# Effect of Dynamic Soil-Pile-Structure Interaction on Seismic Response of Mid-Rise Moment Resisting Frames

By

**Aslan Sadeghi Hokmabadi**

A thesis submitted in fulfilment
of the requirement for the degree of
**Doctor of Philosophy**

Faculty of Engineering and Information Technology
University of Technology Sydney (UTS)

June 2014

# CERTIFICATE OF ORIGINAL AUTHORSHIP

I certify that the work in this thesis has not previously been submitted for a degree nor has it been submitted as part of requirements for a degree except as fully acknowledged within the text.

I also certify that the thesis has been written by me. Any help that I have received in my research work and the preparation of the thesis itself has been acknowledged. In addition, I certify that all information sources and literature used are indicated in the thesis.

Signature of Candidate

---

(Aslan Sadeghi Hokmabadi)

Sydney, June 2014

*Sincerely Dedicated to*

*My Father and Mother*

*Samad and Sorayyah*

# ABSTRACT

Seismic behaviour of structures built on soft soils is influenced by the soil properties and the foundation type, where the response is significantly different from the fixed base condition owing to the interaction between the ground and the structure. Soil-Structure Interaction (SSI) reduces the natural frequency of the system and increases the effective damping ratio of the system, for typical soils and foundations, in comparison with the fixed-base structure. This can considerably alter the response of the building frames under the seismic excitation by influencing the structural demand of the building as well as amplifying the lateral deflections and inter storey drifts of the superstructure. This amplification of lateral deformations due to SSI may change the performance level of buildings in the performance based design approach, which should be considered with great rigor accounting for the influence of SSI significantly influenced by the foundation type (i.e. shallow and deep foundation), in order to provide safe and cost effective design against the natural disasters such as earthquake.

In this study, in order to provide a benchmark to verify and calibrate the numerical model as well as experimentally investigate the influence of SSI on the seismic response of buildings, a series of shaking table tests on the soil-foundation-structure models are conducted at the University of Technology Sydney (UTS) structures laboratory. Different foundation types such as shallow foundation, floating pile foundation, end-bearing pile foundation as well as fixed base condition, excluding SSI interaction, are physically modelled. A laminar soil container is designed and constructed to simulate the free field soil response by minimising boundary effects. Simulating the superstructure as a multi-storey frame during the shaking table tests makes experimental data unique. Accordingly, in the current shaking table tests, by adopting the same soil properties, same superstructure, same input motions, and same test setup, a clear comparison is provided between the structural responses for different types of foundations. The experimental results indicate that soil-structure interaction amplifies the lateral deflections and inter-storey drifts of the structures supported by different types of foundations. However, the choice of the foundation type influences the structural performance significantly and should be addressed carefully in investigating the influence of SSI on the superstructure response during shaking excitations.

A fully nonlinear three-dimensional numerical model employing FLAC3D is developed to perform time-history analysis and simulate the performance of the superstructure considering the seismic soil-structure interaction. Hysteretic damping of the soil is implemented to represent the variation of the shear modulus reduction factor and the damping ratio of the soil with the cyclic shear strain. Free field boundary conditions are assigned to the numerical model and appropriate interface elements, capable of modelling sliding and separation between the pile and soil elements, are considered. The developed numerical model is verified and validated against the conducted shaking table results. Comparison of the numerical predictions and the experimental data shows a good agreement confirming the reliability of the numerical model. Consequently, the proposed numerical model is a reliable method of simulation which can be employed for further numerical investigations concerning the dynamic soil-structure interaction. Practicing engineers can adopt this verified numerical modelling procedure in the design to consider the effect of SSI.

Furthermore, in order to investigate the different characteristics of SSI and its influence on the seismic response of superstructures, parametric studies with respect to different types of foundations are conducted employing the previously verified three-dimensional numerical modelling procedure. A full scale fifteen storey structure (prototype) with four different types of foundations, namely, (i) fixed-base structure representing the situation excluding the soil-structure interaction, (ii) structure supported by a shallow foundation, (iii) structure supported by a pile-raft foundation in soft soil, and (iii) structure supported by a floating (frictional) pile foundation in soft soil, are simulated. According to the results of the numerical investigations, the properties of the in situ soil influence the characteristics of the excitation in terms of peak acceleration and frequency content. Moreover, the reduction ratio of the shear forces of superstructure due to SSI is a function of the foundation type, while the magnitude of this reduction is different for different levels in the superstructure. Accounting for the rocking-dissipation concept, results of this study can help the practicing engineers in selecting the proper foundation type for the structures. The foundation types experiencing considerable amount of rocking during an earthquake, dissipate significant amount of earthquake energy in comparison with the other types of foundations, and this rocking-dissipation in turn results in directing less shear forces to the superstructure and reducing the structural demand of the superstructure.

# ACKNOWLEDGMENT

I would like to express my sincere gratitude and appreciation to the individuals who supported me during my PhD studies. This research work could have not been possible without their support and guidance. I would particularly like to thank my principal supervisor, Dr. Behzad Fatahi, who has provided me with intellectual guidance, encouragement, limitless support, and were always available to discuss this work. I greatly appreciate my co-supervisor, Professor Bijan Samali, for his mentorship and unfailing assistance throughout the course of this research. The author gratefully acknowledges the financial support provided by the University of Technology Sydney (International Research Scholarship) and Centre for Built Infrastructure Research (CBIR) of the Faculty of Engineering and Information Technology, UTS.

I am appreciative to all my friends and co-workers at CBIR, particularly Mohammadreza Hassani, Saad Mahbube Subhani, and Chij Shrestha, for their invaluable friendships and help. Special thanks to Dr. Seyed Hamid Reza Tabatabaeifar (former PhD candidate at UTS) for his collaboration and kind assistance during the experimental phase of the project. Hamid and I conducted the experimental part of this research together to be used in our theses. Furthermore, I owe my gratitude to the staff of the UTS soils and structures laboratories for their extensive assistance in conducting the laboratory experiments. Particularly, I want to thank Peter Brown, for his commitment and remarkable help in technical matters concerning the experimental shaking table tests.

My appreciation is also extended to Professor Ali Fakher and Senior Engineer Jamal Peymani for their guidance, support, and encouragement to continue my postgraduate studies in Australia.

I wish to take the opportunity to express my heartfelt gratitude to my family for their priceless support and confidence in me without which I would never achieve this moment. To my father for instilling in me the value of learning and providing me the outstanding opportunities to follow my dreams. To my mother for every single day that she did not have me nearby, but encouraged me in my endeavour. To my brothers for their countless support, sacrifices, and friendship throughout all these years, and to my beautiful partner for her patience, love, and support.

# LIST OF REFEREED PUBLICATIONS BASED ON THIS RESEARCH

## Journal Articles

1. **HOKMABADI, A. S.**, FATAHI, B. & SAMALI, B. 2014. Physical modelling of seismic soil-pile-structure interaction for buildings on soft soils. *International Journal of Geomechanics,* (DOI: 10.1061/(ASCE)GM.1943-5622.0000396).
2. **HOKMABADI, A. S.**, FATAHI, B. & SAMALI, B. 2014. Seismic Response of Mid-rise Buildings on Shallow and End-bearing Pile Foundations in Soft Soils. *Soils and Foundations,* 54 (3), 345-363.
3. **HOKMABADI, A. S.**, FATAHI, B. & SAMALI, B. 2014. Assessment of soil-pile-structure interaction influencing seismic response of mid-rise buildings sitting on floating pile foundations. *Computers & Geotechnics*, 55, 172–186.
4. **HOKMABADI, A. S.**, FATAHI, B. & SAMALI, B. 2012. Recording inter-storey drifts of structures in time-history approach for seismic design of building frames. *Australian Journal of Structural Engineering*, 13 (2), 175-179.

## Peer-reviewed Conference Papers

5. FATAHI, B., **HOKMABADI, A. S.** & SAMALI, B. 2014. Seismic Performance Based Design for Tall Buildings Considering Soil-Pile-Structure Interaction. *International Conference on Geotechnical Engineering, ASCE, Geoshanghai2014.* Shanghai, China, 333-342.
6. **HOKMABADI, A. S.**, FATAHI, B. & SAMALI, B. 2013. Seismic Response of Superstructure on Soft Soil Considering Soil-Pile-Structure Interaction. In: DELAGE, P., DESRUES, J., FRANK, R., PUECH, A. & SCHLOSSER, F. (eds.) *proceedings of the 18th International Conference on Soil Mechanics and Geotechnical Engineering*. Paris, France, 547-550.
7. **HOKMABADI, A. S.**, FATAHI, B., TABATABAIEFAR, H. R. & SAMALI, B. 2012. Effects of soil-pile-structure interaction on seismic response of moment resisting buildings on soft soil. In: ATALAR, C., CINICIOGLU, F., DAS, B. M.,

SAGLAMER, A. & TOGROL, E. (eds.) *proceeding of the third International Conference on New Developments in Soil Mechanics and Geotechnical Engineering*. Nicosia, North Cyprus: Near East University Press, 377-384.

8. FATAHI, B., TABATABAIEFAR, H. R., **HOKMABADI, A. S.** & SAMALI, B. 2012. Significance of bedrock depth in dynamic soil-structure interaction analysis for moment resisting frames. In: MAUGERI, M. & SOCCODATO, C. (eds.) *proceeding of the second International Conference on Performance-Based Design in Earthquake Geotechnical Engineering*. Taormina, Italy: Associazione Geotecnica Italiana, 1396-1406.

# TABLE OF CONTENTS

# LIST OF FIGURES

# LIST OF TABLES

# LIST OF NOTATIONS

| | |
|---|---|
| $A$ | Area |
| $A_{loop}$ | Area of the hysteresis loop |
| $a$ | foundation width |
| $c$ | damping coefficient of the structure |
| $C$ | cohesion |
| $[C]$ | damping matrix |
| $c_h$ | horizontal damping coefficient of the subsoil |
| $c_\theta$ | rocking damping coefficient of the subsoil |
| $C_s$ | seismic design coefficient of the fixed-based structure |
| $\widetilde{C_s}$ | seismic design coefficient of the flexible-based structure |
| $D$ | dilation angle |
| $E$ | modulus of elasticity (Young modulus) |
| $E_s$ | soil subgrade reaction |
| $f$ | natural frequency of fixed base structure |
| $\widetilde{f}$ | natural frequency of soil-structure system |
| $f_c'$ | specified compressive strength |
| $f_m$ | natural frequency of the model |
| $f_p$ | natural frequency of the prototype |
| $F_s$ | shear force |
| $F_n$ | normal force |
| $F_x$ | unbalanced forces in $x$ direction from the free-field grid |
| $F_y$ | unbalanced forces in $y$ direction from the free-field grid |
| $F_z$ | unbalanced forces in $z$ direction from the free-field grid |
| $F^{ff}_x$ | free-field grid point forces in x direction |
| $F^{ff}_y$ | free-field grid point forces in y direction |
| $F^{ff}_z$ | free-field grid point forces in z direction |
| $\{F_v\}$ | force vector |
| $G$ | shear modulus of the soil |
| $G_0$ | shear modulus of the soil at small strains |
| $G_{max}$ | largest value of the shear modulus |

| | |
|---|---|
| $G_{sec}$ | secant shear modulus |
| $G_{tan}$ | tangent shear modulus |
| $g$ | gravity |
| $h$ | height of the structure |
| $_{h\theta}$ | lateral displacement at the top of the structure due to rotation of the base |
| $I$ | moment of inertia |
| $I_c$ | flexural rigidity of the building columns |
| $I_x$ | second moment of inertia with respect to x-axis |
| $I_y$ | second moment of inertia with respect to y-axis |
| $I_z$ | second moment of inertia with respect to z-axis |
| $J$ | polar moment of inertia |
| $I_r$ | moment of inertia for rocking motion |
| $k$ | stiffness of the structure |
| $k_s$ | shear spring stiffness |
| $k_n$ | normal spring stiffness |
| $k_y$ | lateral stiffness of foundation |
| $k_\theta$ | rocking stiffness of foundation |
| $k_h$ | horizontal stiffness coefficient of the subsoil |
| $\bar{k}$ | stiffness of a fixed-base structure |
| $K$ | bulk modulus |
| $[K]$ | stiffness matrix |
| $K_h$ | horizontal stiffness coefficient of the subsoil |
| $K_r$ | rocking stiffness coefficient of the subsoil |
| $k_x$ | lateral stiffness of the subsoil foundation |
| $L$ | effective contact length |
| $m$ | mass of the structure |
| $[M]$ | mass matrix |
| $M_p$ | plastic moment capacity |
| $M_0$ | overturning moment |
| $M_s$ | secant modulus |
| $M_t$ | tangent modulus |
| $P_x$ | axial load on pile |
| $r$ | radius of the foundation base |
| $S$ | slider |

| | |
|---|---|
| $S_u$ | shear strength |
| $S_p$ | performance factor |
| $S_u$ | soil shear strength |
| $S_{DS}$ | design earthquake motion |
| $T$ | natural period of fixed-base structure |
| $\tilde{T}$ | natural period of soil-structure system |
| $T_s$ | tensile strength |
| $u$ | lateral displacement at the top of the structure due to structural distortion |
| $u_n$ | incremental relative displacement vector in normal direction |
| $u_s$ | incremental relative displacement vector in shear direction |
| $u_0$ | lateral displacement at the top of structure due to translation of the base |
| $u_t$ | total displacement of the base |
| $u_g$ | horizontal seismic excitation |
| $\tilde{u}^g$ | effective input motion |
| $\{u\}$ | nodal displacement |
| $\{\dot{u}\}$ | nodal velocity |
| $\{\ddot{u}\}$ | nodal acceleration |
| $V$ | base shear of fixed base structure |
| $\tilde{V}$ | base shear of the structure in soil-structure system |
| $\Delta V$ | decrease in the base shear due to SSI |
| $V_p$ | compression wave velocity of the soil |
| $V_s$ | shear wave velocity of the soil |
| $V_{s0}$ | shear wave velocity of the soil at small strains |
| $W_D$ | dissipated energy in one hysteresis loop |
| $W_S$ | maximum strain energy |
| $\overline{W}$ | effective seismic weight of structure |
| $y$ | lateral deformation of pile at point x |
| $\Delta z_{min}$ | smallest width of the adjacent zone in the normal direction |
| $\gamma$ | shear strain |
| $\gamma_{ref}$ | numerical fitting parameter |
| $\delta$ | maximum lateral deflection of fixed base structure |
| $\tilde{\delta}$ | maximum lateral deflection of the structure in soil-structure system |

| | |
|---|---|
| $\Delta t$ | time-step |
| $\Delta S_y$ | mean vertical zone size at boundary grid point |
| $\eta$ | material viscosity |
| $\theta$ | foundation rotation |
| $\lambda$ | geometric scaling factor |
| $\lambda_p$ | density scaling factor |
| $\lambda_\varepsilon$ | strain scaling factor |
| $\upsilon$ | Poisson's ratio |
| $v_x^m$ | *x*-velocity of the grid point in the main grid |
| $v_y^m$ | *y*- velocity of the grid point in the main grid |
| $v_z^m$ | *z*- velocity of the grid point in the main grid |
| $v_x^{ff}$ | *x*-velocity of the grid point in the free-field grid |
| $v_y^{ff}$ | *y*- velocity of the grid point in the free-field grid |
| $v_z^{ff}$ | *z*- velocity of the grid point in the free-field grid |
| $\xi$ | equivalent viscous damping ratio |
| $\tilde{\xi}$ | effective damping ratio |
| $\xi_g$ | hysteretic material damping of the soil |
| $\rho$ | soil density |
| $\sigma_y$ | yield stress |
| $\sigma_{xx}^{ff}$ | mean horizontal free-field stress at the grid point |
| $\sigma_{xy}^{ff}$ | mean free-field shear stress at the grid point |
| $\phi$ | friction angle |
| $\tilde{\omega}$ | effective natural frequency |
| $\omega_0$ | natural frequency of the fixed base structure |
| $\tau$ | shear stress |
| $\bar{\tau}$ | normalised shear stress |

# Chapter 1- INTRODUCTION

## 1.1 General

The scarcity of land compels engineers to construct buildings at locations with less favourable geotechnical conditions in seismically active regions. Numerous mid-rise buildings have been built in earthquake prone areas employing different types of foundations. In the selection of the foundation type for the mid-rise buildings, several options such as shallow foundation, pile foundation, or pile-raft foundation, might be considered by design engineers to carry both gravity and earthquake loads. However, different types of foundations behave differently during the earthquake considering the soil-structure interaction (SSI) that may influence the seismic behaviour of the superstructure.

For determining the seismic response of structures, it is a common practice to assume the structure is fixed at the base. In fact, if the ground is stiff enough (e.g. structure founded on solid rock) it is reasonable to assume that the input motion of the structure due to a design earthquake is essentially identical to the motion of the free field, which is defined as the motion experienced at the same point before the structure is built. However, for the structures constructed on soft soils, two modifications should be considered for determining the seismic response. First, the imposed motion to the structure differs from the free field motion due to the presence of the structure and foundation. Secondly, additional dynamic deformations are induced within the structure due to the underneath soft soil. The process, in which response of the soil influences the motion of the structure and response of the structure influences the motion of the soil is referred to as the soil-structure interaction (Kramer, 1996).

## 1.2 Significance of This Study

Complexity of the seismic soil-structure interaction problems and unavailability of standard and validated analysis techniques routinely results in ignoring or greatly simplifying the influence of the foundation for the structural design. The main challenge of the soil-structure interaction problem is that the two disciplines of structural and geotechnical engineering meet simultaneously. However, the analysis usually is conducted in two separate parts in which a geotechnical engineer may idealise a complex multimode superstructure as a single degree of freedom oscillator, and on the other hand structural engineers may ignore the SSI or represent the nonlinear soil-foundation-structure interaction with simple linear springs, where the nonlinear interaction between the superstructure and the substructure is artificially prevented.

Lessons learned from the post seismic observations of the past earthquakes such as 1985 Mexico City, 1995 Kobe, and 2011 Christchurch earthquakes clearly illustrate the importance of accounting for the soil-structure interaction to predict the seismic behaviour of superstructures, where otherwise the loss of life and property is unavoidable. Consequently, there is an obvious need to design structures safely but not costly against natural disasters such as earthquakes. Effects of dynamic soil-structure interaction under extreme loads due to strong earthquakes are significant for many classes of structures and must be included precisely in the design.

The regulated procedures in the available codes such as ASCE (ASCE7-10, 2010), NEHRP (BSSC, 2009), and Australian code (AS1170.4, 2007) do not provide any procedure to account for the different types of foundations in an elaborative manner. Accordingly, a simplified method representing the subsoil by series of springs and dashpots (impedance functions), and the superstructure as single degree of freedom oscillator is adopted in the regulated codes, regardless of the foundation type. Moreover, the linear equivalent behaviour for the subsoil is adopted in the mentioned codes without capturing any soil nonlinearity directly, where soil stiffness and damping are assumed constant during the solution process. Therefore, conducting more research on the influence of SSI in the seismic design of the buildings with great rigor accounting for the higher modes of response and different foundation types, is required.

Model tests in geotechnical engineering offer the advantage of simulating complex systems under controlled conditions providing the opportunity of better understanding of the fundamental mechanisms of these systems. Such tests are often used as calibration benchmarks for numerical or analytical methods, or to make quantitative predictions of the prototype response. Although a number of single gravity (1g) model tests dealing with the SSPSI effects on the seismic response of structures are available in the literature, most of them simplified the superstructure as a single degree of freedom oscillator in which the behaviour of the soil-structure system may not be completely conforming to reality and the effect of higher modes would not be captured. Therefore, conducting shaking table tests adopting multi-storey frame is highly demanded, where the dynamic properties of the prototype structure such as natural frequency of the first and higher modes, and number of stories is simulated during the shaking table tests. Moreover, conducting a complete set of experimental tests in this study with different foundation types (i.e. shallow and deep foundation) leads to experimentally comparable results to determine the influence of the soil-structure interaction on the seismic response of the superstructure supported by different types of foundations.

Pile foundations, which are one of the most common foundation systems for civil engineering structures, are usually employed to transmit foundation loads through soil strata of low bearing capacity to deeper soil or rock strata possessing a high bearing capacity and stiffness. End bearing piles terminate in hard, relatively impenetrable materials such as rock or very dense sand and gravel, while floating piles obtain a greater part of their capacity by skin friction or adhesion and are mostly employed in situations where the bedrock is deep. Determination of the pile foundation seismic response is a multifaceted process involving inertial interaction between the structure and the pile foundation, kinematic interaction between piles and the soil, and the nonlinear response of the soil to strong earthquake motions (Finn, 2005). However, simple methods such as Winkler computational model are often used in engineering practice in which soil–pile interaction is modelled using either linear or nonlinear springs. The reliability of these constitutive models has been questioned by many due to the simplifying assumptions regularly used (Hokmabadi et al., 2011; Ashour et al., 1998). At first, the applied earthquake motion in the time-history analysis is derived from the free field motion ignoring the presence of superstructure and pile elements.

Secondly, Winkler springs which have been developed initially to model single pile–soil interaction, are not directly applicable to simulate pile groups due to the over-lapping displacement fields of piles affecting the individual pile stiffness (Comodromos and Papadopoulou, 2013). The limitations of Winkler methods and availability of advanced computational tools lead the researcher to conduct fully-nonlinear analysis to study the seismic response of pile foundations. However, the adopted numerical models need to be verified against the experimental measurements prior to utilising them as a tool for nonlinear time-history soil-foundation-structure interaction analysis. Therefore, there is a strong need to develop a verified numerical modelling procedure capable of considering important aspects in SSI analysis. Thus, this model can be used for further investigation on the influence of SSI on the seismic response of buildings.

The present research aims to evaluate and quantify the effect of foundation type (shallow and deep foundation) on the response of structures considering SSI, which is significantly important on the performance based design of structures. Different types of foundations can alter the dynamic properties of the system such as stiffness, damping, and natural frequency, which are investigated in this study by conducting both experimental and numerical modelling. A three-dimensional explicit finite difference program, FLAC3D, is used to numerically model and examine the influence of the soil-structure interaction on the seismic response of a fifteen storey moment resiting building. The proposed numerical soil-structure model is verified and validated against a series of experimental shaking table tests conducted at the University of Technology Sydney (UTS). Adopting the verified three-dimensional modelling procedure, the different characteristics of SSI and its influence on the seismic response of the superstructure with respect to different types of foundations are investigated.

## 1.3 Objectives and Scope of This Study

The main objective of this study is to investigate the influence of foundation type on the seismic response of regular mid-rise moment resisting building frames during earthquake excitations in order to ensure the design safety and reliability. The research work consists of four parts: (a) developing an enhanced nonlinear three-dimensional soil-structure model, (b) conducting a series of experimental shaking table test, (c) validation of the soil-structure model employing the experimental shaking table

measurements, and (d) investigating the different characteristics of SSI and its influence of the seismic response of superstructure with respect to the different types of foundations.

The key objectives of the experimental investigations are:

- Investigating the significance of the soil-structure interaction on the seismic response of building frames supported by different types of foundations using experimental shaking table tests.
- Verifying and calibrating the developed numerical soil-structure model as a qualified model which can be employed for further dynamic soil-structure interaction numerical investigations.
- Designing and constructing the soil-structure model components including structural models, pile foundations, a soil mix, and a laminar soil container.

Specific objectives to develop an enhanced soil-structure numerical model in this study are as follows:

- Simulating the complex nature of three-dimensional dynamic soil-foundation-structure interaction as accurate and realistic as possible.
- Treating the dynamic behaviour of soil, foundation, and structure with equal rigor simultaneously.
- Incorporating hysteretic damping algorithm in the dynamic analysis enabling strain-dependent modulus (G/Gmax -$\gamma$) and damping functions ($\xi$ - $\gamma$) to be included directly in order to capture the hysteresis curves and energy absorbing characteristics of the soil.
- Employing a Multi Degree of Freedom (MDOF) structure in order to determine inter-storey drifts directly to be used for investigating the performance levels of the building structures under the influence of dynamic soil-structure interaction.

The main objectives of the investing the influence of foundation type on seismic performance of structures are:

- Studying, in depth, the seismic behaviour and response of regular mid-rise moment resiting building frames supported by different types of foundations (i.e. shallow and deep foundation) subjected to earthquake action embracing the influence of dynamic soil-structure interaction.
- Examining the adequacy of conventional design procedures excluding the influence of foundation type to guarantee the structural safety.
- Acquiring better understanding of key parameters influencing the soil-structure interaction under seismic loads.
- Investigating the effects of the foundation type on the seismic response of superstructure in terms of shear distribution, rocking of the superstructure, amplification of lateral deformations, and the performance levels of structures.

## 1.4 Organisation of the Thesis

Following this introduction, Chapter 2 presents a comprehensive survey of the literature associated with the seismic soil-structure interaction (SSI). The dynamic behaviour of soils, lessons learned from previous earthquakes, modelling techniques to simulate the seismic soil-pile-structure interaction (SSPSI), effects of SSPSI on the behaviour of structural frames, and available building codes on seismic soil-structure interaction are presented. Moreover, previous experimental investigations on SSPSI are reviewed and discussed.

Chapter 3 presents the adopted three-dimensional numerical modelling procedure in this study. In this chapter, different components of the developed numerical model including soil elements, pile elements, structural elements, interface elements, boundary conditions, and the dynamic loading are explained.

Chapter 4 is devoted to the conducted laboratory shaking table tests for verifying the proposed numerical soil-structure model and investigating the influence of different types of foundations on the seismic response of the superstructure. In this chapter, the scaling methodology and utilised scaling factors, design and construction of the soil-pile-structure model components, instrumentations of the model as well as the test preparation and set up are described. In addition, further shaking table tests are carried

out to experimentally investigate the influence of SSPSI on the dynamic response of buildings with various heights.

Chapter 5 illustrates the assessment of the capabilities of the developed numerical model in simulating the SSPSI, while the results of the conducted shaking table tests (reported in Chapter 4) is employed to verify and calibrate the developed numerical model in FLAC3D. Accordingly, the scaled fifteen storey model structure with different types of foundations is simulated numerically and results are compared with the experimental measurements.

Chapter 6 investigates the different characteristics of SSI and its influence on the seismic response of superstructures, while parametric studies with respect to different types of foundations are conducted. For this purpose, the previously verified three-dimensional numerical modelling procedure (see Chapter 5) is adopted, considering four types of foundations. Results are presented and compared in terms of settlement of the superstructure under gravity loads, site effect and soil amplification, shear force distribution in the superstructure, rocking of the superstructure, and lateral deformations and drifts of the fifteen storey superstructure.

Chapter 7 presents the conclusions of the current research and recommendations for further research, followed by the Bibliography.

# Chapter 2- LITERATURE REVIEW

## 2.1 General

The problem of the soil-pile-structure interaction in the seismic analysis and design of structures has become increasingly important, as it may be inevitable to build structures at locations with less favourable geotechnical conditions in seismically active regions. Influence of the underlying soil on the seismic response of the structure can be neglected when the ground is stiff enough, and consequently the structure can be analysed considering fixed-base conditions. However, the same structure behaves differently when constructed on the soft soil deposit. Earthquake characteristics, travel path, local soil properties, and the soil-structure interaction are the key factors affecting the seismic excitation experienced by the superstructure. The result of the first three of these factors can be summarised as free-field ground motion. However, the foundation is not able to follow the deformation of the free field motion due to its stiffness, and the dynamic response of the structure itself would induce deformation of the supporting soil (Kramer, 1996).

Complexity of the Seismic Soil-Pile-Structure Interaction (SSPSI) problem and unavailability of standard and validated analysis techniques routinely results in ignoring or greatly simplifying the presence of pile foundations for the structural design. The main challenge of the soil-structure interaction problem is that the two disciplines of structural and geotechnical engineering meet simultaneously. However, the analysis usually is conducted in two separate parts in which a geotechnical engineer may idealise a complex multimode superstructure as a single degree of freedom oscillator, and on the other hand structural engineers may ignore the SSPSI or represent the nonlinear soil-pile interaction with simple linear springs. In this way, the nonlinear system interaction between the superstructure and the substructure is artificially prevented (Meymand, 1998).

In this chapter, initially the concept of the free field ground motion and the seismic soil-structure interaction together with its influence on the dynamic behaviour of superstructures is presented employing a simplified spring-dashpot model. Hysteresis behaviour of typical soils subjected to the cyclic loading is explained and the adopted backbone curves for cohesive and cohesionless soils are characterised. Then, lessons learned from previous earthquakes emphasising on the importance of the seismic soil-structure interaction for several structures with shallow and pile foundation systems founded on soft soils, are provided. Available modelling techniques to simulate SSPSI are explained and their strengths and shortcomings are discussed. Latest achievements and the state of the art in studying the effects of SSPSI on the behaviour of buildings are provided. Eventually, a general overview on the building codes to consider the effect of the soil-structure interaction on structural behaviour is presented. Moreover, previously conducted experimental works in this area are explained aiming to be employed as a platform for the experimental shaking table investigations in this study.

## 2.2 Free Field Ground Motion

Ground response analysis is used to predict the free field ground motion and in turn to determine the earthquake-induced accelerations applied to the superstructures. In the ideal situation as shown in Figure 2.1a, the complete ground response analysis would model the rupture mechanism of the fault, the propagation of the stress waves through the earth materials till top of the bedrock beneath a site specific soil deposit, and would then consider the effect of the site soil on the ground surface motion. However, in practice due to the complicated mechanism of the fault rupture and other uncertainties, empirical methods together with seismic hazard analysis are used to predict the bedrock motion characteristics at the site. Thus, the problem of the ground response analysis is simplified as a response of the soil deposit to the motion of the bedrock immediately beneath as depicted in Figure 2.1b. It should be mentioned that, according to Kramer (1996), due to the lower wave propagation velocity of shallower materials in comparison with deeper ones, inclined stress waves that strike horizontal layer boundaries are usually refracted to a more vertical direction. By the time the

waves reach the ground surface, multiple refractions often bend the resultant stress waves to a nearly vertical direction as shown in Figure 2.1a.

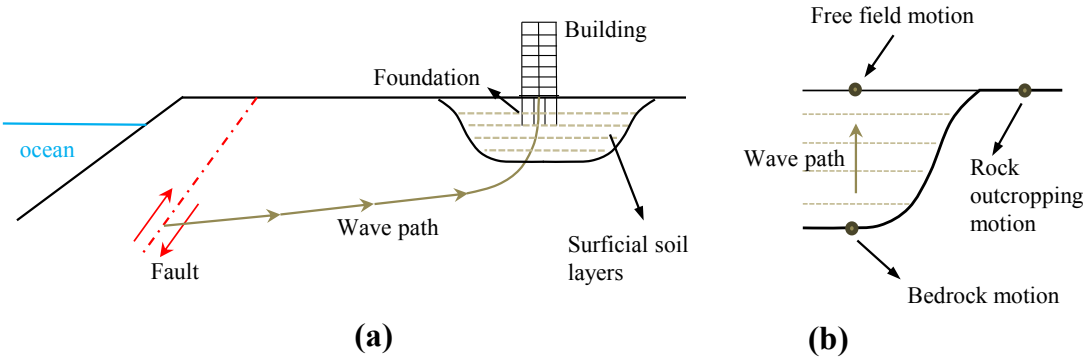


**Figure 2.1** (a) Complete ground response analysis and the resultant vertical wave propagation near the ground surface; (b) free field ground motion

Despite the fact that the seismic waves may travel through tens of kilometres of rock and often less than 100 meters of soil, the soil plays a very important role in determining the characteristics of the ground surface motion (Kramer, 1996). Over the years, a number of techniques and software have been developed for ground response analysis such as commonly used SHAKE software (Schnabel et al., 1972) in which one-dimensional wave propagation equations are adopted. A detailed treatment of these techniques is beyond the scope of the present research and here just the influence of the soft soil deposit on the ground response will be discussed.

Local site effects can significantly influence the characteristics of the ground motion such as amplitude, frequency content, and duration. Idriss (1990) has studied data collected from Mexico City and San Francisco Bay areas and concluded that the peak acceleration at the soft soil sites are likely to be greater than that of on rock sites for low to moderate acceleration levels (less than about 0.4g). However, at higher acceleration levels, low stiffness and nonlinearity of soft soil prevent the development of peak accelerations as large as those observed on the rock.

The frequency content of the free field ground motion is also influenced by the local site conditions. Seed et al. (1976) demonstrated that the deep and soft soil deposits produce greater proportions of long-period (low frequency) motion as shown in Figure 2.2. For example, the dominant period of motion at a soft to medium clay site is about

0.9 second, while the dominant period of motion at rock site is less than 0.2 second. This phenomenon can be extremely important, particularly when long-period structures such as bridges and tall buildings are founded on such deposits.

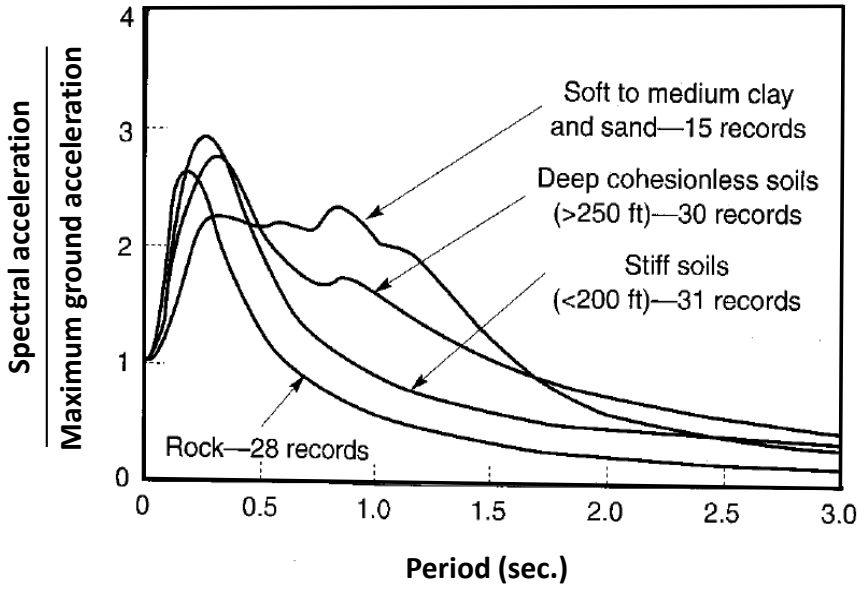


**Figure 2.2** Average normalised response spectrum (5%) for different local site conditions. (Seed et al., 1976)

In the presence of a structure constructed on the soft soil deposit, the pile or shallow foundation is not able to follow the deformation of the free field motion due to its stiffness, and the dynamic response of the structure itself would induce deformation of the supporting soil. This process is referred to as the Seismic Soil-Structural Interaction and will be described further in Section 2.3.

## 2.3 Concept of the Seismic Soil-Structure Interaction

In order to illustrate the concept of SSI and its influence on the response of the superstructure, a simplified model suggested by Wolf (1985) is described here. A single degree of freedom (SDOF) system, which represents either one storey building or an equivalent multi-storey building with respect to its dominant mode, is considered. The structure is characterised by its mass ($m$), stiffness ($k$), and damping coefficient ($c$). When the structure rests on the rigid soil deposit, the natural frequency of the resulting

fixed-base system ($\omega_0$) would depend only on the mass and the stiffness of the structure as follows:

$$\omega_0 = \sqrt{\frac{k}{m}} \tag{2.1}$$

The hysteretic damping ($\xi_0$) would be calculated as:

$$\xi_0 = \frac{c\omega_0}{2k} \tag{2.2}$$

However, when the supporting soil is compliant, the foundation can translate and rotate. Characteristics of such a system can be represented by the translational and rotational springs and dashpots as shown in Figure 2.3, where, $k_h$ and $c_h$ are stiffness and damping in the horizontal direction, and $k_\theta$ and $c_\theta$ are stiffness and damping in the rotational direction, respectively. $h$ is the height of the structure, $2a$ is the width of the foundation, $u_0$ is the amplitude of the base displacement relative to the free-field motion ($u_g$), $u$ is the structural distortion, and $u_t$ is the total lateral displacement of the system.

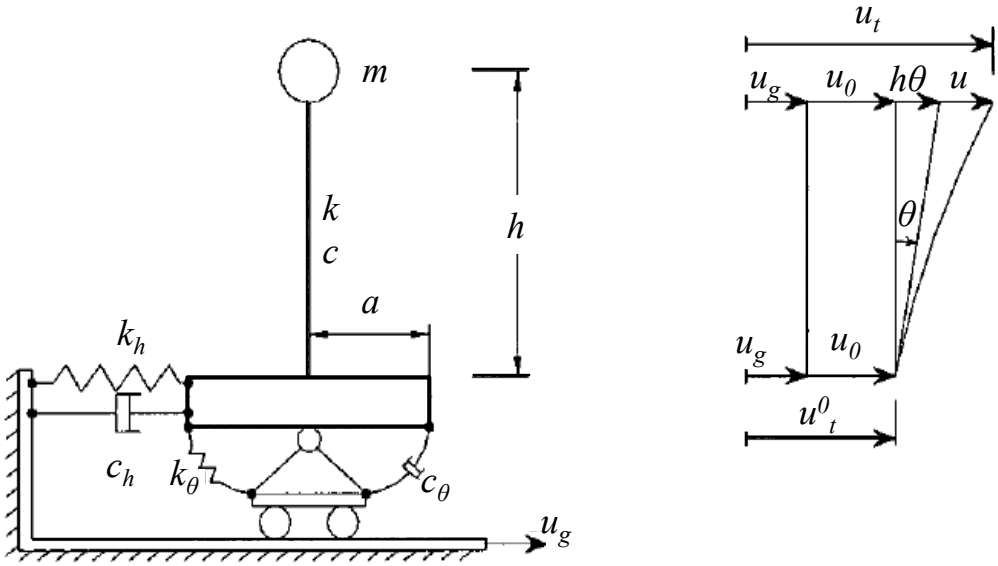


**Figure 2.3** Soil-structure interaction model including SDOF structure and idealised discrete system to represent the supporting soil (after Wolf, 1985)

By assuming a mass-less foundation, the above mentioned three degrees of freedom vibration system can be replaced by an equivalent model as shown in Figure 2.4 with the relevant equilibrium equations as follows:

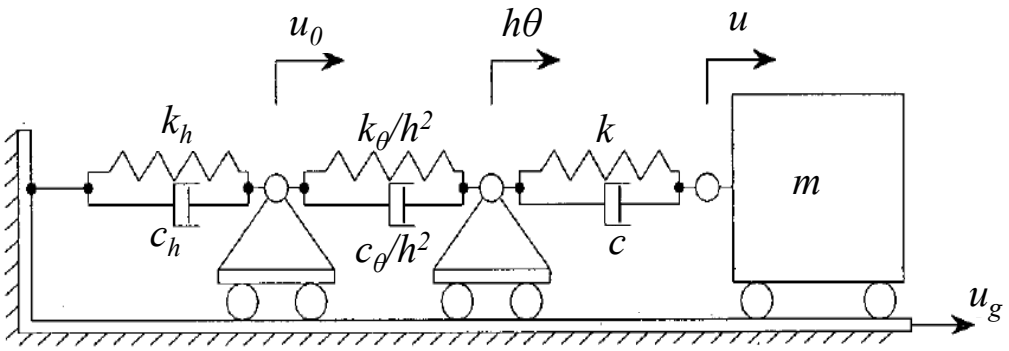


**Figure 2.4** Equivalent soil-structure interaction model (after Wolf, 1985)

$$\begin{bmatrix} k_h + k_\theta/h^2 & -k_\theta/h^2 & 0 \\ -k_\theta/h^2 & k_\theta/h^2 + k & -k \\ 0 & -k & k \end{bmatrix} \begin{Bmatrix} u_0 \\ u_0 + h\theta \\ u_0 + h\theta + u \end{Bmatrix}$$

$$+ \begin{bmatrix} c_h + c_\theta/h^2 & -c_\theta/h^2 & 0 \\ -c_\theta/h^2 & c_\theta/h^2 + c & -c \\ 0 & -c & c \end{bmatrix} \begin{Bmatrix} \dot{u}_0 \\ \dot{u}_0 + h\dot{\theta} \\ \dot{u}_0 + h\dot{\theta} + \dot{u} \end{Bmatrix}$$

$$+ \begin{bmatrix} 0 & 0 & 0 \\ 0 & 0 & 0 \\ 0 & 0 & m \end{bmatrix} \begin{Bmatrix} \ddot{u}_0 \\ \ddot{u}_0 + h\ddot{\theta} \\ \ddot{u}_0 + h\ddot{\theta} + \ddot{u}_0 \end{Bmatrix} = \begin{Bmatrix} 0 \\ 0 \\ -m \end{Bmatrix} \ddot{u}_g \tag{2.3}$$

where,

$$\xi = \frac{c}{2k\omega};\ \xi_h = \frac{c_h}{2k_h\omega_h};\ \xi_\theta = \frac{c_\theta}{2k_\theta\omega_\theta};\ \omega_h = \sqrt{\frac{k_h}{m}};\ \omega_\theta = \sqrt{\frac{k_\theta}{mh^2}};\ \omega_s = \sqrt{\frac{k}{m}} \tag{2.4}$$

After solving the above equations:

$$u_0 = \frac{{\omega_s}^2}{{\omega_h}^2} \frac{1+2i\xi}{1+2i\xi_h} u \tag{2.5}$$

$$h\theta = \frac{{\omega_s}^2}{{\omega_\theta}^2} \left[\frac{1+2i\xi}{1+2i\xi_\theta}\right] u \tag{2.6}$$

Structural distortion, *u,* is expressed as follows:

$$\left(1 + 2\xi - \frac{\omega^2}{{\omega_s}^2} - \frac{{\omega_s}^2}{{\omega_h}^2} \frac{1+2i\xi}{1+2i\xi_h} - \frac{{\omega_s}^2}{{\omega_\theta}^2} \frac{1+2i\xi}{1+2i\xi_\theta}\right) u = \frac{\omega^2}{{\omega_s}^2} u_g \tag{2.7}$$

Figure 2.5 displays the case in which the coupled system is replaced by an equivalent one degree of freedom system the enforcing same structural distortion (*u*),

and same mass ($m$). The equivalent natural frequency ($\tilde{\omega}$), equivalent damping ratio ($\tilde{\xi}$), and equivalent input motion ($\tilde{u}_g$) are:

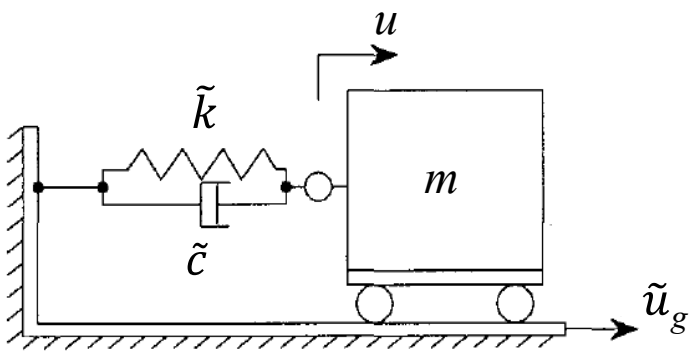


**Figure 2.5** Equivalent one degree of freedom system (after Wolf, 1985)

$$\frac{1}{\tilde{\omega}^2} = \frac{1}{{\omega_s}^2} + \frac{1}{{\omega_h}^2} + \frac{1}{{\omega_\theta}^2} \tag{2.8}$$

$$\tilde{\xi} = \frac{\tilde{\omega}^2}{{\omega_s}^2}\xi + \frac{\tilde{\omega}^2}{{\omega_h}^2}\xi_h + \frac{\tilde{\omega}^2}{{\omega_\theta}^2}\xi_\theta \tag{2.9}$$

$$\tilde{u}_g = \frac{\tilde{\omega}^2}{{\omega_s}^2}u_g \tag{2.10}$$

Equation (2.8) indicates that the natural frequency of the equivalent system considering the seismic soil-structure interaction ($\tilde{\omega}$) is always lower than that of the fixed-base structure ($\omega_0$). In other words, an important effect of SSI is to reduce the natural frequency of the system. Moreover, Equation (2.9) shows that the damping ratio of the equivalent system considering the seismic soil-structure interaction ($\tilde{\xi}$), for typical soils and foundations, is greater than the damping ratio of the fixed-base structure ($\xi_0$) showing the other important impact of the seismic soil-structure interaction by increasing the effective damping ratio of the system.

In order to explain the consequent effect of considering the soil-structure interaction on the total response of the structure, the above mentioned simplified SDOF model is subjected to an arbitrary input motion. For simplicity, foundation stiffness and damping coefficients are assumed to be frequency independent and calculated based on Equations (2.11) and (2.12) as suggested by Gazetas (1991). In these equations, $r$ is the

radius of the rigid circular footing and $V_s$ is the shear wave velocity of the supporting soil.

$$k_x = \frac{8Gr}{2-\upsilon};\ c_x = \frac{4.6}{2-\upsilon}\,\rho V_s\, r^2 \tag{2.11}$$

$$k_\theta = \frac{8Gr^3}{3(1-\upsilon)};\ c_\theta = \frac{0.4}{1-\upsilon}\,\rho V_s\, r^4 \tag{2.12}$$

Figure 2.6 presents the maximum response of the structure considering the soil-structure interaction. Referring to Figure 2.6a, it is obvious that the soil-structure interaction tends to reduce the demand (base shear) of the structure. However, as shown in Figure 2.6b, the soil-structure interaction increases the overall displacement of the structure due to translation and rotation of the foundation (Han and Cathro, 1997). Accordingly, considering the effects of the soil-structure interaction can be important for tall, slender structures or closely spaced structures that may be subjected to pounding when relative displacements become large (Kramer, 1996). Moreover, increase in the total deformation of the structure and in turn secondary P-Δ effect may influence the total stability of the structure.

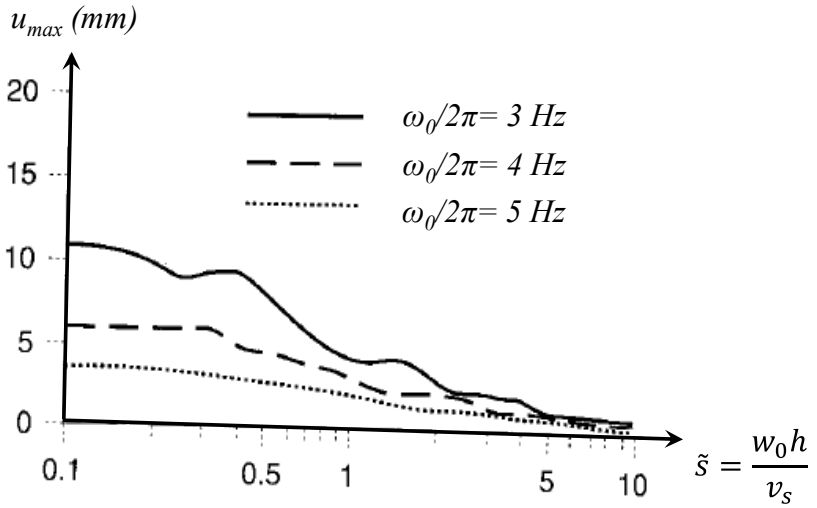


**(a)**

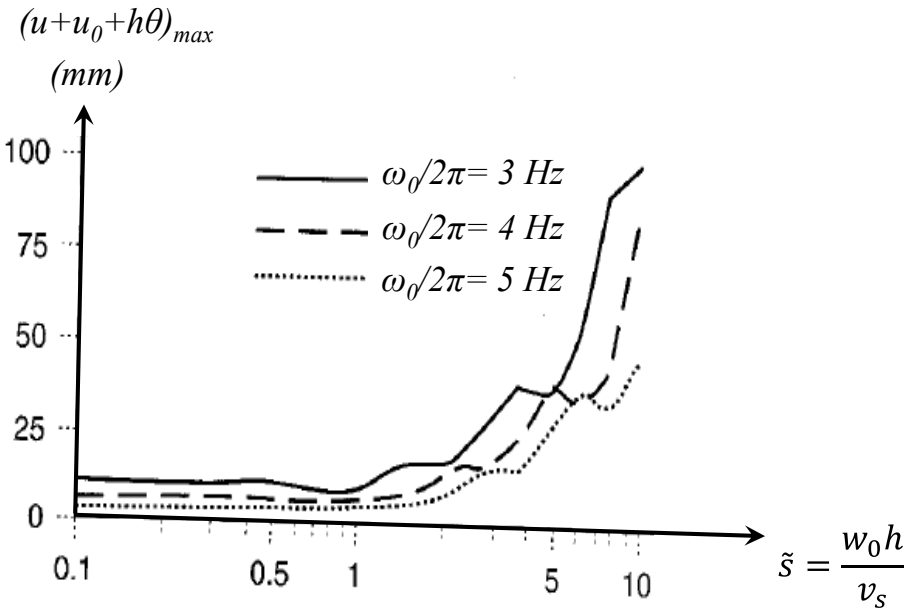


**(b)**

**Figure 2.6** Response of the equivalent soil-structure system: (a) maximum structure demand; (b) maximum total displacement of the structure relative to the free field ground motion (after Wolf, 1985)

Generally, two key mechanisms are involved during the seismic soil-structure interaction:

- *Kinematic Interaction:* The kinematic interaction occurs due to the presence of the stiff shallow foundation or pile foundation elements in the soil resulting in the deviation of the foundation motion from the free field ground motion. Kinematic interaction could be due to the ground motion incoherence, foundation embedment effects, and wave scattering or inclination (Stewart et al., 1999a). This effect can be theoretically modelled by frequency-dependant ratios of the Fourier amplitudes of the foundation input motion to the free field ground motion referring to as *transfer functions*. The foundation input motion, is the theoretical motion of the base slab if the base and the structure were massless. This foundation input motion presents more appropriate motion for the structural response analysis than the free field ground motion (FEMA, 2005).

- *Inertial Interaction:* The inertial interaction results from the inertia developed in the structure due to its own vibration producing base shear, moment and torsional excitation. These loads in turn cause displacements and rotations of the foundation relative to the free field condition (Kramer and Stewart, 2004). The displacements and rotations of the foundation can be described by *Impedance functions* representing frequency-dependant relationships between forces and moments applied to the foundation and the corresponding displacements and rotations of the foundation relative to the free-field motion.

## 2.4 Dynamic Behaviour of Soils

Hysteresis behaviour of typical soils subjected to the cyclic loading is shown in Figure 2.7. This hysteresis response of soils can be described using two important characteristics of the hysteresis loop shape: inclination and breath. As described by Kramer (1996), the inclination of the loop represents stiffness of the soil, which can be described at any point during the loading process by the tangent shear modulus ($G_{tan}$). Obviously, the tangent shear modulus varies throughout a cycle of loading, but its average value over the entire loop can be approximated by the secant shear modulus ($G_{sec}$).

$$G_{sec} = \frac{\tau_c}{\gamma_c} \tag{2.13}$$

where, $\tau_c$ and $\gamma_c$ are the shear stress and shear strain amplitudes at the defined point, respectively. Therefore, $G_{sec}$ describes the general inclination of the hysteresis loop. The breath of the hysteresis loop, which is related to the area of one hysteresis loop, represents the energy dissipation and can be described by the damping ratio ($\xi$) as follows:

$$\xi = \frac{W_D}{4\pi W_S} = \frac{1}{2\pi}\frac{A_{loop}}{G_{sec}\gamma_c^2} \tag{2.14}$$

where, $W_D$ is the dissipated energy in one loop, $W_S$ is the maximum strain energy, and $A_{loop}$ is the area of the hysteresis loop (which is equal to $W_D$).

The parameters $G_{sec}$ and $\xi$ are used to describe the cyclic behaviour of the soil in the equivalent linear analysis and often referred to as the soil equivalent linear

parameters. However, as mentioned by Fatahi and Tabatabaiefar (2013), in order to capture the precise dynamic characteristics of the soil in the nonlinear analysis, the actual path of hysteresis loop should be considered.

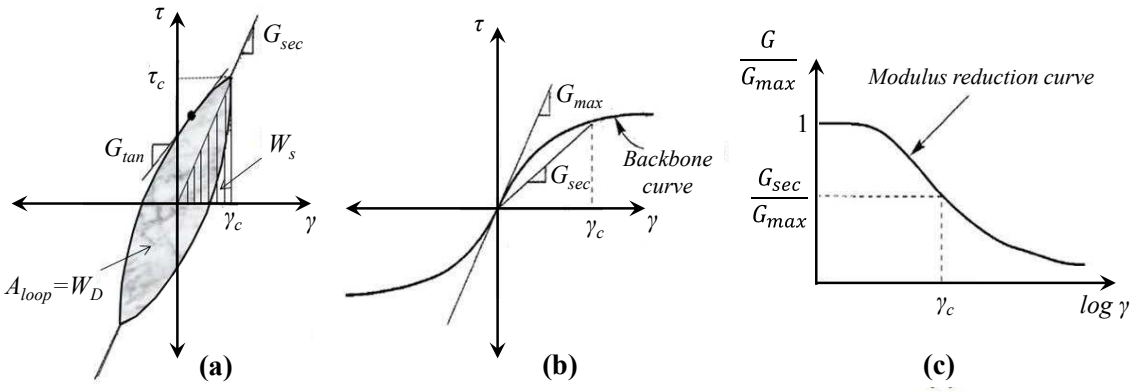


**Figure 2.7** (a) hysteretic stress-strain relationship; (b) backbone curve; (c) typical Modulus reduction curve for soils

The secant shear modulus of a soil element changes with the cyclic shear strain level. At low strain amplitudes, the secant shear modulus is large, but it decreases as the strain amplitude increases. The locus of points corresponding to the tips of hysteresis loops of various cyclic strain amplitudes is called backbone curve as shown in Figure 2.7b. The slope of backbone curve at the origin represents the largest value of the shear modulus represented by $G_{max}$. At greater cyclic shear strain amplitudes, the modulus ratio, $G_{sec}/G_{max}$ drops to values less than one. Therefore, in order to characterise the stiffness of the soil element varying with the cyclic shear strain amplitude, both $G_{max}$ and modulus reduction curve (Figure 2.7c) are required.

In a homogeneous linear elastic material, stress waves travel indefinitely without change in the amplitude. This type of behaviour cannot occur in real materials, such as soil, in which the amplitudes of stress waves attenuate with distance (Das, 1983). In general, soil damping comprises of two distinct parts: material damping (or viscous damping) and geometrical damping (or radiation damping).

- *Material Damping* refers to the absorption of energy by materials during wave propagation resulting in the reduction of the wave amplitude. As described by Kramer (1996), material damping occurs due to the multiple atomic-level actions, such as interface friction and internal hysteresis. Although for specific

soils and structures the operative mechanisms by which the energy is dissipated are not understood sufficiently to allow the explicit modelling, the effects of the various energy loss mechanisms are usually lumped together and represented by some convenient damping mechanism. Das (1983) mentioned that the most commonly used mechanism for representing energy dissipation is viscous damping which assumes the dissipative forces as a function of particle velocity. However, for most soils and structures, energy is dissipated hysteretically by yielding or plastic straining of the material.

- *Geometrical Damping*: Due to the distribution of waves in infinite subsoil media, parts of wave amplitude spread out and dissipate which in turn decrease the specific energy (elastic energy per unit volume) of the media. This reduction in the amplitude due to the spreading of energy over a greater volume, even though the elastic energy is conserved (no conversion to other forms of energy takes place), is often referred to as *Geometrical Damping* (Kramer, 1996). For problems in which energy is released from a finite source, ranging from the large scale fault rupture during an earthquake to the smaller-scale of a vibrating foundation, radiation damping could be extremely important. In such cases, the effects of geometrical damping often dominate those related to the material damping.

Ambrosini (2006) mentioned that the material damping of soil is an important parameter and must be included in the analysis of the soil-structure interaction, especially to determine the maximum top deflection of the superstructure. He also pointed out that the reduction in the base shear force and base overturning moment due to the flexibility of the foundation corresponds, on an average, 70% to geometrical damping and 30% to material damping. For stiff structures having height/width ratios more than one, the rocking motion governs the interaction effect. In this case, especially for low frequency rocking, very little energy is dissipated by the geometric damping of the soil. Thus, the relative importance of the material damping is more pronounced in rocking motion in comparison to translation. Moreover, Ambrosini (2006) concluded that the importance of the soil material damping in the displacement response is very significant leading to reduction of the peak displacements as well as the quick reduction of the free vibrations when the earthquake stops.

## 2.4.1 Backbone Curves for Cohesive Soils

Large number of studies (e.g. Hardin and Drnevich, 1972; Vucetic and Dobry, 1991; Sun et al., 1988) dealing with relationship between shear modulus ratio ($G/G_{max}$) and damping ratio with cyclic shear strain (backbone curves) in cohesive soils have been carried out. Sun et al. (1988) recommended backbone curves for practical use in seismic site-response evaluations for cohesive soils. In those curves, relations between $G/G_{max}$ versus cyclic shear strain (Figure 2.8) and damping ratio versus cyclic shear strain (Figure 2.9) for cohesive soils are illustrated.

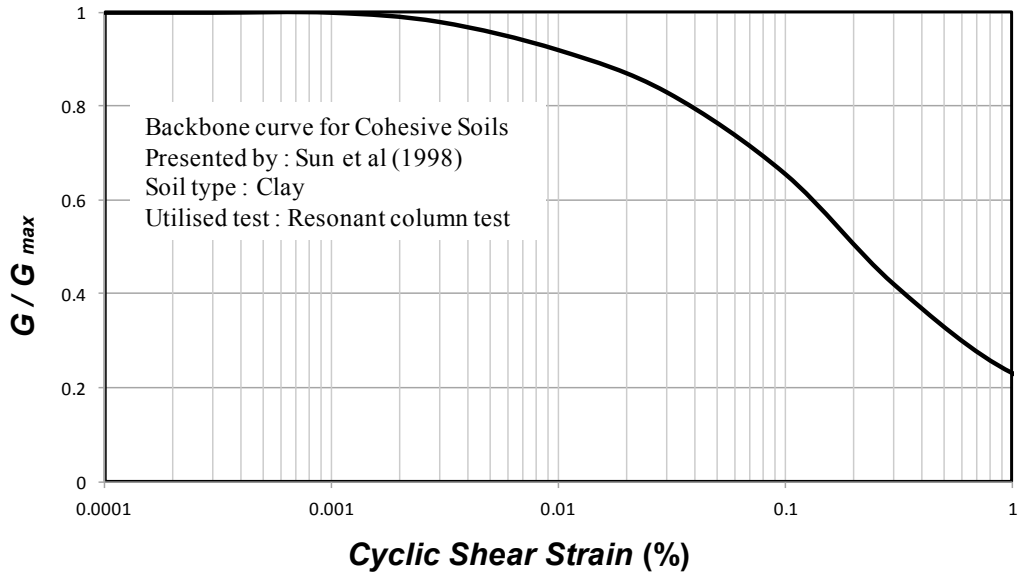


**Figure 2.8** Relations between $G/G_{max}$ versus cyclic shear strain for cohesive soils (after Sun et al., 1988)

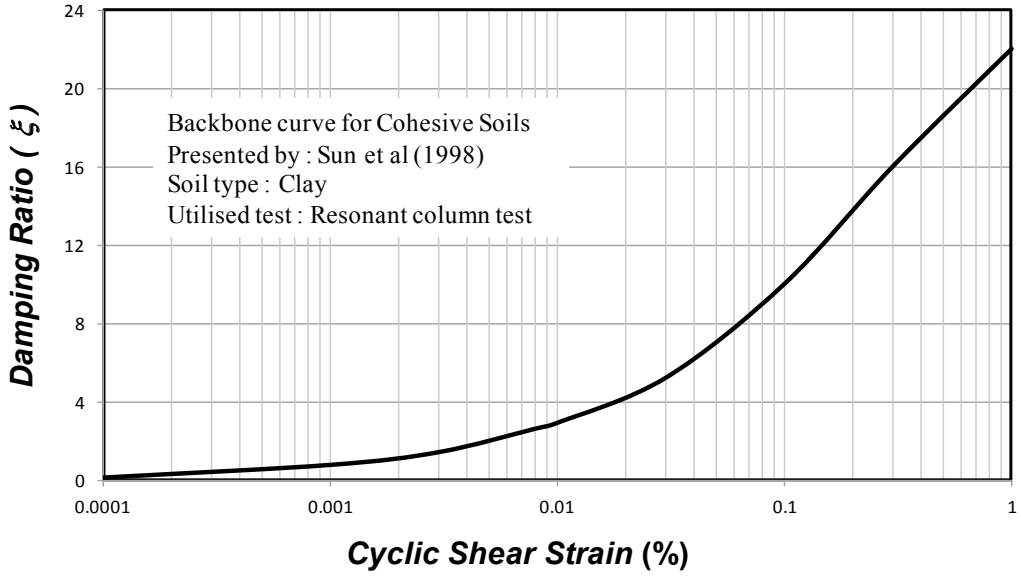


**Figure 2.9** Relations between damping versus cyclic shear strain for cohesive soils (after Sun et al., 1988)

Vucetic and Dobry (1991) conducted a study on number of available cyclic loading results and concluded that the soil Plasticity Index (*PI*) controls the location of the backbone curves for a wide variety of cohesive soils. It should be noted that Sun et al. (1988) backbone curves, employed in this study, take into account the effects of soil plasticity in an average sense, covering common range of soil plasticity indices for cohesive soils.

## 2.4.2 Backbone Curves for Cohesionless Soils

Studies carried out by Hardin and Drnevich (1972) and Seed and Idriss (1969) have shown that while factors such as grain size distribution, degree of saturation, void ratio, lateral earth pressure coefficient, angle of internal friction, and number of stress cycles may have minor effects on the damping ratios of sandy and gravely soils, the main factors affecting the damping ratio are the strain level induced in the soil and the soil effective confining pressure. Seed et al. (1986) represented backbone curves for a wide variety of cohesionless soils as illustrated in Figures 2.10 and 2.11, ignoring the influence of confining pressure for simplicity. Seed et al. (1986) concluded that damping ratio for gravel is very similar to damping ratio for sand. However, the variation pattern of shear modulus ratio with shear strain shown in Figure 2.10 is

generally representative of most sands, but the curve for gravel is a little flatter than the curve for sand.

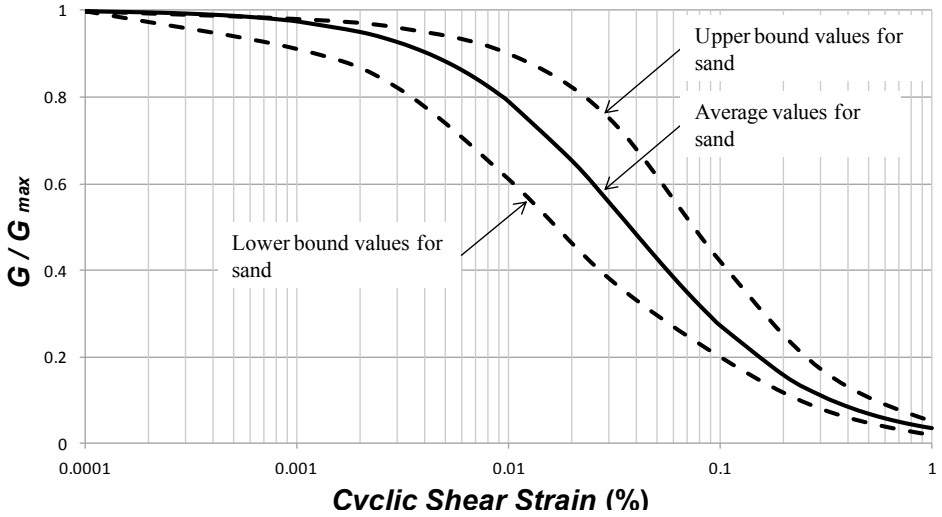


**Figure 2.10** Relations between $G/G_{max}$ and cyclic shear strain for cohesionless soils (After Seed et al., 1986)

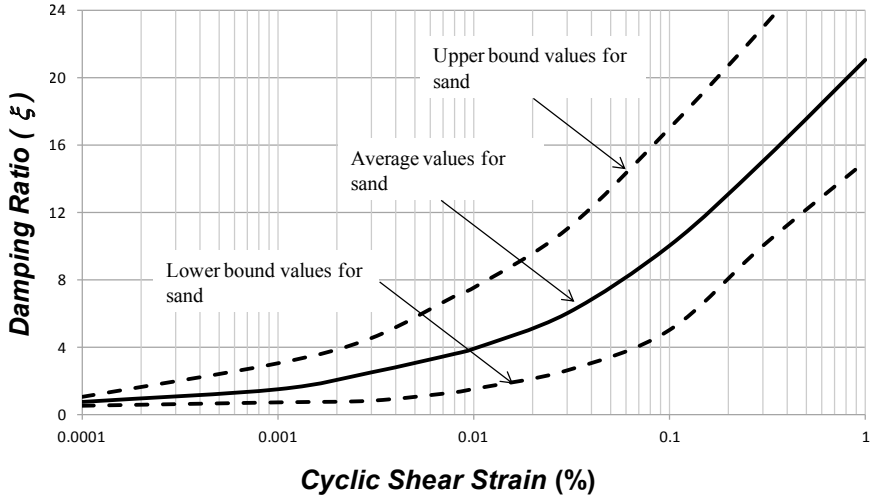


**Figure 2.11** Relations between damping ratio and cyclic shear strain for cohesionless soils (After Seed et al., 1986)

## 2.5 Lessons Learned from Previous Earthquakes

Invaluable knowledge and experience is derived from the study of past earthquakes, either from the effects of particular earthquakes, or the cumulative effects. Especially for engineers, this can answer the question "what happened that was expected, and what was not expected?" in order to get better understating of the phenomena and to improve the design and construction techniques.

During the past earthquakes, several buildings supported by pile foundations were damaged or collapsed. In this section, observations from a number of earthquakes are presented in order to illustrate the behaviour of pile foundations and highlight the importance of SSPSI on the seismic response of superstructures.

### 2.5.1 1985 Mexico City Earthquake, Mexico

The 1985 Mexico City Earthquake with the magnitude of 8.1 occurred with the epicentre being approximately 400 km away from Mexico City, but a convergence of site response factors resulted in huge damage on the Lake Zone of Mexico City. The seismic waves effectively filtered to long period motion in travelling from the epicentre to the Mexico City region. In the Lake Zone due to the existing deep soft clay deposit, the intensity of the shaking greatly amplified with a resulting period of approximately two second. This long period motion induced resonance for many structures of intermediate height, resulting in a damage pattern closely focused on these long period structures. Among them, buildings supported by frictional (floating) pile foundations experienced the most damage (Meymand, 1998; Nghiem, 2009).

Both frictional and end-bearing pile foundations are employed in this area. Considering the high compressibility of Mexico City clays, the key concerns for the foundation design are to limit the settlement and accommodate the negative skin friction on deep foundations. As mentioned by Nghiem (2009), many light to medium weight structures were supported by frictional pile foundations, while the end-bearing pile foundations are utilized for the heavy structures founded on sand layer with a depth up to 38 meters.

Girault (1986) reported 25 buildings on mat foundations supported by frictional piles that experienced large settlement and tilting. These settlements were occurred mainly because of the reduction in the negative skin friction on the piles due to the partial loss of the shear strength of the soil during the cyclic loading. Mendoza and Romo (1989) explained that low factor of safety against bearing capacity and a soil-pile stress state close to yielding with respect to static loading, precipitated foundation failure under seismic loads. Tilting and overturning moments due to cyclic rocking may have been exacerbated by p-$\Delta$ effects. Figure 2.12 illustrates a case of entirely

overturned ten storey building, as one corner sank 6 meters into the soil and the opposite corner rose 3 meters out of the soil, pulling piles out of the ground.

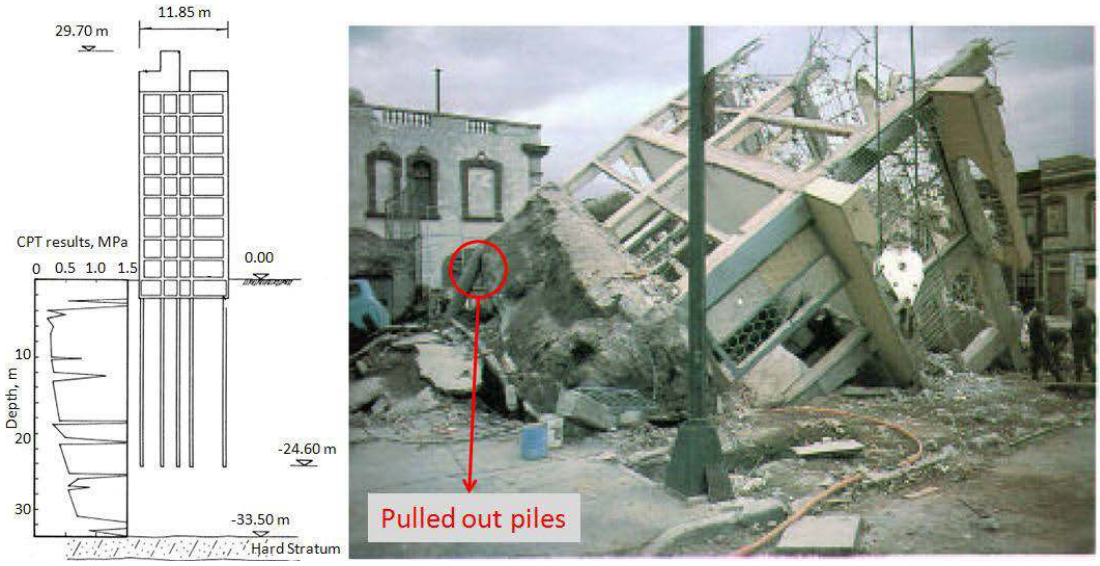


**Figure 2.12** Ten storey building supported by pile foundation on soft soils during the 1985 Mexico City Earthquake; (a) geotechnical conditions of the site (modified after Meymand, 1998); (b) overturned structure (modified after Mendoza and Romo, 1989)

During the 1985 Mexico City earthquake, structures supported by the end-bearing pile foundations had a better performance during earthquake excitation in comparison to the structures sitting on the frictional pile foundations, with smaller settlements and minor failures. Meymand (1998) pointed out that the seismic overturning moments were the main causes of the failure of the pile foundations, although perhaps some cyclic strength degradation contributed to the partial loss of the soil-pile adhesion.

The observations from 1985 Mexico City earthquake are extremely important in terms of the seismic soil-pile-structure interaction. Existing deep soft clay lengthened the period of the ground motion due to the site effect as described in Section 2.1. In the same time, the soil-pile-structure interaction increased the natural period of the system referred to in Section 2.2. Therefore, the long period ground motion came into a resonance with the modified natural period of the system, and as a result significant amount of damage occurred. In addition, SSPSI increases the deflection, referring to Section 2.2, and in turn influences the overall stability of the structure during the

earthquake. Since the seismic overturning moment was pointed out as the main cause of the structural failure during the mentioned earthquake, the importance of considering the effect of SSPSI on the seismic behaviour of structures is clearly highlighted.

### 2.5.2 1995 Kobe Earthquake, Japan

The 1995 Kobe earthquake with the magnitude of 7.2 and depth of 20 km was one of the most destructive earthquakes hit Japan ever. Figure 2.13a shows a collapse of an elevated section of the pile-supported Hanshin Expressway which was one of the most dramatic structural failures during 1995 Kobe earthquake. Gazateas and Mylonakis (1998) present an analysis suggesting that period lengthening due to foundation flexibility may have resulted in the increased structural forces during the earthquake. Figure 2.13b illustrates the ground response spectra due to 1995 Kobe earthquake on three earthquake recording stations.

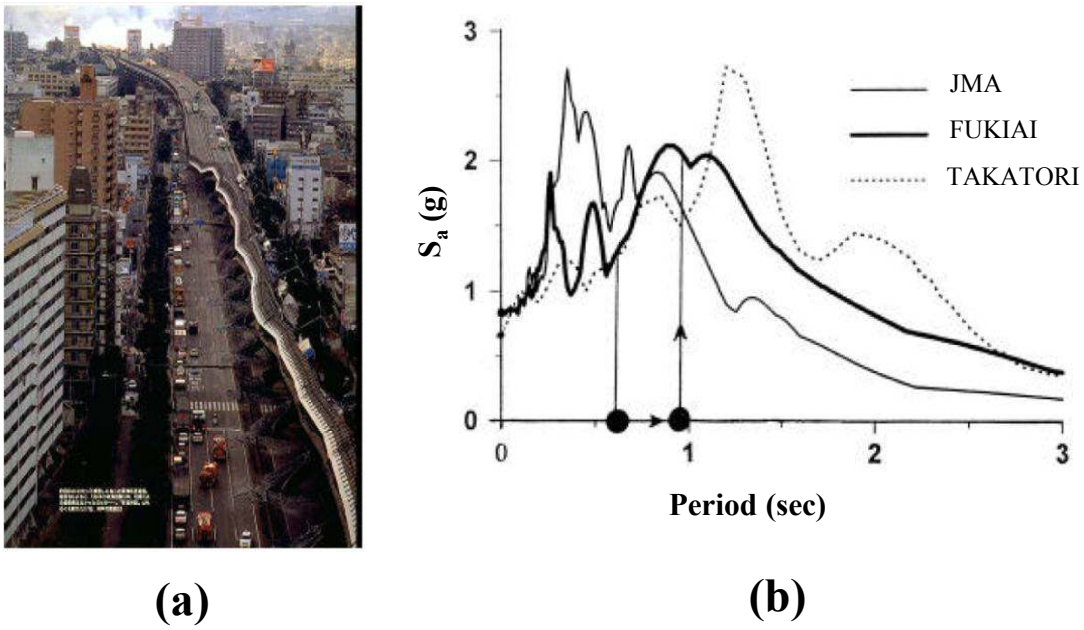


**Figure 2.13** (a) Collapse of Hanshin Expressway during 1995 Kobe earthquake; (b) recorded response spectrum during 1995 Kobe earthquake (After Gazetas & Mylonakis, 1998)

At the site next to the Takatori earthquake recording station (Figure 2.13b), three twelve-storey buildings supported by pile foundations suffered shear and compressive failure (probably due to rocking) near the pile head, and the structures had to be demolished. Mizuno et al. (1996) mentioned that no evidence of liquefaction was noted,

and the damages were attributed to the inertial forces from superstructures. In addition, Hayashi and Takahashi (2004) by studying the soil-structure interaction effect on the structural response during recent earthquakes observed the uplift of the base mat and the separation between the foundation and soil due to the rocking of the superstructure.

### 2.5.3 Recent Earthquakes and Observations

2010 Chile Earthquake with the magnitude of 8.8 was the sixth largest earthquake ever to be recorded by seismographs. Gibson (2010) observed that the majority of buildings performed well, but widespread damage to non-structural elements such as partition walls and building services highlights serious vulnerability that is common elsewhere. The long period and long duration of shaking affected taller buildings more than smaller buildings such as houses, and strong amplification of shaking in the areas with soft soils caused more severe damage to structures and buried services. Moreover, based on the lessons learned from the Chile Earthquake, Bonelli et al. (2012) suggested changes to the design codes emphasising on the importance of considering the soil-structure interaction phenomena.

Lo and Wang (2012) had a comprehensive investigation on the geotechnical aspects of the six recent earthquakes (2005 Sumatra earthquake, Indonesia; 2008 Wenchuan earthquake, China; 2010 Haiti earthquake, Haiti; 2010 Maule earthquake, Chile; 2011 Christchurch earthquake, New Zealand; and, 2011 Tohoku-Oki earthquake, Japan). Accordingly, in areas where earthquake-resistant design codes and engineering practices are kept up-to-date, damage tends to be limited to older and inadequately designed structures or areas with special site conditions, highlighting the impact of the ground condition and the seismic soil-structure interaction on the seismic performance of buildings.

Stewart et al. (1999b) conduct a comprehensive investigation on the effect of SSI on buildings response under strong earthquake motion records at 58 sites, which 34 of them consisted of pile-supported structures. Almost all of the buildings under study experienced the influence of SSPSI to some extent that manifested as period lengthening, increased damping, and spectral deamplification of the pile cap motion relative to the free field ground motion.

As reported by Meymand (1998), according to the observed seismic performance of piles during earthquakes, following points can be mentioned:

- From the instrumented cases, it is observed that SSPSI often results in spectral de-amplification of pile cap motions relative to the free-field motion.
- Soil modulus degradation and soil-pile gapping can inhibit radiation damping, especially at the high level of shaking, which in turn dominates the structure inertial forces reducing the overall effects of the spectral deamplification.
- Strain softening of cohesive soils or liquefaction of cohesionless soils near the pile head results in the loss of bearing capacity. The combination of this effect with the induced rocking mode in the superstructure results in the pile group settlement, punching failure, and/or tensile pull-out failure.

Consequently, as concluded by Nghiem (2009), design of buildings might be inadequate if SSPSI is ignored, and the consideration of SSPSI affects the interpretation of damage as well as altering the design criteria and building specifications.

## 2.6 Modelling Techniques to Simulate SSPSI

Over the past decades, several researchers have studied the seismic soil-pile-structure interaction (SSPSI) phenomenon and its influence on the response of various structures. The developed analytical methods for studying the soil-pile-structure interaction may be categorised into three groups: (1) Beam on Elastic Foundation Methods (or Winkler methods); (2) Elastic Continuum Methods; and (3) Numerical Methods, which are explained below.

### 2.6.1 Beam-on-Elastic Foundation Methods (Winkler methods)

The Winkler's theory assumes that each layer of soil responds independently to the adjacent layers in which series of springs and dashpots are employed to represent the soil behaviour. Figure 2.14 shows the components of beam-on-elastic-foundation method for a single pile. The governing equation for beam-on-elastic-foundation solutions (or subgrade reaction method) was originally provided by Hetenyi (1946) as follows:

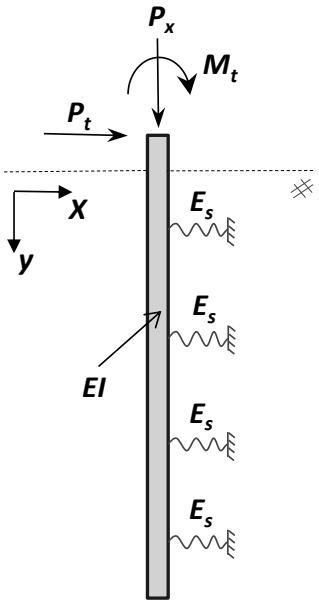


**Figure 2.14** Modelling a single pile using Beam on elastic foundation method

$$EI\left(\frac{d^4y}{dx^4}\right)+P_x\left(\frac{d^2y}{dx^2}\right)+E_s(y)=0 \tag{3.1}$$

where, $EI$ is the bending stiffness of pile, $P_x$ is the axial load on the pile, $y$ is the lateral deflection of the pile at point $x$ along the length of the pile, and $E_s$ is the soil subgrade reaction (the spring's stiffness). A generalised iterative solution method for Equation (3.1) was proposed by Matlock and Reese (1960) for rigid and flexible laterally loaded piles using finite difference method.

Linear or nonlinear soil-pile springs can be employed. p-y curves can be used to model nonlinear soil-pile stiffness, and they have semi-empirical basis typically derived from field tests, so they can implicitly include pile installation effects on the surrounding soil. In more complex models, soil-pile gapping, cyclic degradation, and rate dependency can be captured adopting modified Winkler method (Allotey and El Naggar, 2008; Gazetas and Apostolou, 2004). Malhotra (2010) presented a discussion on the available models and modifications to p-y relationships used to model soil response under seismic conditions.

Allotey and El Naggar (2008) pointed out that the main drawback of Winkler method is idealisation of the soil continuum with discrete soil reactions. In other words, as described by Finn (2005), the shear transfer between the springs is one of the obvious missing fundamental mechanisms in Winkler models. In order to overcome the main

drawback of these methods, Strain Wedge Model (SWM) which creates relationship between the three-dimensional responses of soil-pile to the beam on elastic foundation parameters are suggested for static cases (Ashour et al., 1998), and there have been some developments to consider seismic loads in this method (Hokmabadi et al., 2011), which cannot consider the dynamic behaviour of the soil, precisely.

Mostafa and El Naggar (2002) developed the state-of-the-art modelling techniques based on the subgrade reaction methods as shown in Figure 2.15. In this model, the pile and the soil along the pile shaft are divided into a number of layers, with different soil properties according to the soil profile at each layer. Within each layer, the soil medium is divided into two annular regions (Figure 2.15) including the inner zone adjacent to the pile that accounts for the soil nonlinearity and an outer zone that allows for wave propagation away from the pile and the radiation damping in the soil medium. The soil reactions at both sides of the pile are modelled separately to account for the state of the stress and discontinuity conditions such as slippage and gapping at both sides as the load direction changes. The mass of the inner zone is lumped into two halves, $m_1$ at the node adjacent to the pile and $m_2$ at the node adjacent to the outer field as shown in Figure 2.15.

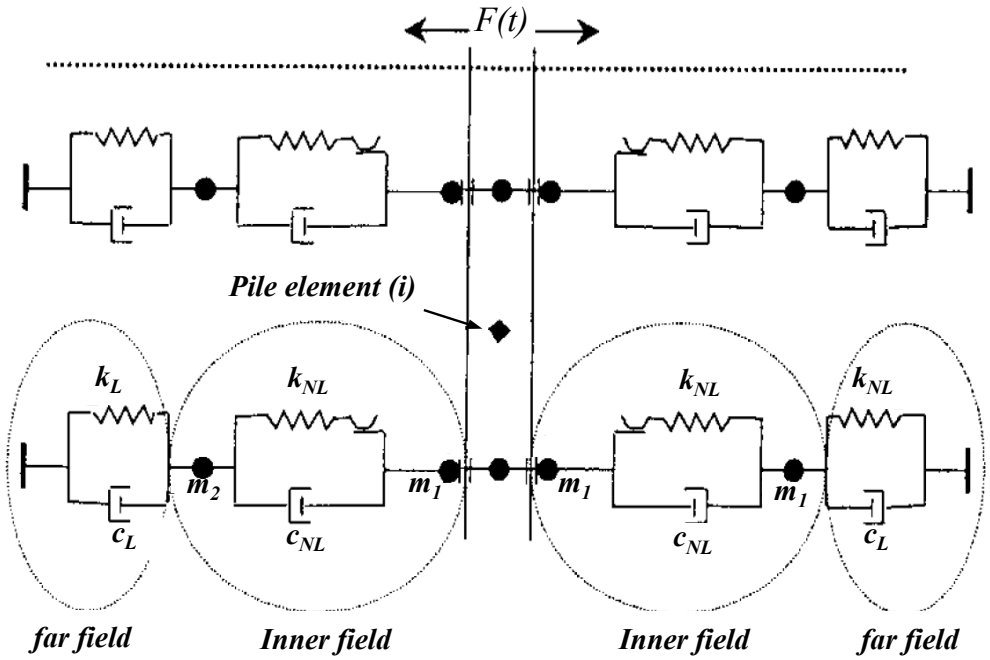


*Where,*
*$K_L$: stiffness of the outer zone,* *$K_{NL}$: stiffness of the inner zone,*
*$C_L$: damping coefficient of the outer zone,* *$C_{NL}$: damping coefficient of the inner zone.*

**Figure 2.15** An element representation of the proposed model based on the subgrade reaction methods to simulate SSPSI (after Mostafa and El Naggar, 2002)

For the cases subjected to the seismic loadings, "free-field" ground motions are usually computed, and then externally applied to the soil-pile springs (Mostafa and El Naggar, 2002). Meymand (1998) mentioned that the multi-step uncoupled approach has the disadvantage of potentially introducing numerical errors in the integration step, and artificially separating the overall soil-pile system response. Winkler methods are attractive to many structural design engineers among other methods due to their simplicity. However, these methods do not account for coupled behaviour of SSPSI and are not able to capture the main aspects of the soil nonlinear cyclic behaviour.

## 2.6.2 Elastic Continuum Methods

The elastic continuum analytical methods are based on Mindlin (1936) closed form solution for the application of point loads to a semi-infinite elastic medium. The accuracy of these solutions depends on the evaluation of soil elastic parameters. In this

approach, it is difficult to incorporate the soil nonlinearity directly, and it is more appropriate to be adopted for small strain and steady state problems.

Tajimi (1969) was the first person who used elastic continuum theory to describe a dynamic soil-pile interaction. Poulos (Poulos, 1971; Poulos and Davis, 1980) have been a major progenitor of using elastic solutions for pile foundation response to axial and lateral loads, and presented a comprehensive set of analysis and design methods for pile foundations based on elastic continuum theory. Gazetas (1991) made a complete survey of foundation vibration problems and included detailed design charts and impedance functions for direct computation of pile head lateral and axial stiffness and damping coefficients representing the soil profile.

### 2.6.3 Numerical Methods

The extensive ability of powerful computers has significantly changed computational aspects making them more popular to study the complex and complicated interactive behaviours. With exploiting these methods, it is possible to conduct the time-history analysis considering various effects such as nonlinear stress-strain behaviour of the soil and superstructure, material and radiation damping, advanced boundary conditions and interface elements. Another advantage of employing numerical methods is the capability of performing the SSPSI analysis on pile groups in a fully-coupled manner, without resorting to independent calculations of site and superstructure response, or application of pile group interaction factors (Meymand, 1998).

Most of the numerical methods such as finite element method (FEM) or finite difference method (FDM) employ extended form of matrix analysis based on variational approach, where the whole perpetual is divided into a finite number of elements connected at different nodal points. Finite element programs often combine the element matrices into a large global stiffness matrix, while this is not usually done with finite difference because it is relatively more efficient to regenerate the finite difference equations at each step. The general principles and applications of finite element and finite difference methods were well documented and explained by Desai and Abel (1972).

Both FDM and FEM methods produce a set of algebraic equations which may be identical for the two methods to be solved. According to Cundall (1976), it is pointless to argue about the relative merits of finite element or finite difference approaches as the resulting equations are the same.

Another well-known numerical method is boundary element method (BEM) which is based on boundary integral equations which presents an attractive computational framework especially for problems involving singularity and unbounded domains. A detailed literature on the formulation of the method and its applications in different fields is addressed in the book by Brebbia et al. (1984). The basic idea of this method is to formulate the equation of motion of the unbounded domain in the form of an integral equation instead of a differential equation. Finally, this integral equation is solved numerically. Katsikadelis (2002) indicated that boundary element method has been applied in various areas of engineering and science. However, for many complex problems boundary element method is significantly less efficient than finite element and finite difference methods.

Gutierrez and Chopra (1978) pointed out that numerical methods are the most appropriate and accurate methods for the soil-structure interaction analysis. Dutta and Roy (2002), after conducting a comprehensive critical review on idealisation and modelling of the soil medium for the dynamic soil-structure interaction problems, concluded that modelling the system through discretisation into a number of elements and assembling the same using the concept of numerical methods have proved to be very useful method, which is recommended to be employed for studying the effects of the soil-structure interaction. In addition, Stewart (1997) emphasised that although simplified models can provide indicative trends of the contribution to lateral and rocking stiffness and radiation made by the piles, more sophisticated models are appropriate to study the SSPSI problem.

According to Bowles (2001) and Dutta and Roy (2002), numerical techniques can incorporate the effects of material nonlinearity (nonlinear stress-strain behaviour), heterogeneous material conditions, stress anisotropy, material and radiation damping as well as changes in geometry of the supporting soil medium in the dynamic soil-structure interaction analysis, due to the case specific nature of any particular problem. Thus, considering the mentioned merits of using numerical methods for the dynamic analysis

of soil-structure systems over the other mentioned approaches, and in order to attain rigorous and realistic results, finite deference method is adopted in this study for seismic analysis of the soil-structure interaction.

Available modelling techniques for SSPSI analysis are conceptually following two scenarios including (*I*) Substructure method and (*II*) Direct method, which are described below:

*I) Substructure method;* in this method the soil-pile-structure system is partitioned into near-field and far-field cases. The near-field case simulates the soil-pile-structure interaction, while the far-field accounts for semi-infinite nature of the soil medium for the site response analysis. As reported by Kramer (1996), the superposition inherent to this approach requires an assumption of linear soil and structural behaviour. Figure 2.16 shows three main steps of substructure method as described below:

- *First step:* evaluation of a Foundation Input Motion (FIM), which is the motion that would occur on the base-slab if the structure and foundation had no mass.
- *Second step:* determination of the impedance function. The impedance function describes the stiffness and damping characteristics of the foundation-soil system.
- *Third step:* dynamic analysis of the structure supported on a compliant base represented by the impedance functions and subjected to a base excitation consisting of the FIM.

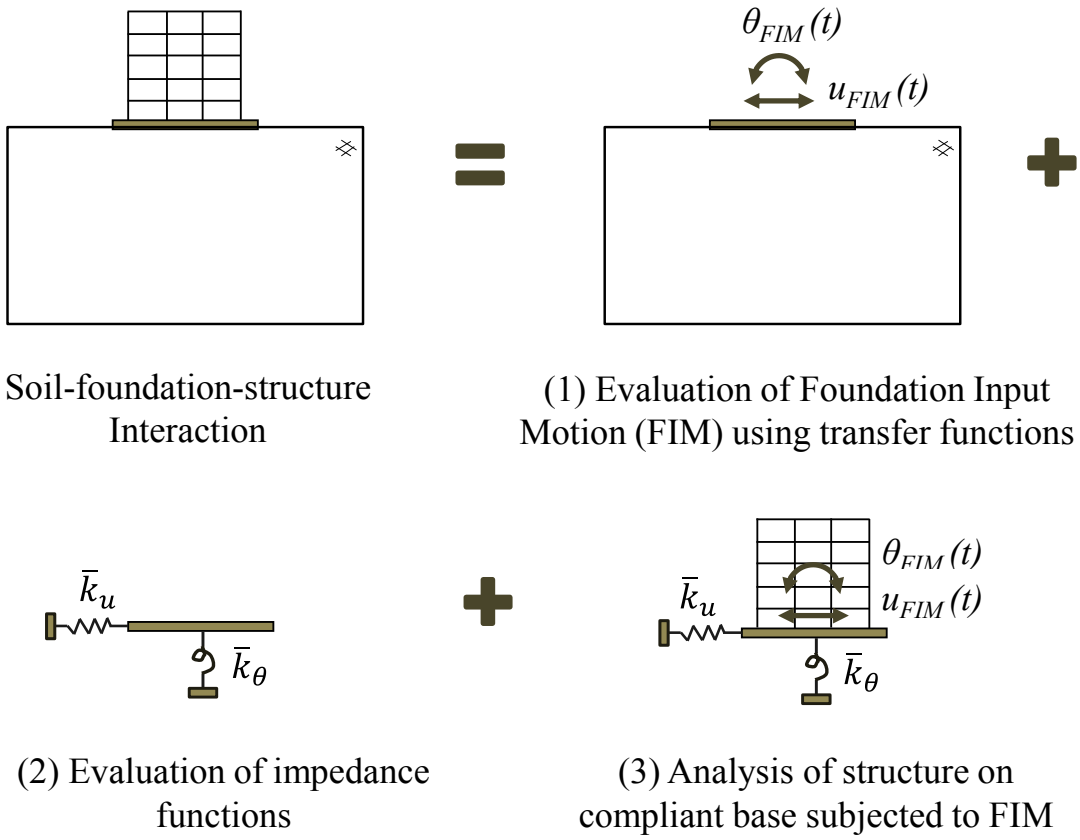


**Figure 2.16** Components of Soil-structure Interaction problem used in Substructure approach

Numerous numerical studies (e.g. Kutanis and Elmas, 2001; Carbonari et al., 2011; Allotey and El Naggar, 2008) have been carried out adopting substructure method in assessing the seismic response of structural systems considering the soil-structure interaction. Gutierrez and Chopra (1978) reported that the principle advantage of the substructure approach is its flexibility. As each step is independent of the others, the analyst can focus resources on the most significant aspects of the problem. According to Wolf (1998), as the method is based on the superposition principle, which is valid only for linear soil and structure behaviour, approximations of the soil nonlinearity by means of iterative wave propagation analyses, may allow the superposition to be applied for moderately-nonlinear systems. Therefore, taking into account the exact nonlinearity of the subsoil in the dynamic analysis may not be easily achievable using this technique. Kutanis and Elmas (2001) noted that much has to be done in investigating the performance of the model and the numerical procedures of substructure method as well as the various factors influencing the response of a soil-structure system.

*II) Direct method;* in this method, entire soil-pile-structure is modelled at the same time and the input motions are specified along the base of the model. Typically, the soil is discretised with solid finite elements while the pile and structure are represented with finite beam elements. Several researchers (e.g. Carbonari et al., 2011; Hayashi and Takahashi, 2004; Chu and Truman, 2004) have studied the seismic response of soil-pile-structure systems adopting the direct method for modelling the soil-structure interaction to achieve accurate and realistic analysis outcomes.

Carr (2008) believes that the advantage of direct method in fact is its versatility to deal with complex geometries and material properties. However, data preparation and complexity of the modelling make it difficult to implement direct method in every-day engineering practice. In addition, more advanced computer programs are required in this method. Since the assumption of superposition is not required, true and accurate nonlinear analyses are possible in this case as mentioned by Borja et al. (1994). Therefore, direct method, which is more capable in modelling the complex nature of the soil-structure interaction in dynamic analysis, is employed in this study.

## 2.7 Effects of SSPSI on Behaviour of Buildings

Ukaja (1975) studied the soil-structure interaction during earthquakes. He developed a coupled two-dimensional model for the soil-structure system employing finite element method to investigate the effects of parameters such as the soil stiffness, soil depth, and building characteristics on SSI, while a linear soil behaviour was assumed. Considering 30 meters of soil depth and 10 meters of foundation embedment, the base shear values were reduced about 30 and 50 percent for the soil damping ratio of 0.33 and 0.11, respectively. Ukaja (1975) reported that the maximum base shear amplification factor coincides with the conditions that natural period ratio of the building to the soil is unity ($\frac{T_{building}}{T_{soil}} = 1$). In addition, soil depth has a similar effect as the soil stiffness, affecting the change in the ratio of the natural period. Ukaja (1975) emphasised the significant effect of the soil stress-strain behaviour on the dynamic response of the system.

Han and Cathrio (1997) analysed a 20-storey building supported by a pile foundation. The building was modelled as a shear frame with additional two degrees of

freedom to consider horizontal and rotational movements of the foundation. By using substructure method, the stiffness and the damping constant of the pile foundations were defined separately and then introduced in the governing equations of the system. Two arrangements of pile foundations were utilised for the building including 5×5 piles and 4×4 piles. The piles were driven pre-cast concrete with 40 cm diameter and 24 meter depth in conjunction with 1.2 m thick reinforced concrete block cap. After performing a time-history analysis, following points were concluded by Han and Cathro (1997):

- The seismic behaviour of the tall building supported on the pile foundation is different from that on the rigid base or the shallow foundation. Comparatively, shallow foundations usually induce higher natural periods and much larger displacements.
- Inclusion of nonlinear response of pile foundation reduces the natural frequencies of the building and increases the displacements in comparison with the linear case.
- The soil nonlinearity and soil-pile-structure interaction are two important factors influencing the seismic response of tall buildings.
- In order to conduct a safe and economic design, a reasonable seismic response analysis of tall buildings considering SSPSI is required.

Shiming and Gang (1998a) conducted three-dimensional linear SSPSI analysis employing substructure model (impedance functions) and finite element method for calculation. Two types of structures (moment resisting frame and frame-shear wall) with 12-storey height in conjunction with two types of foundations (with or without pile) were analysed and compared. The analysis used El Centro and Taft earthquakes with adjustment of the maximum acceleration to 0.35g. By comparing the results, some conclusions were drawn as follows:

- Natural frequencies of the structure with interaction are greater than that of without interaction, related to varying soil properties, structural stiffness, and foundation type (with or without pile).
- The structure with the pile foundation experienced less increase in the natural period in comparison to the structure on the shallow foundation.

- The effect of the SSPSI on the response of the structure (base shear and deflection) is affected by the characteristics of the input seismic motion.

Inaba et al. (2000) modelled the real structure and subsoil during 1995 Kobe earthquake with eight floors above and three floors under the ground employing two dimensional FEM. From the results of the analyses, it was concluded that SSI had a significant effect on the seismic response of the building. Chu and Truman (2004) studied the effects of pile foundation configurations on the seismic soil-pile-structure interaction using a three-dimensional finite element model of a soil-pile-foundation system in the time domain to provide a method for assessing the seismic performance of soil-pile systems with different pile foundation configurations. This work investigated a 2×2 and a 3×3 end-bearing pile foundation system with different soil properties and pile spacing ratios as shown in Figure 2.17. They concluded that although largely spaced pile groups have slightly larger pile head responses than closely spaced pile groups, the general effects of the pile spacing ratio on the seismic responses of the soil-pile systems are insignificant. In addition, this research pointed out that the effects of number of piles on the pile head acceleration are insignificant, while the effects on the pile head displacement are considerable for the studied cases. Chu and Truman (2004) suggested more detailed research on the effects of the pile foundation configuration on the seismic soil-pile-structure interaction.

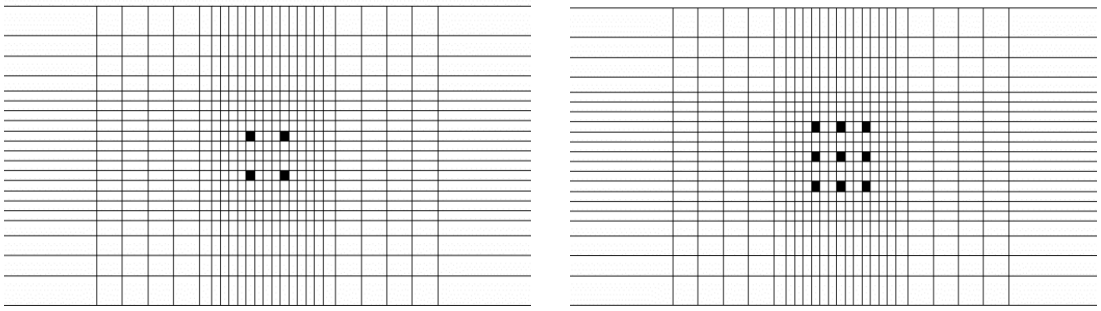


**Figure 2.17** Employed pile foundation configurations to study the seismic soil-pile-structure interaction by Chu and Truman (2004): (a) 2×2 end-bearing pile foundation; (b) 3×3 end-bearing pile foundation

Hayashi and Takahashi (2004) surveyed the effects of the base mat uplift and separation between the ground exterior wall and the soil around, on a 9-story building under 1995 Kobe earthquake using two-dimensional FEM. The building is modelled

adopting linear elements and its underground stiffness is assumed to be rigid as shown in Figure 2.18. Equivalent linear behaviour for the subsoil is adopted during the analysis and viscous boundaries are modelled to absorb outgoing waves. It was concluded that the maximum lateral force coefficient of the model with uplift is about half of that without uplift. Consequently, as pointed out by Nghiem (2009), the uplift effects result in reduced structural damages for slender buildings.

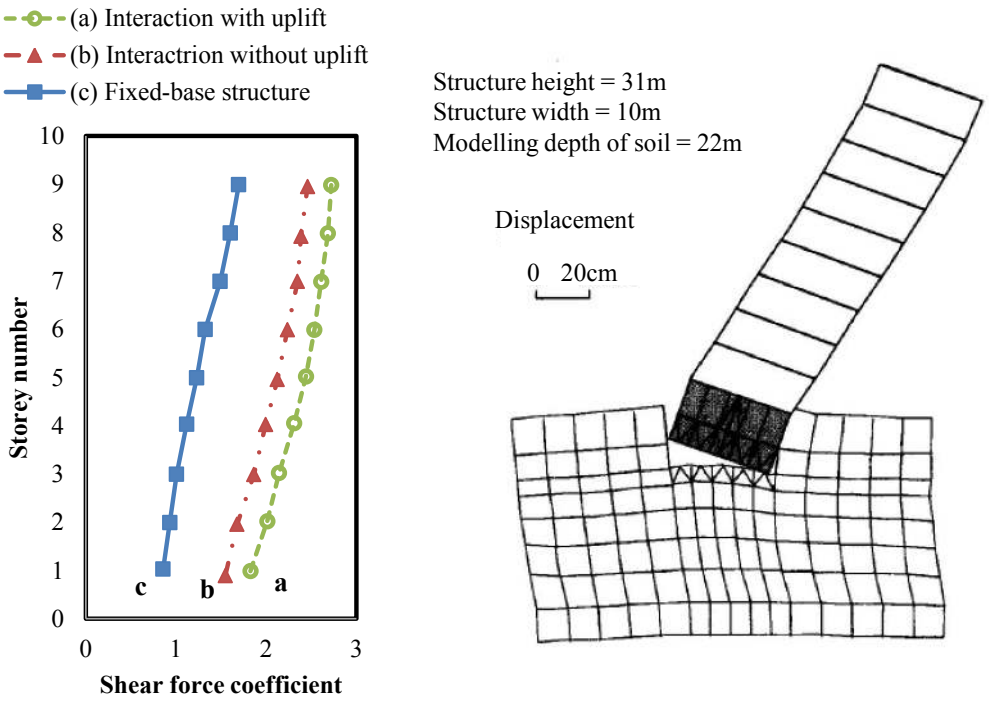


**Figure 2.18** (a) Maximum response value of shear force for structure with and without uplift; (b) developed two-dimensional FEM (after Hayashi and Takahashi, 2004)

Carbonari et al. (2011) studied the linear soil–structure interaction of coupled wall–frame structures on pile foundations. A linear finite element procedure for a complete dynamic interaction analysis was developed in the frequency domain accounting for the soil–pile interaction and radiation damping. Three different soil profiles were considered together with real earthquake records as input motions. The calculated results, expressed in terms of the response parameters most significant for the description of damage (e.g. deflections, inter-storey drifts, accelerations and stress resultants), were compared with those obtained from a conventional fixed-base model. Applications demonstrated that performing complete soil–structure interaction analyses may be crucial for the reliable evaluation of the behaviour of such systems.

Consequently, previous researchers have emphasised the significance of SSPSI on the response of superstructures and clarified some aspects of it. Some of the previous investigations used substructure model (or impedance functions) to represent the soil behaviour. It means that they treated the soil and structure separately, thus the models were not able to capture the coupled behaviour of SSPSI. The other group of researchers, modelled all relevant components such as soil, pile, and superstructure simultaneously, but they assumed a linear or an equivalent linear behaviour for the subsoil and linear behaviour for the superstructure without accounting for the full nonlinear coupled behaviour of both soil and structural elements.

In addition, based on the literature review, following parameters influence the structural response when SSPSI is considered:

- Building characteristics such as the height and the natural frequency,
- Soil properties including the dynamic stiffness, damping ratio, and the thickness of the soil,
- Pile group configuration and the nonlinear interaction between piles and the soil,
- Type of the foundation such as shallow, pile, or raft-pile foundations, and
- Characteristics of the input motion (earthquake type).

## 2.8 Building Codes Concerning Seismic Soil-Structure Interaction

Building codes, as mentioned by Lo and Wang (2012), are living documents, periodically reviewed and updated to reflect current understanding of the local site seismicity, structural earthquake performance and latest analysis and design technologies. In this section, a number of building codes recommendations for considering the effects of the soil-structure interaction are reviewed and summarised. Rayhani (2007) concluded that although a number of design codes incorporate simplified soil-structure interaction analysis methods, they acknowledge the need for site specific studies for structures on soft soils subjected to strong ground shakings. The effect of the soil-structure interaction is usually taken into account by modifying the dynamic properties of the structure on the fundamental mode of vibration. In addition,

the influence of the kinematic interaction is assumed to be beneficial to the structure and is usually neglected in the building codes resulting in taking the building foundation excitation equal to the free field ground motion. In this study, ASCE, NEHRP, New Zealand, and Australian codes are reviewed.

### 2.8.1 American Society of Civil Engineers (ASCE 7-10)

ASCE code entitled "*Minimum Design Loads for Buildings and Other Structures*" (ASCE7-10, 2010) in chapter nineteen denotes that if the option to incorporate the effects of the soil-structure interaction is exercised, the following method is permitted to be used in the determination of the design earthquake forces and the corresponding displacements of the structure in the case that the model used for structural response analysis does not directly incorporate the effects of the foundation flexibility.

The code accounts for decreasing the base shear due to the soil-structure interaction corresponding to the fundamental (first) mode of vibration, by using the following equation:

$$\tilde{V} = V - \Delta V \tag{3.1}$$

$$\Delta V = \left[C_s - \widetilde{C_s}\left(\frac{0.05}{\tilde{\xi}}\right)^{0.4}\right]\overline{\mathrm{W}} < 0.3\,V \tag{3.2}$$

where, $\tilde{V}$ is the modified base shear, $V$ is the base shear of the fixed-base structure, $\Delta V$ is the decrease in the base shear due to the soil-structure interaction, $C_s$ is the seismic design coefficient computed based on the fundamental natural period of the fixed-base structure ($T$), $\widetilde{C_s}$ is the seismic design coefficient computed based on the fundamental natural period of the flexible-based structure ($\tilde{T}$), $\tilde{\xi}$ is the fraction of critical damping for the structure-foundation system, and $\overline{W}$ is the effective seismic weight of the structure.

In order to calculate the modified period and damping ratio of the structure due to the soil-structure interaction, ASCE code employs a spring-dashpot model with SDOF structure similar to what has been illustrated in Figure 2.3. The modified period of the structure is evaluated from Equation (3.3) which clearly emphases on the increase in the natural period of the system due to the soil-structure interaction.

$$\tilde{T} = T\sqrt{1 + \frac{\bar{k}}{k_y}\left(1 + \frac{k_y \bar{h}^2}{k_\theta}\right)} \tag{3.3}$$

$$\bar{k} = 4\pi^2\left(\frac{\bar{W}}{gT^2}\right) \tag{3.4}$$

where, $\bar{k}$ is the stiffness of the structure fixed at the base, $k_y$ and $k_\theta$ are lateral and rocking stiffnesses of the foundation, respectively, and $g$ is the gravity acceleration. ASCE code does not give any equations to obtain foundation stiffness parameters (i.e. $k_y$ and $k_\theta$), and it simply suggests to use established principles of foundation mechanics and soil properties to calculate the stiffness of the springs representing the foundation dynamic behaviour.

The employed soil dynamic properties including shear stiffness ($G$), and shear wave velocity, ($V_s$) should be compatible with the soil strain levels associated with the design earthquake motion ($S_{DS}$) referring to Table 2.1. $V_{so}$ is the average shear wave velocity for the soil deposit beneath the foundation at small strain levels ($10^{-3}$ percent or less), $G_0$ (= $\gamma V^2_{so}/g$) is the average shear modulus for the soil deposit beneath the foundation at small strain levels, and γ is the average unit weight of the soil deposit. The design earthquake motion is provided in the code, and the site is classified based on the upper 30m of the site profile with respect to the soil properties such as the shear wave velocity.

**Table 2.1** Values of $G/G_0$ and $V_s/V_{so}$ considering strain compatibility (ASCE7-10, 2010)

| | Value of $V_s/V_{so}$ | | | Value of $G/G_0$ | | |
|---|---|---|---|---|---|---|
| | $S_{DS}/2.5$ | | | $S_{DS}/2.5$ | | |
| Site Class | ≤0.1 | 0.4 | ≥0.8 | ≤0.1 | 0.4 | ≥0.8 |
| A | 1.00 | 1.00 | 1.00 | 1.00 | 1.00 | 1.00 |
| B | 1.00 | 0.97 | 0.95 | 1.00 | 0.95 | 0.90 |
| C | 0.97 | 0.87 | 0.77 | 0.95 | 0.75 | 0.60 |
| D | 0.95 | 0.71 | 0.32 | 0.90 | 0.50 | 0.10 |
| E | 0.77 | 0.22 | a | 0.60 | 0.05 | a |
| F | a | a | a | a | a | a |

Note. Use straight-line interpolation for intermediate values of $S_{DS}/2.5$
[a] should be evaluated from site specific analysis

In addition, the modified deflection ($\tilde{\delta}_x$ ) shall be determined as follows:

$$\tilde{\delta}_x = \frac{\tilde{V}}{V}\left[\frac{M_0 h_x}{K_\theta} + \delta_x\right] \quad (3.5)$$

where, $M_0$ is the overturning moment, $h_x$ is the height of the building, and $\delta_x$ is the deflection of the fixed-base structure excluding the soil-structure effect. The code mentions that the modified storey drifts and p-Δ effects shall be evaluated using the modified base shear (Equation 3.1) and the modified deflection as presented in Equation (3.5).

According to Equation (3.5), the soil-structure interaction reduces the structural distortion as a result of reduction in the base shear of the structure ($\frac{\tilde{V}}{V}\delta_x$), while the rocking component ( $\frac{\tilde{V}}{V}\frac{M_0 h_x}{K_\theta}$) is adding up to the total deformation of the structure. Therefore, although the structural demand and in turn distortion of the superstructure reduces, the seismic soil-structure interaction may increase the overall displacement of the superstructure in comparison to the fixed-base condition due to the rotation of the foundation (Guin and Banerjee, 1998).

ASCE7-10 employs a simplified method to account for the soil-structure interaction. This method represent the subsoil by series of springs and dashpots (impedance functions), and the superstructure as SDOF oscillator. Thus, it does not address the coupled behaviour of the soil-structure system. Additionally, linear equivalent behaviour for the subsoil is assumed. In addition, this method does not capture directly any nonlinearity of the soil as it assumes linear behaviour for the soil during the solution process. Strain-dependent modulus and damping functions (Figures 2.9-2.11) are only taken into account in an average sense (Table 2.1), in order to approximate some effects of soil nonlinearity, and for the soft soils (Class F) site specific analysis are required.

The above mentioned process is for shallow foundations and ASCE07-10 does not offer any procedure for pile foundations. The process explained in ASCE 7-10 can also be found in Veletsos (1993) and Stewart et al. (1998). International Building Code (IBC, 2012) refers to the similar procedure to account for the effects of the soil-structure interaction in structural designs.

### 2.8.2 National Earthquake Hazard Reductions Program (NEHRP)

The 1997 edition of NEHRP titled "Recommended Provisions for Seismic Regulations for New Buildings and Other Structures", from Buildings Seismic Safety Council (BSSC, 1997) provides detailed procedure including the impedance functions for incorporating the influence of the soil-structure interaction in the determination of design earthquake forces and lateral deflections of structures. Incorporating these effects has a direct result on reducing the base shear applied to the structure, and consequently the lateral forces and overturning moments, while those effects can either increase or reduce the lateral deflections.

The foundation stiffness factors can be derived from a simple model of a rigid mat bonded to an elastic half space following the method initially developed by Gazetas (1991). The model can take into account foundation shape, embedment, and the condition of the soft soil over the stiff layer. In addition, simplified expressions for the pile axial and rocking stiffness values and the influence of the pile cap on the pile group seismic response are provided by NEHRP (BSSC, 1997). However, the suggested method in NEHRP suffers from the shortcomings corresponding to the application of the substructure method, such as assuming linear behaviour for the soil during the excitation and using general approximation to estimate the material and geometric damping properties for the soil.

Applied Technology Council code, ATC-40 (1996), suggests a similar procedure to account for the effects of the soil-structure interaction. Moreover, simplified recommendations to model the deep foundations are provided. NEHRP from 2003 edition onward, including 2009 version (BSSC, 2009) eliminates the detailed procedure to derive foundation stiffness factors and covers almost the same materials as in ASCE07-10.

### 2.8.3 New Zealand and Australian Codes

New Zealand code (NZS1170.5, 2004) denoted that "Foundation flexibility should be included in the modelling of the structure. Ignoring foundation flexibility will be conservative with respect to strength but non-conservative with respect to

deflection". Also, it is mentioned that foundations including piles and other soil supporting structures should be treated as a part of the overall building structure during the analysis. Although New Zealand code (NZS1170.5, 2004) highlighted the importance of considering the effects of the soil-structure interaction, it does not suggest detailed procedure for considering these effects.

Australian code (AS1170.4, 2007) does not address the soil-structure interaction effects for seismic design of structures explicitly and consequently structural designers are not able to include those important effects in the analysis and design procedure using the mentioned standard. As a result, the seismic design of moment resisting building frames resting on relatively soft grounds employing this standard could not be adequately safe due to amplification of lateral deflections and corresponding inter-storey drifts which can possibly change the performance levels of the buildings.

By reviewing the way building codes treat the effects of the soil-structure interaction on the structural response, building codes can be categorised in three types: (1) codes that provide a simplified linear method together with SDOF structure to account for SSI, (2) codes that appreciate the importance of the soil-structure interaction in analysis and design, but do not provide any practical procedure to consider this phenomenon in the analysis, and (3) codes that do not highlight the importance of SSI on the seismic behaviour of the structures. In particular, the influence of pile elements and the generated soil-pile-structure interaction on the seismic behaviour of structures during the earthquake is the missing part in the most of the building codes, perhaps due to the complexity of the problem.

All the reviewed seismic design codes permit the use of alternate methods of design to those prescribed in their seismic requirements with the approval of regularity agency having due jurisdiction. It seems to be necessary to do further research and update the seismic design procedures to account for the items such as the kinematic interaction, the nonlinear hysteretic behaviour of the soil and the influence of SSI on the higher modes of vibration especially in tall buildings. In addition, the accuracy of simplified linear spring models in chaptering the main aspects of SSI needs to be further validated particularly in the cases that the superstructure sits on soft soils subjected to strong ground motions.

## 2.9 Previous Experimental Investigations on SSPSI

Model tests in geotechnical engineering offer the advantage of simulating complex systems under controlled conditions providing the opportunity of better understanding the fundamental mechanisms of these systems. Such tests are often used as calibration benchmarks for numerical or analytical methods, or to make quantitative predictions of the prototype response (Rayhani et al., 2008). Shaking table test is an experimental technique used in earthquake engineering to simulate ground motions. Since the emergence of shaking table tests in the 1920s, large numbers of earthquake model tests have been performed. Shaking table tests have been considered as 1g modelling, in which the gravity acceleration of the model and prototype are always the same. Shaking table test is relatively cheap and easy to model complex prototypes, although there is a lack of accuracy due to 1g manner (e.g. low confining pressure of model affects test results especially in sandy soils). It should be noted that, in centrifuge tests, by increasing the gravity force via rotating the model, it is possible to accurately model the soil stress-strain condition similar to the prototype. In comparison, as described by Jakrapiyanun (2002), although centrifuge test models the stress-strain conditions accurately, it is difficult to build complex prototypes, and due to small size of the model, fewer instruments can be installed.

The geotechnical models cannot be directly mounted on shake table because of the requirements of confinement. To model the soil in shaking table tests, a container is required to hold the soil in place. In literature, this container is called Soil Container, Soil Tank, or Shear Stack. During the past few decades, several researchers have carried out shaking table tests on soil-structure systems using various types of soil containers and structural models as summarised in Table 2.2.

**Table 2.2** Past performed shaking table tests on soil-structure systems using various types of soil containers

| Container type | References | Comments |
|---|---|---|
| **Rigid** | Gohl and Finn (1987)<br>Yan and Byrne (1989)<br>Valsangkar et al. (1991)<br>Zen et al. (1992)<br>Sato et al. (1995)<br>Bathurst et al. (2007)<br>Ha et al. (2011)<br>Anastasopoulos et al. (2012a) | *Adopted superstructural model*: retaining wall, no superstructure, SDOF (single Degree of Freedom) aluminium structure.<br><br>*Adopted foundation type*: Hollow aluminium tubing, and hollow aluminium piles, aluminium footing<br><br>*Adopted soil type*: Dry Ottawa sand, saturated sand, saturated sand mixed with treated soil, dry Longstone sand |
| **Flexible** | Stanton et al. (1998)<br>Richards et al. (1990)<br>Kanatani et al. (1995)<br>Meymand (1998)<br>Maugeri et al. (2000)<br>Lu et al. (2004)<br>Moss et al. (2010) | *Adopted superstructural model:* SDOF (single Degree of Freedom) steel structure.<br><br>*Adopted foundation type*: Steel piles only, wooden shallow foundation, and aluminium piles<br><br>*Adopted soil type:* Dry sand, saturated sand, and reconstituted clayey soil. |
| **Laminar** | Jafarzadeh and Yanagisawa (1995)<br>Taylor et al. (1995)<br>Ishimura et al. (1992)<br>Taylor (1997)<br>Tao et al. (1998)<br>Endo and Komanobe (1995)<br>Jakrapiyanun (2002)<br>Prasad et al. (2004)<br>Pitilakis et al. (2008)<br>Chau et al. (2009)<br>Tang et al. (2009)<br>Turan et al. (2009)<br>Chen et al. (2010)<br>Lee et al. (2012)<br>Tsukamoto et al. (2012)<br>Massimino and Maugeri (2013) | *Adopted superstructural model:* SDOF (single Degree of Freedom) structure<br><br>*Adopted foundation type*: Steel piles only, concrete piles only, structure on shallow foundation, and structure on concrete piles.<br><br>*Adopted soil type:* Dry sand, moist sand, poorly graded river sand, and saturated sand. |

A number of previous experiments were only performed on the soil inside the container without modelling the structural elements (e.g. Sato et al., 1995; Kanatani et al., 1995; Taylor, 1997; Prasad et al., 2004; Lee et al., 2012) aiming to investigate the dynamic behaviour of the soil under the influence of earthquake loads, while some other tests were undertaken on the soil-foundation system to observe the dynamic interaction of the shallow or the pile foundation with the underlying soil (e.g. Richards et al., 1990; Stanton et al., 1998; Tao et al., 1998). In addition, most of the conducted shaking table tests on the soil-structure systems (e.g. Ishimura et al., 1992; Meymand, 1998; Jakrapiyanun, 2002; Lu et al., 2004; Pitilakis et al., 2008; Chau et al., 2009) simplified the superstructure as a single degree of freedom oscillator in which the behaviour of the soil-structure system may not be completely conforming to reality and the effects of higher modes would not be captured. In this study, unlike the previous efforts, a multi-storey frame for the superstructure is adopted, representing the dynamic properties of the prototype structure such as natural frequency of the first and higher modes, number of stories, and density. As a result, a realistic seismic response of a multi-storey frame could be determined experimentally and compared with the numerical modelling predictions.

Soil containers can be cllasified into three main categorise, namely, rigid, flexible, and laminar containers. Rigid containers are the simplest type consisting of no moving parts. According to Jakrapiyanun (2002), studying earth retaining structures such as retaining walls, bridge abutments, and quay walls seems to be appropriate on rigid wall containers as the soil on one side of the earth retaining structure is lower than the other side. Therefore, the soil on the shallower depth is less restricted. As shown in Figure 2.19, the main drawback of the rigid containers is distorting the free field boundary conditions. This occurs because firstly the rigid walls cannot move along with the soil, and secondly there may be excessive energy reflections from their boundaries. In order to provide the free field conditions in this type of container, an extremely large container is required which is not feasible in most cases. Another option to reduce the reflecting energy is to attach energy absorbing layers to the container walls. Steedman and Zeng (1991) concluded that only one third of incident waves could reflect from these kinds of absorbent boundaries. Despite the fact that using absorbent boundaries decreases the reflection of outward propagating waves back into the model from the boundary walls, those boundaries may cause additional modelling variables like

stiffness and friction of the layers (Gohl and Finn, 1987). Valsangkar et al. (1991) employed 25-mm thick Styrofoam as the absorbing layers in their rigid container. The layers were attached to both end walls perpendicular to the shaking direction.

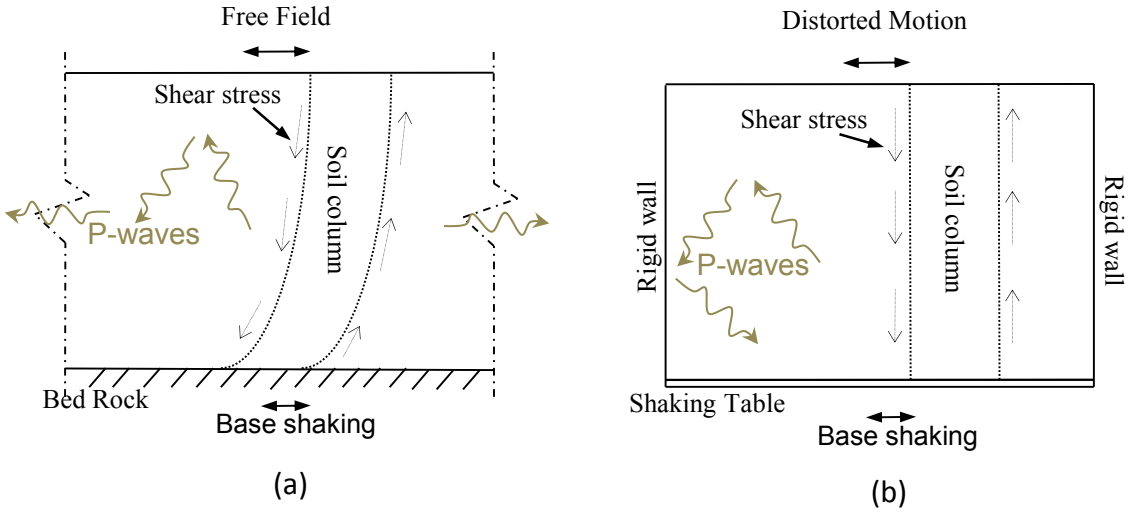


**Figure 2.19** Comparison of (a) the free field ground motion, and (b) the simulated motion employing rigid soil container on shaking table

Flexible containers allow the modelled soil inside them to move more analogous to the free field ground motion in comparison with rigid containers. In addition, reflection of outward propagating waves back into the model from the walls could be reduced more efficiently. An example for flexible soil containers is a flexible cylindrical soil container shown in Figure 2.20 designed by Meymand (1998). This container is cylindrically shaped which is 2440 mm (7.5 ft) in diameter and 2130 mm (7 ft) in height. The top ring and the base plate were made of steel plates. The top ring was supported by four steel pipes in order to provide the container with full translational and rotational freedom. A rubber membrane was bolted to the top ring and the base plate with compression rings in between. 50 mm (2.0 in) wide bands were arrayed circumferentially around the exterior of the membrane. Combination of the rubber membrane and bands provided the desired lateral flexibility and radial stiffness (to avoid bulging). In addition, the base plate of the container was roughened by epoxying a high friction coating containing angular crushed gravel pieces onto its surface, and the soil was isolated from the top ring by not filling the container to the top.

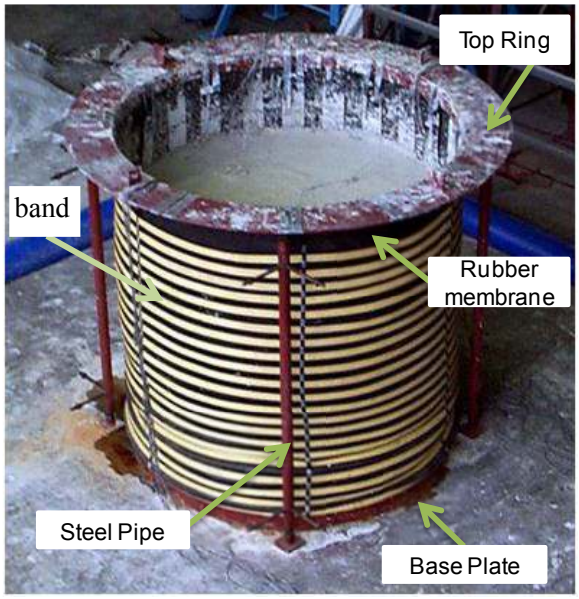


**Figure 2.20** Flexible cylindrical soil container (Meymand, 1998)

Gazetas (1982) pointed out that laminar soil containers can realistically simulate the free field conditions in comparison with rigid and flexible containers. Several types of inter-layer sliding systems for laminar soil containers have been used over the past few decades such as commercial ball bearings (Ishimura et al., 1992), sliding systems such as Teflon (Chau et al., 2009), and elastic materials such as rubber (Taylor, 1997).

Figure 2.21 illustrates the laminar soil container designed by Taylor (1997). The container had inside dimensions of 5m length, 1m width, and 1.15 m height, made of rectangular aluminium frames. Small rubber blocks were inserted between frames with 0.5 m spacing in the longitudinal sides. The noticeable and major points of modelling techniques utilised by Taylor (1997) are as follows:

- As the same tuning stiffness for the container and the soil is required in the desired strain level, and based on the selected maximum strain level for the soil, the natural frequency of the soil was determined. Afterwards, the natural frequency of empty container was fitted to the estimated natural frequency of the soil,
- Sand was glued to the base of the container and end walls to provide frictional contact between the soil and container's base and end walls, and
- The estimated weight of the container was 33% of the soil weight. It is preferable to reduce this portion as much as possible.

By satisfying the above conditions in design of Taylor's laminar soil container, authentic conditions of the free field ground motion could be captured in shaking table tests. Thus, lateral movements of the container in shaking table tests may be almost identical to the free field ground motion in reality.

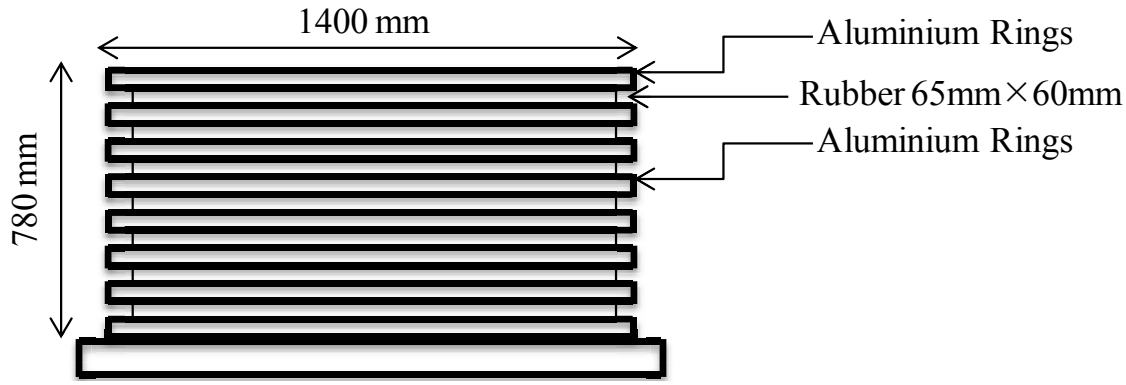


**Figure 2.21** Schematic view of the laminar soil container developed by Taylor (1997)

Many researchers (e.g. Gazetas, 1982; Taylor et al., 1995; Pitilakis et al., 2008; Tang et al., 2009) concluded that the laminar soil container is the most suitable and efficient type of the soil container. Based on the conclusions made by the above mentioned researchers, the merits of adopting laminar soil containers in shaking table tests over the other types of soil containers are as follows:

- Well-designed laminar soil containers can better model the free field conditions in comparison with rigid and flexible containers as the lateral deformations in laminar soil containers are almost identical to the free field movements,
- Uniform lateral motion exists in each horizontal plane,
- Lateral motion of the entire depth follows the sinusal shape which represents authentic conditions of the free field ground motion, and
- Most of the recent experimental shaking table tests, conducted over the past 10 years, have been carried out using the laminar soil container due to its accuracy in modelling the free field ground motion during the experimental tests.

According to the above mentioned merits of using laminar soil containers over the other types of containers (flexible and rigid soil containers) and in order to perform

rigorous and reliable experimental shaking table tests, a laminar soil container is employed in this study.

## 2.10 Summary

Base on the simplified models described in this chapter, it has been shown that the soil-structure interaction reduces the natural frequency of the system and increases the effective damping ratio of the system, for typical soils and foundations, in comparison with the fixed-base structure. This can considerably alter the response of the building frames under the seismic excitation by amplifying the lateral deformation and inter storey drifts of the superstructure. The increase in the lateral deformation of the building can change the performance level of the structure and is especially important for tall, slender structures or for closely spaced structures that can be subjected to pounding when relative displacements become large. The lessons learned from post seismic observations of the past earthquakes such as 1985 Mexico City and 1995 Kobe earthquakes provide sufficient reasons to believe that the soil-structure interaction can have important effects on the structural damage during earthquake and should be investigated with greater rigor and precision.

A number of building codes recommend a simplified linear method together with SDOF structure to account for the effects of the soil-structure interaction. Australian code (AS1170.4, 2007) does not address the soil-structure interaction effects in seismic design of structures explicitly and consequently structural designers are not able to include those important effects in the analysis and design procedure using the mentioned standard. In particular, the influence of pile elements and the generated soil-pile-structure interaction on the seismic behaviour of structures during the earthquake is the missing part in the most of the building codes, perhaps due to the complexity of the problem. As a result, conducting more research to consider those detrimental effects of the soil-pile-structure interaction in the seismic design of building structures with respect to different types of foundations (e.g. shallow and deep foundations) are required.

The existing analytical methods for studying the soil-pile-structure interaction including Winkler methods, elastic continuum methods, and numerical methods have

been presented and the advantages and shortcomings of each method have been discussed. Consequently, the direct numerical model, in which the entire soil-pile-structure is modelled at the same time and the input motions are specified along the base of the model, is more capable in modelling the complex nature of the soil-structure interaction in dynamic analysis and is employed in this study. The developed 3D numerical model will be verified and validated in this study against a series of experimental shaking table test results prior to be employed for investigating the influence of different parameters on the soil-pile-structure interaction phenomenon.

The previous efforts to experimentally investigate the influence of SSPSI on seismic response of buildings have been summarised. Accordingly, the employed soil containers can be categorised into three main categorise, namely, rigid, flexible, and laminar containers. By comparing the advantages and disadvantages of each type, and considering the mentioned merits of using laminar soil containers over the other types of containers (flexible and rigid soil containers), a laminar soil container is employed in this study to perform rigorous and reliable experimental shaking table tests.

# Chapter 3- NUMERICAL MODELLING

## 3.1 General

In order to conduct a fully coupled analysis of the entire soil-pile-structure system, a three-dimensional numerical soil-structure model has been developed in this study which treats the behaviours of the soil and the structure with equal rigor. Adopting direct method of analysis, the numerical model can perform fully nonlinear time-history dynamic analysis to simulate realistic dynamic behaviour of the soil and the structure under seismic excitations. According to Chu (2006), time domain analysis is necessary to compute the nonlinear dynamic responses of soil-pile-structure systems as the frequency domain analysis can deal only with linear responses without considering any nonlinearities. In this study, three-dimensional explicit finite difference based program FLAC3D (Fast Lagrangian Analysis of Continua) version 4.0 has been employed following the other researchers experience (e.g. Comodromos and Papadopoulou, 2012; Rayhani and El Naggar, 2008). This program can simulate behaviour of different types of structures and materials by elements which can be adjusted to fit the geometry of the model. Each element behaves according to a prescribed constitutive model in response to the applied forces or boundary restraints. The program offers a wide range of capabilities to solve complex problems in mechanics such as inelastic analysis including plastic moment and simulation of hinges for structural systems.

There are two main analytical procedures to model soil for dynamic analysis of soil-structure systems under seismic loads, namely equivalent-linear and fully nonlinear methods. The equivalent-linear method, as discussed by Seed and Idriss (1969), cannot capture directly any nonlinearity effects during the solution process and uses linear properties for each element remaining constant throughout the history of shaking, and

are estimated from the mean level of dynamic motion. Therefore, the strain-dependent modulus and damping functions for the soil (Section 2.4) are only taken into account in an average sense, in order to approximate some effects of nonlinearity. As a result, during the low amplitude shakings in the excitation history, soil elements will be modelled overdamped and too soft, and during the strong shaking, soil elements will be modelled underdamped and too stiff. In contrast, as explained by Fatahi and Tabatabaiefar (2013), employing fully nonlinear method, nonlinearity in the soil stress-strain law is followed directly by each soil element and the dependence of damping and apparent modulus on strain level is automatically modelled. Byrne et al. (2006) and Beaty (2001) provided some overviews of the above mentioned methods and concluded that the most appropriate method for a dynamic analysis of soil-structure system is a fully nonlinear method. In addition, Lu et al. (2011) studies illustrated the potential for further reliance on the computer simulation in the assessment of the nonlinear seismic ground response using the nonlinear dynamic analysis. Consequently, fully nonlinear method to model soil for dynamic analysis of soil-structure systems has been employed in this study.

It should be noted that there are some other rigorous approaches to model soil behaviour under cyclic loads such as isotropic kinematic constitutive models (Gajo and Muir Wood, 1999), incrementally nonlinear models (Darve et al., 1995), or hypoplastic models (Chambon et al., 1994). However, the modulus reduction approach is the most common approach to model the soil for dynamic analysis of soil-structure systems, and is employed in this study.

In this chapter, different components of the developed numerical model including soil elements, pile elements, structural elements, interface elements, boundary conditions, and dynamic loading are explained. Due to the complexity of the model, fast computation facilities at University of Technology Sydney (UTS) were employed to run the developed SSPSI analysis models in this study.

## 3.2 Governing Equation of Motion for Soil-Structure Systems

The governing equations of motion for the structure incorporating foundation interaction and the method of solving these equations are relatively complex. The main

reason for this complexity lies in the fact that unlike the ordinary dynamic time-history equations of motions, the right hand side of the dynamic equation of motion of the soil and structure system (shown in Equation 3.1) consists of a combination of different vectors and matrices corresponding to the soil and the structure. This combination makes the equation mathematically sophisticated to be solved by conventional methods. Therefore, direct numerical method, the method in which the entire soil-structure system is numerically modelled in a single step, is employed in this study.

The dynamic equation of motion for the soil and structure system can be written as follows:

$$[M]\{\ddot{u}\} + [C]\{\dot{u}\} + [K]\{u\} = -[M]\{1\}\ddot{u}g + \{Fv\} \quad (3.1)$$

where, *[M]*, *[C]* and *[K]* are the mass, damping, and stiffness matrices of the structure, respectively. *{u}*, *{u̇}*, and *{ü}* are the relative nodal displacements, velocities and accelerations of the structure with respect to the underlying soil foundation, respectively. $\{\ddot{u}_g\}$ is ground acceleration, and $\{F_v\}$ is the force vector corresponding to the viscous boundaries. This vector is nonzero only when there is a difference between the motion on the near side of the artificial boundary and the motion in the free field (Wolf, 1985). It is more appropriate to use the incremental form of Equation (3.1) when plasticity is included, and then the matrix *[K]* should be the tangential matrix and $\{\ddot{u}_g\}$ is the earthquake induced acceleration at the level of the bedrock. An incremental equation is a form of equation that requires satisfaction of equilibrium at the end of the iteration. Further details about the form and application of incremental equation have been provided by Wolf (1998).

## 3.3 Three-dimensional Finite Difference Software, FLAC3D

FLAC3D, Fast Lagrangian Analysis of Continua, version 4.0 (Itasca, 2009) is an explicit finite difference program to numerically study the mechanical behaviour of a continuous three-dimensional medium. In order to achieve mathematical model description, general principles such as strain definition and motion laws together with the use of constitutive material equations are implemented in FLAC3D. The resulting mathematical expressions are a set of partial differential equations, relating mechanical (stress) and kinematic (strain rate, velocity) variables, which are to be solved for

particular geometries and properties, given specific boundary and initial conditions (Itasca, 2009).

The solution method in FLAC3D employs following three main approaches: (1) finite difference approach, in which finite differences are used to approximate the first-order space and time derivatives of a variable, assuming linear variations of the variable over finite space and time intervals, respectively; (2) discrete-model approach, in which the continuous medium is replaced by a discrete equivalent and all the involved forces are concentrated at the nodes of a three-dimensional mesh in order to represent the medium; and (3) dynamic-solution approach, in which the inertial terms in the equations of motion are used as numerical means to reach the equilibrium state of the system under consideration. Employing these approaches, the motion laws for the continuum are converted into discrete forms of Newton's law at the nodes. Afterward, the resulting ordinary differential equations system is solved numerically adopting the finite difference approach.

For the purpose of defining velocity variations and corresponding space intervals, the medium is discretised into constant strain-rate of tetrahedral shape elements as illustration in Figure 3.1. Comparing tetrahedral with other types of three-dimensional constant strain-rate elements, tetrahedral have the advantage of not generating hourglass deformations which is the deformation patterns formed by combinations of nodal velocities producing no strain rate, and thus no nodal force increments. However, since tetrahedral elements do not provide enough modes of deformation (see Nagtegaal et al., 1974), using these elements in the framework of plasticity may cause slightly stiffer response in comparison to the theoretical predictions. A process of *mixed discretization* is applied in FLAC3D to overcome this problem, which has been broadly explained by Marti and Cundall (1982) and Itasca (2009).

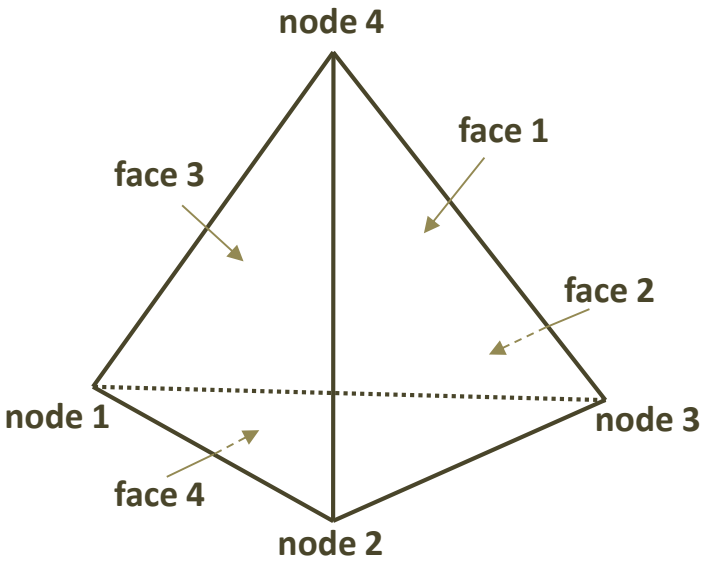


**Figure 3.1** Tetrahedron shape elements employed in FLAC3D to discretise the continuous medium

## 3.4 Soil Elements

In the numerical modelling process, soil medium is represented by elements, and each element behaves according to a prescribed linear or nonlinear stress/strain law in response to the applied forces or boundary restrains. Accordingly, a proper constitutive model representing the geomechanical behaviour of soil elements should be implemented in FLAC3D in order to conduct a rigorous SSI analysis.

Nonlinear Mohr-Coulomb model has been adopted in this study to simulate the nonlinear soil behaviour and possible shear failure in the soil elements during the excitation. The adopted Mohr-Coulomb model is a nonlinear elastic-perfectly plastic model that has been employed by many researchers (e.g. Conniff and Kiousis, 2007; Rayhani and EL Naggar, 2008) to simulate soil behaviour under seismic loads in soil-structure systems. The associated failure envelope for this model corresponds to a Mohr-Coulomb criterion (shear yield function) with tension cut-off (tension yield function).

Following soil parameters are required to be defined for soil elements in FLAC3D, where Mohr-Coulomb model is implemented:

- $\Phi$ : Friction angle (*deg*)

- $C$ : Cohesion ($Pa$)
- $\rho$ : Mass density ($kg/m^3$)
- $G$ : Shear modulus ($Pa$)
- $K$ : Bulk modulus ($Pa$)

### 3.4.1 Implementation of Soil Backbone Curves in FLAC3D

Soil nonlinearity during the earthquake plays an important role in the dynamic response of soil-structure systems. In order to accommodate fully nonlinear SSI analysis, despite the linear elastic behaviour of conventional Mohr-Coulomb model, variation of shear modulus and damping ratio of the soil elements during the shaking excitations in accordance with the developed shear strain level as explained in Section 2.4 has been adopted in this study.

Modulus degradation curves imply nonlinear stress-strain curves. In case of an ideal soil in which the stress depends only on the strain (not on the number of cycles, or time), an incremental constitutive relation from the degradation curve can be described by the strain-dependent normalised secant modulus ($M_s$) as follows:

$$M_s = \frac{\bar{\tau}}{\gamma} \tag{3.2}$$

where, $\bar{\tau}$ is the normalised shear stress and $\gamma$ is the shear strain. The normalised tangent modulus, $M_t$, is then obtained as:

$$M_t = \frac{d\bar{\tau}}{d\gamma} = M_s + \gamma \frac{dM_s}{d\gamma} \tag{3.3}$$

The incremental shear modulus in a nonlinear simulation is then given by $G \times M_t$, where, $G$ is the secant shear modulus described in Equation (2.13). The formulation described above is implemented in FLAC3D by modifying the strain rate calculation. Therefore, the mean strain rate tensor (averaged over all subzones) is calculated prior to any calls are made to constitutive model functions. At this stage, the hysteretic logic is invoked, returning a modulus multiplier which is passed to any called constitutive model. The model then uses the multiplier $M_t$ to adjust the apparent value of tangent shear modulus of the full zone.

Three built-in tangent modulus functions are available in FLAC3D to implement hysteretic damping by representing the variation of the shear modulus reduction factor ($G/G_{max}$) and the damping ratio ($\xi$) with the cyclic shear strain ($\gamma$) as follows:

1. ***Default Model***: The default hysteresis model is developed by the S-shaped curve of modulus versus logarithm of cyclic strain, representing a cubic equation, with zero slopes at both low and high strains. Thus, the secant modulus ($M_s$) can be calculated as:

   $$M_s = s^2 (3-2s) \tag{3.4}$$

   where,

   $$s = \frac{L_2 - L}{L_2 - L_1} \tag{3.5}$$

   and $L$ is the logarithmic strain,

   $$L = Log_{10}(\gamma) \tag{3.6}$$

   The model is defined by two parameters, $L_1$ and $L_2$, which are the extreme values of logarithm of the shear strain.

2. ***Sigmoidal Models****:* These curves are monotonic within the defined range, and have the required asymptotic behaviour. Thus, the functions are well-suited to the purpose of representing modulus degradation curves. Two types of sigmoidal models (Sig3 includes $a$, $b$, and $x_0$ and Sig4 consists of a, $b$, $x_0$ and $y_0$ as model fixing parameters) are defined as follows:

   *Sig3 Model*

   $$M_s = \frac{a}{1 + \exp(-(L - x_0)/b)} \tag{3.7}$$

   *Sig4 Model*

   $$M_s = y_0 + \frac{a}{1 + \exp(-(L - x_0)/b)} \tag{3.8}$$

3. ***Hardin/Drnevich Models**:* The model was presented by Hardin and Drnevich (1972), known as Hardin model which is defined by Hardin/Drnevich constant ($\gamma_{ref}$) as follows:

$$M_s = \frac{1}{1+\gamma/\gamma_{ref}} \tag{3.9}$$

Any of the above mentioned models generate backbone curves presented in Sections 2.4.1 and 2.4.2 for granular soils (Seed et al., 1986) and cohesive soils (Sun et al., 1988) adopting the required numerical fitting parameters summarised in Table 3.1.

**Table 3.1** Numerical fitting parameters in FLAC3D for implementing soil backbone curves

| Soil type | Clay | Sand |
|---|---|---|
| Default Model | $L_1$= -3.156, $L_2$= 1.904 | $L_1$= -3.325, $L_2$= 0.823 |
| Sig3 Model | $a$= 1.017, $b$= -0.587, $x_0$= -0.633 | $a$= 1.014, $b$= -0.4792, $x_0$= -1.249 |
| Sig4 Model | $a$= 0.922, $b$= -0.481 $x_0$= -0.745, $y_0$= 0.0823 | $a$= 0.9762, $b$= -0.4393 $x_0$= -1.285, $y_0$= 0.03154 |
| Hardin Model | $\gamma_{ref}$= 0.234 | $\gamma_{ref}$= 0.06 |

*Note: for cohesive soils adopting Sun et al. (1988), and for granular soils adopting Seed et al. (1986) backbone curves.

## 3.5 Pile Elements

For the numerical simulation of pile foundations, one of the possible approaches is to use the pile structural elements (pileSELs) provided in FLAC3D. Pile structural elements are similar to the beam structural elements, while in addition to providing the structural behaviour of a beam (including the ability to define a plastic moment capacity), frictional interaction in both normal (perpendicular to the pile axis) and shear direction (parallel with the pile axis) occurs between the pile and the surrounding soil (Figure 3.2). According to Itasca (2009), PileSELs elements are suitable to model

structural-support members, such as foundation piles, where the analysis and design of the pile elements is targeted.

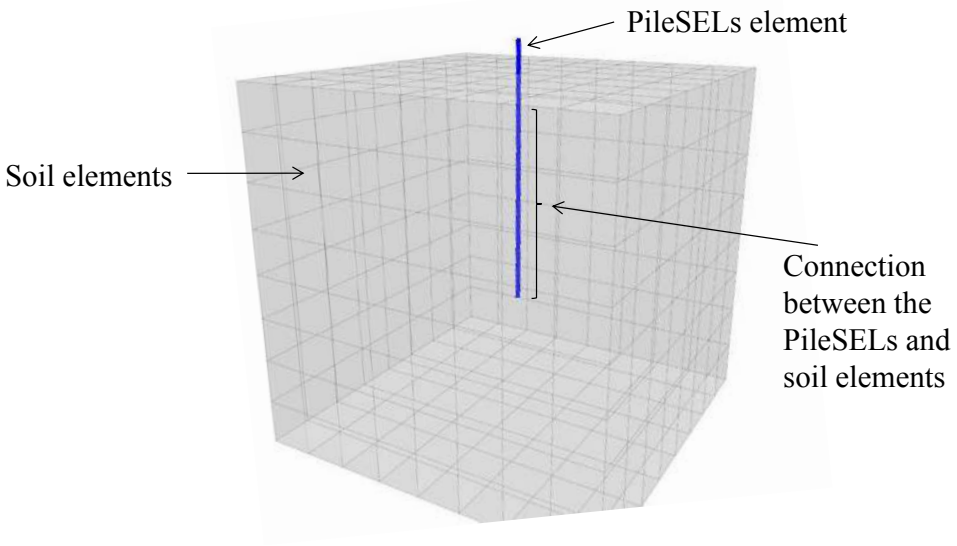


**Figure 3.2** Pile structural elements (pileSELs) in FLAC3D

In contrast, one of the main features of the presence of pile foundation in SSPSI analysis is the stiffness of pile elements. In other words, the volume of the stiff pile elements, which is replaced into the soft soil medium, affects the equivalent stiffness of the ground which in turn can influence the dynamic properties of the whole system such as the natural frequency and the damping. Therefore, employing pileSELs, which do not possess any volume in the generated grid, would not be appropriate to represent the pile foundation in SSPSI numerical simulation.

Solid elements are adopted to simulate the pile foundation in this study as suggested by several researchers (e.g. Comodromos and Papadopoulou, 2012; Ghee and Guo, 2010). Pile elements, as shown in Figure 3.3, have rigid connection with the pile cap, while appropriate interface elements (see Section 3.6), capable of accounting for possible gap and slide generation in pile elements, are adopted to connect the pile grid points and the surrounding soil.

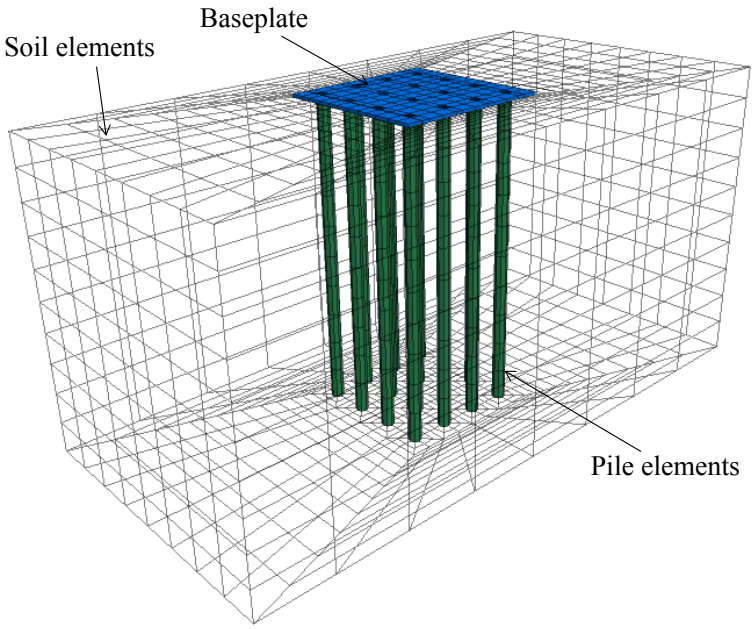


**Figure 3.3** Simulating pile elements in this study for SSPSI analysis

The formulation adopted in this study to simulate the inelastic behaviour of pile elements assumes elastic-perfectly plastic behaviour with yielding criteria for the elements (Figure 3.3) to control the possibility of inelastic behaviour in pile elements. Accordingly, in order to validate the capability of the applied procedure in modelling the pile elements, a FLAC3D analysis was first conducted on a cantilever pile while the pile was fixed at one end into the ground without the surrounding soil and different lateral loads were applied on the free end of the cantilever pile. The recorded deflection from the FLAC3D model showed less than 2% difference from the existing analytical predictions, confirming the accuracy of the adopted modelling procedure.

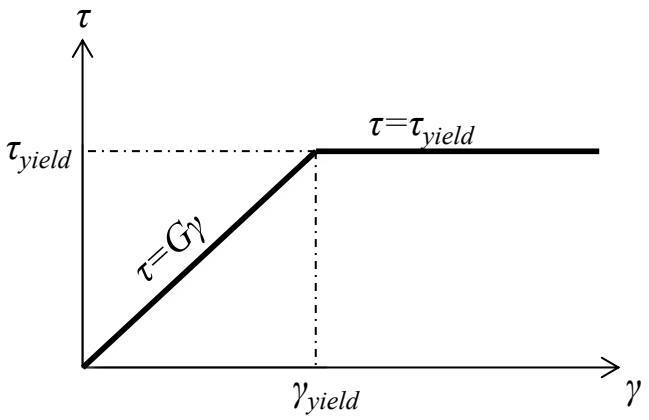


**Figure 3.3** Simulating the inelastic behaviour of pile elements

## 3.6 Structural Elements

Beam structural elements (beamSELs) are implemented in this study to model the superstructure. The adopted structural elements are two nodded, straight, finite elements with six degrees of freedom per node including three translational components, and three rotational components. Figure 3.4 shows the local coordinate system and the twelve active degrees-of-freedom for the beam finite element. Accordingly, for each degree of freedom the generalised displacement (translation and rotation) corresponds to the relevant force (force and moment) in that degree of freedom. The stiffness matrix of the beam finite element includes all six degrees of freedom at each node representing axial, shear and bending action within a beam structure.

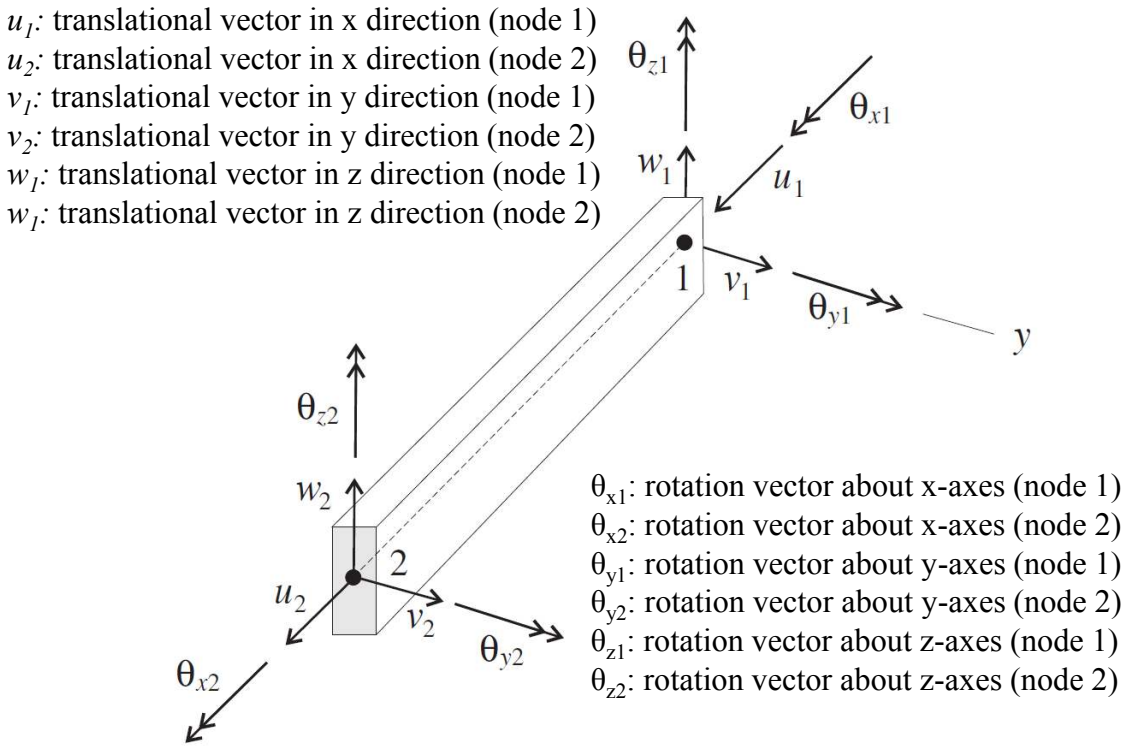


**Figure 3.4** Developed twelve degrees-of-freedom beam structural element for the 3D numerical simulation (after Itasca 2009)

Nodal responses including forces and moments as well as translational and rotational velocities and displacements are computed for each node of beamSEL. The implemented structural elements follow the same explicit, Lagrangian solution procedure as the rest of the code. Large displacements, including geometric nonlinearity, can be accommodated by specifying a large-strain solution mode, and the

full dynamic response of the system in the time domain can also be obtained with the dynamic-analysis option.

### 3.6.1 Properties of Beam Structural Elements

Each beam structural element is defined by its geometric and material properties. A beamSEL is assumed to be a straight segment with uniform bisymmetrical cross-sectional properties lying between two nodal points. Geometric properties of the adopted beam elements adopted in this study to simulate the superstructures are defined using the following cross sectional parameters referring to Figure 3.5:

- $A$ : Cross-sectional area ($m^2$)
- $I_y$ : Second moment of inertia with respect to y-axis ($m^4$)
- $I_z$ : Second moment of inertia with respect to z-axis ($m^4$)
- $J$: Polar moment of inertia ($m^4$)

FLAC3D automatically calculates $z$, $y$ dimensions for two principal axes of the beam cross section using the above defined cross sectional parameters.

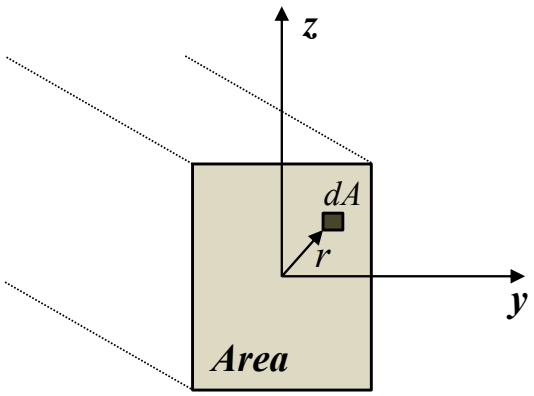


**Figure 3.5** Cross-section of the beam structural element cross-section in y-z plane (after Itasca, 2009)

The implemented polar moment of inertia ($J$), and second moment of inertia with respect to $y$ axis ($I_{y,}$) and $z$ axis ($I_{z,}$) are determined using the following integrals:

$$J = \int_A r^2 dA \tag{3.10}$$

$$I_y = \int_A z^2 dA \tag{3.11}$$

$$I_z = \int_A y^2 dA \tag{3.12}$$

In addition, the following material properties are defined in this study for the beam structural elements:

- $\rho$ : Mass density ($kg/m^3$)
- $E$ : Young modulus ($Pa$)
- $v$ : Poisson's ratio
- $M_p$ : Plastic moment capacity ($N.m$)

Plastic moment capacity ($M_p$) is exercised for inelastic structural analysis. For elastic analysis, the plastic moment capacity value is assumed to be infinite. It should be noted that by default, beam structural elements are linear elastic materials, without any failure limit. However, plastic moment capacity (plastic hinge) can be introduced to model the inelastic behaviour of the structures. In this case, elastic-perfectly plastic behaviour (Figure 3.6) for the beam structural elements are assumed, where each element behaves elastically until reaching the plastic moment, and then it continues to deform without generating additional resistance.

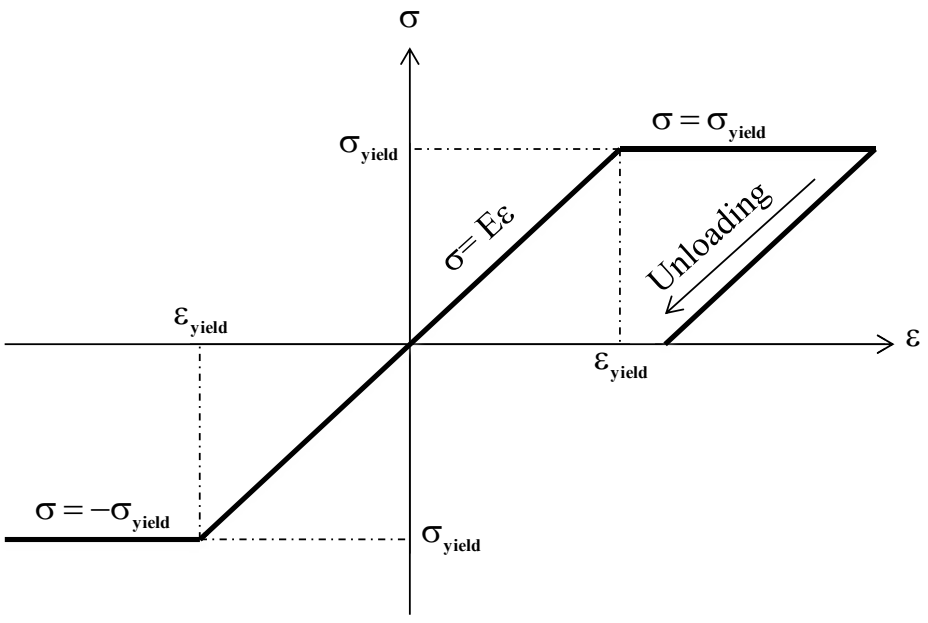


**Figure 3.6** Elastic-perfectly plastic behaviour of beam structural elements

The value of plastic moment capacity of a flexural structural member can be calculated using the following equation:

$$M^p = \sigma_y (\frac{bh^2}{4}) \tag{3.13}$$

where, $b$ is the width of the element cross-section, $h$ is the height of the element cross-section, and $\sigma_y$ is the yield stress of the material. The plastic-moment capacity limits the internal moment carried by each beam structural element. As pointed out by Ziemian (1993), the computational expense required for the above mentioned plastic hinge method could be hundred times less than other methods such as plastic zone approach. Therefore, as concluded by Chan and Chui (2000), the plastic hinge method is a preferable method offering the advantage of cost-effectiveness and accuracy meeting the requirement of practicing engineers.

## 3.7 Interface Elements

Because of the different characteristics of the soil and the superstructure/piles, sliding and separation may occur at the soil-structure interfaces (Maheshwari and Watanabe, 2006). Three sets of interface elements are modelled in this study. For the shallow foundation case, the interface elements are placed between the foundation and the soil surface as shown in Figure 3.7a. For the floating pile foundation case, the interface elements are attached to the outer perimeter and bottom of the piles as shown in Figure 3.7b. Finally, for the end-bearing pile foundation case, the interface elements are only attached to the outer perimeter of the piles (Figure 3.7c) and fixed base connection between the pile tips and the bedrock is considered, in order to compel the end bearing behaviour and prevent any possible sliding between the piles and the bedrock.

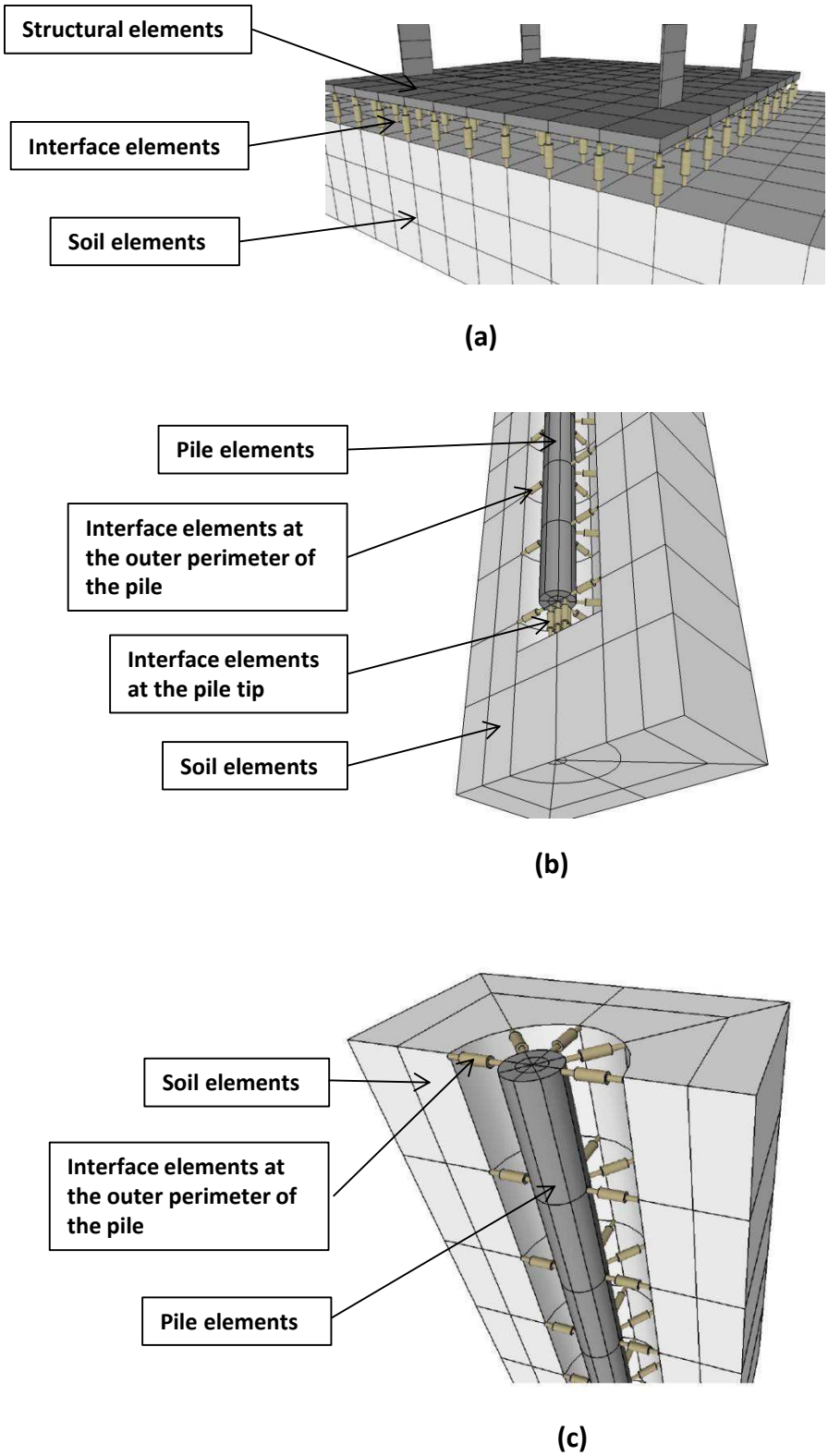


**Figure 3.7** Interface elements adopted in this study: (a) interface elements between the shallow foundation and the soil element; (b) interface elements at the outer perimeter and tip of the floating piles and surrounding soil; (c) Interface elements at the outer perimeter of the end-bearing piles and surrounding soil

It should be noted that in the pile foundation cases, there is no interface or attachment between the foundation and the surface soil as some gap in the shaking table tests is considered to avoid any pile-raft behaviour. Therefore, there is no direct stress transfer in the pile foundation cases between the foundation slab and the subsoil in the pile foundation case. However, for the pile-raft foundations, as discussed in Chapter 6, interface elements are defined between the foundation and the surface soil as well as the outer perimeter of the piles to represent the stress transfer of the pile-raft behaviour.

According to Figure 3.8, the normal and shear forces that describe the interface response in the elastic range are determined at the calculation time ($t+\Delta t$) using the following relations (Itasca, 2009):

$$F^{(t+\Delta t)}_{n} = k_n u_n A + \sigma_n A \tag{3.14}$$

$$F^{(t+\Delta t)}_{si} = F^{(t)}_{si} + k_s \Delta u^{(t+(1/2)\Delta t)}_{si} A + \sigma_{si} A \tag{3.15}$$

where, $F^{(t+\Delta t)}_{n}$ and $F^{(t+\Delta t)}_{si}$ are the normal and shear force vectors at time $(t+\Delta t)$, respectively, $u_n$ is the absolute normal penetration of the interface node into the target face, $\Delta u_{si}$ is the incremental relative shear displacement vector, $\sigma_n$ and $\sigma_{si}$ are the additional normal and shear stresses added due to interface stress initialisation, respectively, $k_n$ and $k_s$ are the normal and shear stiffnesses, respectively, and $A$ is the representative area associated with the interface node. The adopted interfaces in FLAC3D are one-sided which is different from the formulation of two-sided interfaces in two-dimensional FLAC (Itasca, 2010). FLAC3D interfaces are like a “shrink-wrap” which is stretched over the desired surface, causing the surface to become sensitive to interpenetration with any other face with which it may come into contact.

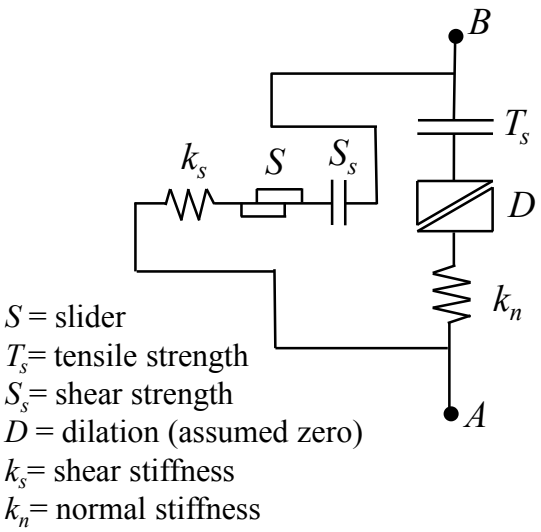


**Figure 3.8** components of the interface constitutive model adopted in this study

The lateral and axial stiffnesses of the interface elements are set to ten times the equivalent stiffness of the neighbouring zone, based on the recommended relationship by Rayhani and El Naggar (2008) and Itasca Consulting Group (Itasca, 2009) for the isotropic soil medium, as follows:

$$k_s = k_n = 10\left[\frac{K + \frac{4}{3}G}{\Delta z_{\min}}\right] \tag{3.16}$$

where, $K$ and $G$ are bulk and shear modulus of neighbouring zone, respectively, and $\Delta z_{min}$ is the smallest width of an adjoining zone in the normal direction. This is a simplifying assumption that has been used to ensure that the interface stiffness has minimal the influence on the system compliance by avoiding the intrusion of adjacent zones (a numerical effect) and preventing excessive computation time (Rayhani and El Naggar, 2008). In addition, shear strength of the interfaces was defined by Mohr–Coulomb failure criterion and the tensile strength of the interfaces are set to zero in order to allow gapping between the piles and the supporting soil in the pile foundation case and uplift in the shallow foundation case.

## 3.8 Boundary Conditions

Simulation of SSPSI problem revolves around media which are more appropriate to be modelled as unbounded half-space media. However, numerical methods, relying on the discretisation of a finite region of space, require appropriate conditions to be enforced at the artificial numerical boundaries. The boundary conditions in the numerical models are prescribed at the boundaies of the numerical grids. Each of the two main steps of SSPSI numerical analysis, static analysis and dynamic analysis, requires particular types of boundaries. During the static analysis step, where the model should be analysis under gravity loads in order to achieve the static equilibrium, preliminary boundary conditions should be adopted at the boundaries of the numerical grids. In the preliminary boundary conditions as shown in Figure 3.9, soil side boundaries are fixed in the horizontal directions while free movement is allowed in the vertical direction. Also, the base boundary is fixed in all direction (Rayhani, 2007). Lu et al. (2012) emphasised on the influence of the gravity load on contact state of the soil–structure interface mentioning that significant error in the analysis may occur if gravity is not taken into account in the dynamic analysis.

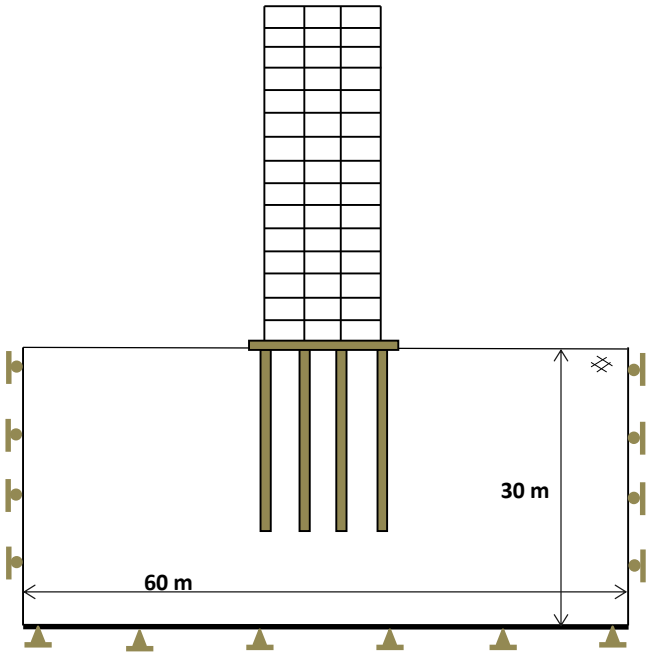


**Figure 3.9** Preliminary boundary conditions for the static analysis under the gravity loads

Prescribing the preliminary boundary conditions for the dynamic analysis causes the reflection of outward propagating waves back into the model, and do not allow the

necessary energy radiation. It is possible to minimise the problem by using a larger model as material damping will absorb most of the energy in the waves reflected from distant boundaries. However, increasing the size of the model leads to a significantly large computational burden. Roesset et al. (1973), after a comprehensive study on the performance of different types of soil boundary conditions for dynamic problems, proposed quiet (or absorbing) boundaries as the best solution to the problem. Detailed explanation of the adopted boundary conditions is provided in the following sections.

### 3.8.1 Quiet (viscous) Boundaries

During the dynamic time-history analysis, the quiet (viscous) boundaries have been adopted in order to avoid the reflection of the outward propagating waves back into the model. As shown in Figure 3.10, independent dashpots in the normal and shear directions are placed at the lateral boundaries of the soil medium. Viscous damping on the boundaries is a function of soil density and the velocity of the propagated p-wave and s-wave in the soil medium. Referring to Lysmer and Kuhlemeyer (1969), the employed viscous normal and shear tractions are as follows:

$$t_n = -\rho\, C_p\, V_n \tag{3.17}$$

$$t_s = -\rho\, C_s\, V_s \tag{3.18}$$

where, $V_n$ and $V_s$ are the normal and shear components of the velocity at the boundaries, respectively, $\rho$ is the mass density, and $C_p$ and $C_s$ are the velocities of the p-wave and s-wave, respectively. In the adopted numerical analysis procedure, the above mentioned viscous terms are implemented as boundary loads at every time step. Alternatively, these viscous terms can be introduced directly into the equations of motion of the grid points lying on the boundaries.

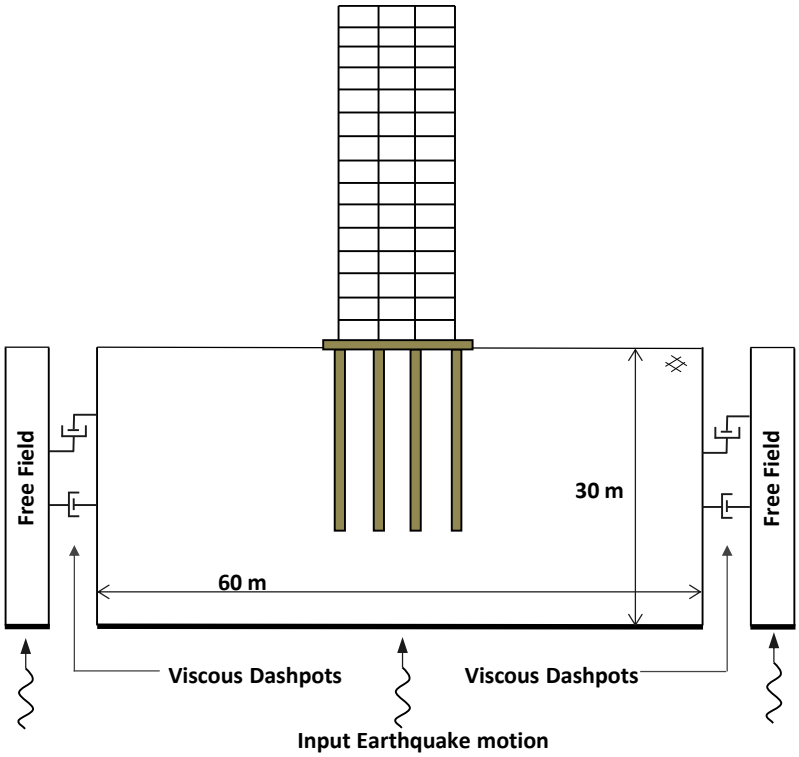


**Figure 3.10** Simulating boundary conditions for the dynamic analysis of the soil-pile-structure interaction system.

The above mentioned viscous boundaries have the advantage of operating in time domain. More efficient energy absorption (particularly in the case of Rayleigh waves) requires the use of frequency-dependent elements called consistent boundaries, which can only be used in frequency-domain analyses (e.g Lysmer and Waas, 1972). However, as Chu (2006) mentioned, time domain analysis is necessary to compute the nonlinear dynamic responses of soil-pile-structure systems as the frequency domain analysis can deal only with linear responses without considering any nonlinearities. A comparative study of the performance of different types of preliminary, viscous and consistent boundaries was documented by Roesset and Ettouney (1977).

## 3.8.2 Free Field Boundaries

In order to accurately simulate SSPSI problem, the side boundary conditions of the numerical model must account for the free-field ground motion which would exist in the absence of the structure and pile foundation as explained in Section 2.2. The adopted techniques in FLAC3D execute the free-field calculation in parallel with the main-grid

analysis. As shown in Figure 3.10, the lateral boundaries of the main grid are coupled to the free-field grids by viscous dashpots of quiet boundaries at the sides of the model, and the unbalanced forces from the free-field grid are applied to the main-grid boundary. The unbalanced forces from the free-field grid along one side-boundary plane, with its normal in the direction of the *x*-axis, are expressed in the following equations (similar expressions may be written for the other sides and corner boundaries):

$$F_x = -\rho C_p (v_x^m - v_x^{ff}) A + F_x^{ff} \tag{3.19}$$

$$F_y = -\rho C_s (v_y^m - v_y^{ff}) A + F_y^{ff} \tag{3.20}$$

$$F_z = -\rho C_s (v_z^m - v_z^{ff}) A + F_z^{ff} \tag{3.21}$$

where, $F_x$, $F_x$, and $F_x$ are unbalanced forces from the free field grid in *x*, *y*, and *z* directions, respectively, ρ is the density of the soil, $C_p$ and $C_s$ are the velocities of the p-wave and s-wave, $A$ is the area of influence of free-field boundary, $v_x^m$ , $v_x^m$ , and $v_z^m$ are the x-velocity, y-velocity, and z-velocity of the grid point in the main grid, respectively, $v_x^{ff}$ , $v_x^{ff}$ , and $v_z^{ff}$ are the x-velocity, y-velocity, and z-velocity of the grid point in the free-field grid, respectively, and $F_x^{ff}$ , $F_x^{ff}$ , and $F_z^{ff}$ are the free field grid point forces in *x*, *y*, and *z* directions, respectively.

Prior to applying free field boundaries to the model, the model should be in static equilibrium and the dynamic boundary conditions at the base of the model should be specified. After invoking the free field boundary, the static equilibrium and base conditions are automatically transferred to the free field region for the dynamic analysis. Thus, plane waves propagating upward undergo no distortion at the boundary because the free-field grid supplies conditions identical to those in an infinite model. It should be noted that if the main grid is uniform, and there is no surface structure, the lateral dashpots are not exercised because the free-field grid and the main grid experience the same motion. The adopted boundary conditions, main grid, and free field grid are shown in Figure 3.11.

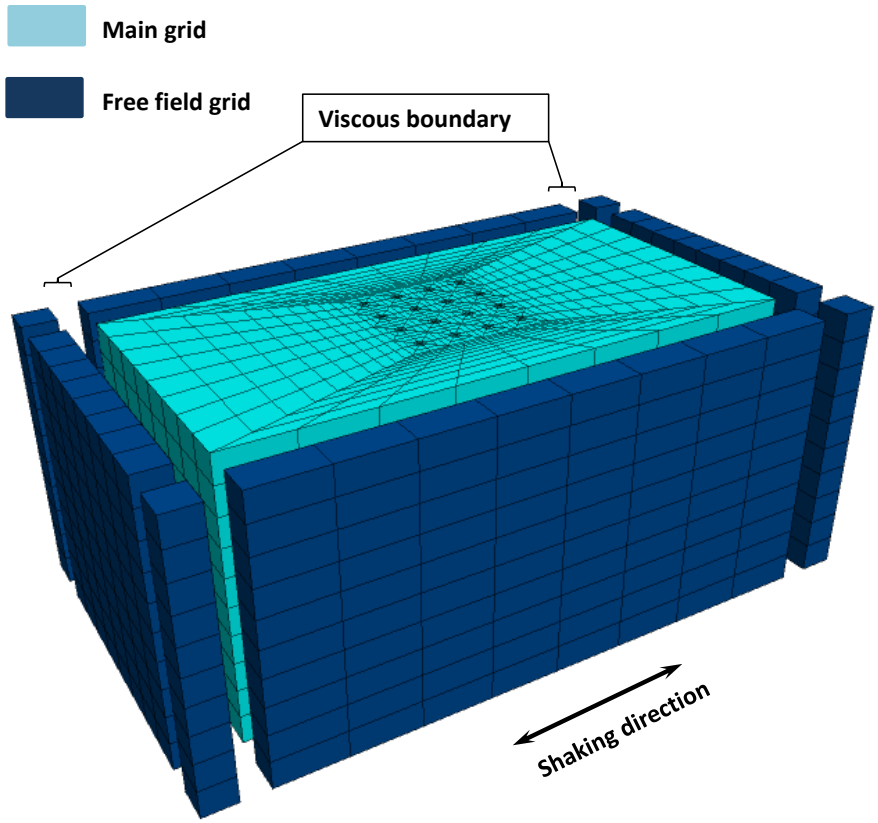


**Figure 3.11** Adopted boundary conditions, main grid, and boundary grid for the dynamic analysis of SSPSI in this study

### 3.8.3 Bedrock Boundary Condition and Size of the Numerical Model

In this study, rigid boundary condition is adopted to simulate the bedrock (bottom of the soil medium grid) in the seismic soil-structure interaction analysis as suggested by other researchers (e.g. Dutta and Roy, 2002; Spyrakos et al., 2009). As explained by Kocak and Mengi (2000), employing complaint boundary conditions for the bedrock, the entire reflected waves from the surface will be absorbed by the viscous dashpots at the base of the model. As a result, the effect of the upward-propagating wave between the bedrock and the soil surface cannot be considered in the dynamic analysis. Consequently, assuming rigid boundary condition for simulation of the bedrock in the dynamic soil-structure analysis is more appropriate and realistic which is implemented in the developed numerical model in this study.

Rayhani and El Naggar (2008), after undertaking comprehensive numerical modelling and centrifuge model tests, concluded that the horizontal distance of the soil lateral boundaries should be at least five times the width of the structure in order to

avoid reflection of outward propagating waves back into the model. They also recommended 30 metres as the maximum bedrock depth in the numerical analysis as the most amplification occurs within the first 30 metres of the soil profile, which is in agreement with most of modern seismic codes (e.g. ATC-40, 1996; BSSC, 2003). These seismic codes evaluate local site effects just based on the properties of the top 30 meters of the soil profile. Thus, in this study, the bedrock depth of 30 metres is adopted. The horizontal distance of the soil lateral boundaries is assumed to be 60 metres (five times the width of the structure which is 12 metres) in the shaking direction. Considering the characteristics of the employed shaking table in this study, the input shaking excitation is applied just in one direction. Therefore, in order to optimise the computational burden, the horizontal distance of the soil lateral boundaries in the direction perpendicular to the shaking direction is assumed to be 36 metres (three times the width of the structure) following the previous researchers (e.g. Ishimura et al., 1992; Tao et al., 1998; Chau et al., 2009). In addition, experience gained from the parametric studies helped to finalise the adopted mesh size and the maximum unbalanced force at the grid points to optimise the accuracy and the computation speed, simultaneously.

## 3.9 Dynamic Loading

Conducting time-history analysis in FLAC3D, the earthquake input motions should be applied at the bedrock horizontally propagating upward through the entire model. For dynamic inputs with high frequency the stability requirements may necessitate a very fine spatial mesh and a corresponding small time step which may lead to a prohibitively time and memory consuming analysis. For such cases, where most of the power for the input history is contained in lower-frequency components, it is possible to adjust the input by filtering the history and removing high frequency components. The adopted filtering procedure is accomplished with a low-pass filter routine called Fast Fourier Transform technique. In this study, the recorded input motions from the shaking table tests are filtered with a 50 Hz low-pass filter. It means that the frequency component above 50 Hz are filtered and removed from the input motion. The reason for choosing 50 Hz as an upper bond of input motion is that according to characteristics of the UTS shaking table, the frequency limit of the generated input motion by shaking table is between 0-50 Hz. Therefore, the high

components (above 50 Hz) of the recorded input motion by sensors include noises and should be filtered before imposing them to the numerical simulations. By removing high frequency components, a coarser mesh can be used in the numerical model without significantly affecting the results. For instance, the filtered and unfiltered acceleration records of scaled 1940 El Centro earthquake with the relevant frequency content being subjected to the 50 Hz low-pass filter are illustrated in Figure 3.12 and 3.13. Accordingly, by filtering this record, the frequency components above 50 Hz are removed, while the peak acceleration remains the same.

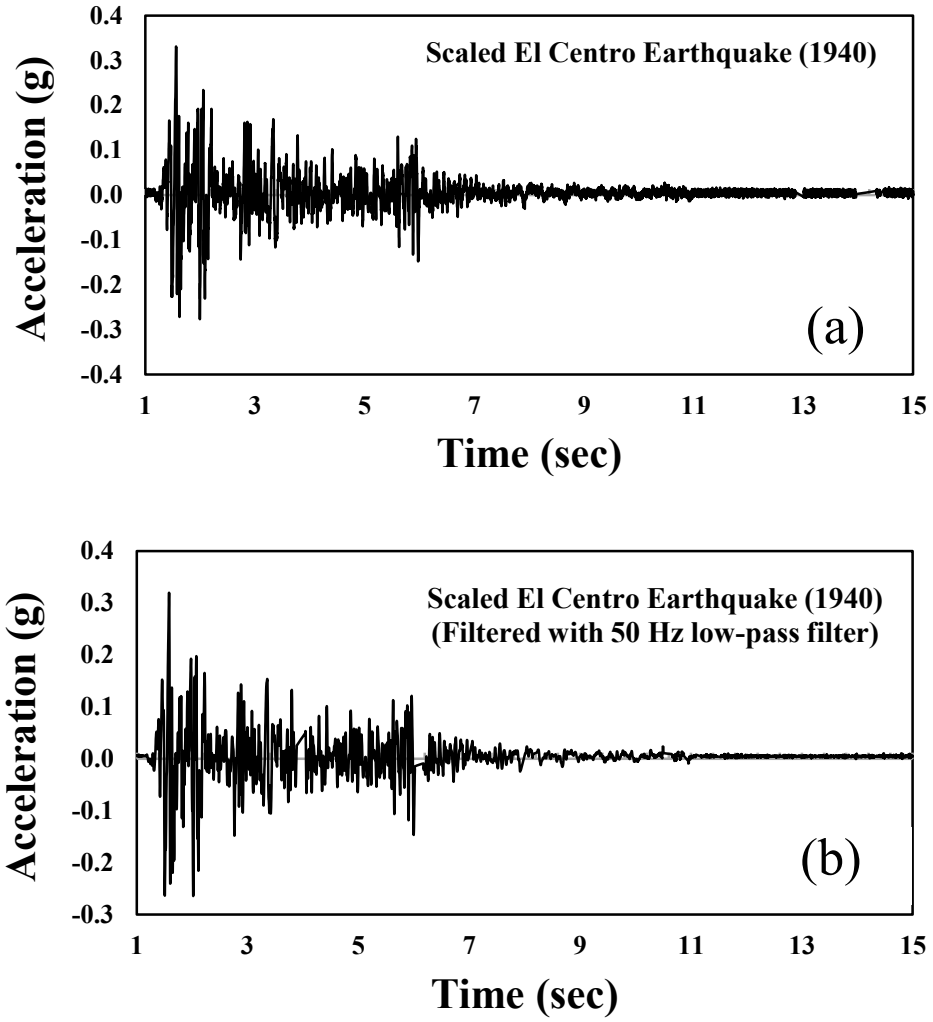


**Figure 3.12** (a) Unfiltered acceleration records of scaled 1940 El Centro earthquake subjected to the 50 Hz low-pass filter; (b) filtered acceleration records of scaled 1940 El Centro earthquake subjected to the 50 Hz low-pass filter

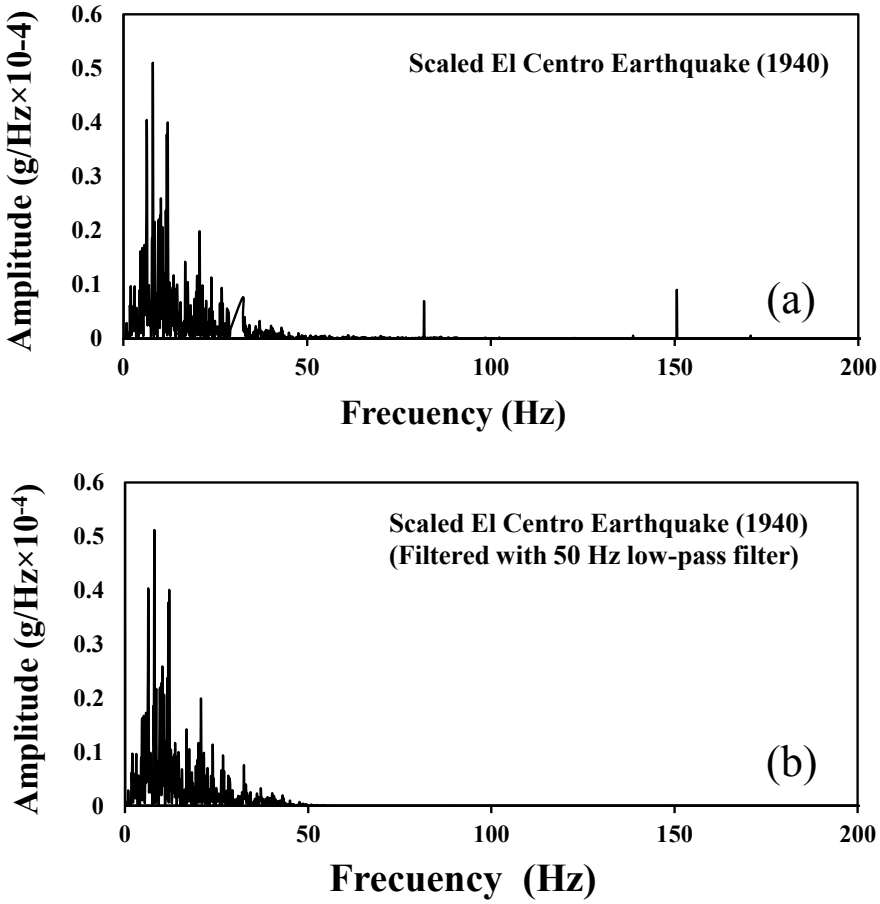


**Figure 3.13** (a) Unfiltered frequency content of scaled 1940 El Centro earthquake subjected to the 50 Hz low-pass filter; (b) filtered frequency content of scaled 1940 El Centro earthquake subjected to the 50 Hz low-pass filter.

Earthquake records can be applied to the model boundaries in terms of accelerations, velocities or forces. If an acceleration or velocity record from a site is used as a time-history, the numerical model may exhibit continuing velocity or residual displacements after the motion has finished. This arises from the fact that the integral of the complete time-history may not be zero. For example, the time-history record of the scaled 1940 El Centro earthquake (Figure 3.12b) after integration produces the time-dependent velocity and the displacement curves as shown in Figure 3.14a and 3.14b, respectively.

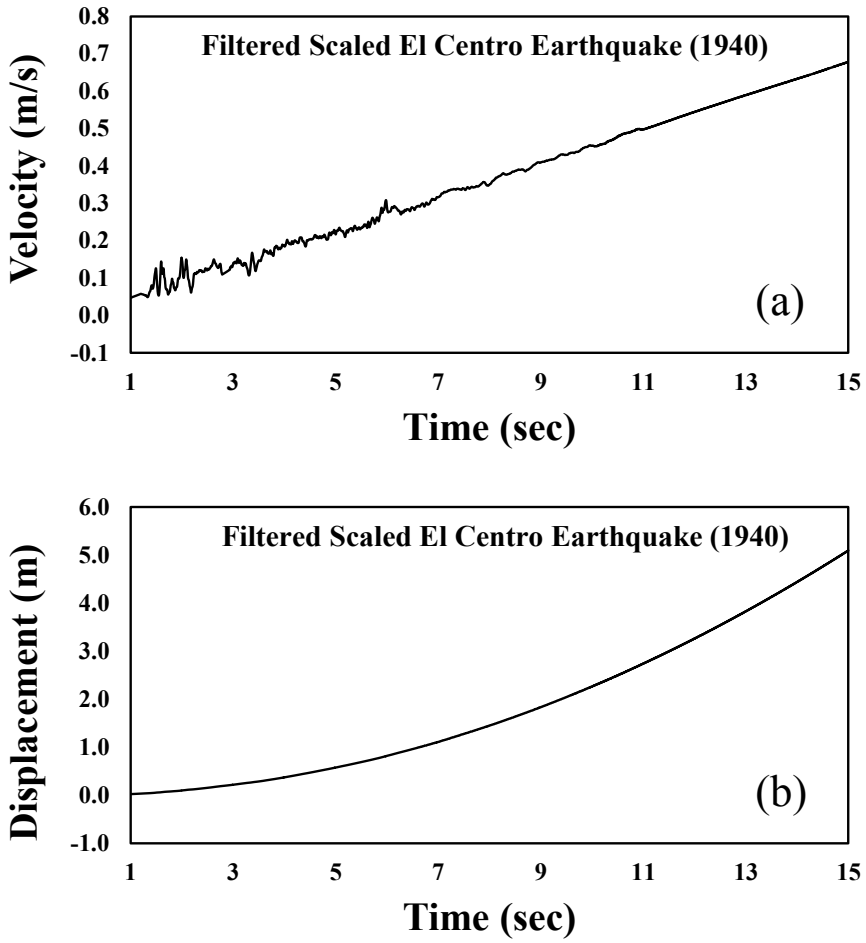


**Figure 3.14** (a) time-history velocity record of scaled 1940 El Centro earthquake; (b) time-history displacement record of scaled 1940 El Centro earthquake

It is possible to define a low frequency wave (Figure 3.15) which, when added to the original history, produces a final displacement of zero (Figure 3.16b). This process, which is called "baseline correction", is applied to correct the input motion before time-history analysis, although the physics of the numerical simulation usually will not be affected if it is not done (Akkar and Boore, 2009; Itasca, 2009). Boore (2001) mentioned that the residual displacements derived from the earthquake records can be sensitive to the choice of baseline correction, but the response of oscillators with periods less than about 20 sec are usually not sensitive to the baseline corrections. This is good news for engineering purposes, for which most structures are not influenced by such long periods.

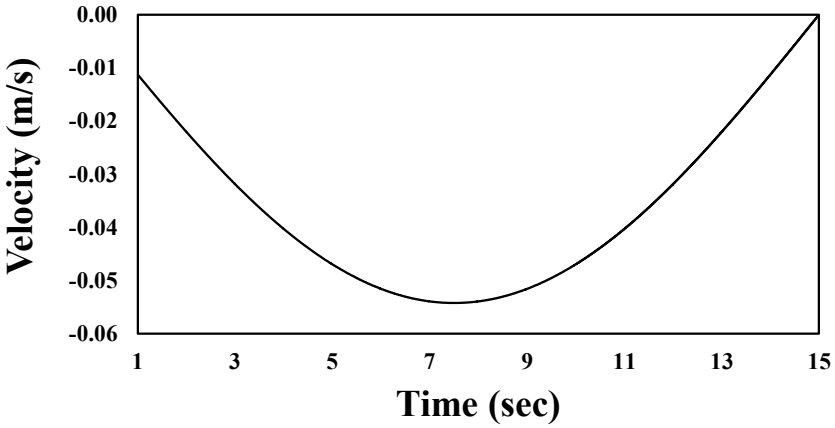


**Figure 3.15** Low frequency velocity wave for baseline correction

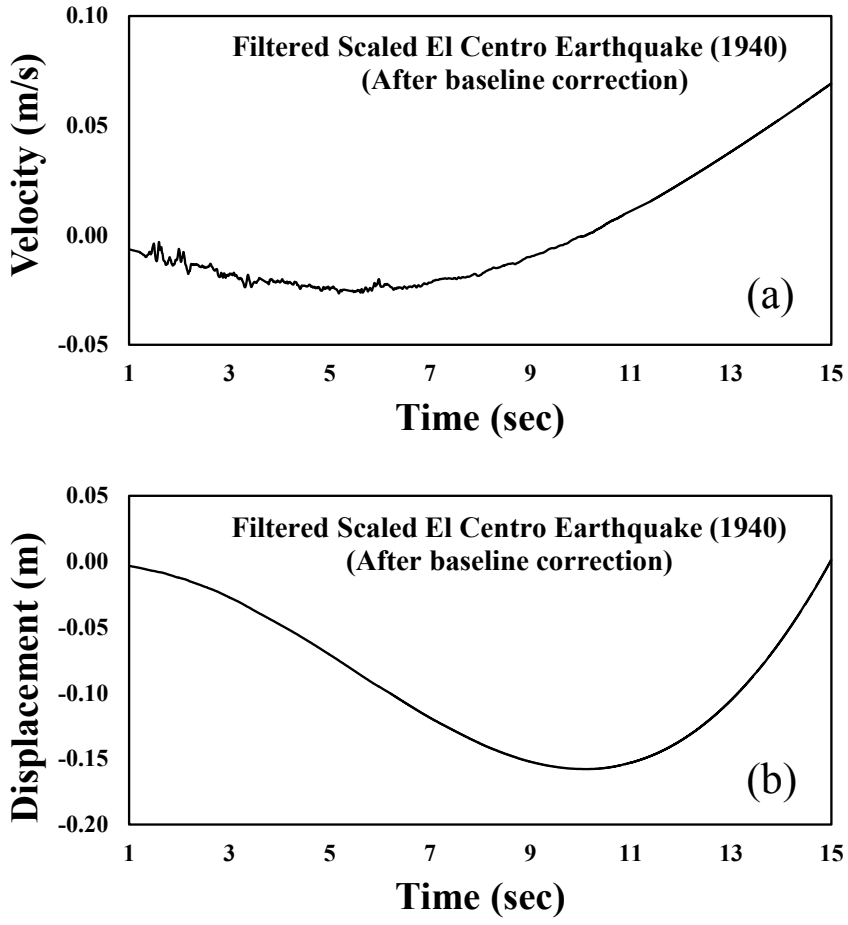


**Figure 3.16** (a) time-history velocity record of scaled 1940 El Centro earthquake after baseline correction; (b) time-history displacement record of scaled 1940 El Centro earthquake applying baseline correction

Eventually, after applying above mentioned filtration and baseline correction, the desired earthquake records are imposed to the entire base of the numerical model horizontally.

## 3.10 Summary

In this chapter, the characteristics of the developed 3D numerical model using FLAC3D to investigate the influence of SSPSI on the behaviour of superstructures under seismic loads have been explained. The developed numerical model performs SSPSI analysis in a fully coupled manner, without resorting to independent calculations of site or superstructure response, or application of pile group interaction factors. The main feature of the developed numerical modelling is incorporating the nonlinear behaviour of both soil and structural elements simultaneously during the three-dimensional numerical analysis.

Nonlinear Mohr-Coulomb model has been adopted in this study to simulate the nonlinear soil behaviour and possible shear failure in the soil elements during the excitation. Moreover, hysteretic damping of the soil is implemented to represent the variation of the shear modulus reduction factor and the damping ratio of the soil with the cyclic shear strain.

Solid elements are adopted to simulate the pile foundation, where an elastic-perfectly plastic behaviour with yielding criteria is considered. In addition, plastic moment capacity is exercised in the beam structural elements (beamSELs) to account for inelastic behaviour of the structural elements.

Adjusting the boundary conditions for the static analysis, in which the system is under the gravity loads only, the bottom face of the model is fixed in all directions, while the side boundaries are fixed in the horizontal direction. During the dynamic time-history analysis, in order to avoid reflection of outward propagating waves back into the model, quiet (viscous) boundaries comprised of independent dashpots in the normal and shear directions are placed at the lateral boundaries of the soil medium. Employing appropriate viscous dashpots, the lateral boundaries of the main grid are coupled to the free-field grids at the sides of the model to simulate the free field motion which would exist in the absence of the structure and the pile foundation.

Due to the different characteristics of the soil and the superstructure/piles, sliding and separation may occur at the soil-structure interfaces. Two sets of interface elements are modelled in this study. For the shallow foundation case, the interface elements are placed between the foundation and the soil surface. However, for the pile foundation case, the interface elements were attached to the outer perimeter of the piles. The adopted interfaces were modelled as spring–slider systems, while the shear strength of the interfaces was defined by Mohr–Coulomb failure criterion.

In this study, the developed 3D numerical model is used to simulate and investigate the influence of the soil-pile-structure interaction on the seismic response of building frames. The proposed numerical soil-structure models are verified and validated against the conducted experimental shaking table test (Chapter 4).

# Chapter 4- SHAKING TABLE EXPERIMENTS

## 4.1 General

Model tests in geotechnical engineering offer the advantage of simulating complex systems under controlled conditions providing the opportunity of better understanding the fundamental mechanisms of these systems. Such tests are often used as calibration benchmarks for numerical or analytical methods, or to make quantitative predictions of the prototype response (Rayhani et al., 2008). In most previously conducted shaking table tests (e.g. Chau et al., 2009; Ishimura et al., 1992; Jakrapiyanun, 2002; Pitilakis et al., 2008) the superstructure is simplified as a single degree of freedom oscillator in which the behaviour of the soil-structure system may not be completely conforming to reality and the effect of higher modes would not be captured. In the current model tests, unlike the previous efforts, a multi-storey frame for the superstructure is adopted, representing the dynamic properties of the prototype structure such as natural frequency of the first and higher modes, number of stories, and density. Moreover, an advanced laminar soil container is designed to simulate the free field soil response by minimising the boundary effects. Consequently, in the current shaking table tests, by adopting the same soil properties, same superstructure, same input motions, and same test setup, a clear comparison is provided between the structural responses for different types of foundations (i.e. shallow foundation, floating pile foundation, end-bearing pile foundation). In addition, further experimental tests were conducted to investigate the influence of SSPSI on the dynamic response of buildings with various heights (i.e. five storey, ten storey, and fifteen storey buildings).

The experimental model tests were carried out utilising the shaking table facilities located at structures laboratory of the University of Technology Sydney (UTS). Table 4.1 summarises the specifications of UTS shaking table.

**Table 4.1** UTS shaking table specifications

| | |
|---|---|
| Size of table | 3m × 3 m |
| Maximum Payload | 10 tonnes |
| Overturning Moment | 100 kN-m |
| Maximum Displacement | ±100 mm |
| Maximum Velocity | ±550 mm/sec |
| Maximum Acceleration | ±2.5g or 0.9g (full load) |
| Testing Frequency | 0.1 – 100 Hz |

## 4.2 Prototype Characteristics

A fifteen storey concrete moment resisting building frame with the total height of 45 m and width of 12 m consisting of three spans in each direction, representing the conventional types of mid-rise moment resisting buildings, is selected for this study. The spacing between the frames into the page is 4 m. Natural frequency of the prototype building is 0.384 Hz and its total mass is 953 tonnes. The structural sections are specified after conducting the routine design procedure as regulated in the relevant building codes. For this purpose, SAP2000(CSI, 2010) software is employed. Details of the designing process have been explained in Section 6.2. The soil medium beneath the structure is a clayey soil with the shear wave velocity of 200 m/s and density of 1470 kg/m$^3$. As discussed in Section 3.7, the horizontal distance of the soil lateral boundaries and bedrock depth was selected to be 60 m and 30 m, respectively.

Aiming to evaluate and quantify the effect of foundation type on the response of structures considering SSI, which is significantly important on the performance based design of structures, four different cases were modelled on the shaking table test, as follows:

- Fixed-base structure representing the situation excluding the soil-structure interaction (Figure 4.1a).
- Structure supported by shallow foundation on the soft soil, in which the structural frame is sitting on a footing with 1 m thickness and 15 m width (Figure 4.1b).

- Structure supported by floating pile foundation in the soft soil, in which a 4×4 reinforced concrete pile group with pile diameter and length of 1.2 m and 20 m, respectively, is adopted (Figure 4.2a).
- Structure supported by end-bearing pile foundation in the soft soil, in which a 4×4 reinforced concrete pile group with pile diameter and length of 1.2 m and 30 m, respectively, is adopted. (Figure 4.2b).

In the pile foundation cases, piles are closed-end and have rigid connection with the pile cap. Moreover, the end-bearing piles are embedded into the bedrock representing typical end-bearing pile foundations. It should be noted that in the pile foundation cases, some gap between the foundation and the surface soil is allocated to avoid any pile-raft behaviour. Therefore, there is no direct stress transfer between the foundation slab and the subsoil in the pile foundation cases.

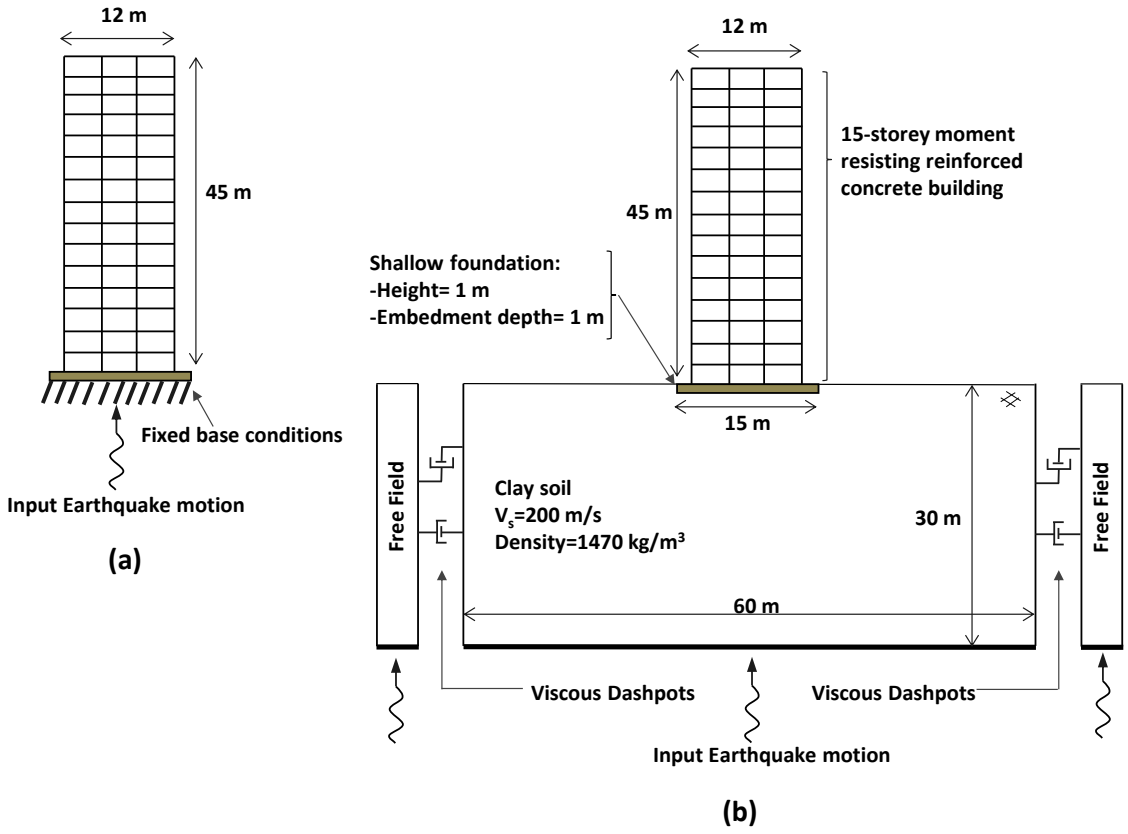


**Figure 4.1** (a) Prototype fixed-base structure; (b) prototype structure supported by shallow foundation

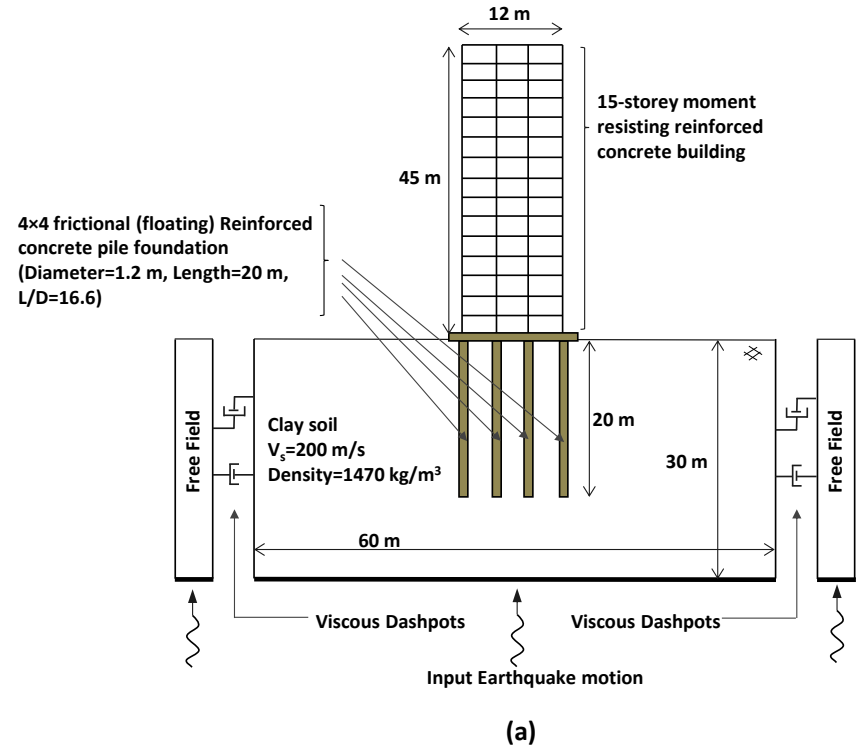


**Figure 4.2** (a) Prototype structure supported by floating (frictional) pile foundation; (b) prototype structure supported by end-bearing pile foundation

In addition to the above mentioned cases, further shaking table tests were carried out in this study (Section 4.11) to experimentally investigate the influence of SSPSI on the dynamic response of buildings with various heights. For this purpose, three moment resisting building frames with total heights of 15 m (five storey), 30 m (ten storey), and 45 (fifteen storey) supported by end-bearing pile foundations are modelled, and results are compared with the fixed-base assumption.

## 4.3 Scaling Factors for Shaking Table Tests

The use of scaled models in engineering offers the advantage of simulating complex systems under controlled conditions and studying their behaviour in the feasible and economical way. For such applications, it is necessary to have a set of scaling relations relating the observed model and predicted prototype behaviours (Meymand, 1998). Scale models can be defined as having geometric, kinematic, or dynamic similarities to the prototype (Langhaar, 1951; Sulaeman, 2010). Geometric similarity defines a model and prototype with homologous physical dimensions. Kinematic similarity refers to a model and a prototype with homologous particles at homologous points at homologous times. Dynamic similarity describes a condition where homologous parts of the model and prototype experience homologous net forces.

Scale models meet the requirements of similitude to the prototype to differing degrees, and researchers may apply nomenclature such as “true”, “adequate”, or “distorted” to the model (Moncarz and Krawinkler, 1981). A true model fulfils all the similitude requirements. An adequate model correctly scales the primary features of the problem, with secondary influences allowed to deviate while the prediction equation is not significantly affected. Distorted models refer to those cases in which deviation from similitude requirements distorts the prediction equation, or where compensating distortions in other dimensionless products are introduced to preserve the prediction equation.

In addition, Moncarz and Krawinkler (1981) elucidated that in 1-g scale modelling, where, $\rho$ is density, $E$ is modulus of elasticity, $a$ is acceleration, and $g$ is gravitational acceleration, the dimensionless product $a/g$ (Froude’s number) must be kept equal to unity implying that the ratio of model to prototype specific stiffness ($E/\rho$)

is equal to the geometric scaling factor λ. This is known as "Cauchy condition" which can also be stated in terms of shear wave velocity as follows:

$$\frac{(V_S)_p}{(V_S)_m} = \sqrt{\lambda} \tag{4.1}$$

where, subscripts *p* and *m* stand for prototype, and model, respectively, and $V_s$ is shear wave velocity. Satisfying the Cauchy condition is a necessary requirement for simultaneous replication of restoring forces, inertial forces, and gravitational forces in a dynamic system (Moncarz and Krawinkler, 1981).

Iai (1989) derived a comprehensive set of scaling relations for a soil-structure system under the dynamic loading and defined the entire problem in terms of geometric, density, and strain scaling factors. This method relates the geometric ($\lambda$) and density ($\lambda_p$) scaling factors, and then derives the strain scaling factor ($\lambda_\varepsilon$) from shear wave velocity tests on both the model and prototype soil, as presented in Equation (4.2).

$$\lambda_\varepsilon = \left[ \frac{\lambda}{(\frac{(V_S)_p}{(V_S)_m})^2} \right] \tag{4.2}$$

Meymand (1998) and Moss et al. (2010) explained that no governing equation can be written describing the entire soil-structure system, nor can dimensional analysis or similitude theory be directly applied to this complex system to achieve "true" model similarity. The viable scale modelling approach for application of scale model similitude therefore consists of identifying and successfully modelling the primary forces and processes in the system, while suppressing secondary effects, thereby yielding an "adequate" model.

Several researchers (e.g. Meymand, 1998; Turan, 2009; Moss et al., 2010) pointed out that in order to achieve an adequate model for the dynamic soil-structure interaction simulation in shaking table tests, Cauchy condition (Equation 4.1), should be satisfied. In addition, the strain scaling factor ($\lambda_\varepsilon$) should be kept equal to one. It should be noted that when Cauchy condition is satisfied, obviously, the result of substituting the value of $(V_s)_p/(V_s)_m$ from Equation (4.1) into Equation (4.2) is equal to one.

The objective of the scale modelling procedure for this test program is to achieve "dynamic similarity", where model and prototype experience homologous forces. For this purpose, adopted methodology by Meymand (1998) is the framework for scale model similitude in this study. According to this approach, three principle test conditions establish many of the scaling parameters. The first condition is that testing is conducted in a 1-g environment, which defines model and prototype accelerations to be equal. Secondly, a model with similar density to the prototype is desired, fixing another component of the scaling relations. Thirdly, the test medium is primarily composed of saturated clayey soil, whose undrained stress-strain response can be reasonably assumed independent of confining pressure, thereby simplifying the constitutive scaling requirements. In addition to the above mentioned three principle test conditions, Meymand (1998) pointed out that the natural frequency of the prototype should be scaled by an appropriate scaling relation.

By defining scaling conditions for density and acceleration, the mass, length, and time scale factors can all be expressed in terms of the geometric scaling factor (λ), and a complete set of dimensionally correct scaling relations (ratio of prototype to model) can be derived for all variables being studied. The scaling relations for the variables contributing to the primary modes of system response are shown in Table 4.2 (e.g. Meymand, 1998; Turan, 2009; Moss et al., 2010; Sulaeman, 2010; Lee et al., 2012).

**Table 4.2** Scaling relations in terms of geometric scaling factor (λ)

| | | | | | |
|---|---|---|---|---|---|
| Mass Density | **1** | Acceleration | **1** | Length | **λ** |
| Force | $\boldsymbol{\lambda^3}$ | Shear Wave Velocity | $\boldsymbol{\lambda^{1/2}}$ | Stress | **λ** |
| Stiffness | $\boldsymbol{\lambda^2}$ | Time | $\boldsymbol{\lambda^{1/2}}$ | Strain | **1** |
| Modulus | **λ** | Frequency | $\boldsymbol{\lambda^{-1/2}}$ | EI | $\boldsymbol{\lambda^5}$ |

According to Table 4.2, the shear wave velocity scaling factor ($(V_s)_p/(V_s)_m$) is equal to $\lambda^{1/2}$. Therefore, Cauchy condition (Equation 4.1) is met in the scaling relations. In addition, strain scaling factor ($\lambda_\varepsilon$), which can be determined by substituting the value of $(V_s)_p/(V_s)_m$ from Equation (4.1) into Equation (4.2), is kept equal to one. Thus, as mentioned earlier, both requirements for achieving an adequate model for the dynamic soil-structure interaction simulation in shaking table tests are satisfied

Adopting an appropriate geometric scaling factor (λ) is one of the important steps in scale modelling on shaking table tests. Although small scale models could save cost, the precision of the results could be substantially reduced. Considering the mentioned specifications of UTS shaking table, scaling factor of 1:30 provides the largest achievable scale model with rational scales, maximum payload, and overturning moment meeting the facility limitations. Thus, geometric scaling factor (λ) of 1:30 is adopted for experimental shaking table tests on the scale model in this study. According to Table 4.2, apart from the geometric scaling which should be imposed to all the components, the required scaled natural frequency for the structural model and the required scaled shear wave velocity and density of the soil mix should be 2.11 Hz, 36 m/s and 1470 kg/m$^3$, respectively. Moreover, the required scaled natural frequency of the soil mix inside the soil container needs to be 10 Hz which is used as a benchmark to design the laminar soil container. The application of the scaling relations in developing the different components of the model soil-pile-structure system is discussed in the following sections.

## 4.4 Model Components of Shaking Table Tests

The developed soil-structure model for shaking table tests possesses four main components including the model structure, the model pile foundations, the laminar soil container, and the soil mix together with the imposed shaking events. Details and characteristics of these components are explained below.

### 4.4.1 Model Structure

Employing geometric scaling factor of 1:30, height, length, and width of the structural model are determined to be 1.50 m, 0.40 m, and 0.40 m, respectively. In addition, according to the scaling relationship as shown in Table 2, the required natural frequency of the structural model is 2.11 Hz. Moreover, the density of the model and prototype should be equal. Thus, the total mass of 106 kg for the model structure is obtained. It should be noted that, considering the required scaled dimensions and dynamic properties for the model structure, constructing the model structure from reinforced concrete material is not feasible. Therefore, equivalent steel model

structure, which is constructible and adjustable to the test environment, is adopted following the required scaled characteristics.

In order to simulate the prototype structure more accurately on the shaking table, the model structure was preliminary designed employing SAP2000 (CSI, 2010) software considering the required characteristics of the model structure. The 3D numerical model consists of fifteen horizontal steel plates as the floors and four vertical steel plates as the columns. Steel plate grade 250, according to Australian standards (AS/NZS3678, 2011), with the minimum yield stress of 280 MPa and the minimum tensile strength of 410 MPa, was adopted in the design. The thickness of the steel plates was determined in the design process after several cycles of trial and error in order to fit the required natural frequency and mass of the model structure. The finalised base plate is a 500×500×10 mm steel plate while the floors consist of 400×400×5 mm plates and four 500×40×2 mm steel plates are used for the columns. The connections between the columns and floors are provided using stainless steel metal screws with 2.5 mm diameter and 15 mm length. After the numerical modelling and design, the structural model was constructed in house. The completed structural model is shown in Figure 4.3.


**Figure 4.3** The completed model structure for shaking table tests

### 4.4.2 Model Pile Foundation

Similar to the model structure, the model pile should be subjected to the competing scale model criteria. In order to achieve a successful model pile design, the principle governing factors of pile response such as slenderness ratio L/d, moment curvature relationship, flexural stiffness EI, relative soil/pile stiffness, yielding behaviour/mechanism, and natural frequency of vibration should be addressed (Meymand, 1998). By adopting the geometric similitude, the overall pile slenderness and relative contact surface area would be preserved in the model. This also guarantees that pile group relative spacing and consequent group interaction would be replicated at the model scale. Thus, by considering the geometric scaling factor ($\lambda$) of 1:30 in this study, the model piles should have a diameter of 40 mm with L/d ratio of 16.6 and 25 for the floating and end-bearing pile foundations, respectively.

The moment-curvature relation criterion represents pile response to the lateral loading which is a function of the flexural rigidity and the yielding behaviour. Since in the present study piles are intended to respond in the elastic range (this assumption is confirmed numerically), this criterion is achieved by scaling the flexural rigidity (*EI*) of the piles according to Table 2 ($\lambda^5$, $\lambda=1/30$) in addition to ensuring that the yielding point of the model pile is equal to or greater than the scaled prototype. Furthermore, by scaling the stiffness of the soil and pile consistently, the relative soil/pile stiffness parameter will be satisfied inevitably. Therefore, the soil-pile interaction should then be accurately reproduced in the model.

Previous researchers (e.g. Bao et al., 2012; Chau et al., 2009; Tao et al., 1998) used different types of materials like aluminium tubes, steel bars, and reinforced concrete to build a model pile. Considering the selected scaling factor in this study ($\lambda=1/30$) and in turn the required stiffness and yielding stress for the model piles, a commercial Polyethylene high pressure pipe with Standard Dimension Ratio (SDR) of 7.4 according to the Australian Standard (AS/NZS4130, 2009), is the selected candidate which falls in the range of acceptable criteria with 5% deviation from the target value for EI. Moreover, Polyethylene pipes can tolerate large deformation prior to the yielding without any brittle failure. Characteristics of the model pile used in this study are summarised in Table 4.3.

**Table 4.3** Characteristics of the model pile built from Polyethylene pressure pipe

| | | | |
|---|---|---|---|
| Outer Diameter (mm) | 40 | Young's modulus (MPa) | 1.16E+3 |
| Wall Thickness (mm) | 5.5 | Density (kg/m$^3$) | 955 |
| Cross-sectional Area (mm$^2$) | 5.78E+2 | Poisson's ratio | 0.4 |
| Moment of Inertia (mm$^4$) | 8.33E+4 | Flexural yield stress (MPa) | 32 |

### 4.4.3 Soil Mix

A synthetic clay mixture was designed to provide soil medium for the shaking table testing. Previous researchers (e.g. Meymand, 1998; Turan et al., 2009; Moss et al., 2010) reported that a reconstituted soil would not be able to satisfy the competing scale modelling criterion of shear wave velocity with enough bearing capacity for the

foundation in shaking table tests while synthetic clay mix can provide adequate undrained shear strength to mobilise the required bearing capacity underneath the structural model meeting the scale modelling criterion of the shear wave velocity. It should be noted that, without providing enough bearing capacity for the structural model foundation, the underneath soil may experience failure or excessive settlements while testing process is being undertaken. In order to find out the most appropriate mix for the test program, three different mixes (A, B, and C) were produced and examined in the UTS soils laboratory. The proportion of different mix components for three mixes are summarised in Table 4.4. Mix A, which is the closest mix to what was proposed by Meymand (Meymand, 1998), has higher percentages of kaolinite and bentinite, lower percentage of class F fly ash and lime, and the same percentage of water content compared to Mix B. Mix B and Mix C have the same dry component percentages, but the water content was increased by 20% in Mix C in comparison to Mix B in order to achieve better mixibility and workability for the mix.

**Table 4.4** Proportion of different components for the examined mixtures

| Mix Components | Mix A | Mix B | Mix C |
|---|---|---|---|
| Q38 kaolinite clay | 67.5 % | 60 % | 60 % |
| ActiveBond 23 bentonite | 22.5 % | 20 % | 20 % |
| Class F fly ash+ Lime† | 10 % | 20% | 20% |
| Water * | 100% | 100% | 120% |

* % of the dry mix weight.

† Weight ratio of lime to dry class F fly ash is 4:1

During the mixing procedure, first dry kaolinite and bentonite were added to the mixing container and mixed in dry condition using spatula. Then, fly ash and lime, which had been combined separately, added to the dry mix and completely mixed using spatula in order to form a homogenous dry mix. Afterwards, water was added in a slow and successive manner while the whole components were being mixed inside the mixing container. Alternating hand and mechanical mixing was introduced to ensure a homogenous mix for all samples. The resulting mixtures were of reasonable workability for placement into the moulds; particularly, Mix C had the

highest workability among the other mixtures. In an effort to minimise entrapped air and to provide compaction, the mixture was placed into the mould in several layers and worked into the mould with palette knives (Figure 4.4).

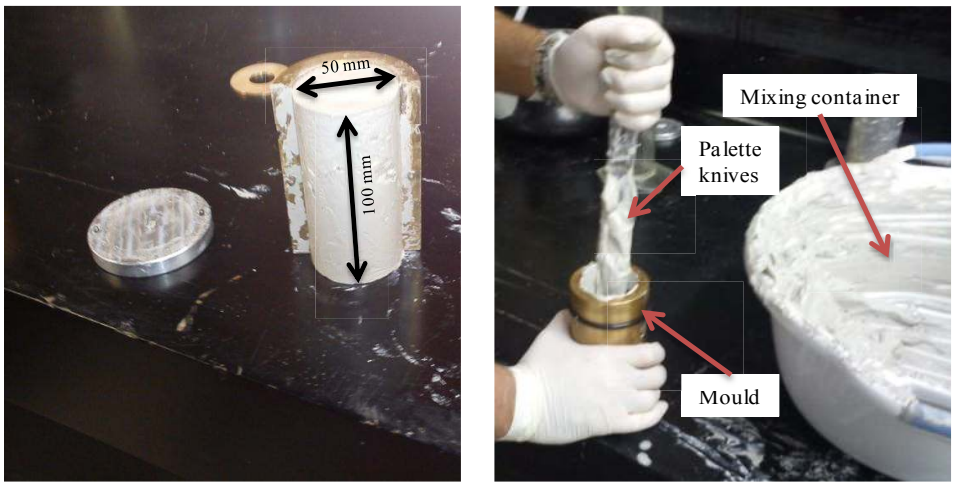


**Figure 4.4** Soil mix cylindrical test specimen; (b) placing the mixtures into the mould with palette knives

Each proposed mix was prepared three times to control repeatability of the test and each time three cylindrical test specimens of size D=50 mm and h=100 mm were taken for the bender element test which was performed to measure the shear wave velocity of the soil over the curing age. The elapsed time from specimen preparation to testing is termed “curing age”. To carry out bender element tests, the soil specimens were placed between bender elements as shown in Figure 4.5a; and the shear wave velocity of each soil specimen was obtained by measuring the time required for the wave to travel between two bender elements using PC running GDS bender element control software. The adopted system has a data acquisition speed of 2 MSamples/s, 16 bit resolution of data acquisition and the connection to the control box through USB link. In this study, the propagated shear wave type was sine waves with amplitude of 10 V and a period of 1 second. Figure 4.5b shows the schematic graphical signal processing to measure the shear wave travel time at the bender element test.

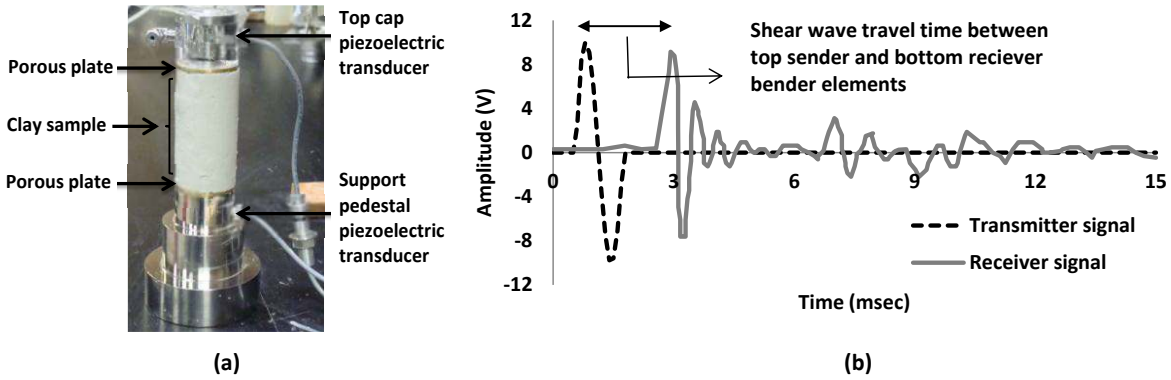


**Figure 4.5** (a) Bender element test setup; (b) schematic graphical signal processing to measure the shear wave travel time between the sender and receiver bender elements

The extracted average shear wave velocities versus curing ages for the three different mixes over the period of two weeks are illustrated in Figure 4.6. As shown in Figure 4.6, the examined soil mixes gain stiffness, and consequently shear wave velocity increases with the curing age as expected (e.g. Wartman, 1996; Riemer et al., 1998; Moss et al., 2010). However, only Mix C produces the required shear wave velocity of 36 m/s for the soil model on the second day of its curing age while the other two mixes are unable to produce such a low shear wave velocity as required. In addition, in order to ensure that the undrained shear strength of the proposed soil mix is adequate to satisfy the required foundation bearing capacity underneath the structural model, Unconfined Compression Tests were performed on three soil specimens in accordance with AS5101.4-2008 (AS5101.4, 2008). Eventually, desired soil mix consisting of 60% Q38 kaolinite clay, 20% Active-bond 23 Bentonite, 20% class F fly ash and lime, and 120% water (% of the dry mix) was adopted for the shaking table tests in this study. Table 4.5 summarises the soil mix properties at the second day of its curing age. Accordingly, soil density on the second day was determined to be 1450 kg/m$^3$ being almost equal to the prototype soil density (1470 kg/m$^3$) as required. Therefore, the designed soil mix possesses the required dynamic similitude characteristics. It should be noted that the prototype soil acquires the properties of the cemented soil that can be found in nature or the treated soil.

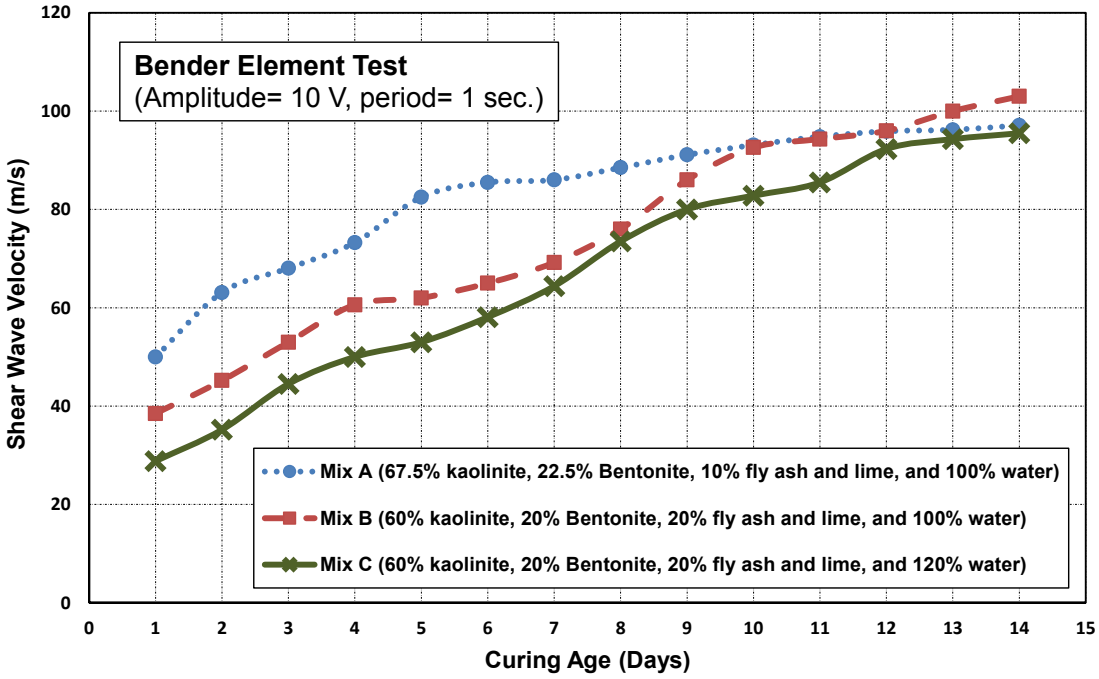


**Figure 4.6** Average shear wave velocity for three mixes obtained from bender element test

**Table 4.5** Properties of the soil mix on the second day of curing

| Soil Properties | Value |
|---|---|
| Mass density (kg/m$^3$) | 1450 |
| Shear wave velocity (m/s) | 36 |
| Maximum shear modulus, $G_{max}$ (kPa) | 1776 |
| Undrained shear strength, $S_u$ (kPa) | 3.1 |
| Liquid Limit, *LL (%)* | 32 |
| Plastic Limit, *PL (%)* | 72 |
| Plasticity Index, *PI (%)* | 42 |

### 4.4.5 Shaking Events

The input ground motions in this study are represented by a set of real earthquakes defined at the outcropping bedrock. Each test model was subjected to two near-field shaking events including 1994 Northridge (Figure 4.7a), 1995 Kobe (Figure 4.7b), two far-field earthquakes including 1940 El Centro (Figure 4.7c), and 1968 Hachinohe (Figure 4.7d), and Sine Sweep test. It is well known that the intensity of shaking

decreases as the distance increases from the seismic fault where the earthquake shaking is generated (Towhata, 2008). In addition, high frequency components lose energy more quickly than low frequency components while traveling through the ground. As a result, near-field earthquakes generate higher ground peak acceleration and frequency component in comparison with the far-field earthquakes. The characteristics of the mentioned earthquakes suggested by the International Association for Structural Control and Monitoring for benchmark seismic studies (Karamodin and Kazemi, 2010) are summarised in Table 4.6.

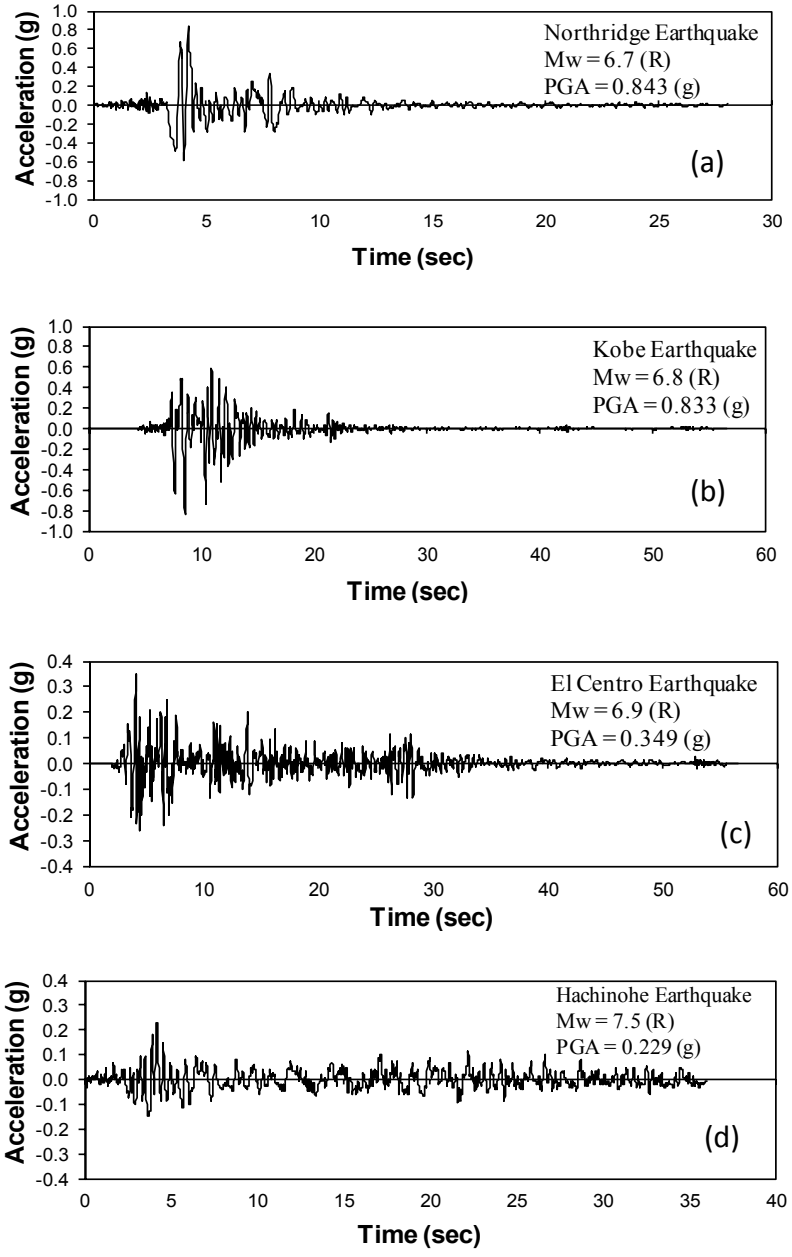


**Figure 4.7** Utilised earthquake records in this study: (a) 1994 Northridge earthquake; (b) 1995 Kobe earthquake; (c) 1940 El Centro earthquake; (d) 1968 Hachinohe earthquake

**Table 4.6** Characteristics of the utilised earthquake base motions

| Earthquake | Country | Year | PGA (g) | Mw (R) | Duration (s) | Type | Hypocentral Distance* (km) |
|---|---|---|---|---|---|---|---|
| Northridge | USA | 1994 | 0.843 | 6.7 | 30.0 | Near-field | 9.2 |
| Kobe | Japan | 1995 | 0.833 | 6.8 | 56.0 | Near-field | 7.4 |
| El Centro | USA | 1940 | 0.349 | 6.9 | 56.5 | Far-field | 15.69 |
| Hachinohe | Japan | 1968 | 0.229 | 7.5 | 36.0 | Far-field | 14.1 |

* Obtained from PEER (PEER, 2012)

Referring to Table 4.2, in order to scale the shaking events, although the model earthquake magnitude remains the same as the prototype, time intervals of the original records should be reduced by the factor of 5.48 ($\lambda^{1/2}$, $\lambda=1/30$) which means that the scaled earthquakes contain higher frequencies and shorter durations. The scaled acceleration records of the four adopted earthquakes together with the relevant frequency content obtained from Fast Fourier Transform are illustrated in Figures 4.8a-d.

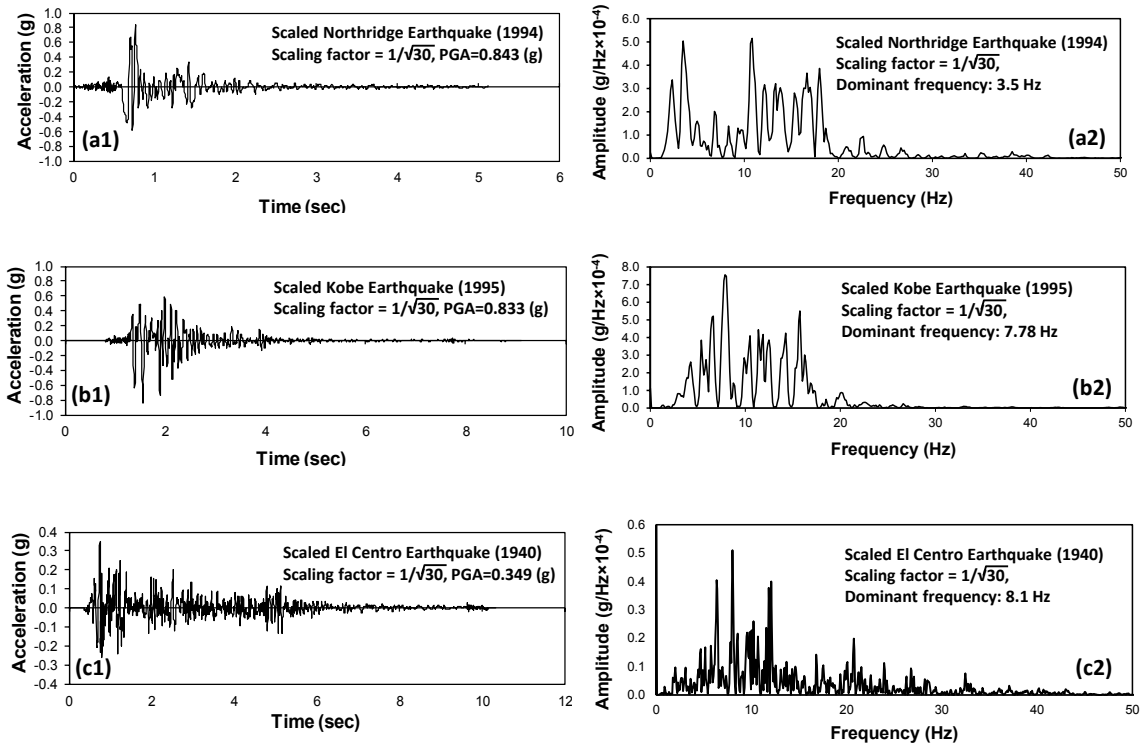

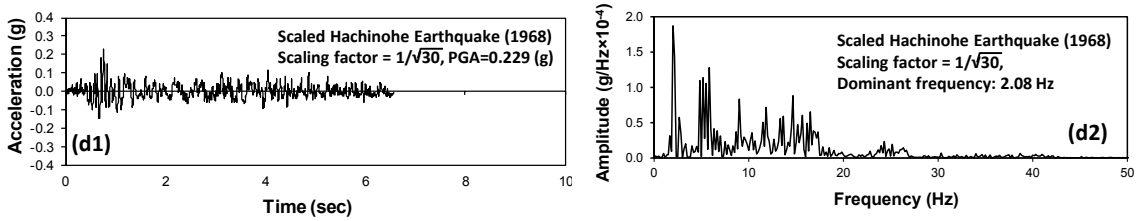


**Figure 4.8** Scaled shaking events adopted in the shaking table experimental tests: (a) scaled 1994 Northridge earthquake; (b) scaled 1995 Kobe earthquake; (c) scaled 1940 El Centro earthquake; (d) scaled 1968 Hachinohe earthquake

In addition, exponential sine sweep wave with amplitude of 0.05g, exponential increase rate of 0.5 Hz/min., and frequency range of 1- 50 Hz was applied to the test models in order to identify the dynamic characteristics of the model. The frequency of the wave as a function of time is obtained employing Equation (4.3), as follows:

$$f = f_0 \times k^t \tag{4.3}$$

where, *f (t)* is the frequency of the wave at time *t, $f_0$* is the starting frequency (at *t*=0), and *k* is the exponential increase rate. Figure 4.9 displays a schematic view of the applied exponential sine sweep waves in this study.

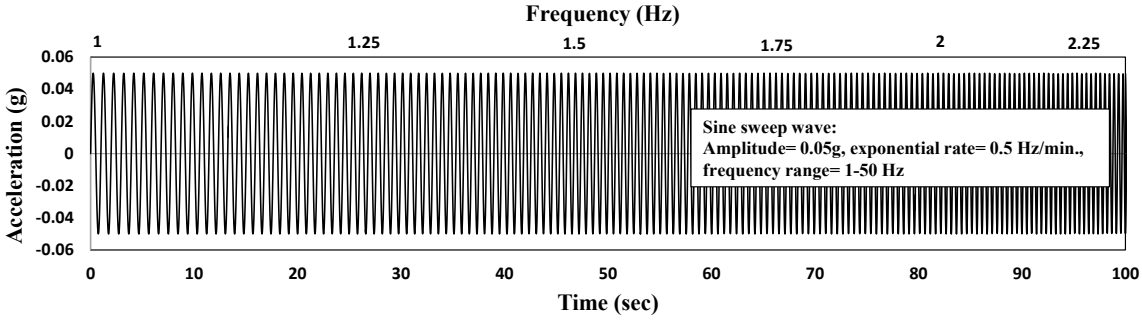


**Figure 4.9** Exponential sine sweep wave adopted in the shaking table experimental tests

## 4.4.6 Laminar Soil Container

In conducting the earthquake model tests, one of the main concerns is the boundary effects created by artificial boundaries of a model container. The premier task of the soil container is to hold the soil in place during imposed excitation and to provide confinement. However, the ideal soil container should simulate the free field soil behaviour as it exists in the prototype, by minimising the boundary effects. The key parameter in the design of the soil container is to satisfy the same dynamic shear

stiffness between the soil container and the adjacent soil deposit in order to achieve the strain similitude. Moreover, this criterion leads to minimising the interaction between the soil and the container during the shaking table test, and avoiding the generation of primary (compressive) waves from the end walls. According to Zeng and Schofield (1996), the same dynamic shear stiffness means that the soil container should have the same natural frequency and deflection as the soil deposit in the model container.

Three-dimensional explicit finite difference based program FLAC3D (Fast Lagrangian Analysis of Continua) version 4.0 (Itasca, 2009) was employed to design the laminar soil container for the shaking table tests. Adopting FLAC3D, fully nonlinear time-history dynamic analysis can be performed to simulate the realistic dynamic behaviour of the soil and the container under seismic excitations. Initially, the extensive uniform soil layer was modelled to predict the response of the soil deposit without being interrupted by the artificial boundaries which was used as a benchmark to design the laminar soil container. Solid elements are employed to model the soil deposit, and free field boundary conditions are applied. Nonlinearity of the soil medium plays a very important role on the seismic behaviour of the soil-pile-structure system (Kim and Roesset, 2004; Maheshwari and Sarkar, 2011). The built-in tangent modulus function developed by Hardin and Drnevich (1972) as discussed in Section 3.3.1 is adopted to implement hysteretic damping of the soil representing the variation of the shear modulus reduction factor and damping ratio with cyclic shear strain of the soil. This model is defined as follows:

$$M_s = 1/(1+(\gamma/\gamma_{ref})) \tag{4.4}$$

where, $M_s$ is the secant modulus ($G/G_{max}$), $\gamma$ is the cyclic shear strain, and $\gamma_{ref}$ is Hardin/Drnevich constant. In this study, $\gamma_{ref}$ = 0.234 is adopted representing the backbone curves suggested by Sun et al. (1988) for fine grained soils as illustrated in Section 2.4.1. The maximum deformations of the soil deposit under the four earthquakes are shown in Figure 4.10. In addition, applying the Sine Sweep wave, the natural frequency of the soil deposit is determined to be equal to 10 Hz which was used for the primary design of the laminar soil container.

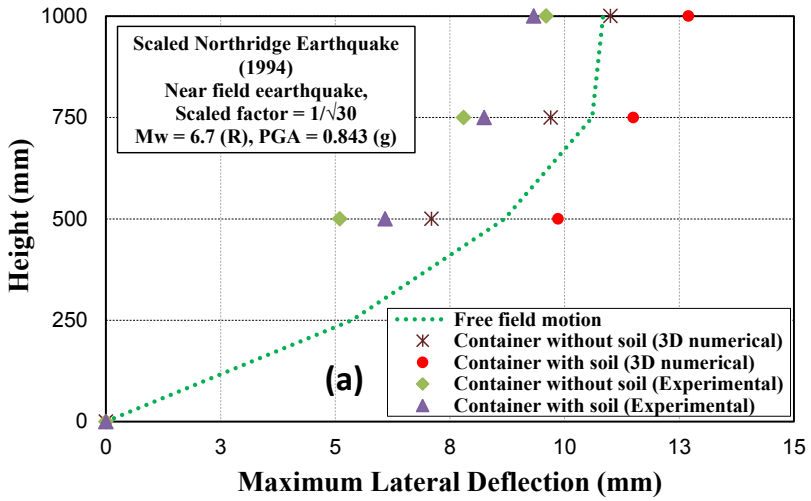
Scaled Northridge Earthquake (1994)
Near field eearthquake,
Scaled factor = 1/√30
Mw = 6.7 (R), PGA = 0.843 (g)
Free field motion
Container without soil (3D numerical)
Container with soil (3D numerical)
Container without soil (Experimental)
Container with soil (Experimental)
(a)
Height (mm)
Maximum Lateral Deflection (mm)
0
250
500
750
1000
0
3
5
8
10
13
15

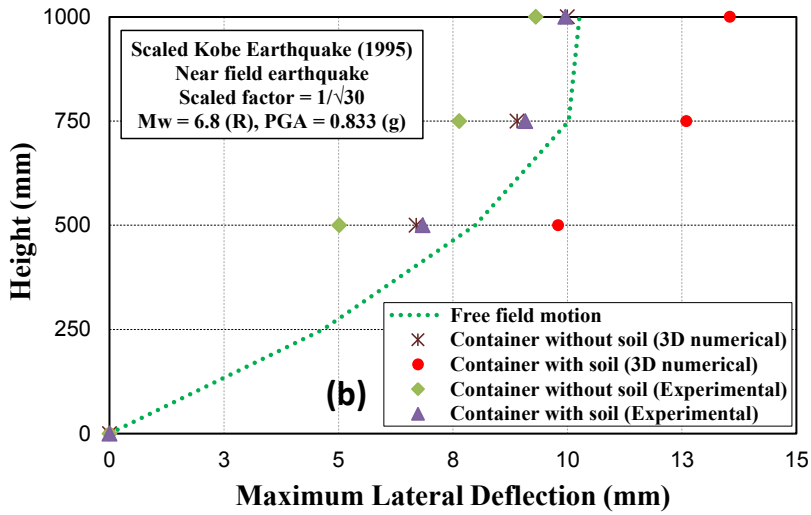
Scaled Kobe Earthquake (1995)
Near field earthquake
Scaled factor = 1/√30
Mw = 6.8 (R), PGA = 0.833 (g)
Free field motion
Container without soil (3D numerical)
Container with soil (3D numerical)
Container without soil (Experimental)
Container with soil (Experimental)
(b)
Height (mm)
Maximum Lateral Deflection (mm)
0
250
500
750
1000
0
3
5
8
10
13
15

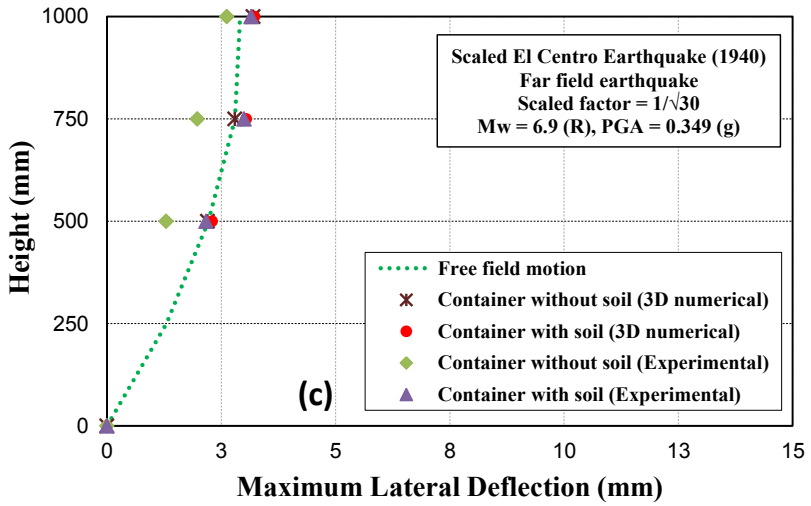
Scaled El Centro Earthquake (1940)
Far field earthquake
Scaled factor = 1/√30
Mw = 6.9 (R), PGA = 0.349 (g)
Free field motion
Container without soil (3D numerical)
Container with soil (3D numerical)
Container without soil (Experimental)
Container with soil (Experimental)
(c)
Height (mm)
Maximum Lateral Deflection (mm)
0
250
500
750
1000
0
3
5
8
10
13
15

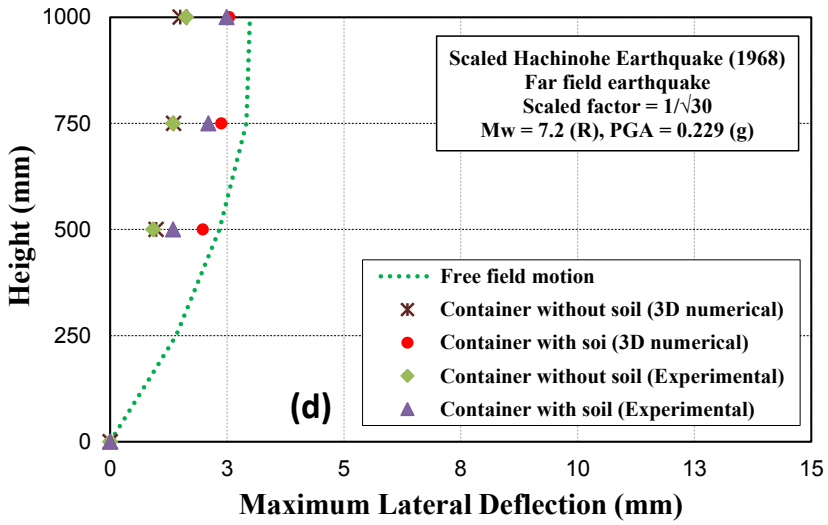


**Figure 4.10** 3D numerical predictions versus experimental measurements of the maximum lateral deformation of the soil container under the influence of: (a) 1994 Northridge earthquake; (b) 1995 Kobe earthquake; (c) 1940 El Centro earthquake; (d) 1968 Hachinohe earthquake

Based on the adopted geometric scaling factor (1:30) and allowing a further 10 mm on each side for construction purposes similar to Prasad et al. (2004), the final length, width, and depth of the laminar soil container are selected to be 2.10 m, 1.30 m, and 1.10 m, respectively. The employed laminar soil container consists of a rectangular laminar box made up of aluminium rectangular hollow section frames separated by rubber layers. The aluminium frames provide lateral confinement of the soil, while the rubber layers allow the container to deform in a shear beam manner. The numerical model components of the container in FLAC3D are shown in Figure 4.11. The predicted maximum deformations of the empty container and the container filled with the desired soil mix are compared with the free field deformation of the soil deposit as shown in Figure 4.10. The employed soil container possesses the natural frequency of 10.8 Hz and 10.4 Hz for the empty and filled conditions, respectively, which is in a good agreement with the predicted value (10 Hz).

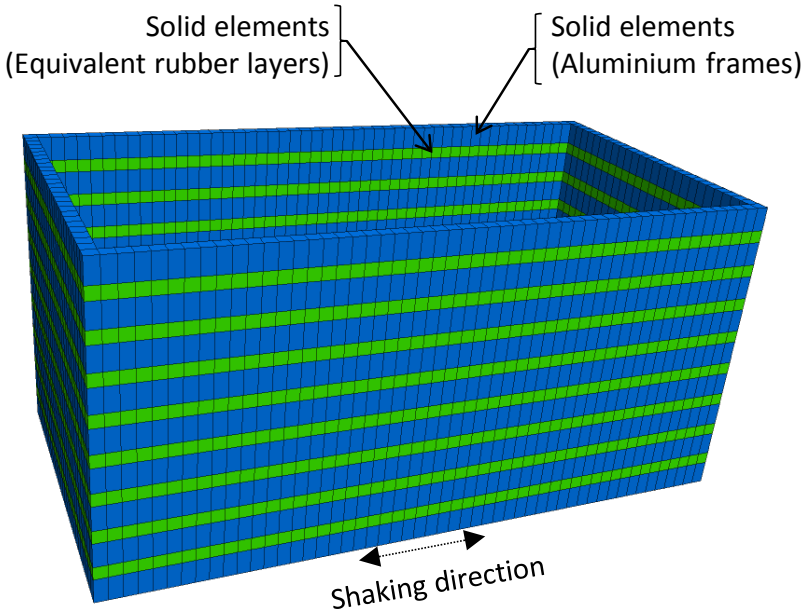


**Figure 4.11** Numerical grid and model components of laminar soil container in FLAC3D

The soil container was constructed in house and the required rubber sections were manufactured specifically for this project. The container was secured on the shaking table using eight M38 bolts passing through the provided holes. The internal surface of the soil container was covered and sealed with two layers of black plastic sheeting. According to Gohl and Finn (1987) and Valsangkar et al. (1991), 25mm thick absorbing layers of Polystyrene foam sheets were installed at the end walls of the soil container to simulate viscous boundaries in the free field condition and minimise the reflection of the outward propagating waves back into the model. In addition, a layer of well graded gravel was glued to the bottom of the soil container to create a rough interface between the soil and the base during the test. This layer provides friction between the timber base plate (as a bedrock) and the in-situ soil mix to aid the transmission of shear waves ensuring negligible relative slip between the soil and the bottom surface of the container. Moreover, the side walls, parallel to the shaking direction, are lubricated to be frictionless in order to avoid the generation of shear stresses on the side walls. Figure 4.12 shows details of the constructed laminar soil container adopted in this study.

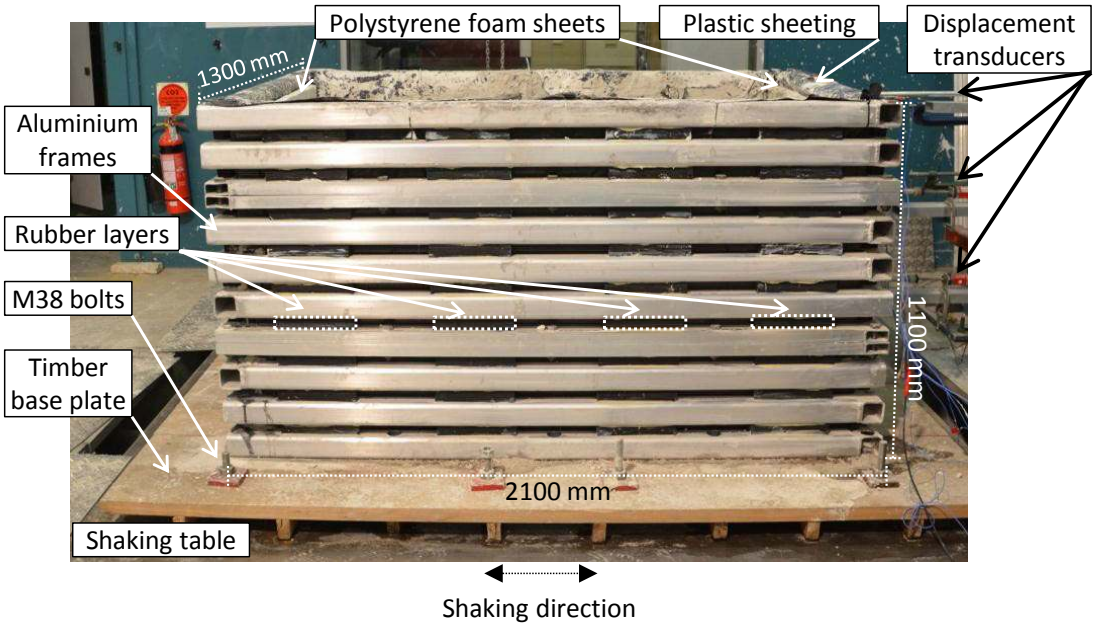


**Figure 4.12** Components of the constructed laminar soil container on the shaking table

As mentioned earlier, the constructed container was exposed to the same shaking events and the results in terms of the maximum lateral deformation are presented in Figure 4.10. Accordingly, measurements are in a good agreement with the predictions confirming the dynamic shear stiffness similarity between the laminar container and the ideal free field behaviour of the soil deposit. As mentioned earlier, the soil deposit has a fully nonlinear behaviour and its stiffness is changing under the cyclic loading; however, the stiffness of the container is constant during a test. As a result, during the excitations with lower shear strain range (smaller deformation), soil dynamic shear stiffness is much closer to the container in comparison to the earthquakes with higher intensity in which more reduction in the initial shear stiffness of the soil is generated (see Figure 2.8) resulting in more disparities in terms of the maximum lateral deformations.

After ensuring the adequacy of the dynamic characteristics of the constructed laminar soil container, 2 cubic meters of the designed soil mix (Mix C: 60% kaolinite, 20% Bentonite, 20% class F fly ash and lime, and water (120% of the dry mix)) was produced and placed into the laminar soil container. As explained in Section 4.4.3, the desired soil mix acquires the required stiffness and consequently the shear wave velocity after two days of curing. As a result, the entire mixing process and filling the

laminar soil container were completed in one day, and the soil mix inside the container was left to be cured for two days while the surface of the soil container was covered and sealed. On the second day, same excitation events were applied to the filled container and results were compared with the predicted values (Figure 4.10).

## 4.5 Instrumentation and Data Acquisition System

Different classes of measuring instruments were utilised in the current shaking table test programme. Displacement transducers (Figure 4.13a) and accelerometers (Figure 4.13b) were used to measure structural deformations and accelerations, respectively. In addition, strain gauges (Figure 4.13c) were installed on the model piles to measure the generated strain and in turn flexural moments along the pile elements during the shaking excitations.

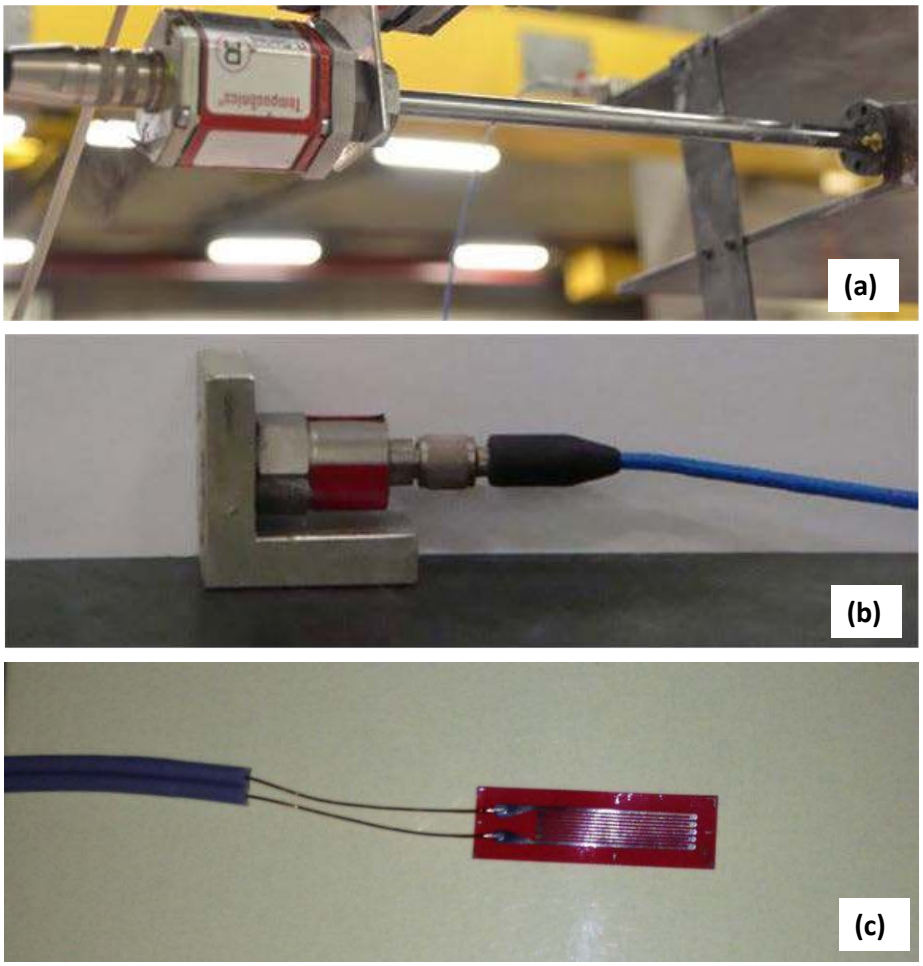


**Figure 4.13** Utilised measuring instruments in the shaking table tests: (a) displacement transducer; (b) accelerometer; (c) strain gauge

The utilised measuring instruments possess the following specifications:

Displacement transducers:

- Model : GH Rod-style position sensor
- Digital pulse accuracy : ± 0.005 mm
- Update times : less than 1 ms
- Repeatability : ± 0.001%
- Operating temperature range : -40 to +80 ºC

Accelerometers:

- Model : PCB triaxial accelerometer
- Frequency range : ± 5%
- Measurement range : ± 490 m/s-2
- Measurement accuracy : ± 0.006 m/s-2
- Operating temperature : -54 to +121 ºC

Strain Gauges:

- Model: FLA-10-11-3L
- Gauge length: 10 mm
- Gauge width: 2.5 mm
- Backing: epoxy
- Gauge factor: 2.09 (± 1%)
- Strain limit: $50000 \times 10^{-6}$
- Gauge resistance 119.6±05 Ω
- Transverse sensitivity: -0.4%
- Operating temperature : -20 to +80 ºC

The instruments were directly connected (Figure 4.14 a) to a data acquisition system managed by the integrated software package, which is run on a desktop computer and interfaces with the MTS (MTS System Corp.) shaking table control system. Each of the sensors was individually calibrated before installation to ensure high accuracy (Figure 4.14b). An online calibration check was performed just before each shaking table test through the data acquisition system, thereby identifying any malfunctioning or miswired sensors. With the calibration routine embedded in the data acquisition system, the acquired data was automatically transformed into engineering units.

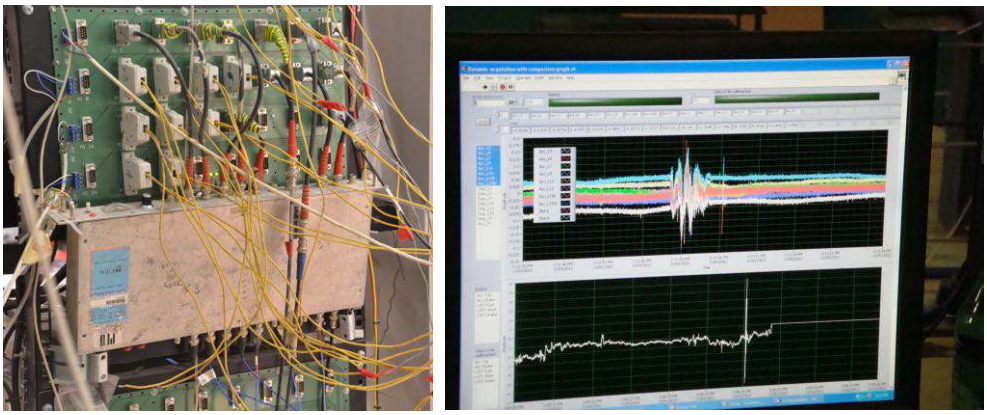

(a) (b)

**Figure 4.14** (a) sensors connection to the data acquisition system; (b) calibration of the sensors prior to the shaking table test

## 4.6 Shaking Table Tests on the Fixed-base Model Structure

The first stage of the shaking table tests was carried out under the fixed-base condition, in which the constructed structures were directly fixed on top of the shaking table (Figure 4.15), to ensure the structural model possesses the target natural frequency and determine the damping ratio of the model structure. To achieve the above, the constructed structural model as explained is Section 4.4.1, was fixed and secured on the shaking table. The arrangement of the installed displacement transducers and accelerometers on the fifteen storey model structures are given in Table 4.7, which were employed to monitor the dynamic response of the structures and to primarily measure the structural lateral displacements. The recorded accelerations can be used to check the consistency and accuracy of the obtained displacements through a double integration in

time domain. In addition, by recording the accelerometers which are installed on two edges of the top floor, any possible torsion of the structure during the seismic excitations could be monitored.

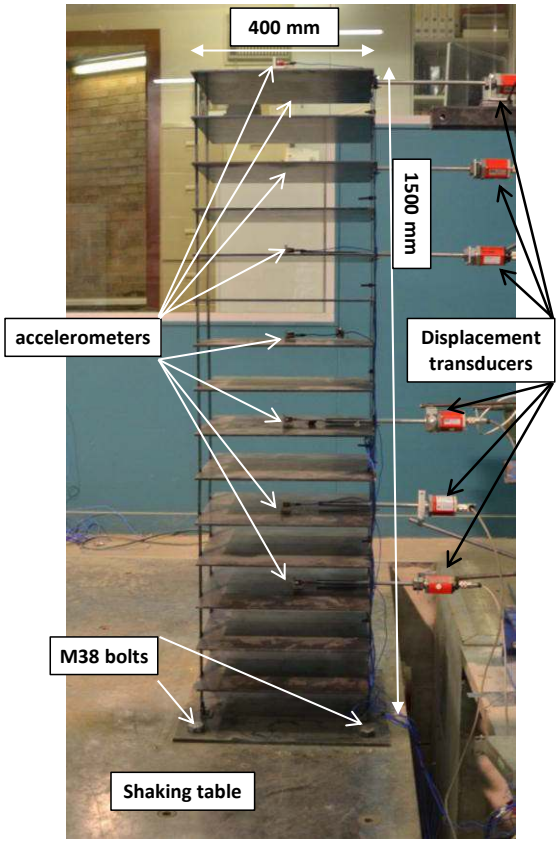


**Figure 4.15** Shaking table tests on the fixed-base model structure

**Table 4.7** Characteristics of the fifteen storey model structure

| Model Structure | Height (m) | Length (m) | Width (m) | Natural Frequency (Hz) | Mass (kg) | Location of displacement transducers | Location of accelerometers |
|---|---|---|---|---|---|---|---|
| 15-storey | 1.5 | 0.40 | 0.40 | 2.19 | 104 | 3, 5, 7, 11, 13, 15 | 3, 5, 7, 9, 11, 13, 15 |

Initially, Sine Sweep test was performed on the structural model to determine the natural frequency of the model. Sine Sweep test involves a logarithmic frequency sweep holding a specified acceleration constant at the base of the structure. For the current Sine Sweep test (Figure 4.9), by increasing the frequency of the shaking table from 0.1 Hz to 50 Hz, the first resonance between the shaking table and the structural model frequencies showed the fundamental natural frequency of the model. The test was repeated three times to ensure the determined natural frequency is adequately accurate.

The resulting natural frequency of the constructed structural model obtained from Sine Sweep test results was 2.19 Hz which is in a very good agreement with the desired natural frequency of the structural model (2.11 Hz). Therefore, the constructed structural model, with the natural frequency of 2.19 Hz and the total mass of 104 kg, possesses the required characteristics to meet the dynamic similitude criteria.

After ensuring the adequacy of the structural model dynamic characteristics to model the prototype, shaking table tests were performed by applying scaled earthquake acceleration records of 1994 Northridge (Figure 4.8a), 1995 Kobe (Figure 4.8b), 1940 El Centro (Figure 4.8c), and 1968 Hachinohe (Figure 4.8d) to the fixed-base structural model and the results in terms of maximum lateral deflections are presented in Figures 4.16 – 4.19. Figures 4.20 illustrate a sample of time-history deformation records used to obtain the maximum lateral deformations of the fifteen storey model structure reported in Figures 4.16-4.19. In determining the lateral deflections, the movement of the shaking table was subtracted from the storey movements. Therefore, all the records are relative to the base movements. It should be noted that the presented data are based on the lateral deformation of each storey when the maximum deflection at the top level occurred. This approach gives more reasonable pattern of the structural deformation in comparison with the approach that maximum absolute storey deformation irrespective of occurrence time are recorded.

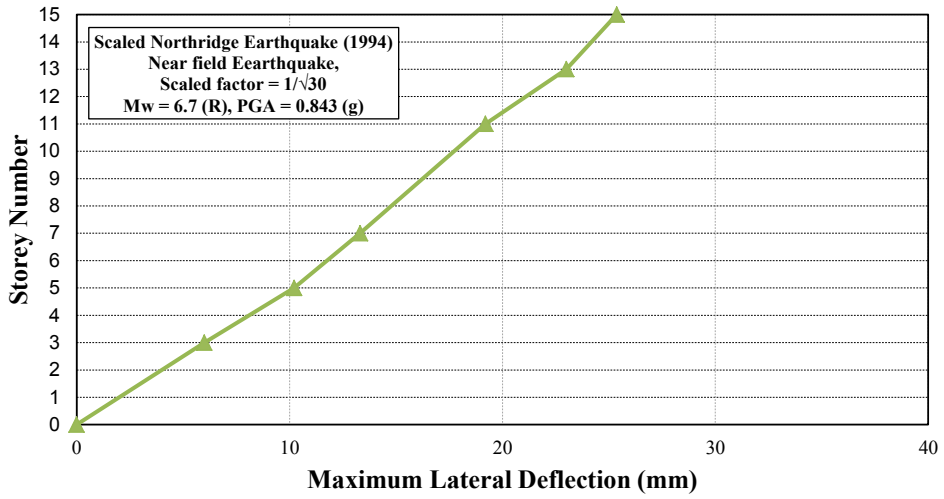


**Figure 4.16** Recorded maximum lateral deflections of fixed-base fifteen storey model structure under the influence of scaled 1994 Northridge earthquake

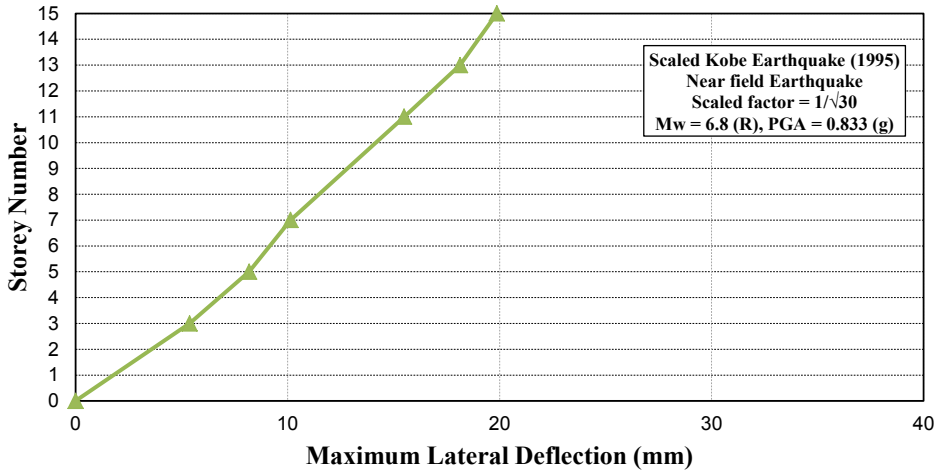


**Figure 4.17** Recorded maximum lateral deflections of fixed-base fifteen storey model structure under the influence of scaled 1995 Kobe earthquake

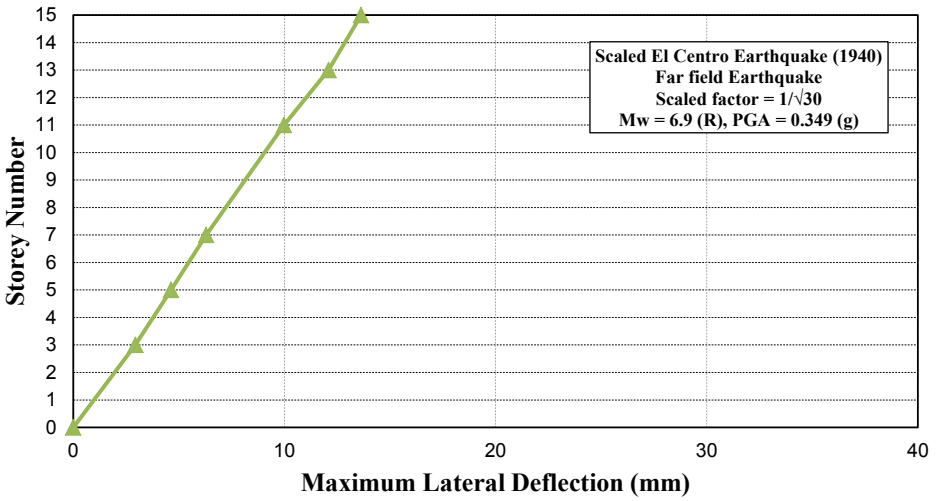


**Figure 4.18** Recorded maximum lateral deflections of fixed-base fifteen storey model structure under the influence of scaled 1940 El Centro earthquake

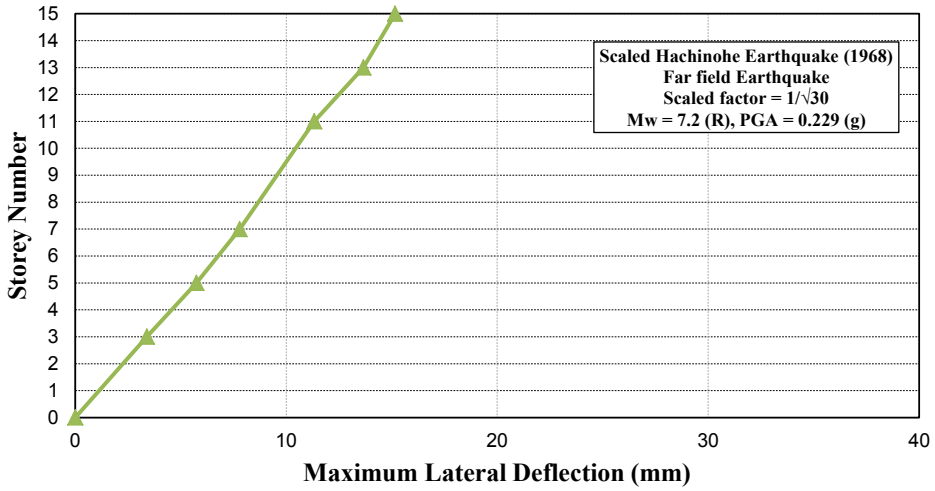


**Figure 4.19** Recorded maximum lateral deflections of fixed-base fifteen storey model structure under the influence of scaled 1968 Hachinohe earthquake

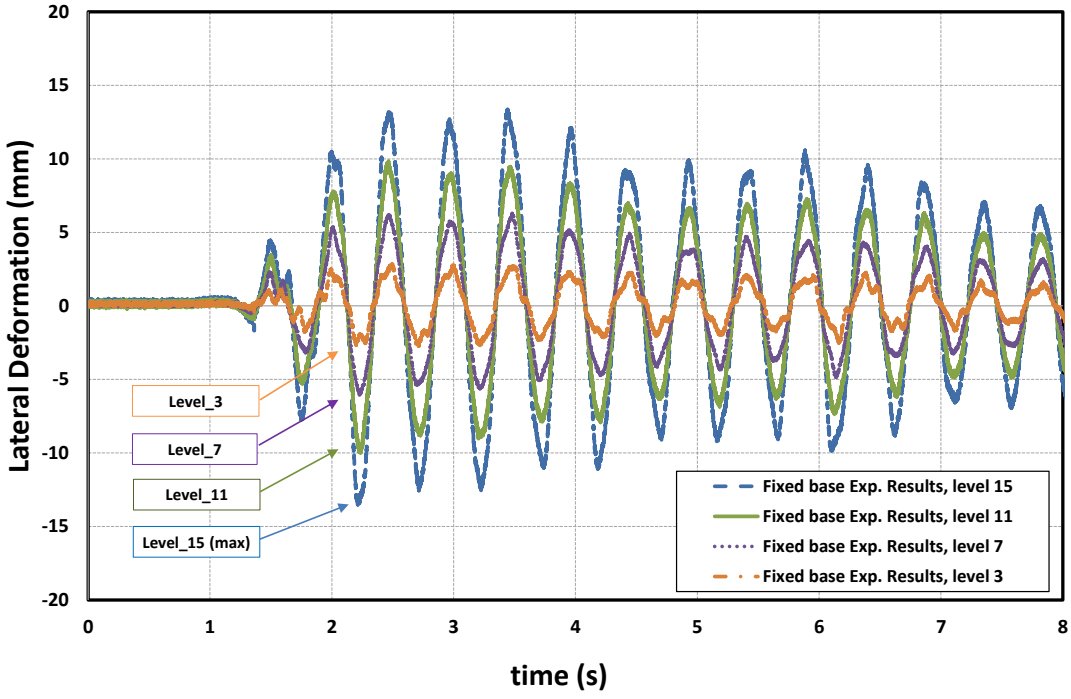


**Figure 4.20** Sample experimental time-history displacement results for the fixed-base fifteen storey model structure under the influence of 1940 El Centro earthquake

### 4.6.1 Damping Ratio of the Model Structure

The estimated value of the structural damping ratio of the constructed structural model was determined from the free vibration lateral displacement records of the structural model using the following Taylor series expansion (Craig and Kurdila, 2006):

$$\frac{U_n}{U_{n+m}} = e^{2\pi m\xi} = 1 + \sum_{n=1}^{\infty} \frac{(2\pi m\zeta)^n}{n!} = 1 + 2\pi m\xi + \frac{(2\pi m\xi)^2}{2!} + \ldots \quad (4.5)$$

where, $\xi$ is the structural damping ratio and $U_n$ and $U_{n+m}$ are two positive peaks of the free vibration response of the structure which are $m$ cycles apart. Substituting the values of $U_n$ and $U_{n+m}$ for the two positive peaks of the free vibration lateral displacement records in Equation (4.5), which are 10 cycles apart, and repeating the whole process several times, the damping ratio of the constructed structural model was determined to be equal to 1.1%.

## 4.7 Shaking Table Tests on Model Structure supported by Shallow Foundation

The second set of the shaking table tests was to study the effects of the soil-structure interaction under the shallow foundation. As explained in Section 4.4.4, after securing the laminar soil container on the shaking table and conducting the tests on the empty container to validate the required dynamic properties of the container, 2 cubic meters of the designed soil mix (Mix C: 60% Q38 kaolinite clay, 20% Active-bond 23 Bentonite, 20% class F fly ash and lime, and water, 120% of the dry mix) was produced and placed into the laminar soil container. Referring to Section 4.4.3, the desired soil mix acquires the required stiffness and consequently the shear wave velocity after two days of curing. As a result, the time frame for the testing process was very tight and time sensitive. Therefore, soil mixing and placement needed to be carried out in one day in order to produce a homogenous soil mix, and after two days of curing, the final tests had to be performed.

During the soil mixing process, ten cylindrical soil samples of D=50 mm and h=100 mm were taken from the soil mix for quality control of the mix. The entire mixing process and filling the laminar soil container were completed in one day. Then,

the soil mix inside the container was left to be cured for two days while the surface of the soil container was covered and sealed.

Initially, the filled soil container (without structure) was subjected to the shaking events and the results were compared with the predicted values, as broadly discussed in Section 4.4.4, to assess the capability of the constructed laminar soil container in minimising the boundary conditions. Later on, the structural model was lifted up and placed on the designated location (Figure 4.21), without observing any excessive settlement or failure underneath the base plate as predicted.

**Figure 4.21** Placing the fifteen storey model structure on top of the soil mix for the shaking table tests

Instrumentation of the structure in the soil-structure system was similar to the fixed-base structure. In addition, vertical displacement transducers were placed on the level of base plate of the structure (simulating the foundation) to determine the vertical displacements of the structure during the testing process as shown in Figure 4.22.

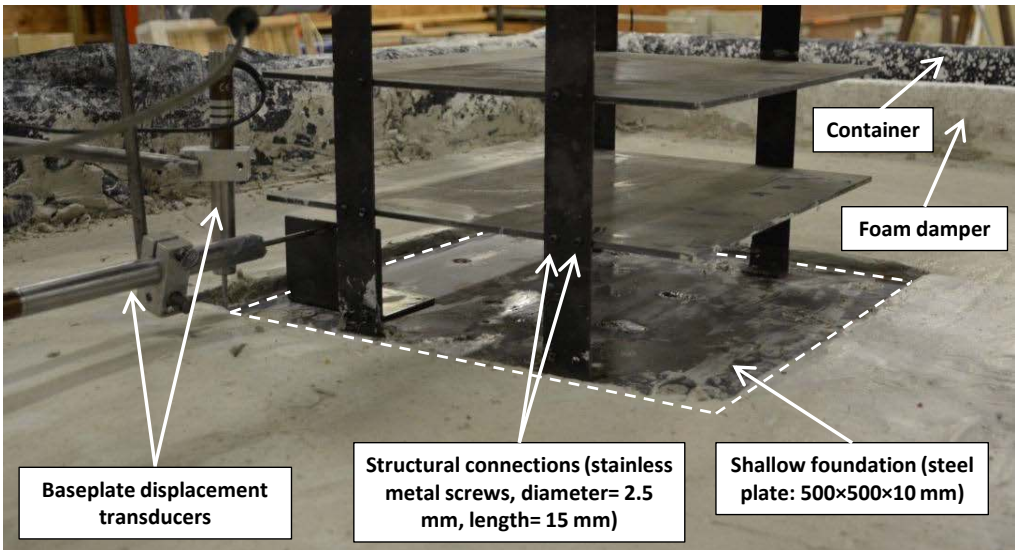


**Figure 4.22** Shaking table tests setup and connections for model shallow foundation

Before applying the scaled earthquake acceleration records, Sine Sweep test was carried out in order to estimate the natural frequency of the shallow foundation model. Accordingly, the natural frequency of the soil-structure model from the performed Sine Sweep test was measured to be 1.60 Hz. The results of the carried out shaking table tests for the model structure supported by shallow foundation under the influence of 1994 Northridge (Figure 4.8a), 1995 Kobe (Figure 4.8b), 1940 El Centro (Figure 4.8c), and 1968 Hachinohe (Figure 4.8d) earthquakes in terms of maximum lateral deflections are presented in Figures 4.23 – 4.26. Figures 4.27 illustrate a sample of time-history deformation records used to obtain the maximum lateral deformations of the fifteen storey model structure reported in Figures 4.23-4.26.

It should be noted that during the shaking table tests, pore water pressure is generated in the soil under the seismic loads. However, due to the fast nature of the applied loads and the low permeability of the clayey soil mix, undrained condition exists, and the behaviour of the soil is predicted under the total stress conditions. Thus, drainage boundary conditions will not influence the behaviour. In most cases, the development of excess pore water pressure in the soil types such as saturated silt, fine sand or sandy silt have become the focus of earthquake engineering since the liquefaction potential energy are easily accumulated during earthquake action (Ivšić, 2006). Referring to Zhang et al. (2009) and Gratchev et al. (2006) it is not a common practice to study the characteristic of excess pore water pressure in clayey soils under

earthquake actions. Therefore, the excess pore water pressure of the soil mix was not measured during the shaking table tests in this study.

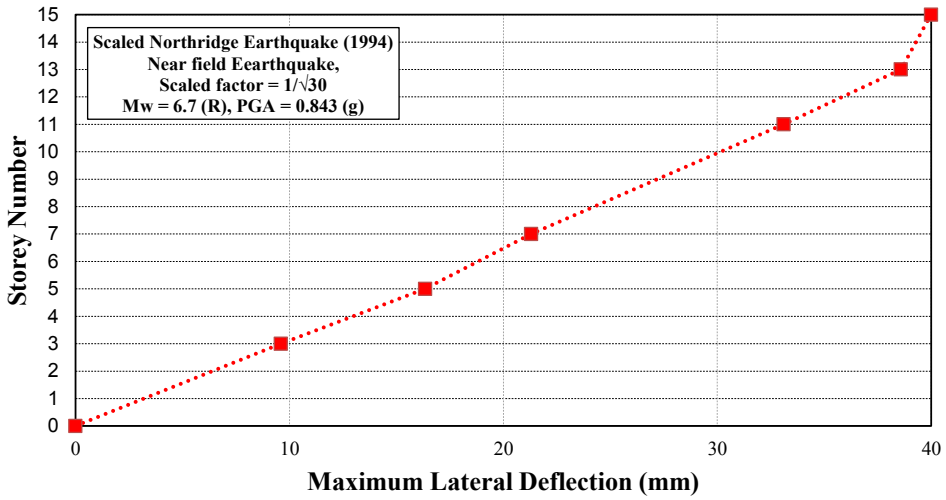


**Figure 4.23** Recorded maximum lateral deflections of fifteen storey model structure supported by shallow foundation under the influence of scaled 1994 Northridge earthquake

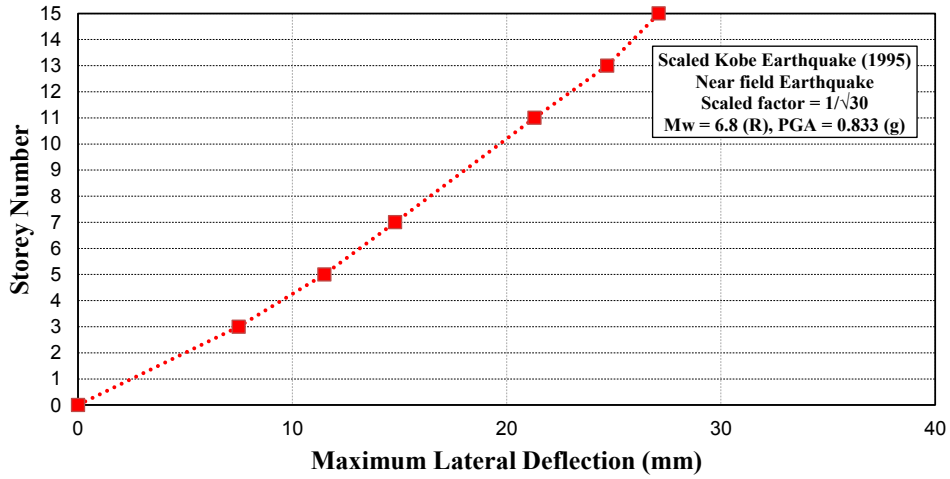


**Figure 4.24** Recorded maximum lateral deflections of fifteen storey model structure supported by shallow foundation under the influence of scaled 1995 Kobe earthquake

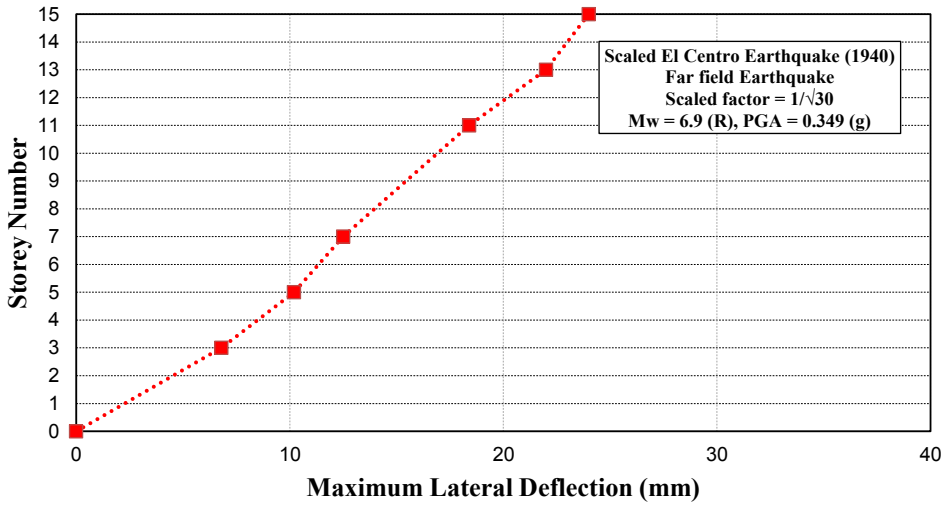


**Figure 4.25** Recorded maximum lateral deflections of fifteen storey model structure supported by shallow foundation under the influence of scaled 1940 El Centro earthquake

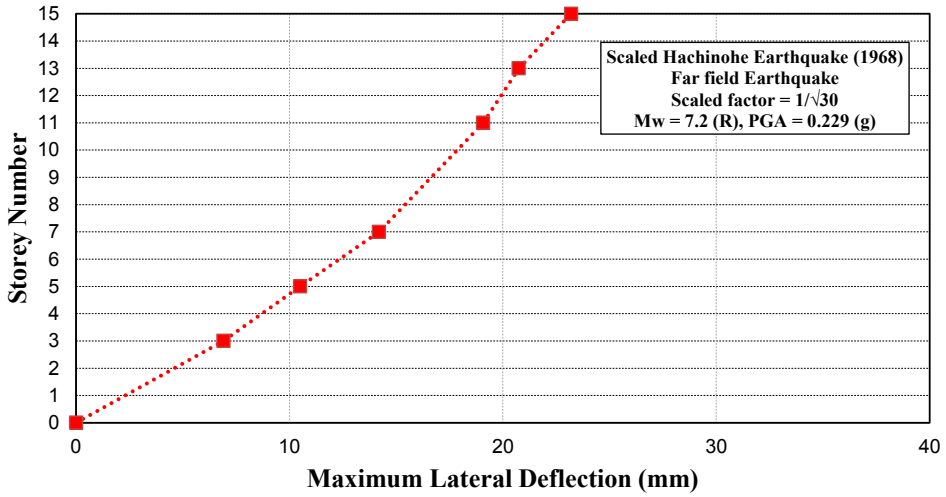


**Figure 4.26** Recorded maximum lateral deflections of fifteen storey model structure supported by shallow foundation under the influence of scaled 1968 Hachinohe earthquake

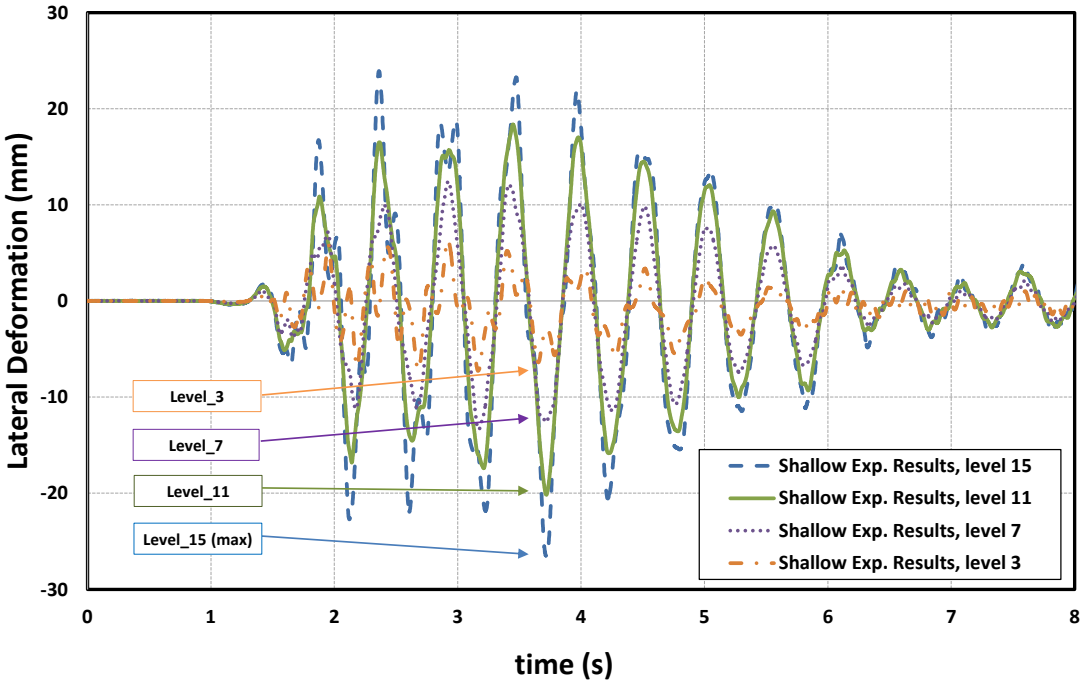


**Figure 4.27** Sample experimental time-history displacement results for the fifteen storey model structure supported by shallow foundation under the influence of 1940 El Centro earthquake

Moreover, the maximum vertical displacement of the foundation (base plate) and the relevant rocking angles were obtained from the vertical displacement transducers installed at the level of the base plate for each earthquake, as illustrated in Table 4.8. Figures 4.28 illustrate a sample of time-history vertical displacement records used to obtain the maximum vertical displacement of the base plate reported in Table 4.8.

**Table 4.8** Maximum vertical displacement and rocking angle of the base plate obtained from shaking table tests for the model structure supported by shallow foundation

| Scaled Earthquake Acceleration Record | Maximum Vertical Displacement | Rocking Angle of the Foundation |
|---|---|---|
| Northridge (1994) | 2.54 mm | 0.58° |
| Kobe (1995) | 1.32 mm | 0.30° |
| El Centro (1940) | 1.98 mm | 0.45° |
| Hachinohe (1968) | 1.47 mm | 0.33° |

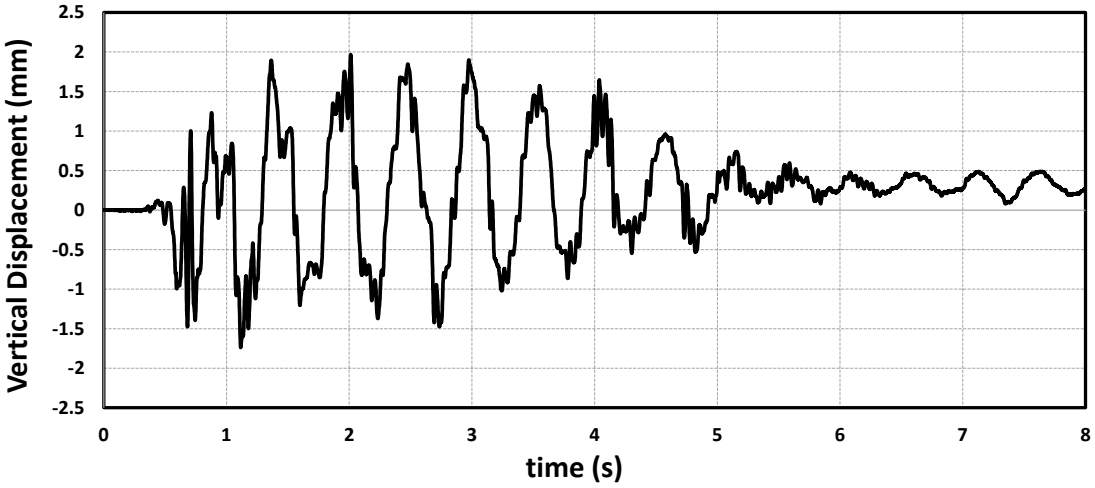


**Figure 4.28** Sample experimental time-history results of the vertical displacement of the base plate for the fifteen storey model structure supported by shallow foundation under the influence of 1940 El Centro earthquake

## 4.8 Shaking Table Tests on Model Structure supported by Floating Pile Foundation

The third case of the shaking table tests was to consider the floating pile foundation and investigate the influence of the soil-pile-structure interaction on the seismic response of the superstructure by comparing this case with the previously mentioned fixed-base and shallow foundation cases. Since the properties of the designed soil mix is time dependent, this stage needed to be carried out at the same age as for the shallow foundation case to make the results comparable, without any variation of the dynamic soil properties.

Commercial Polyethylene pressure pipe was employed to build the model piles as explained in Section 4.4.2. The length of the model floating piles is 660mm, leaving 340mm distance between the piles toe and the base. Wooden tips were fitted to the model piles to provide a closed end condition. The model piles were driven into the soil through a 150 mm tall wooden template to ensure location and verticality. Moreover, employing template during the installation process helps to achieve full connection between the piles and the surrounding soil without generating any gap due to the installation process. The template was constructed with special cut outs to accommodate a few millimetres of extra room for piles with external strain gages aiming to prevent any possible damage to the strain gages during the installation.

After installation of the model piles, the template was removed and the steel plate (simulating the foundation) with prefabricated holes was fitted over the group. Sixteen M12 bolts were used to provide fixed connection between the piles' head and the steel plate as shown in Figure 4.29. The required nuts were fixed to the pile top with strong glue and steel rings before the test and the strength and capability of this connection technique were examined successfully. Then, the model structure was suspended from the overhead crane and connected to the steel plate from the pre-located connections.

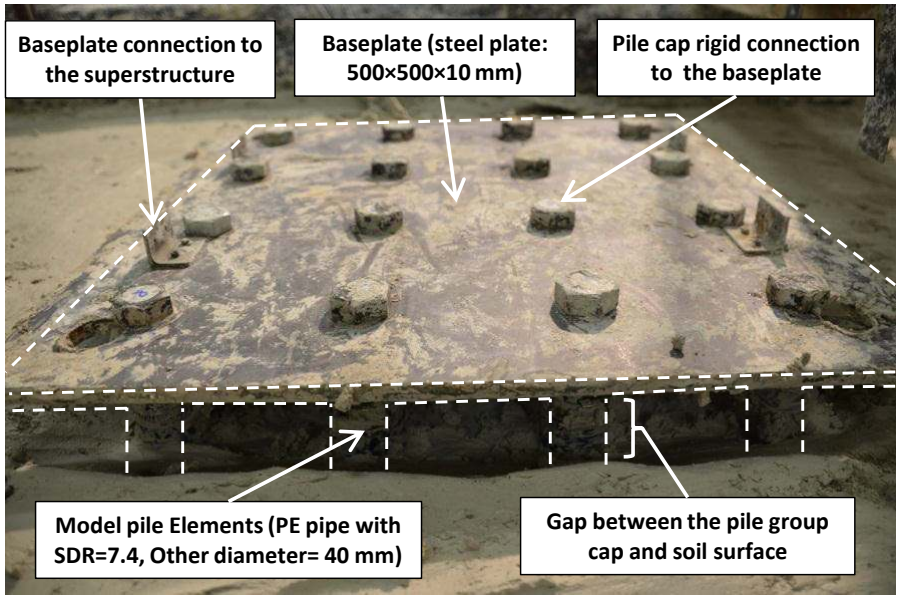


**Figure 4.29** Connection details for the pile foundation cases

All the components of the system including the container, soil, piles, and superstructure were installed, and same arrangement of displacement transducers and accelerometers was used on the structure and the steel plate (simulating the foundation).

Similar shaking events including Sine Sweep test and four scaled earthquake records were applied to the floating pile foundation system. The natural frequency of the soil-pile-structure model from the performed Sine Sweep test was measured to be 1.8 Hz. The results of the conducted shaking table tests under the influence of four scaled earthquake acceleration records in terms of the maximum lateral deflections of various stories of the structure are presented in Figures 4.30- 4.33. Figure 4.34 illustrate a sample of time-history deformation records used to obtain the maximum lateral deformations of the fifteen storey model structure reported in Figures 4.30-4.33.

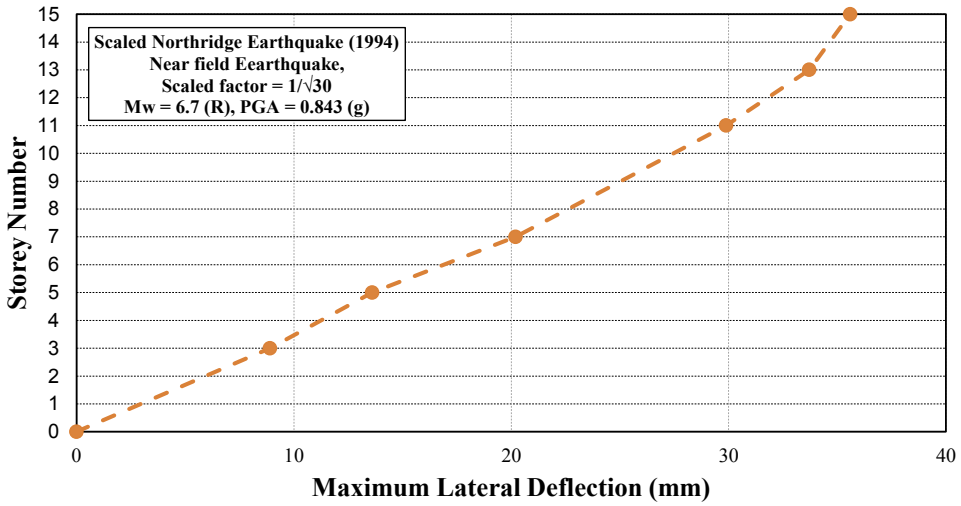


**Figure 4.30** Recorded maximum lateral deflections of fifteen storey model structure supported by floating pile foundation under the influence of scaled 1994 Northridge earthquake

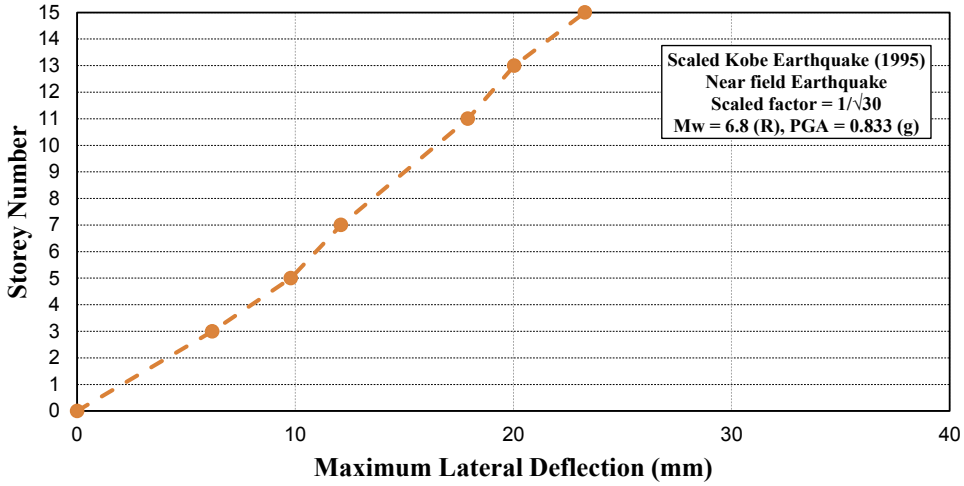


**Figure 4.31** Recorded maximum lateral deflections of fifteen storey model structure supported by floating pile foundation under the influence of scaled 1995 Kobe earthquake

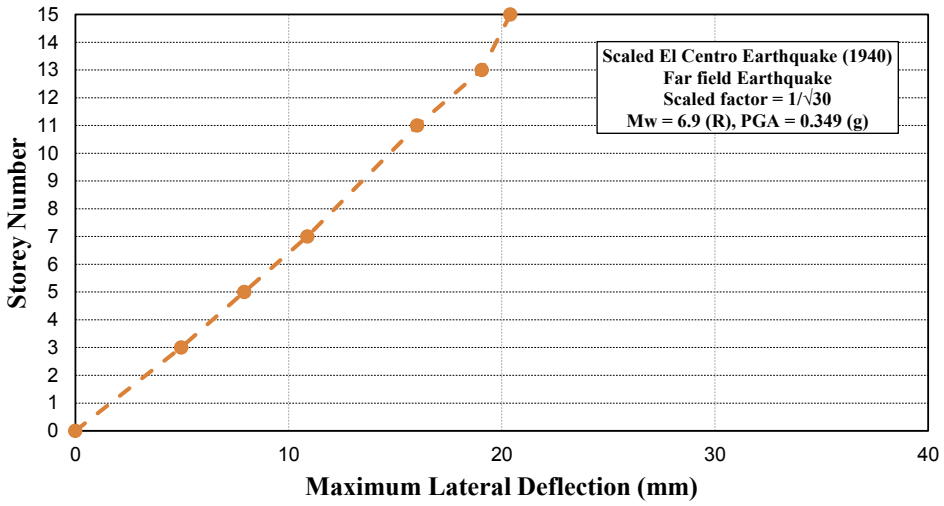


**Figure 4.32** Recorded maximum lateral deflections of fifteen storey model structure supported by floating pile foundation under the influence of scaled 1940 El Centro earthquake

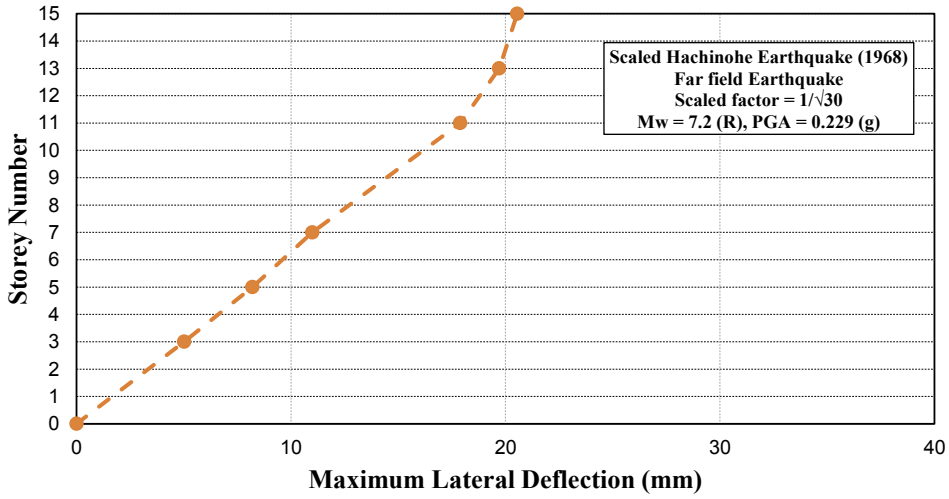


**Figure 4.33** Recorded maximum lateral deflections of fifteen storey model structure supported by floating pile foundation under the influence of scaled 1968 Hachinohe earthquake

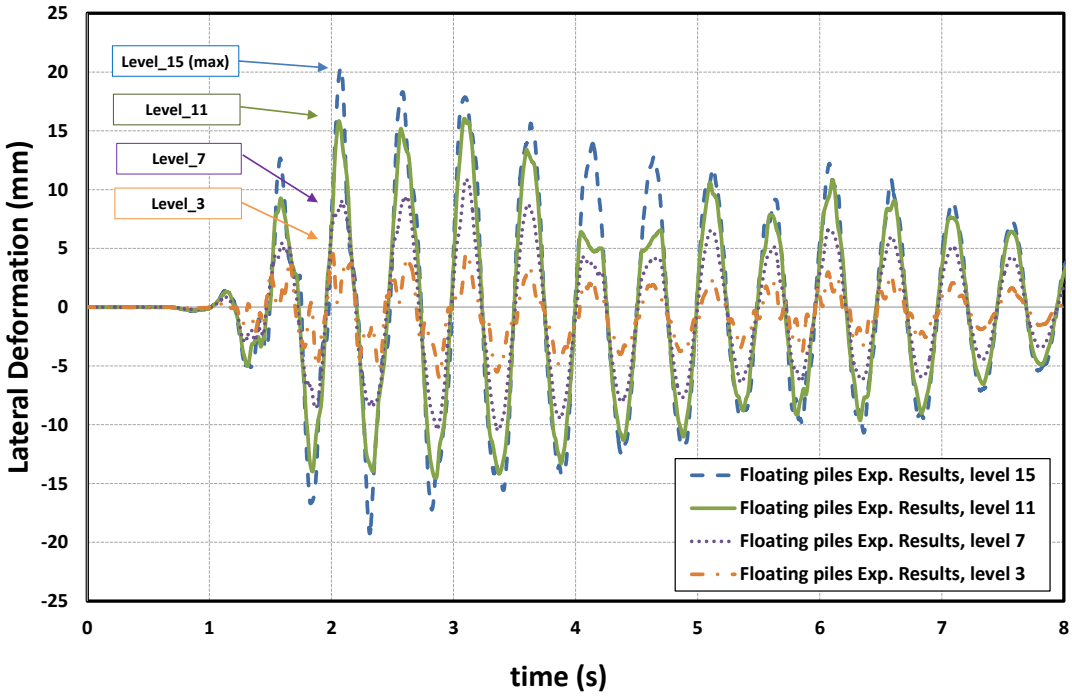


**Figure 4.34** Sample experimental time-history displacement results for the fifteen storey model structure supported by floating pile foundation under the influence of 1940 El Centro earthquake

The maximum vertical displacement and rocking angle of the base plate obtained from shaking table tests for the model structure supported by the floating pile foundation are summarised in Table 4.9. Figures 4.35 illustrate a sample of time-history vertical displacement records used to obtain the maximum vertical displacement of the base plate reported in Table 4.9.

**Table 4.9** Maximum vertical displacement and rocking angle of the base plate obtained from shaking table tests for the model structure supported by floating pile foundation

| Scaled Earthquake Acceleration Record | Maximum Vertical Displacement | Rocking Angle of the Foundation |
|---|---|---|
| 1994 Northridge | 1.9 mm | 0.43° |
| 1995 Kobe | 0.43 mm | 0.1° |
| 1940 El Centro | 1.27 mm | 0.29° |
| 1968 Hachinohe | 0.93 mm | 0.21° |

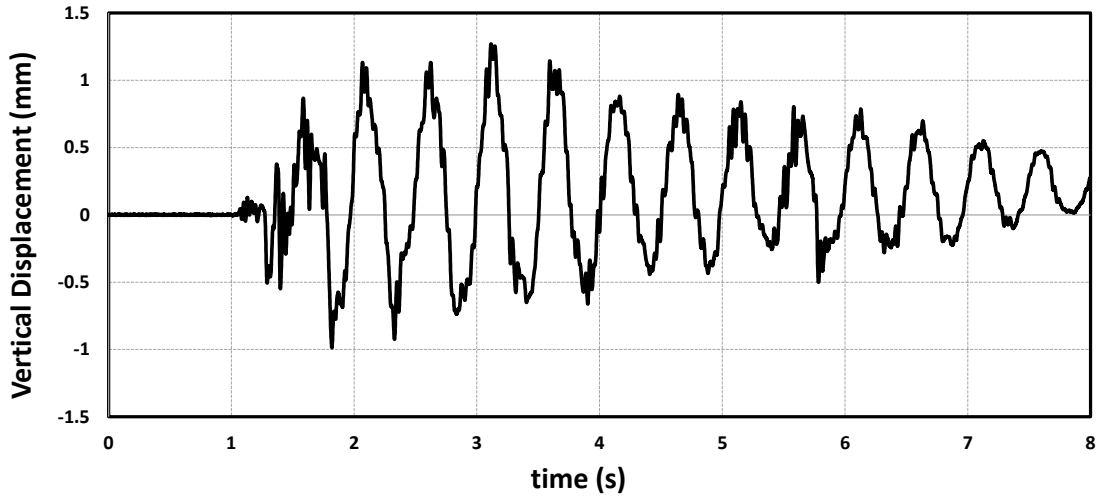


**Figure 4.35** Sample experimental time-history results of the vertical displacement of the base plate for the fifteen storey model structure supported by floating pile foundation under the influence of 1940 El Centro earthquake

## 4.9 Shaking Table Tests on Model Structure supported by End-bearing Pile Foundation

In this case, the fifteen storey model structure is supported by an end-bearing pile foundation while subjected to the shaking excitations. Considering the time dependent behaviour of the soil mix, this stage is also carried out in the same curing age as for the shallow foundation and floating pile foundation cases, making the results comparable.

For the end-bearing pile foundation, model piles with the length of 1000mm are adopted. After fitting wooden tips to the model piles to provide a closed end condition, in order to compel the end-bearing behaviour and prevent any possible sliding between the piles and the container base plate, pile tips were equipped with bolts which were driven into the wooden base-plate during the installation. This is to prevent any possible sliding between the piles and the container base plate (simulating the bedrock) during the shaking table test. The installation technique and other test setups for the end-bearing piles were similar to the floating piles. The final setup of the tests including the displacement transducers and accelerometers at different levels of the structural model for the end-bearing pile foundation system on the shaking table are presented in Figure 4.36.

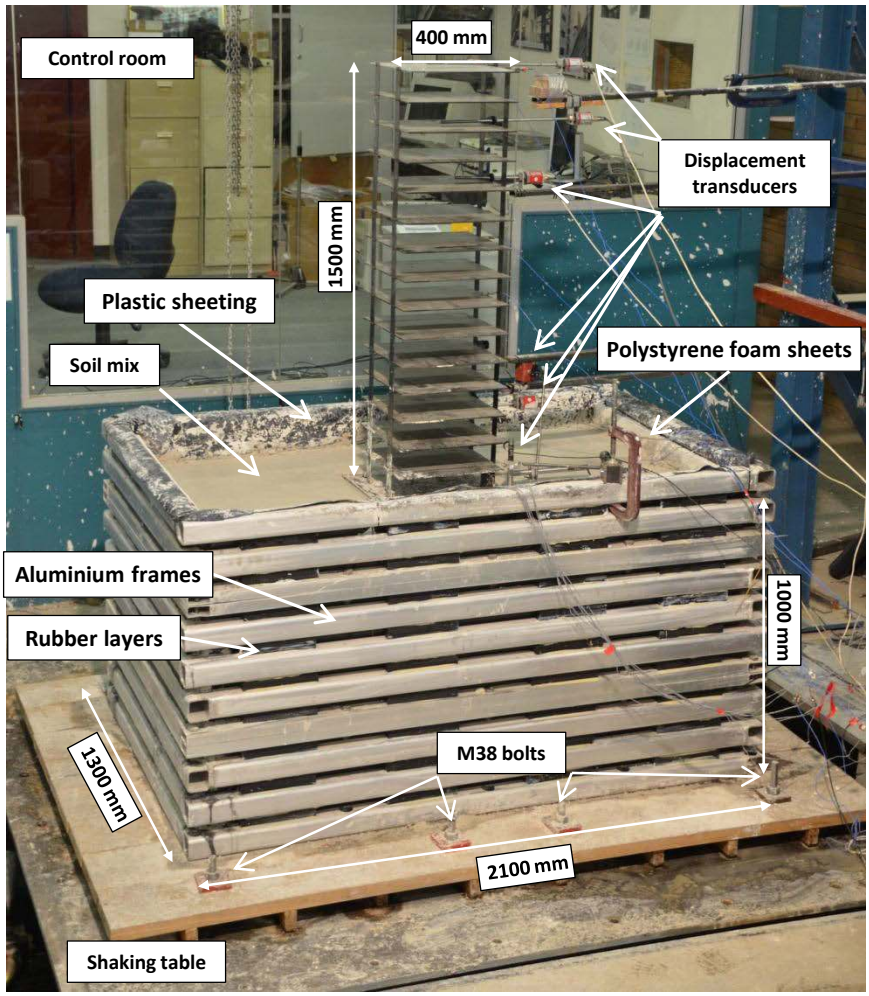


**Figure 4.36** Various components of the shaking table tests for the structure with pile foundation adopted in this study

The natural frequency of the soil-pile-structure model from the performed Sine Sweep test was measured to be 1.93 Hz. The results of the conducted shaking table tests under the influence of four scaled earthquake acceleration records in terms of the maximum lateral deflections of various stories of the structure are presented in Figures 4.37-4.40. Figures 4.41 illustrate a sample of time-history deformation records used to obtain the maximum lateral deformations of the fifteen storey model structure reported in Figures 4.37-4.40.

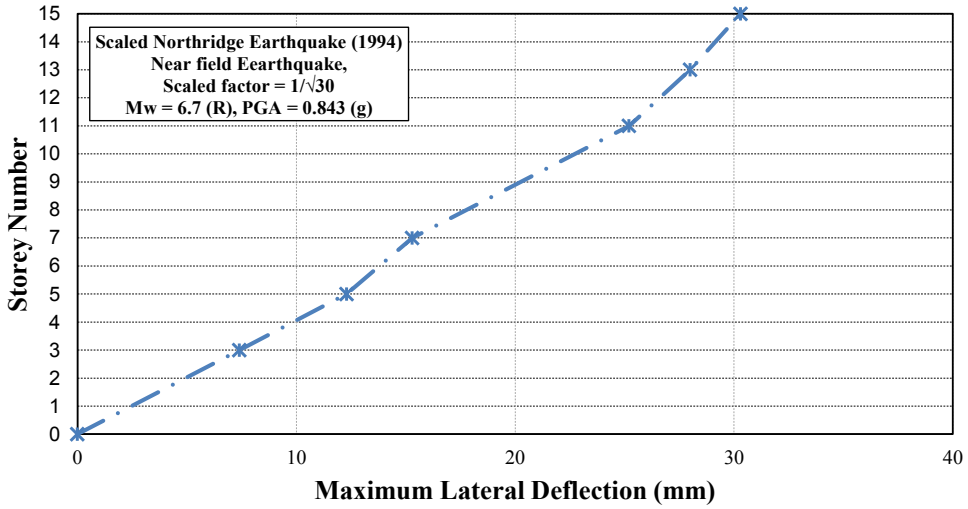


**Figure 4.37** Recorded maximum lateral deflections of fifteen storey model structure supported by end-bearing pile foundation under the influence of scaled 1994 Northridge earthquake

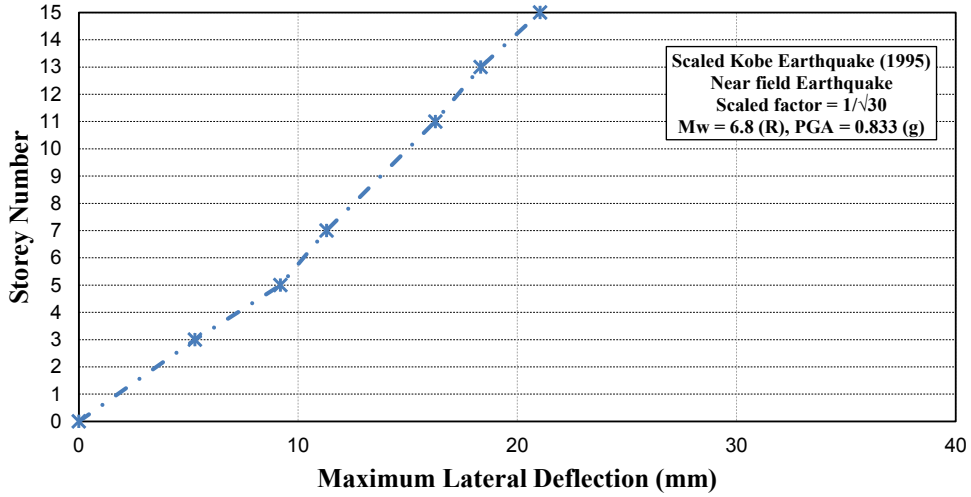


**Figure 4.38** Recorded maximum lateral deflections of fifteen storey model structure supported by end-bearing pile foundation under the influence of scaled 1995 Kobe earthquake

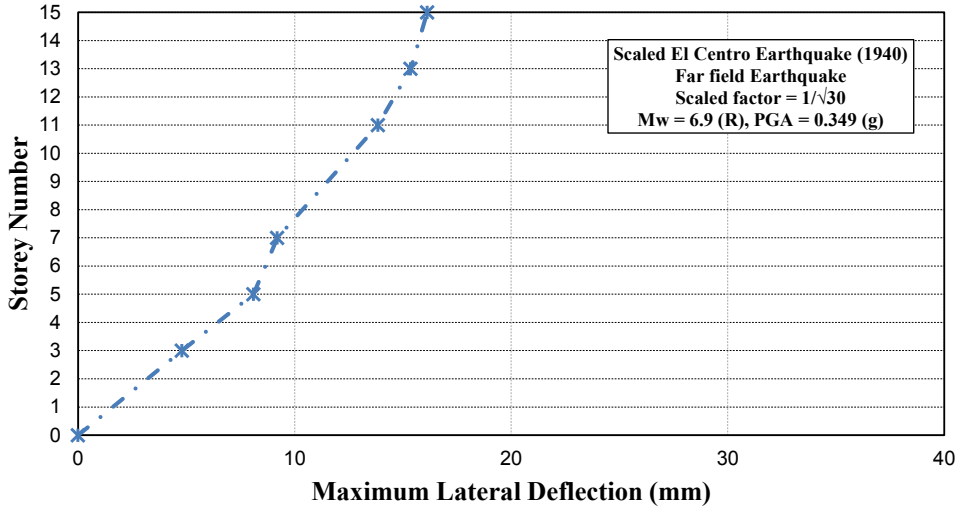


**Figure 4.39** Recorded maximum lateral deflections of fifteen storey model structure supported by end-bearing pile foundation under the influence of scaled 1940 El Centro earthquake

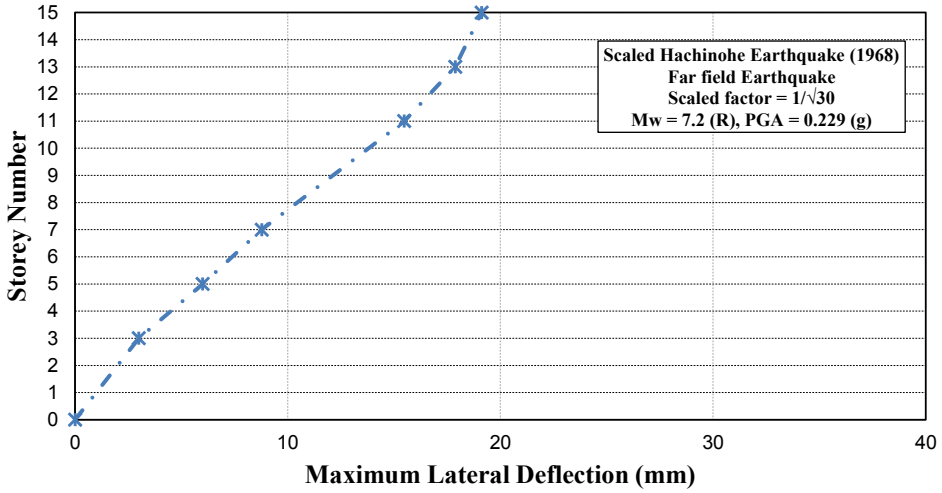


**Figure 4.40** Recorded maximum lateral deflections of fifteen storey model structure supported by end-bearing pile foundation under the influence of scaled 1968 Hachinohe earthquake

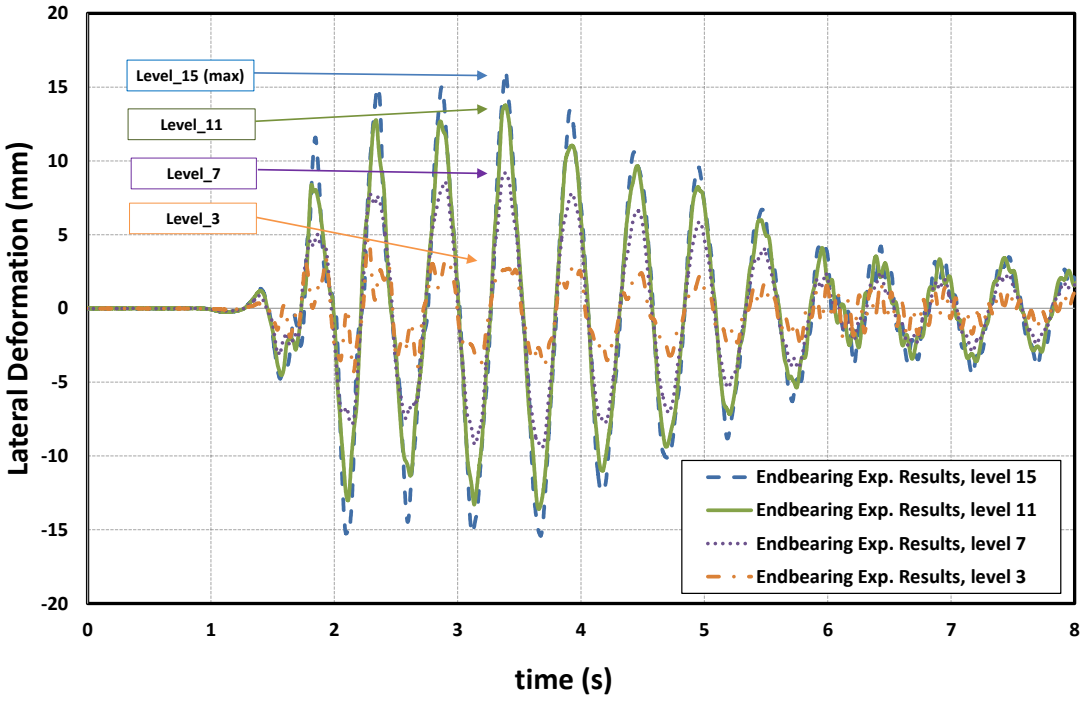


**Figure 4.41** Sample experimental time-history displacement results for the fifteen storey model structure supported by end-bearing pile foundation under the influence of 1940 El Centro earthquake

The maximum vertical displacement and rocking angle of the base plate obtained from shaking table tests for the model structure supported by end-bearing pile foundation are summarised in Table 4.10. Figures 4.42 illustrate a sample of time-history vertical displacement records used to obtain the maximum vertical displacement of the base plate reported in Table 4.10. Comprehensive discussion on the results of the conducted shaking table tests with respect to the different types of foundations is provided in Section 4.10.

**Table 4.10** Maximum vertical displacement and rocking angle of the base plate obtained from shaking table tests for the model structure supported by end-bearing pile foundation

| Scaled Earthquake Acceleration Record | Maximum Vertical Displacement | Rocking Angle of the Foundation |
|---|---|---|
| 1994 Northridge | 0.97 mm | 0.22° |
| 1995 Kobe | 0.39 mm | 0.09° |
| 1940 El Centro | 0.62 mm | 0.14° |
| 1968 Hachinohe | 0.86 mm | 0.20° |

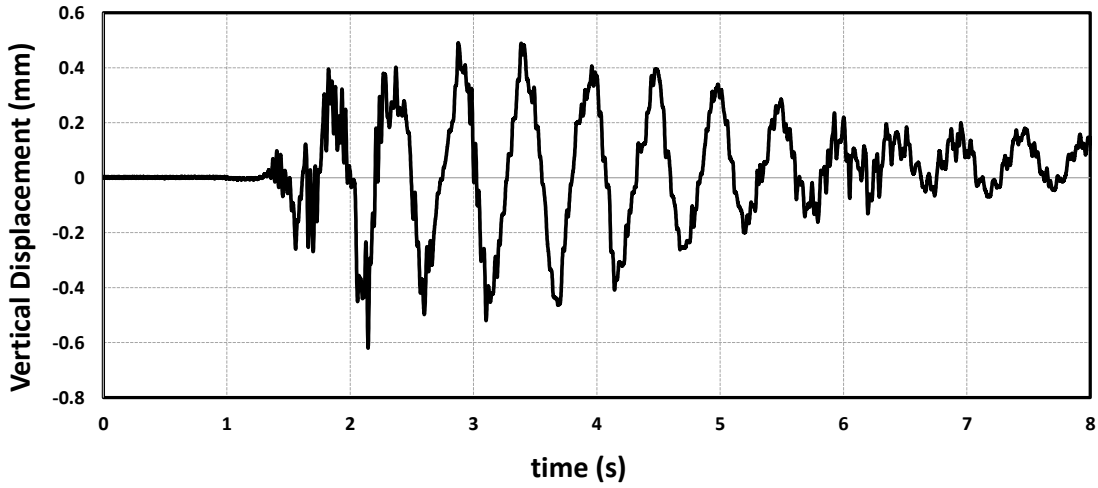


**Figure 4.42** Sample experimental time-history results of the vertical displacement of the base plate for the fifteen storey model structure supported by end-bearing pile foundation under the influence of 1940 El Centro earthquake

It should be noted that all the foundations are initially designed in the way which can carry both gravity and earthquake loads during shaking table tests without experiencing any failure. Accordingly, during the shaking table tests no excessive settlement or failure is observed under the shaking excitations for different types of foundations including shallow foundation, floating-pile foundation, and end-bearing pile foundations, as expected.

## 4.10 Discussion on the Results

Figure 4.43 compares the recorded maximum lateral deflection of the fifteen storey model structure from the shaking table tests for the fixed-base, shallow foundation, floating pile foundation, and end-bearing pile foundation cases under the influence of the four mentioned shaking events. Accordingly, the maximum lateral deformation of the structure during the shaking excitations amplifies due to the presence of the soft soil and the foundation system. In comparison to the fixed-base structure, the maximum lateral deflection of the structure supported by end-bearing and floating pile foundations increases on average by 17%, and 34% based on the experimental measurements, respectively. Moreover, the maximum lateral deflection of the structure

supported by the shallow foundation is increased by 55% in comparison to the results obtained from the fixed-base structure.

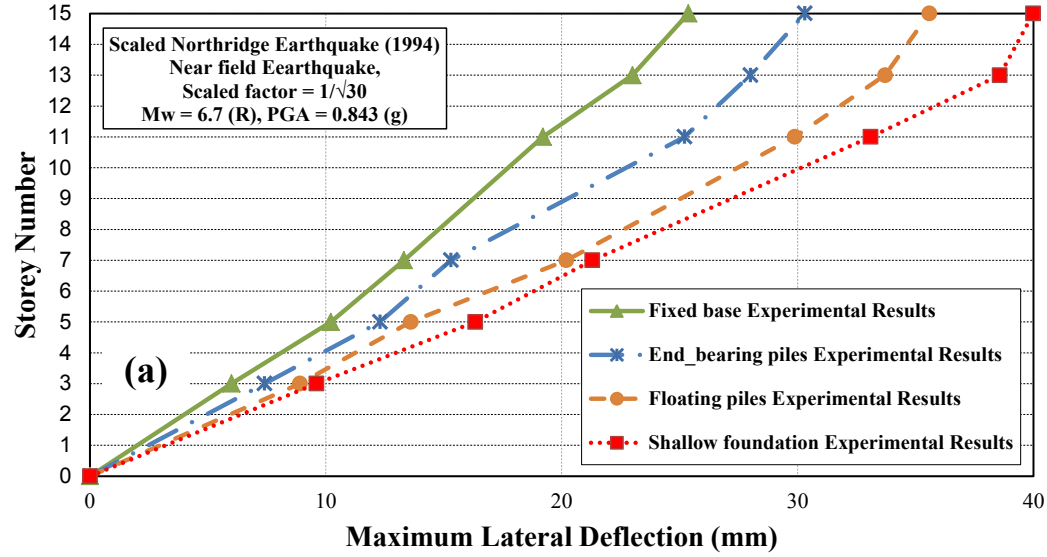


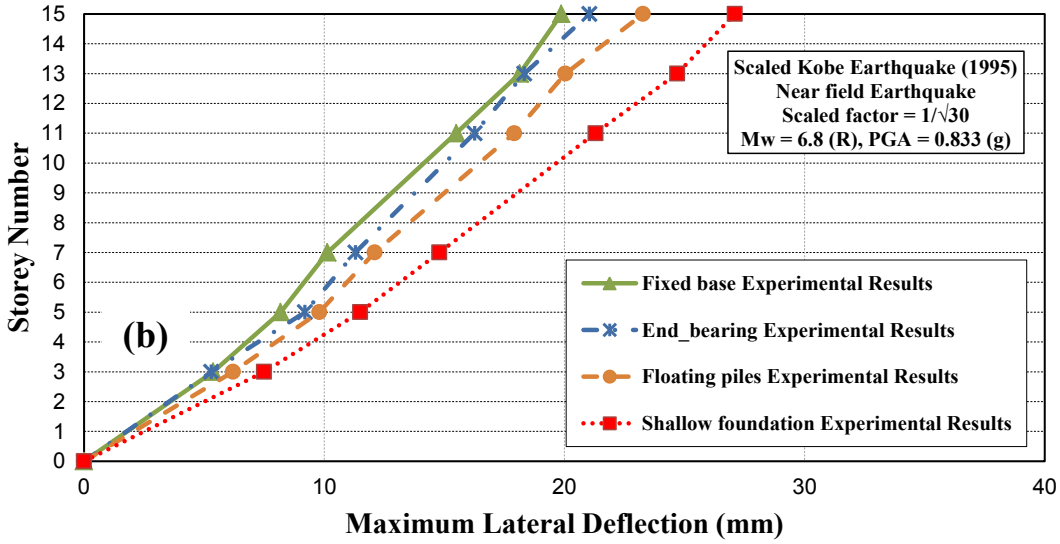

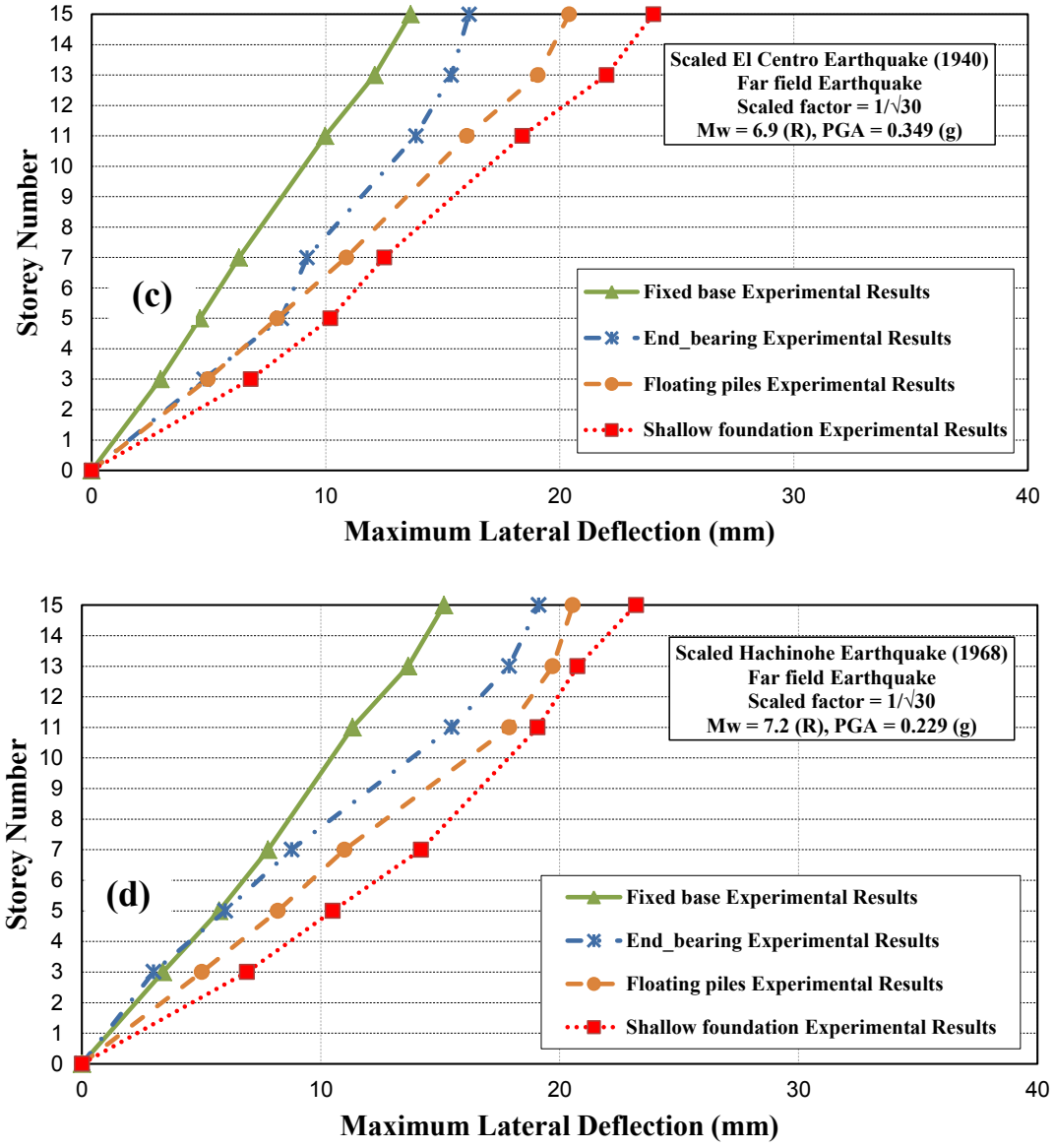


**Figure 4.43** Comparing the maximum lateral deflection of the fifteen storey model structure from the shaking table tests for the fixed-base, shallow foundation, floating pile foundation, and end-bearing pile foundation cases under the influence of: (a) 1994 Northridge earthquake; (b) 1995 Kobe earthquake; (c) 1940 El Centro earthquake; (d) 1968 Hachinohe earthquake

Based on the recorded values from sine sweep test, the natural frequency of the system reduces due to the soil-structure interaction (2.19 Hz for the fixed-base condition, 1.93 Hz for the end-bearing pile foundation, 1.8 Hz for the floating pile foundation, and 1.60 Hz for the shallow foundation case). Therefore, such decreases in the natural frequency (increases in the natural period) considerably alter the response of the building frame under the seismic excitation. This is due to the fact that the natural period of the system lies in the long period region of the response spectrum curve, and the displacement response tends to increase. The pile foundations reduce the lateral

displacements in comparison to the shallow foundation case since the presence of the stiff pile elements in the soft soil increases the equivalent stiffness of the ground and thus influences the dynamic properties of the whole system such as the natural frequency and the damping. Clearly, end-bearing pile foundations provide stiffer base for the building in comparison to the frictional piles and shallow foundations, resulting in the structural results comparable with the fixed-base condition.

Rocking component plays an important role in the lateral deformation of the superstructure. According to Kramer (1996), relative lateral structural displacements under the influence of the soil-structure interaction consist of rocking and distortion components. The Maximum vertical displacement and rocking angle of the base plate obtained from shaking table tests for the fixed-base, shallow foundation, floating pile foundation, and end-bearing pile foundation cases under the influence of the adopted shaking events are summarised and compared in Tables 4.11- 4.12.

**Table 4.11** Maximum vertical displacement of the base plate obtained from shaking table tests obtained from shaking table tests

| **Scaled Earthquake Acceleration Record** | **Maximum Vertical Displacement** | | | |
|---|---|---|---|---|
| | Fixed-base | Shallow foundation | Floating Pile Foundation | End-bearing Pile Foundation |
| 1994 Northridge | 0 | 2.54 mm | 1.9 mm | 0.97 mm |
| 1995 Kobe | 0 | 1.32 mm | 0.43 mm | 0.39 mm |
| 1940 El Centro | 0 | 1.98 mm | 1.27 mm | 0.62 mm |
| 1968 Hachinohe | 0 | 1.47 mm | 0.93 mm | 0.86 mm |

**Table 4.12** Maximum rocking angle of the base plate obtained from shaking table tests

| **Scaled Earthquake Acceleration Record** | **Rocking Angle of the Foundation** | | | |
|---|---|---|---|---|
| | Fixed-base | Shallow foundation | Floating Pile Foundation | End-bearing Pile Foundation |
| 1994 Northridge | 0 | 0.58° | 0.43° | 0.22° |
| 1995 Kobe | 0 | 0.30° | 0.1° | 0.09° |
| 1940 El Centro | 0 | 0.45° | 0.29° | 0.14° |
| 1968 Hachinohe | 0 | 0.33° | 0.21° | 0.20° |

Accordingly, considering the recorded maximum vertical displacements of the foundation (Table 4.11) and the rocking angles (Table 4.12), together with the maximum lateral displacements reported in Figure 4.43, it is noted that for the end-bearing pile foundation cases, approximately 20% of the maximum lateral deflections were due to the rocking component, while 80% took place due to the distortion component. For the floating pile foundation cases, approximately 27% of the maximum lateral deflections were due to the rocking component, while 73% took place due to the distortion component. These values for the shallow foundation cases are 37% and 63%, respectively. For example, under the influence of 1940 El Centro earthquake, maximum lateral deflection at the top of the fixed-base model was measured to be 13.63 mm due to distortion component, while maximum lateral deflection at the top of the structure supported by end-bearing pile foundation was 16.12 mm with 3.72 mm of that value being due to rocking component and 12.4 mm took place due to distortion component. In the pile foundation cases, rocking occurs due to the axial deformation of the pile elements. The area replacement ratio of the pile group was 8% in this study and as a result piles attract significant axial forces. However, clearly the rocking of the structure in the shallow foundation case, without pile elements, is much more than the case with pile foundations resulting in further amplification of the lateral deformations.

Consequently, based on the results obtained from the conducted shaking table tests, it is observed that the lateral deflections of structures siting on the end-bearing or floating pile foundations amplified in comparison to the fixed-base model. This amplification for the structure siting on the shallow foundation is more severe. Therefore, the choice of the foundation type is dominant and should be included in investigating the influence of SSI on the superstructure response during shaking excitations, and conventional design procedures excluding the soil-structure interaction are not adequate to guarantee the structural safety for the moment resisting buildings resting on soft soils.

## 4.11 Shaking Table Tests on Five and Ten Storey Model Structures

In the present research, further shaking table tests were carried out to experimentally study the effects of the seismic-soil-pile-structure interaction (SSPSI) on the dynamic response of buildings with various heights. For this purpose, a five storey

and ten storey moment resisting building frames with the total heights of 15 m and 30 m, respectively, are simulated, and results are compared with the previously conducted shaking table tests on the fifteen storey model structure. Two types of foundations for each case are investigated including: (i) fixed-base structure representing the situation excluding the soil-structure interaction, and (ii) structure supported by end-bearing pile foundation in the soft soil.

Each frame consists of three spans with total width of 12 m, and the spacing between the frames into the page is 4 m. Natural frequencies of the prototype buildings are 1.05 Hz and 0.51 Hz for five storey and ten storey buildings, respectively. Moreover, the total mass of the prototype buildings are 387 tonnes and 671 tonnes for five storey and ten storey buildings, respectively. For the end-bearing pile foundation case, similar to the previously conducted shaking table tests on the fifteen storey model structure, the soil medium beneath the structures is a clayey soil with the shear wave velocity of 200 m/s and density of 1470 kg/m$^3$. The horizontal distance of the soil lateral boundaries and bedrock depth was selected to be 60 m and 30 m, respectively. The buildings are resting on a footing which is 1 m thick and 15 m wide connecting to a 4×4 reinforced concrete pile group with pile diameter and length of 1.2 m and 30 m, respectively. The equal spacing of the piles is four times the diameter (4d). The piles are embedded into the bedrock representing typical end-bearing piles. Characteristics of the prototype five storey and ten storey buildings are presented in Figure 4.44 and 4.45.

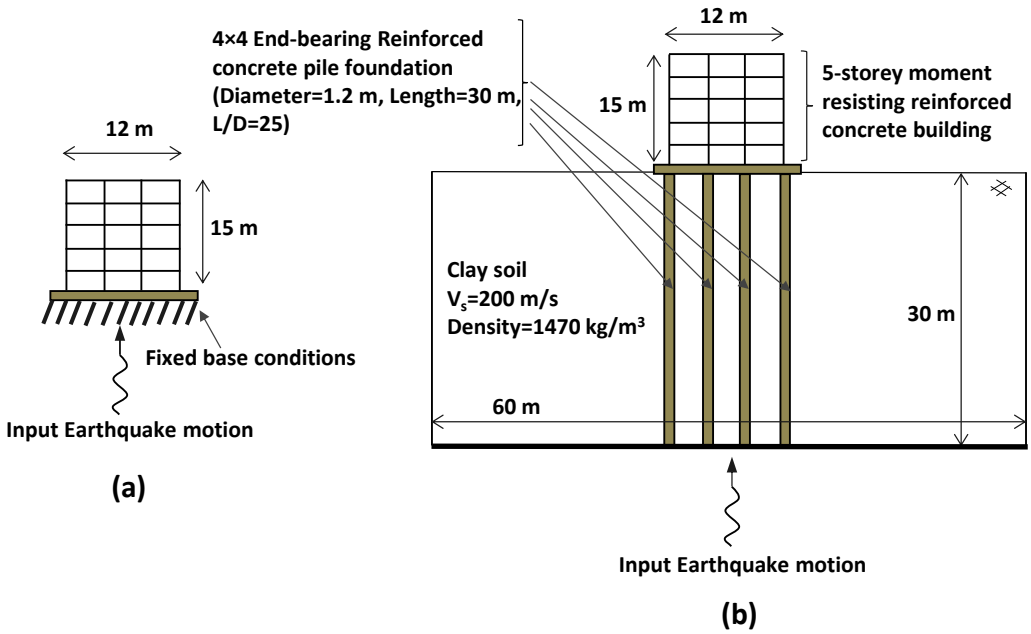


**Figure 4.44** (a) Prototype fixed-base five storey building; (b) prototype five storey building supported by end-bearing pile foundation

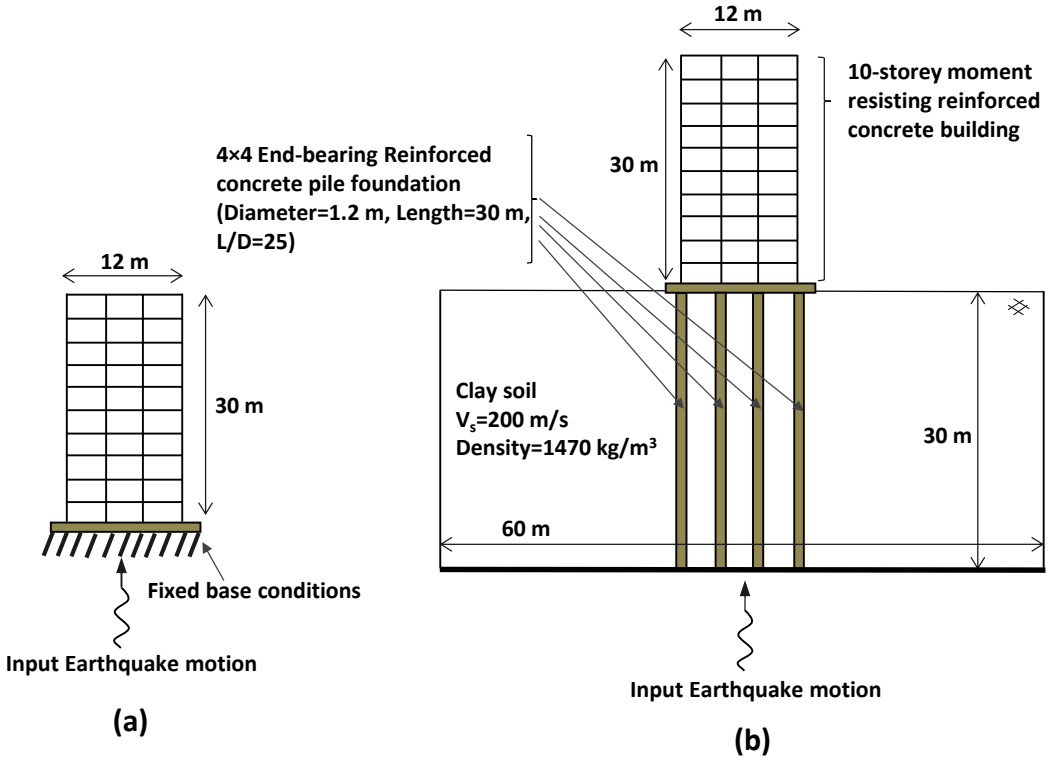


**Figure 4.45** (a) Prototype fixed-base ten storey building; (b) prototype ten storey building supported by end-bearing pile foundation

Making the results comparable, same test setup and scaling factor, as for the fifteen storey model structure, were adopted. Accordingly, the required scaled natural frequency for the structural models should be 5.83 Hz are 2.83 Hz, for five storey and ten storey buildings, respectively. The model structures are constructed from the same material, as for the fifteen storey (Section 4.4.1), and characteristics of the model structures are presented in Table 4.13. The properties of the other test components including soil mix, pile elements, and shaking excitation were explained in Section 4.4. The arrangement of the installed displacement transducers and accelerometers on the five storey and ten storey model structures are given in Table 4.13, which were employed to monitor the dynamic response of the structures and to primarily measure the structural lateral displacements

**Table 4.13** Characteristics of the model structures

| Model Structure | Height (m) | Length (m) | Width (m) | Natural Frequency (Hz) | Mass (kg) | Location of displacement transducers | Location of accelerometers |
|---|---|---|---|---|---|---|---|
| 5-storey | 0.5 | 0.40 | 0.40 | 5.6 | 43 | 1, 3, 5 | 1, 2, 3, 4, 5 |
| 10-storey | 1.0 | 0.40 | 0.40 | 2.85 | 74.6 | 1, 3, 5, 7, 9, 10 | 1, 3, 5, 7, 8, 9, 10 |

Figure 4.46 and Figure 4.47 illustrate the shaking table tests on the fixed-base ten storey and five storey model structures, respectively. The resulting natural frequencies of the constructed structural models obtained from Sine Sweep test results were 5.6 Hz and 2.85 Hz for the five storey and ten storey model structures, respectively, which are in a very good agreement with the desired natural frequency of the structural models (5.83 Hz and 2.83 Hz, respectively).

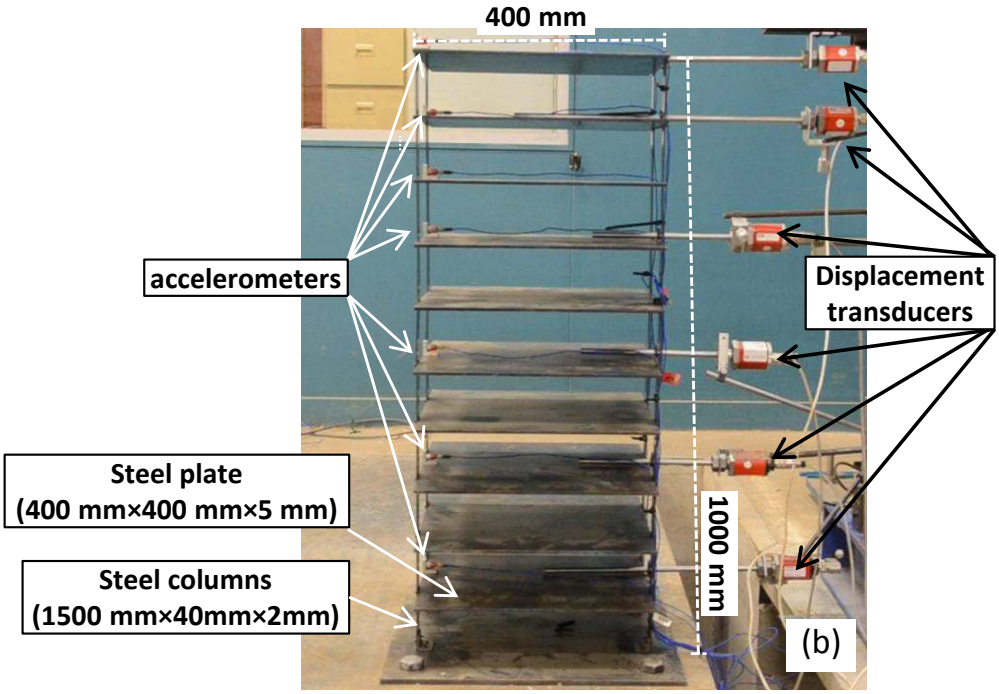


**Figure 4.46** Ten storey fixed-base model structure for shaking table tests

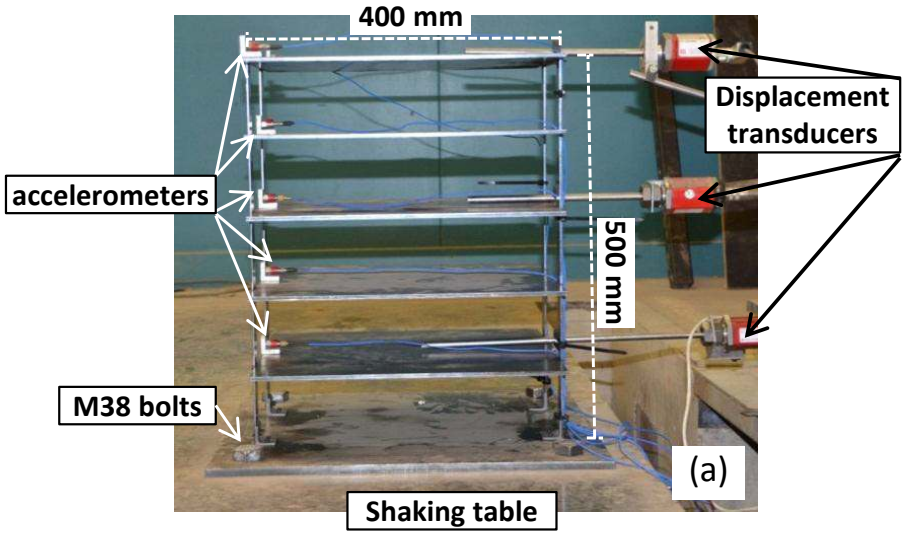


**Figure 4.47** Five storey fixed-base model structure for shaking table tests

Accordingly, shaking table tests were performed by applying scaled earthquake acceleration records of 1994 Northridge (Figure 8a), 1995 Kobe (Figure 8b), 1940 El Centro (Figure 8c), and 1968 Hachinohe (Figure 8d) to the fixed-base structural models and the results in terms of maximum lateral deflections are presented and discussed in Section 4.11.1.

For the case of structures supported by end-bearing pile foundations same test setup, as explained earlier for the fifteen storey model structure, is adopted. Figure 4.48 and Figure 4.49 illustrate the characteristics of the shaking table tests on the ten storey and five storey model structures with pile foundations, respectively. Performing Sine Sweep test, the natural frequency of the soil-pile-structure model was measured to be 5.2 Hz and 2.6 Hz for the five storey and ten storey model structures, respectively. The results of the conducted shaking table tests under the influence of four scaled earthquake acceleration records in terms of the maximum lateral deflections for five storey and ten storey model structures are presented and discussed in Section 4.11.1.

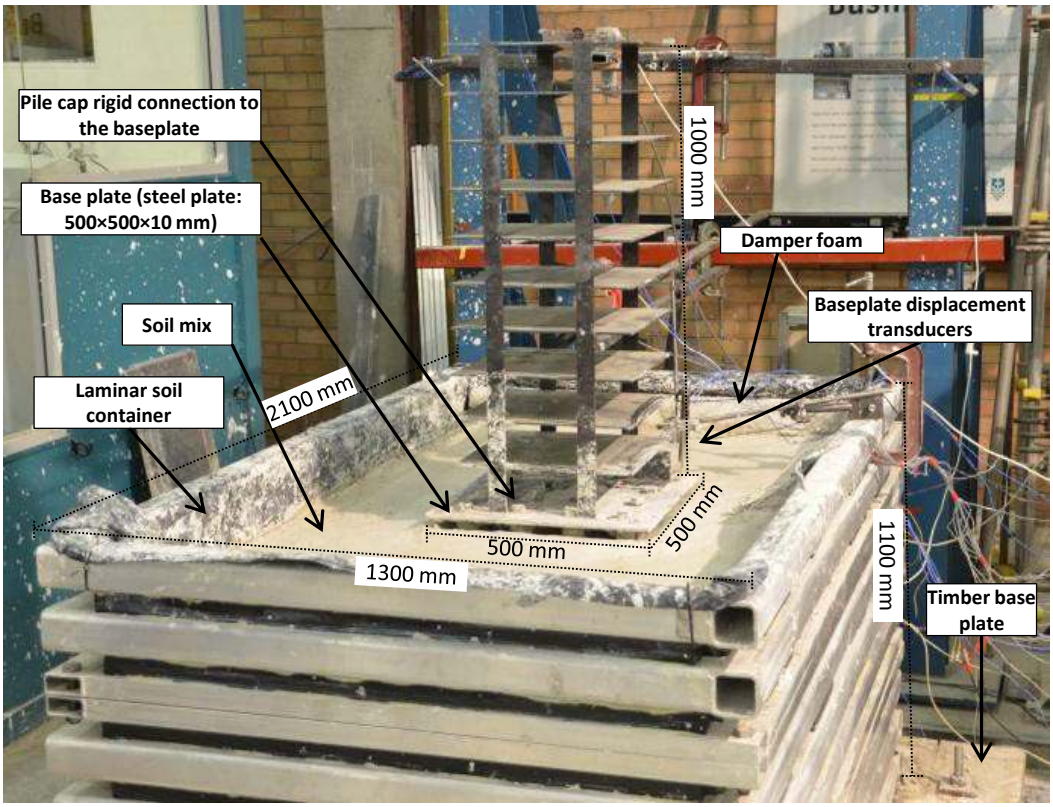


**Figure 4.48** Shaking table tests for the ten storey model structure with end-bearing pile foundation.

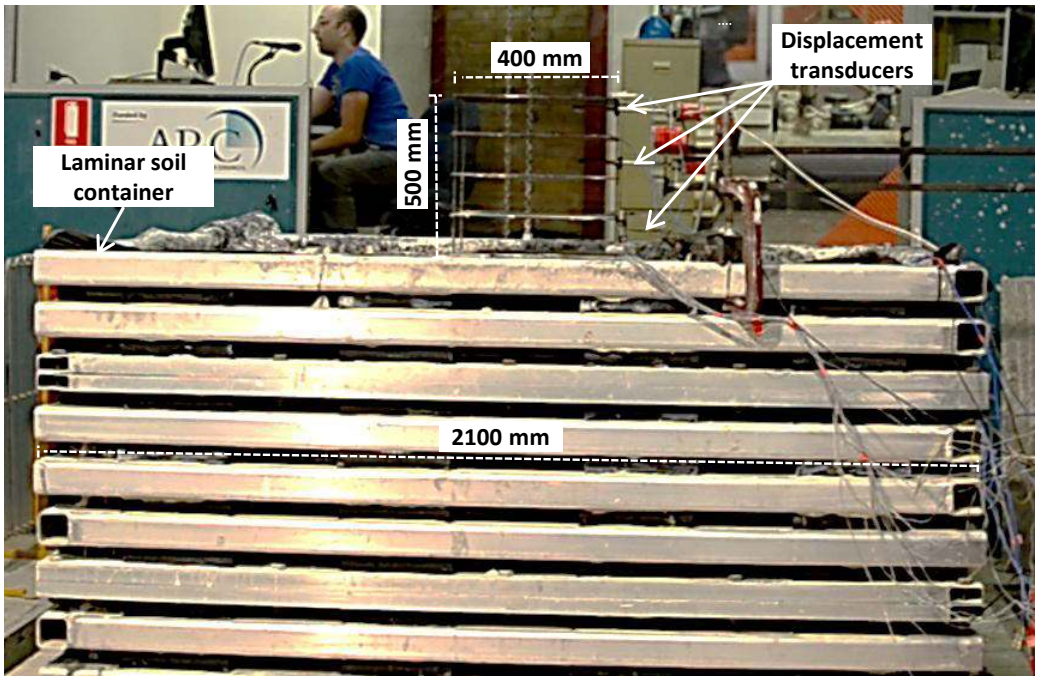


**Figure 4.49** Shaking table tests for the five storey model structure with end-bearing pile foundation.

### 4.11.1 Results and Discussion on the Model Structures with Various Heights

The results of conducted shaking table tests on the five storey and ten storey model structure in terms of the maximum lateral deformation are shown in Figure 4.50 and Figure 4.52, respectively. Figures 4.51 and 4.53 illustrate samples of time-history deformation records used to obtain the maximum lateral deformations of the five storey and ten storey model structure reported in Figures 4.50 and Figure 4.52, respectively. Accordingly, in comparison to the fixed-base structure the maximum lateral deformation of the five storey structure supported by the end-bearing pile foundation increases by 12%, 37%, 8%, and 14% under the influence of 1994 Northridge, 1995 Kobe, 1940 El Centro, and 1968 Hachinohe earthquakes, respectively. For ten storey structure (Figure 4.52) the maximum lateral deformation increases by up to 16% in comparison to the fixed-base structures. Moreover, the fifteen storey model structure supported by the end-bearing pile foundation experiences up to 26% increase in the maximum lateral deformation (Figure 4.43) in comparison to the fixed-base fifteen storey model structure. As an example, the lateral deformation of five, ten, and fifteen storey buildings subjected to the 1994 Northridge earthquake increase by 12%, 16%,

18% due to the SSPSI, in comparison to the fixed-base condition. In the meantime, in comparison to the fixed-base structure the natural frequency of the system reduces due to the seismic soil-pile-structure interaction (from 5.6 Hz, to 5.2 Hz for the five storey structure; from 2.85 Hz, to 2.60 Hz for the ten storey structure; and from 2.19 Hz, to 1.93 Hz for the fifteen storey structure). Therefore, as mentioned earlier, such decreases in the natural frequency (increases in the natural period) alter the response of the building frames under the seismic excitation to some extent. This is due to the fact that the natural period of the system lies in the long period region of the response spectrum curve, and the displacement response tends to increase, while inertia force decrease.

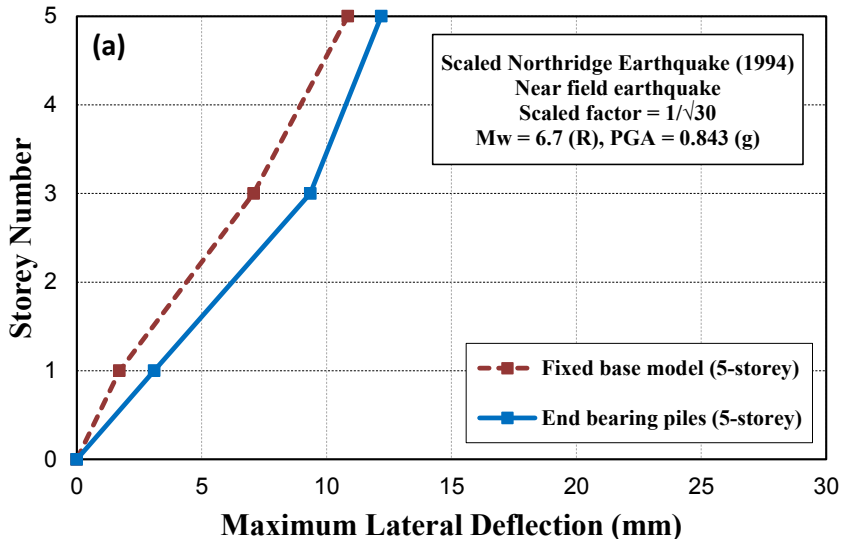


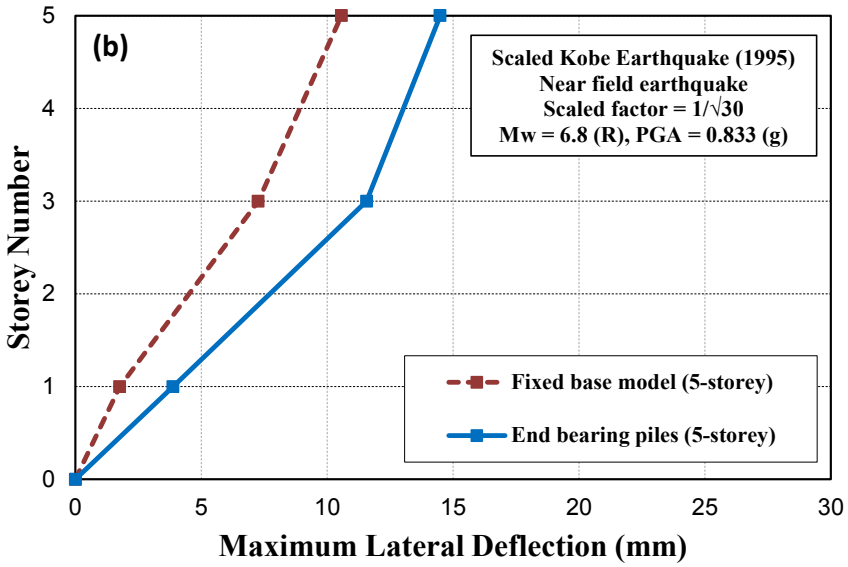

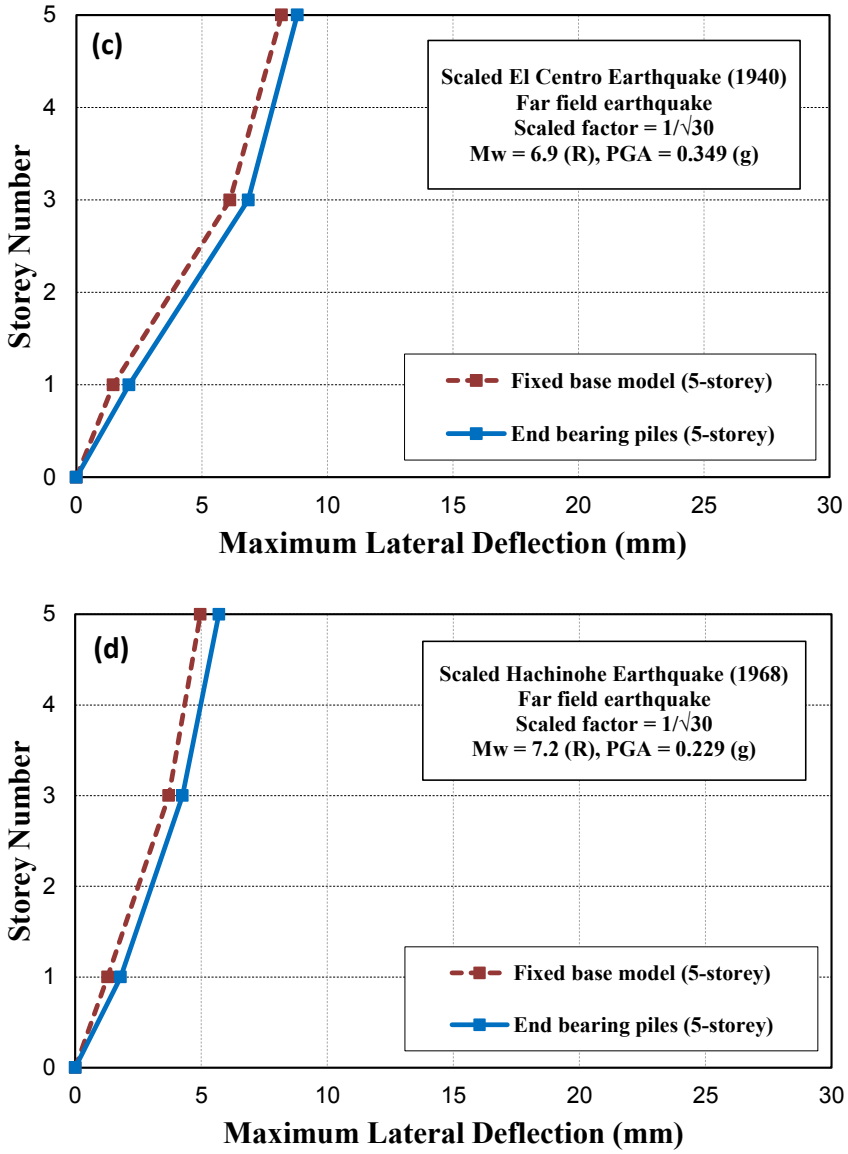


**Figure 4.50** Recorded maximum lateral deflection of the five storey model structure from the shaking table tests under the influence of: (a) 1994 Northridge earthquake; (b) 1995 Kobe earthquake; (c) 1940 El Centro earthquake; (d) 1968 Hachinohe earthquake

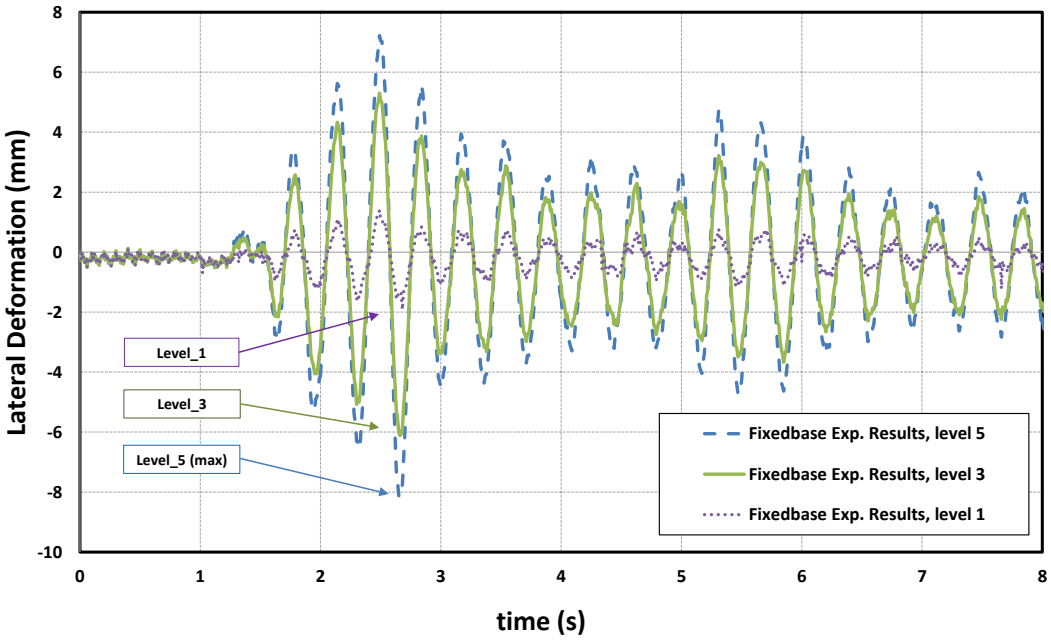


**Figure 4.51** Sample experimental time-history displacement results for the fixed-base five storey model structure under the influence of 1940 El Centro earthquake

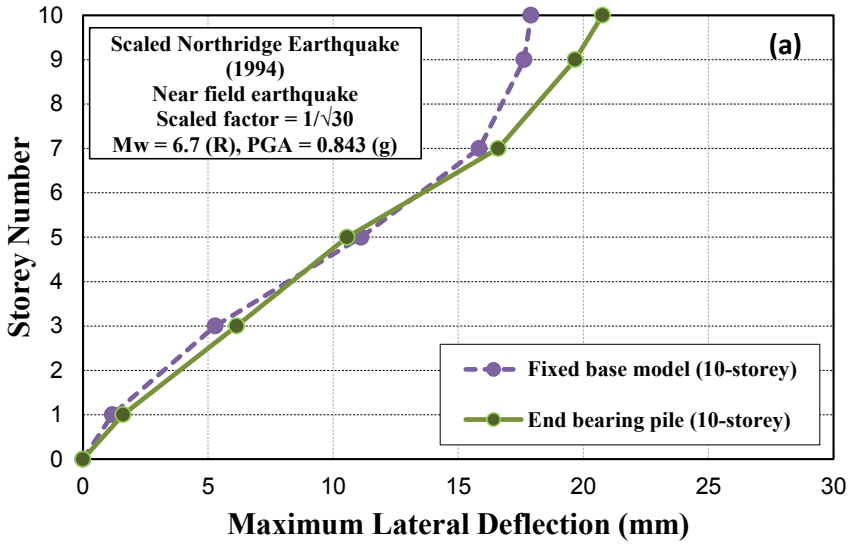

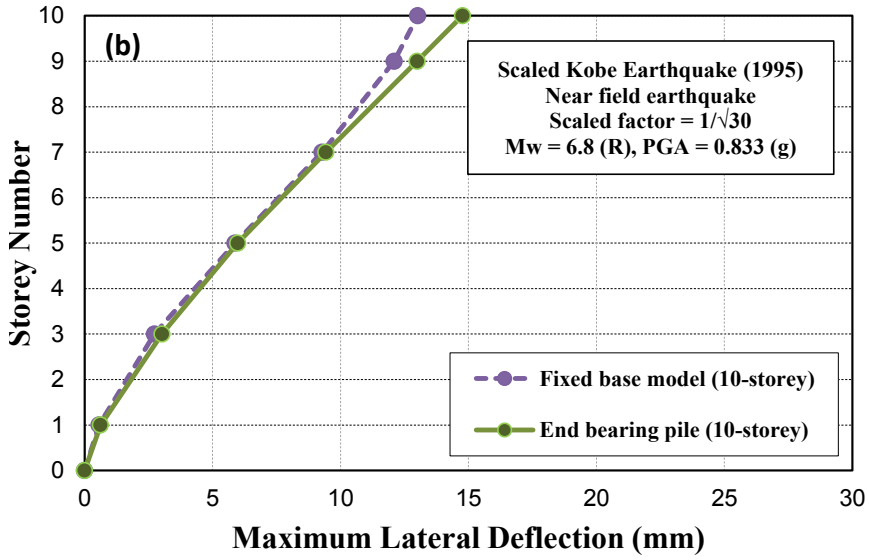
(b)
Scaled Kobe Earthquake (1995)
Near field earthquake
Scaled factor = 1/√30
Mw = 6.8 (R), PGA = 0.833 (g)
Fixed base model (10-storey)
End bearing pile (10-storey)
Storey Number
Maximum Lateral Deflection (mm)
0
1
2
3
4
5
6
7
8
9
10
0
5
10
15
20
25
30

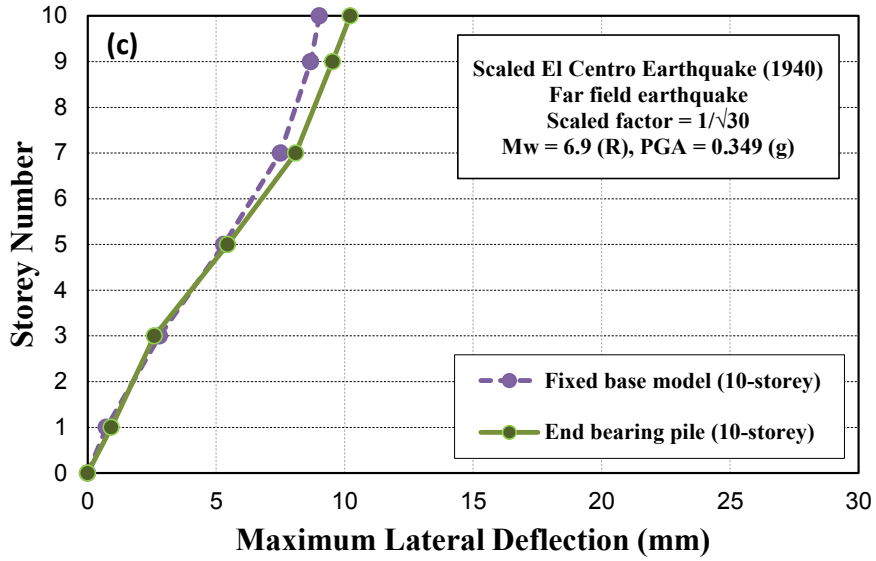
(c)
Scaled El Centro Earthquake (1940)
Far field earthquake
Scaled factor = 1/√30
Mw = 6.9 (R), PGA = 0.349 (g)
Fixed base model (10-storey)
End bearing pile (10-storey)
Storey Number
Maximum Lateral Deflection (mm)
0
1
2
3
4
5
6
7
8
9
10
0
5
10
15
20
25
30

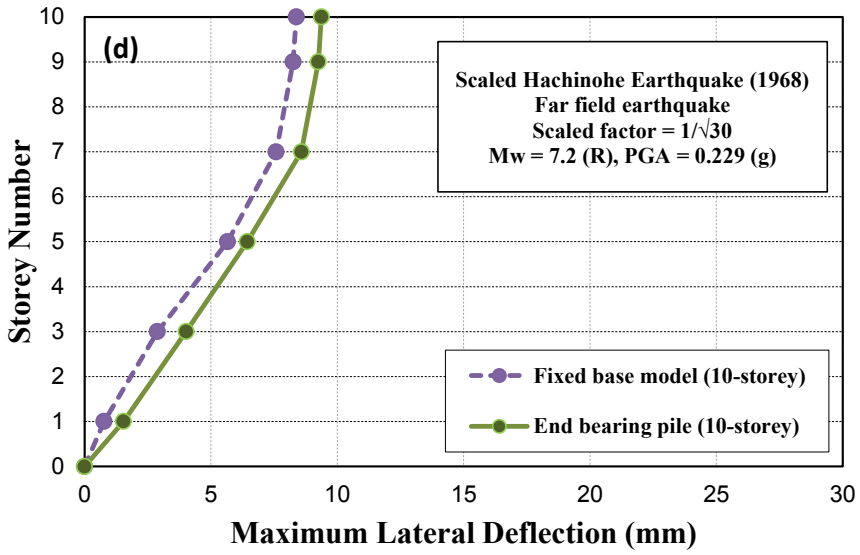


**Figure 4.52** Recorded maximum lateral deflection of the five storey model structure from the shaking table tests under the influence of: (a) 1994 Northridge earthquake; (b) 1995 Kobe earthquake; (c) 1940 El Centro earthquake; (d) 1968 Hachinohe earthquake

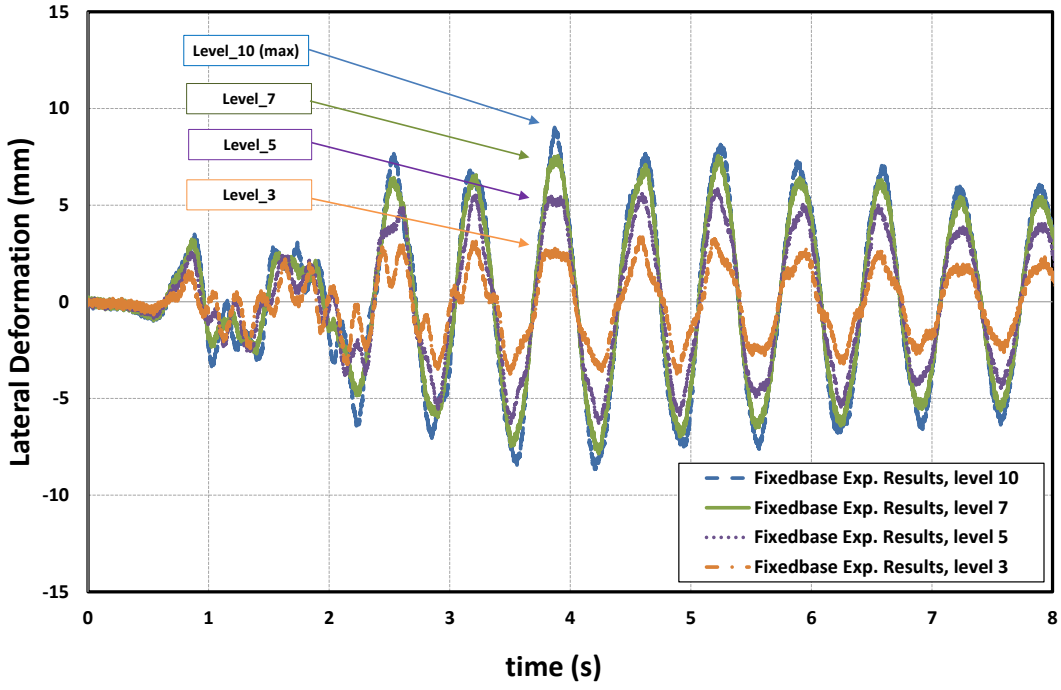


**Figure 4.53** Sample experimental time-history displacement results for the fixed-base ten storey model structure under the influence of 1940 El Centro earthquake

The recorded maximum vertical displacement and rocking angle of the base plate from the conducted shaking table tests for the five storey and ten storey model structures are represented in Table 4.14 and Table 4.15, respectively. Comparing Figure

4.50 with table 4.14, in the five storey model structure on average 16.9% of the maximum lateral deflections were due to the rocking component, while 83.1% took place due to the distortion component. In addition, comparing Figure 4.52 with table 4.14, in the ten storey model structure on average 18.8% of the maximum lateral deflections were due to the rocking component, while 81.2% took place due to the distortion component. These values for the fifteen storey structures (Section 4.10) are 19.7% and 80.3%, respectively. For example, under the influence of 1940 El Centro earthquake, the maximum lateral deflection at the top of the fixed-base ten storey model was measured to be 9.02 mm due to distortion component, while the maximum lateral deflection at the top of the same structure supported by end-bearing pile foundation was 10.22 mm with 2.35 mm of this value being due to rocking component and 7.9 mm took place due to distortion component.

**Table 4.14** Maximum vertical displacement of the base plate obtained from shaking table tests

| **Scaled Earthquake Acceleration Record** | **Maximum Vertical Displacement** | | | |
|---|---|---|---|---|
| | **Five storey model structure** | | **Ten storey model structure** | |
| | Fixed-base | End-bearing Pile Foundation | Fixed-base | End-bearing Pile Foundation |
| 1994 Northridge | 0 | 0.77 mm | 0 | 0.85 mm |
| 1995 Kobe | 0 | 1.82 mm | 0 | 0.64 mm |
| 1940 El Centro | 0 | 0.42 mm | 0 | 0.58 mm |
| 1968 Hachinohe | 0 | 0.47 mm | 0 | 0.52 mm |

**Table 4.15** Maximum rocking angle of the base plate obtained from shaking table tests

| **Scaled Earthquake Acceleration Record** | **Rocking Angle of the Foundation** | | | |
|---|---|---|---|---|
| | **Five storey model structure** | | **Ten storey model structure** | |
| | Fixed-base | End-bearing Pile Foundation | Fixed-base | End-bearing Pile Foundation |
| 1994 Northridge | 0 | 0.18° | 0 | 0.19° |
| 1995 Kobe | 0 | 0.42° | 0 | 0.15° |
| 1940 El Centro | 0 | 0.10° | 0 | 0.13° |
| 1968 Hachinohe | 0 | 0.11° | 0 | 0.12° |

Comparing the three model structures, the increase in the maximum lateral deflection is more severe for the fifteen storey model structure in comparison with the ten storey and five storey model structures. This is due to the fact that the rocking component results in more deformation as the height of the structure increases. It is interesting to point out that the influence of SSPSI on the five storey model structure is considerably higher under the 1995 Kobe earthquake in comparison to the other earthquakes. This can be due to the nature of the imposed seismic motion and its frequency content which hits the structure (with the modified dynamic properties due to SSPSI) and is close to the natural frequency of the system resulting in attraction of extra energy by the superstructure and getting close to the resonant conditions. This phenomenon is similar to what occurred on the lake zone of Mexico City during 1985 Mexico City earthquake in which many intermediate height structures with natural periods close to the dominant frequency of the earthquake (recorded on the ground surface) experienced the most damage (Nghiem, 2009; Mendoza and Romo, 1989).

The locations of the installed strain gauges on the pile elements are shown in Figure 4.54. Pile numbers 1, 6, 11, and 16 were instrumented, and in three points along the piles, strain and in turn flexural moments were measured during the tests. For instance, the measured moment distribution along the pile number 1, supporting five storey, ten storey, and fifteen storey model structures subjected to the four mentioned earthquake excitations at the instant of peak pile head deflection are presented in Figure 4.55. According to the theory of elasticity and Hooke's law (Timoshenko, 1940), the generated flexural moment in the pile section is a function of the recorded strain in the strain gauges, referring to the following equation:

$$M = \frac{2EI}{D} \times \varepsilon \tag{4.6}$$

Where, $E$ is the Young modulus, $I$ is the moment of inertia, $D$ is the outer diameter of the pile, and ε is the recorded strain in the strain gauges. The distribution of the moment amplitude along the pile shows that the bending moments are large at the top of the piles while small bending were generated at the tips. In addition, by increasing the height of the model structure more bending moments were generated in the pile elements. This is due to the fact that the fifteen storey model structure, due to its larger mass, attracts more inertial force from the same seismic excitation in comparison to the ten storey or five storey model structures. As a result, extra lateral forces and

flexural moments are induced in the pile foundation system for the fifteen storey building. It should be noted that for the five storey model structure under 1995 Kobe earthquake, as mentioned earlier, due to getting closer to the resonant conditions, extra energy were attracted by the superstructure resulting in the amplified pile foundation response in comparison with the other cases as shown in Figure 4.55b.

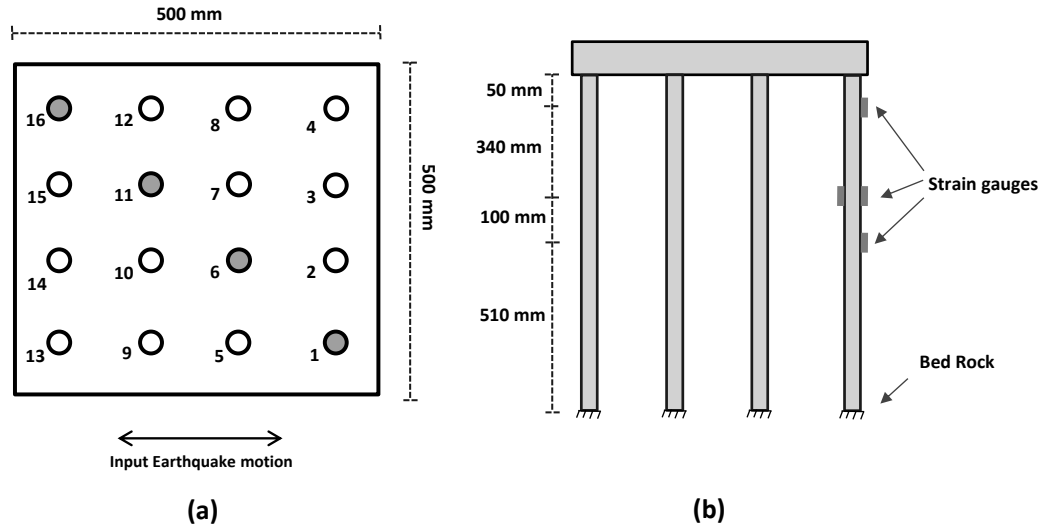


**Figure 4.54** (a) Plan of the pile group foundation for the shaking table tests; (b) Location of the installed strain gauges on the pile elements

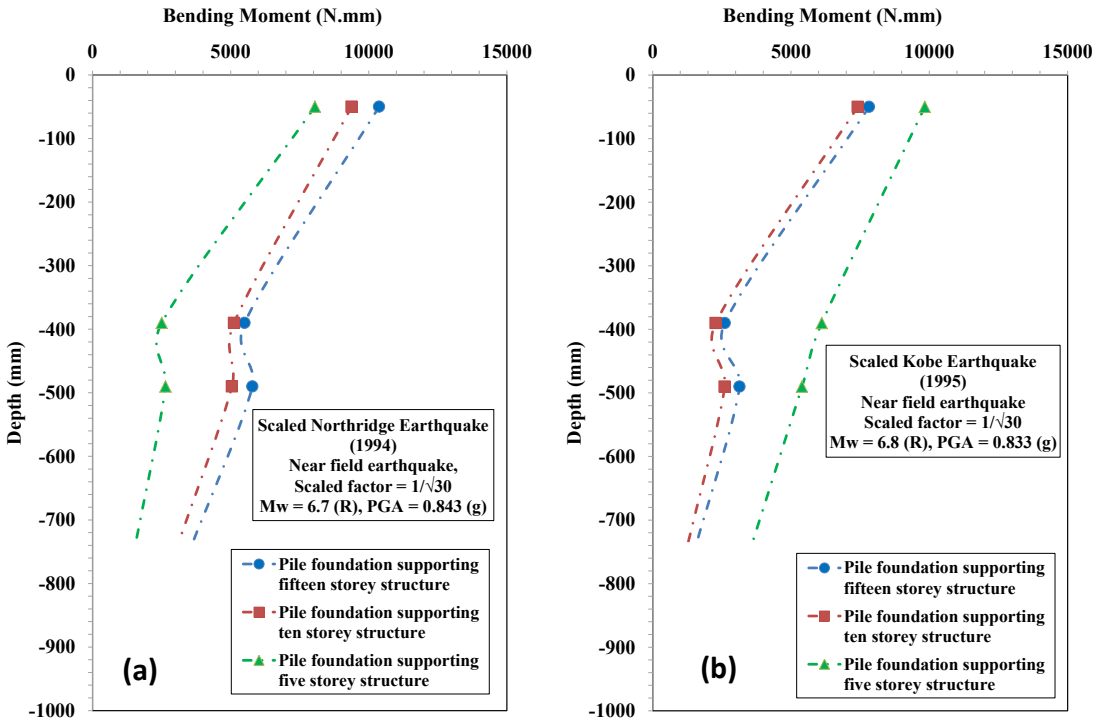

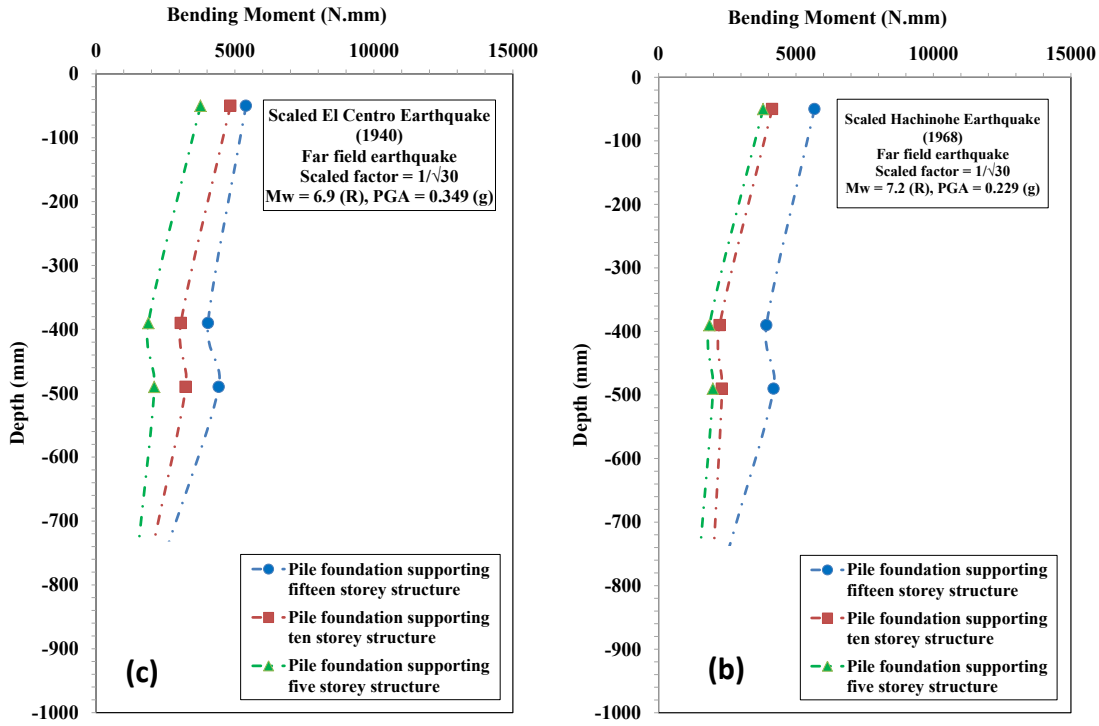


**Figure 4.55** Recorded bending moment distribution along the pile number 1 supporting five storey, ten storey, and fifteen storey model structures under the influence of: (a) 1994 Northridge earthquake; (b) 1995 Kobe earthquake; (c) 1940 El Centro earthquake; (d) 1968 Hachinohe earthquake

The corresponding inter-storey drifts of the model structures were calculated (Figures 4.56-4.58) using the following equation based on the Australian standard (AS1170.4, 2007):

$$Drift = (d_{i+1}-d_i) / h \qquad (4.7)$$

where, $d_{i+1}$ is deflection at $(i+1)$ level, $d_i$ is deflection at $(i)$ level, and $h$ is the storey height. In the performance-based seismic design, the seismic performance (performance level) is described by considering the maximum allowable damage state (damage performance) for an identified seismic hazard (hazard level). Performance levels describe the state of structures after being subjected to a certain hazard level, and based on FEMA273/274 (BSSC, 1997) are classified as: fully operational, operational, life safe, near collapse, or collapse. Overall lateral deflection, ductility demand, and inter-storey drifts are the most commonly used damage parameters. The above mentioned five qualitative levels are related to the corresponding quantitative maximum inter-storey drifts (as a damage parameter) of: <0.2%, <0.5%, <1.5%, <2.5%, and >2.5%, respectively (BSSC, 1997). In addition, most of the force-based design codes employ an

additional check in terms of limiting inter-storey drifts to ensure that particular deformation-based criteria are met. For example, ASCE (ASCE7-10, 2010) defines allowable storey drift for structures considering type and risk category of the structure. Australian Earthquake Code (AS1170.4, 2007) indicates 1.5% as the maximum allowable storey drift.

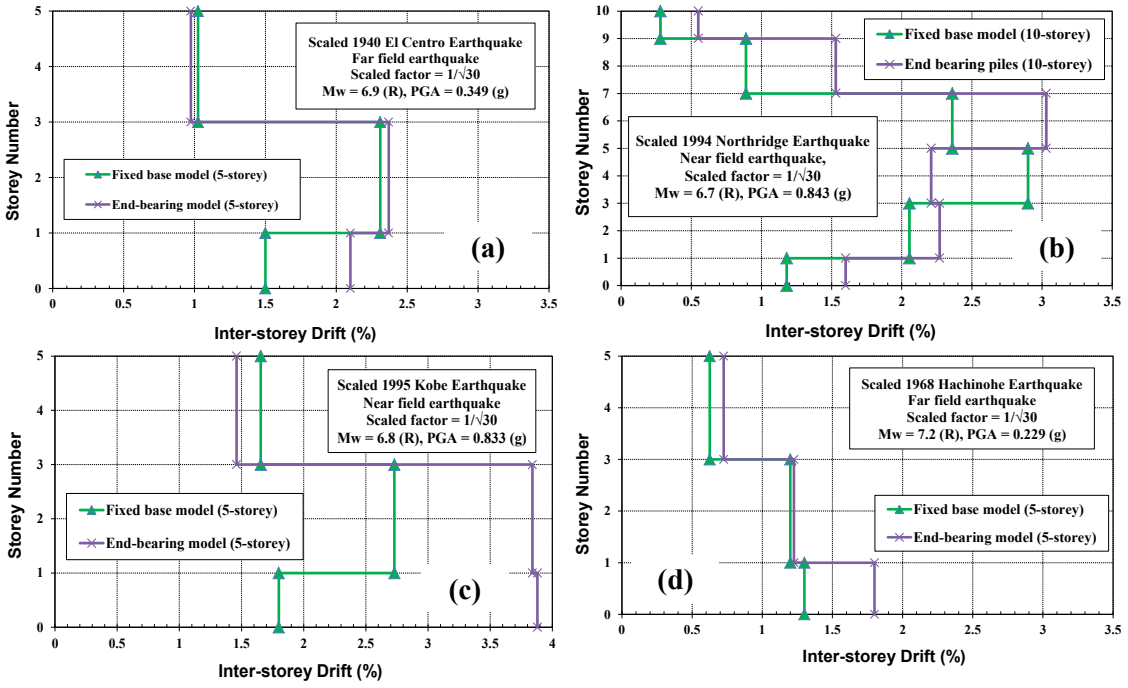


**Figure 4.56** Recorded maximum lateral deflection of the five storey model structure from the shaking table tests under the influence of: (a) 1994 Northridge earthquake; (b) 1995 Kobe earthquake; (c) 1940 El Centro earthquake; (d) 1968 Hachinohe earthquake

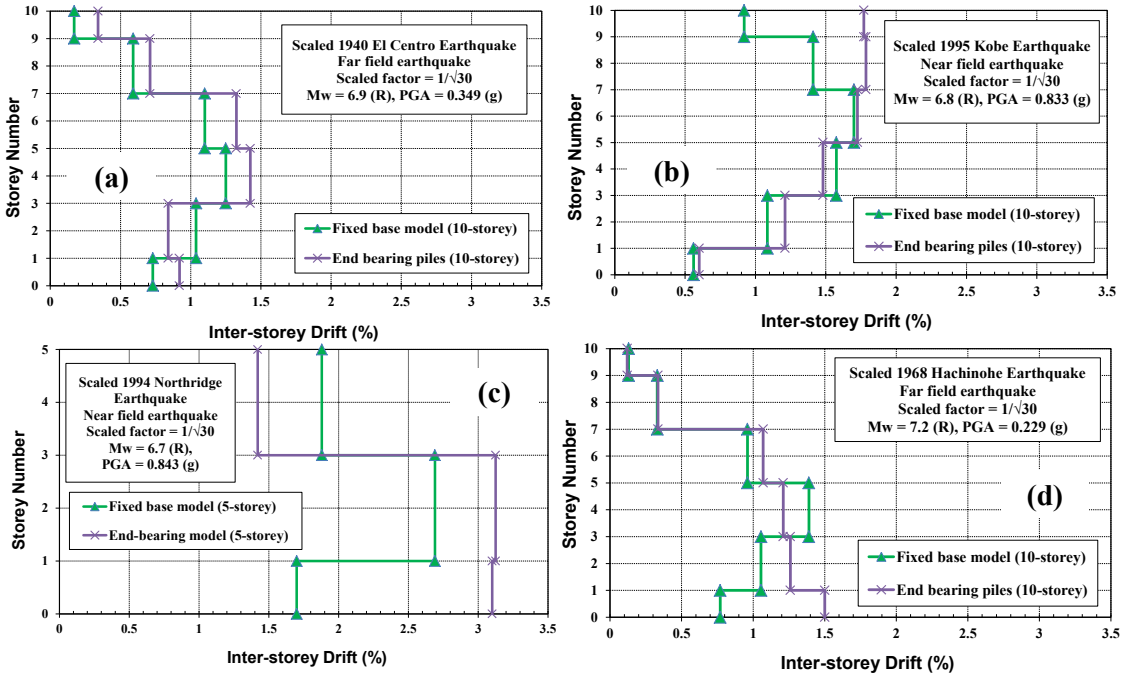


**Figure 4.57** Recorded maximum lateral deflection of the ten storey model structure from the shaking table tests under the influence of: (a) 1994 Northridge earthquake; (b) 1995 Kobe earthquake; (c) 1940 El Centro earthquake; (d) 1968 Hachinohe earthquake

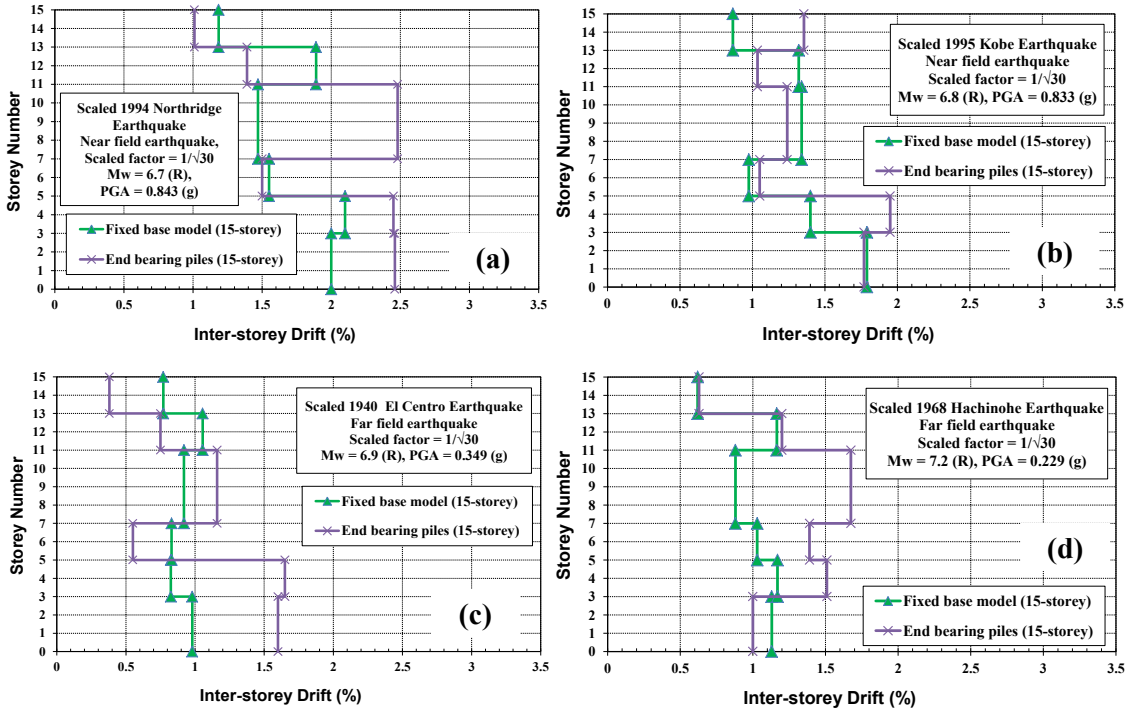


**Figure 4.58** Recorded maximum lateral deflection of the fifteen storey model structure from the shaking table tests under the influence of: (a) 1994 Northridge earthquake; (b) 1995 Kobe earthquake; (c) 1940 El Centro earthquake; (d) 1968 Hachinohe earthquake

According to Figures 4.56-4.58, considering the effect of SSPSI increases the generated inter-storey drifts in the model structures during the applied earthquakes. For example, the maximum recorded inter-storey drift of the fifteen storey fixed-base structure subjected to 1940 El Centro earthquake is measured to be 1.05%, while the corresponding value for the end-bearing pile foundation case is 1.65%. In other words, SSPSI induces 56% increase in the recorded maximum inter-storey drifts in this case. For ten and five storey model structures subjected to 1940 El Centro earthquake, considering the effect of SSPSI, induces 14% and 3% increase in the recorded inter-storey drifts, respectively. This increase in the inter-storey drifts of the superstructures due to SSPSI can shift the performance level of the structures toward near-collapse or collapse levels (BSSC, 1997), which is of crucial importance in the performance based design of the structures . Therefore, the amplified values of the inter-storey drifts due to SSPSI should be controlled and minimised for both structural and non-structural elements. The extent that the presence of the pile foundation influences the structural seismic response depends on the characteristics of the superstructure such as the structural height.

Consequently, by comparing the experimental results on structures with different heights, it can be concluded that considering the effects of SSPSI can alter the dynamic characteristics of the superstructure with different heights. In addition, the lateral deflections of structures siting on end-bearing pile foundations were amplified in comparison to the fixed-base model. Generally, this amplification which is mainly due to the rocking component is more severe for taller buildings (e.g. under 1994 Northridge, 1940 El Centro, and 1968 Hachinohe earthquakes) considering the range of the buildings investigated in this study.

## 4.12 Summary

Employing pile foundations, either floating or end-bearing, is a common practice to transfer structural loads through the soft soil to the underlying bedrock or the stiffer layers in order to increase the bearing capacity and reduce the settlement of the superstructure. In the seismic design of structures supported by different types of foundations, structural engineers often ignore or simplify the soil-pile-structure interaction, and design the structure under the fixed-based condition. In order to assess

the accuracy of this assumption and to investigate the effects of soil-pile structure interaction on the seismic response of buildings, series of shaking table experimental tests were conducted in this study. A laminar soil container was designed to simulate the free field soil response by minimising boundary effects, and the superstructure was simulated as a multi-storey frame representing most of the dynamic properties of the prototype structure. Four sets of shaking events including 1995 Kobe Earthquake, 1994 Northridge Earthquake, 1940 El Centro Earthquake, and 1968 Hachinohe Earthquake were applied. The improved physical modelling techniques in this study such as designing the soil mix and the laminar soil container were explained in details which can be used by other researchers to achieve more accurate simulation of the soil-structure interaction in 1g shaking table tests.

According to the shaking table test results, the maximum lateral deflection of the fifteen storey structure supported by end-bearing and floating pile foundations increases on average by 17% and 34% in comparison to the fixed-base structure, respectively. Moreover, the maximum lateral deflection of the structure supported by the shallow foundation is increased by 55% in comparison to the results obtained from the fixed-base structure. Therefore, comparing different types of foundations, pile foundations increase the lateral displacements of the superstructure in comparison with the fixed-base assumption, and reduce the lateral displacements in comparison to the shallow foundation case due to the rocking components. Consequently, the choice of the foundation type is dominant and should be included in investigating the influence of SSI on the superstructure response during shaking excitations, and conventional design procedures excluding the soil-structure interaction are not adequate to guarantee the structural safety for the moment resisting buildings resting on soft soils.

In addition, further experimental tests were conducted to investigate the influence of SSPSI on the dynamic response of buildings with various heights (i.e. five storey, ten storey, and fifteen storey buildings). By comparing the experimental results obtained from the model structures, it can be concluded that considering the effects of SSPSI can alter the dynamic characteristics of the superstructure. In addition, the lateral deflections of structures siting on end-bearing pile foundations were amplified in comparison to the fixed-base model. Generally, this amplification which is mainly due to the rocking component is more severe for taller buildings considering the range of the buildings

investigated in this study. As a particular case, the five storey model structure experienced considerably high amount of amplification under the influence of the 1995 Kobe earthquake, while accounting for SSPSI. This can be due to the nature of the imposed seismic motion and its frequency content which hits the structure (with the modified dynamic properties due to SSPSI) and is close to the natural frequency of the system resulting in attraction of extra energy by the superstructure and getting close to the resonant conditions.

The seismic soil-pile-structure interaction can increase the lateral deflection and in turn inter-storey drifts of the structures sitting on the soft soil. This increase in the inter-storey drifts of the structure can change the performance level of the structure to near collapse or even collapse levels in the performance based design methods. Therefore, ignoring the real deformability of the soil-pile system may affect the predicted damage level of structural and non-structural elements during earthquake as well as the lateral load carrying mechanism of soil-structure systems.

Consequently, considering the effects of the soil-pile-structure interaction can alter the dynamic characteristics of the superstructure, and ignoring the real deformability of the soil-pile system may affect the predicted damage level of structural and non-structural elements during earthquake as well as the lateral load carrying mechanism of soil-structure systems.

The results of the conducted experimental investigation in this chapter were employed to verify and calibrate the developed 3D numerical model in this study as explained in Chapter 5.

# Chapter 5- VERIFICATION OF THE DEVELOPED 3D NUMERICAL MODEL

## 5.1 General

Adopting the performance base design for structures involves achieving the target performance level under the anticipated loads. In order to provide a specified performance level for a structure at reasonable cost, conducting accurate analysis accounting for the entire soil-foundation-structure system is required. For this purpose, efficient and trustable analytical tools amenable for use by both structural and geotechnical engineers are required.

In this chapter, to assess the capabilities of the developed numerical model in simulating the SSPSI, the results of the conducted shaking table tests (Chapter 4) has been employed to verify and calibrate the developed numerical model in FLAC3D. Accordingly, the scaled fifteen storey model structure with four different types of foundations, namely: (i) fixed-base structure representing the situation excluding the soil-structure interaction, (ii) structure supported by shallow foundation, (iii) structure supported by floating (frictional) pile foundation in soft soil, and (iii) structure supported by end-bearing pile foundation, are simulated numerically and results are compared with the experimental measurements. The developed 3D nonlinear numerical model accounts for the various phenomena observed in SSPSI experimental study, providing further understanding on the influence of the SSPSI on the seismic response of the superstructure.

## 5.2 Numerical Model Setup

In the first stage, a three-dimensional numerical simulation of the constructed model structure with the fixed-base assumption, shown in Figure 5.1, was built in

FLAC3D employing the same dimensions as the scaled model structure used in the laboratory experiments (see Section 4.4.1). After defining the geometry of the model structure and proper mesh generation, the required structural parameters including density ($\rho$), bulk modulus of steel ($K$), shear modulus of Steel ($G$), Yield stress of steel ($F'_y$), and structural damping ratio ($\xi$), summarised in Table 5.1, were extracted from the construction details (Section 4.4.1), and adopted in the numerical simulation of the structure in FLAC3D.

**Table 5.1** Adopted parameters for 3D numerical simulation of the model structure

| Structural Properties | Value |
|---|---|
| Mass density, $\rho$ (kg/m$^3$) | 7560 |
| bulk modulus of steel, $K$ (*kPa*) | 1.65E8 |
| Shear modulus of Steel, G (*kPa*) | 7.6E7 |
| Structural damping ratio, $\xi$ *(%)** | 1.1 |
| Yield stress of steel, $F'_y$ *(MPa)* | 280 |

* Obtained from the free vibration results (see Section 4.6.1)

It should be noted that solid elements in FLAC3D are used to numerically model the scaled structure providing more accurate simulation of the employed steel plates and connections of the constructed model structure in the laboratory. Figure 5.1 illustrates the characteristics of the developed numerical model for the fixed-base model structure.

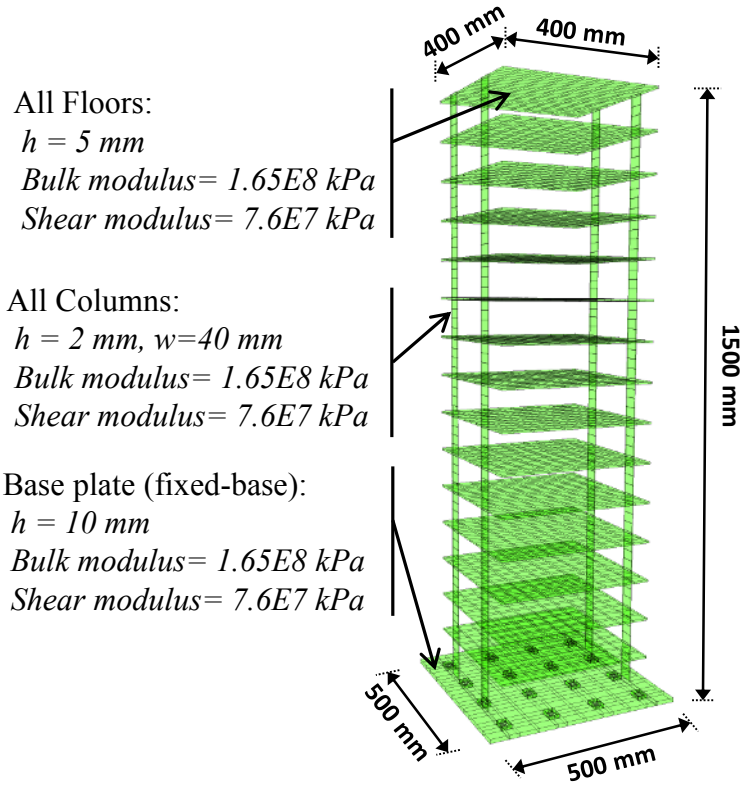


**Figure 5.1** Numerical grid and model components of fixed-base fifteen storey model structure in FLAC3D

Initially, static analysis, where the model should be analysis under gravity loads, is performed in order to achieve the static equilibrium. For the dynamic stage, fully nonlinear time-history analyses, as described in Chapter 3, were carried out under the influence of four scaled earthquake acceleration records including 1994 Northridge (Figure 4.8a), 1995 Kobe (Figure 4.8b), , 1940 El-Centro (Figure 4.8c), and 1968 Hachinohe (Figure 4.8d). Filtration and baseline correction are applied to the earthquake records derived from the experimental tests as explained in Section 3.8.

Geometric nonlinearity of the structures, capturing P-Delta effects, was accommodated by specifying large-strain solution mode in FLAC3D software in the structural analyses of fixed-base and flexible base models. In addition, running the analysis in large strain mode increases the accuracy of the analysis in determination of the deformations.

The results obtained from the numerical time-history analysis are compared with the previously measured experimental values as shown in Figure 5.2. To determine the

lateral deflections, the movement of the base plate (foundation) was subtracted from the storey movements. Therefore, all the records are relative to the base movements. Similar to the reported experimental results, the reported data are based on the lateral deformation of each storey when the maximum deflection at the top level occurred.

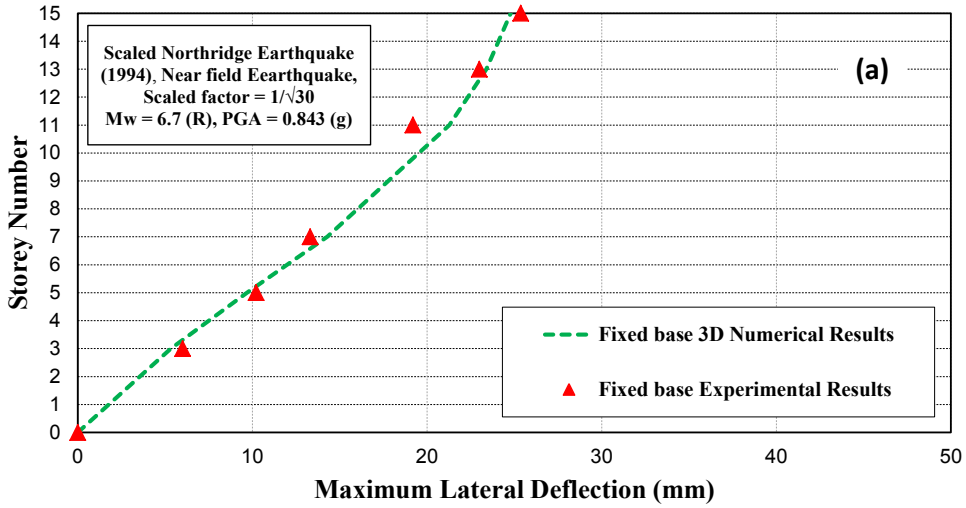


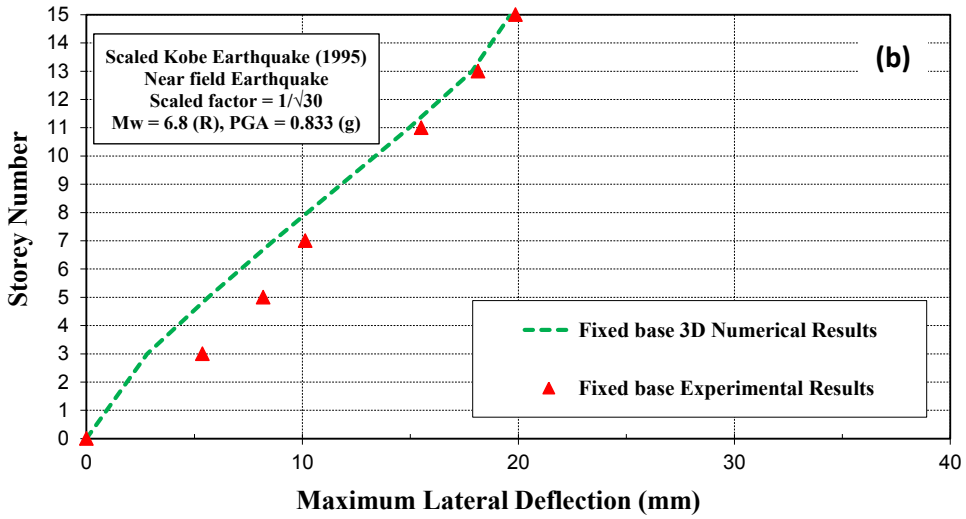

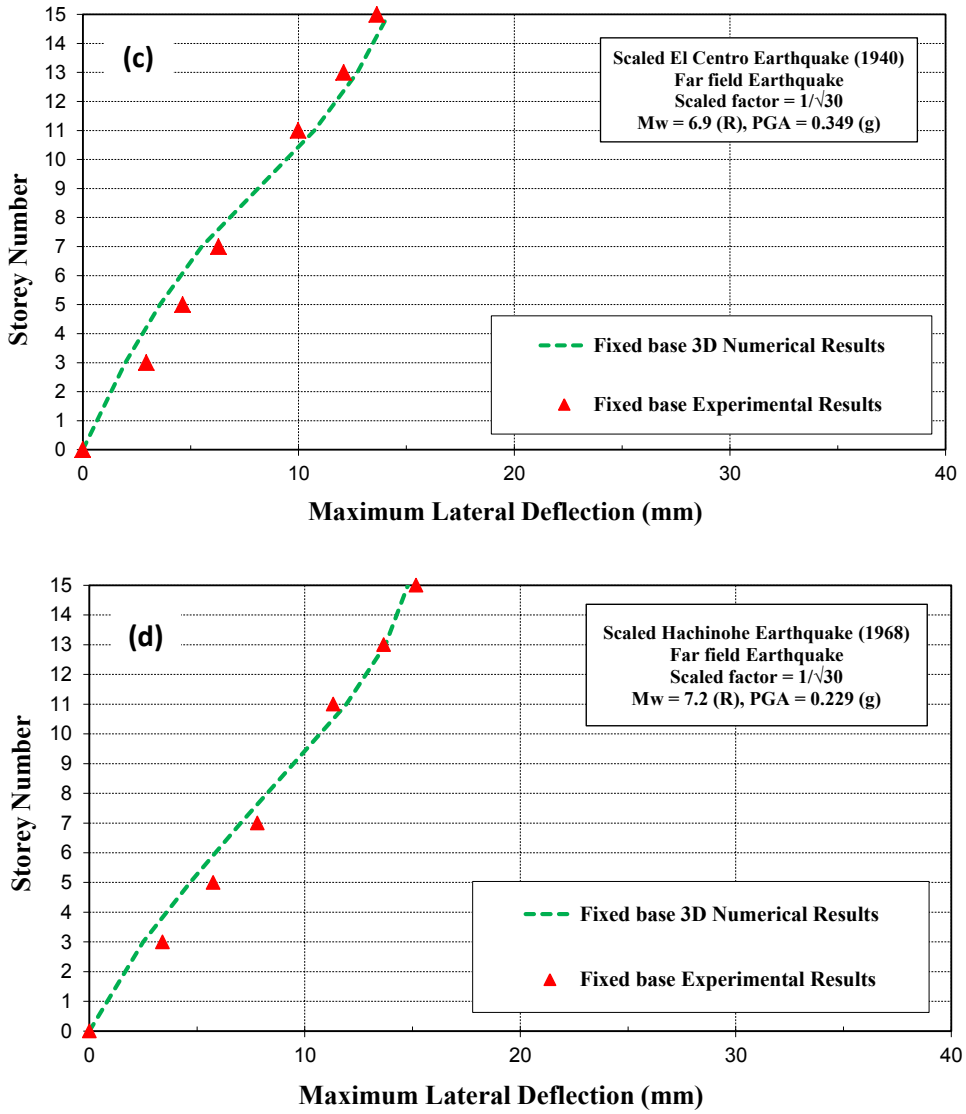


**Figure 5.2** 3D numerical predictions versus experimental measurements of the maximum lateral deformation of the fixed-base fifteen storey model structure under the influence of: (a) 1994 Northridge earthquake; (b) 1995 Kobe earthquake; (c) 1940 El Centro earthquake; (d) 1968 Hachinohe earthquake

For the shallow foundation cases, all the components of the model are simulated simultaneously as shown in Figure 5.3, where the same dimensions as the scaled model are adopted. In Figure 5.3 just half of the model is shown for more clarification. Experience gained from the parametric studies helped to finalise the adopted mesh size and the maximum unbalanced force at the grid points to optimise the accuracy and the computation speed, simultaneously.

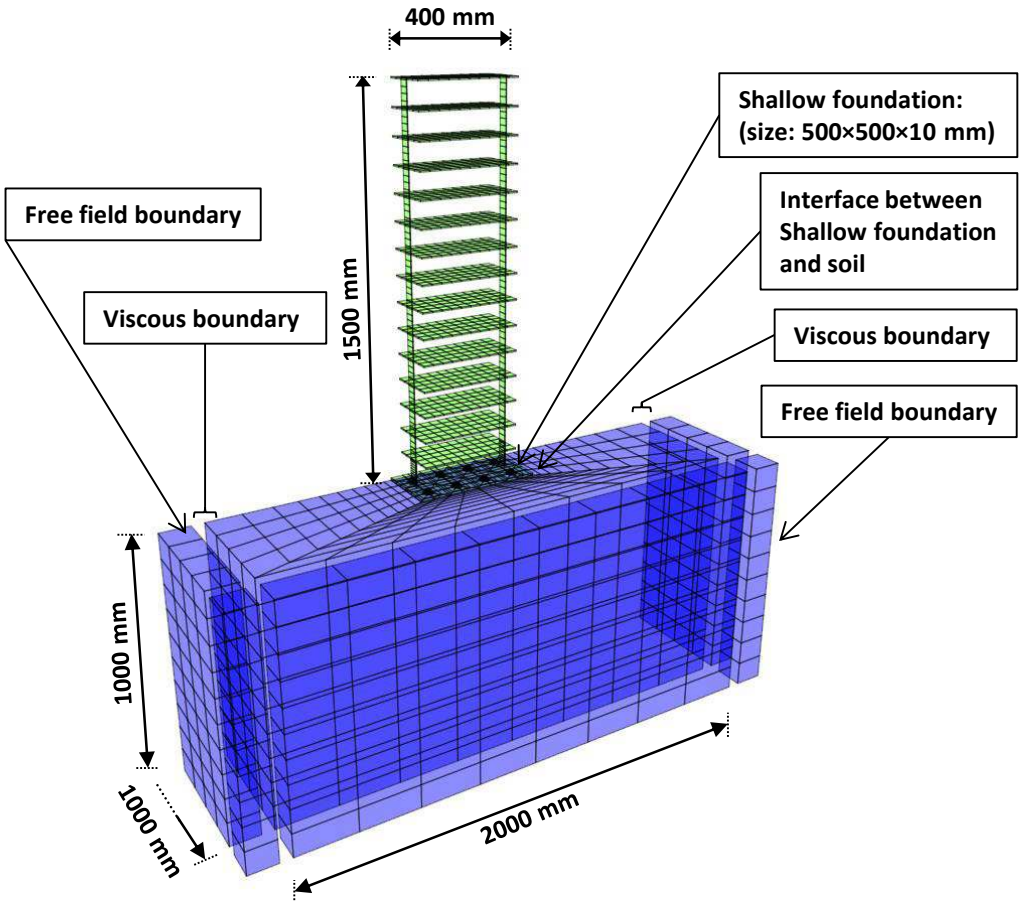


**Figure 5.3** Numerical grid and model components of the model structure supported by the shallow foundation in FLAC3D

In order to mathematically define Sun et al. (1988) backbone curves, the available hysteretic damping algorithm in FALC3D is employed. The numerical model adopts hysteretic damping algorithm representing the variation of the shear modulus and damping ratio of the soil with the cyclic shear strain capturing the energy absorbing characteristics of the soil. For this purpose, Hardin (Hardin and Drnevich, 1972) built-in tangent-modulus function for clay (see section 3.3.1) with the value of $\gamma_{ref} =$ 0.234 was adopted in this study as illustrated in Figure 5.4. A value of $\gamma_{ref}$ = 0.234, giving the coefficient of determination ($R^2$) equal to 0.91, produces the best match to the backbone curves suggested by Sun et al. (1988) for fine grained soils as illustrated in Figure 5.4, and thus was adopted in this study. The required soil parameters are derived from ten cylindrical soil specimens that were taken from the soil mix during the experimental tests (Section 4.7). The obtained values from the specimens were in conformity to the initial laboratory test results (Table 4.5), which were implemented to the developed

numerical model. Table 5.2 summarises the soil properties adopted in the 3D numerical simulation.

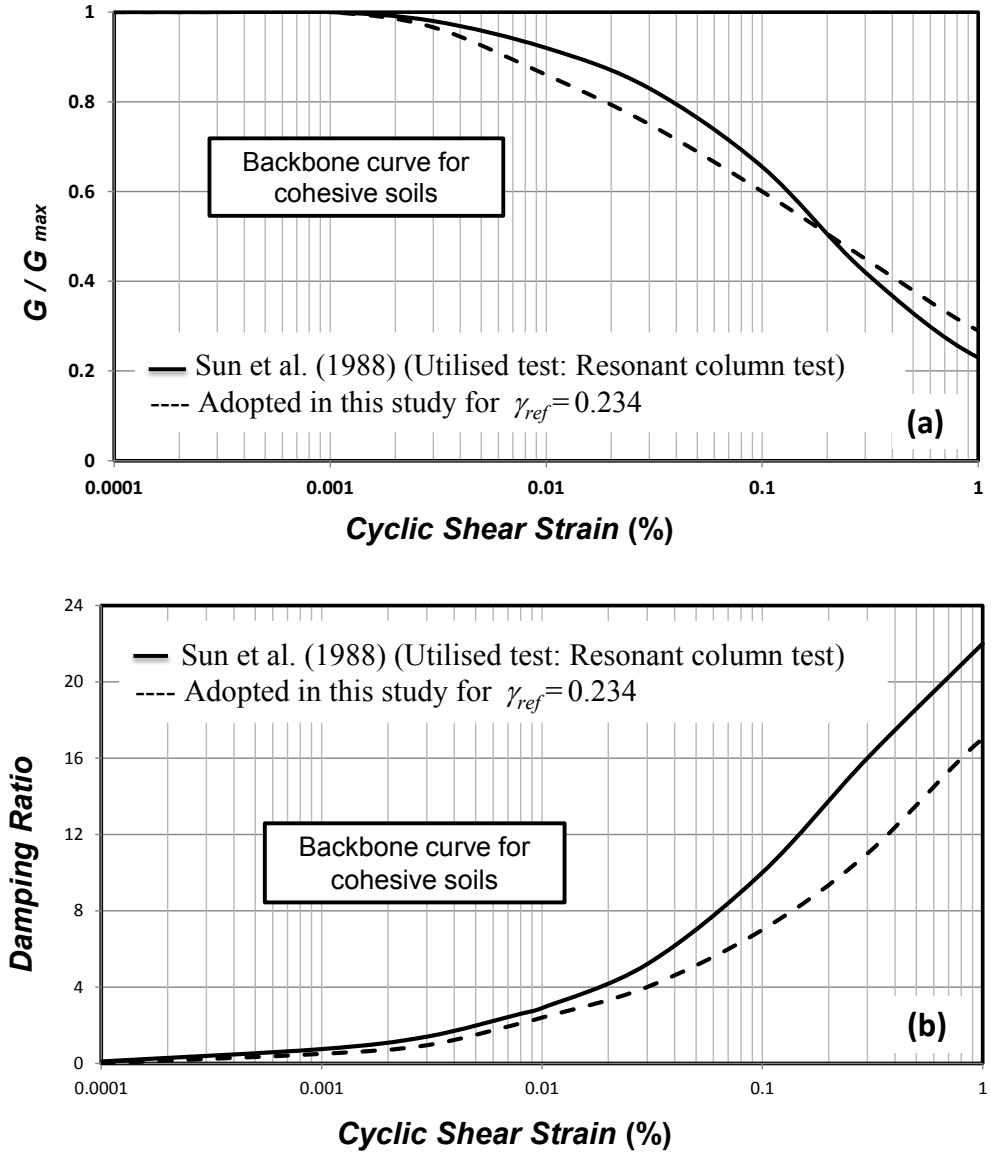


**Figure 5.4** Adopted fitting curve for fine grained soil in this study (after Sun et al. 1998): (a) relations between $G/G_{max}$ and cyclic shear strain; (b) relations between damping ratio and cyclic shear strain

**Table 5.2** Properties of the adopted soil properties in 3D numerical simulation

| Soil Properties | Value |
|---|---|
| Mass density, $\rho$ (kg/m$^3$) | 1450 |
| bulk modulus of steel, $K$ ($kPa$) | 13712 |
| Maximum shear modulus, $G_{max}$ (kPa) | 1776 |
| Shear wave velocity (m/s) | 35 |
| Undrained shear strength, $C_u$ (kPa) | 3.1 |
| Undrained friction angle, $\varphi_u$ (kPa) | 0 |
| Dilation angle, $\psi$ (degree) | 0 |

Appropriate interface elements between the soil surface and the shallow foundation base are considered to capture the possible uplift and sliding of the foundation. Referring to Section 3.6, properties of the adopted interface elements in terms of shear stiffness ($K_s$), normal stiffness ($K_n$), tensile strength ($T_s$), shear strength ($S_s$), and dilation angle ($\psi$) are summarised in Table 5.3.

**Table 5.3** Properties of the adopted interface elements in 3D numerical simulation

| Interface Properties | Value |
|---|---|
| Shear stiffness, $K_s$ (kPa/m) | 3E8 |
| Normal stiffness, $K_n$ (kPa/m) | 3E8 |
| Shear strength, $S_s$ (kPa) | 2.06E3 |
| Tensile strength, $T_s$ (kPa) | 0 |
| Dilation angle, $\psi$ (degree) | 0 |

Preliminary boundary conditions, as broadly discussed in Section 3.7, are defined for the static analysis step. During the dynamic time-history analysis, free field boundary conditions are assigned to the numerical model, which were connected to the main grid with the viscous dampers to avoid the reflection of the outward propagating waves back into the model. For future details of the adopted boundary conditions refer to Section 3.7. The four mentioned earthquake input motions are imposed to the entire base of the numerical model horizontally. Figure 5.5 compares the results of 3D numerical predictions with the previously recorded experimental measurements from

the shaking table tests, for the fifteen storey model structure supported by the shallow foundation.

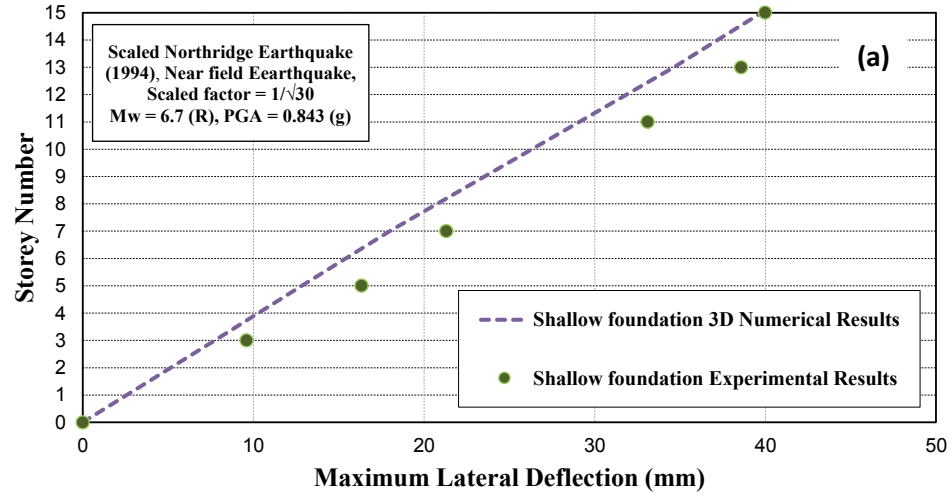


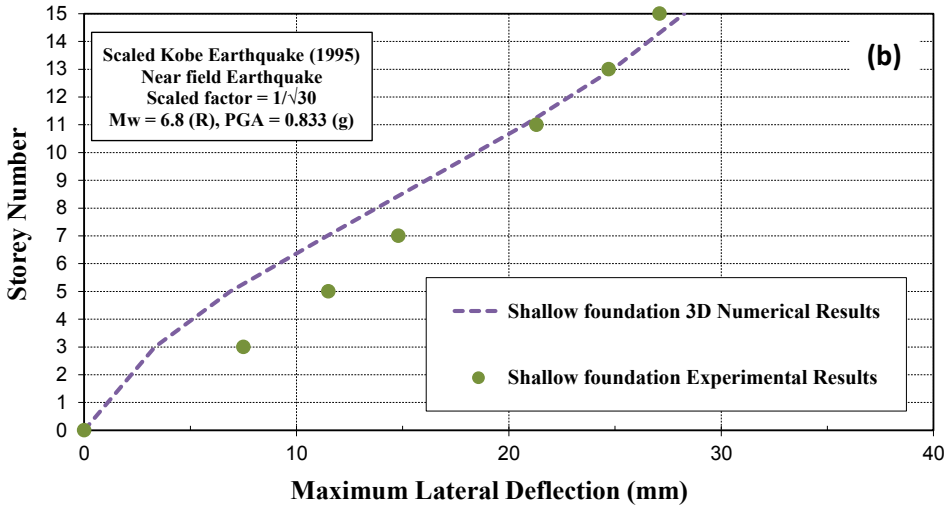


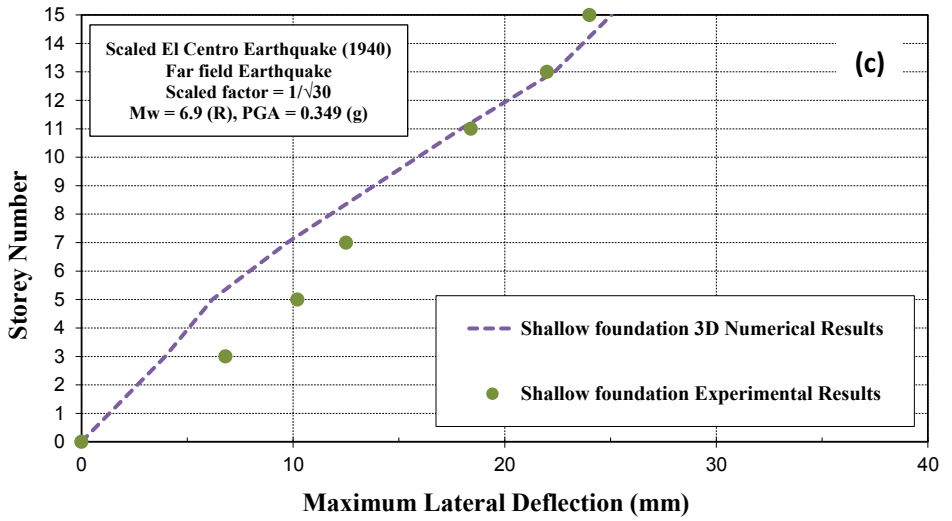

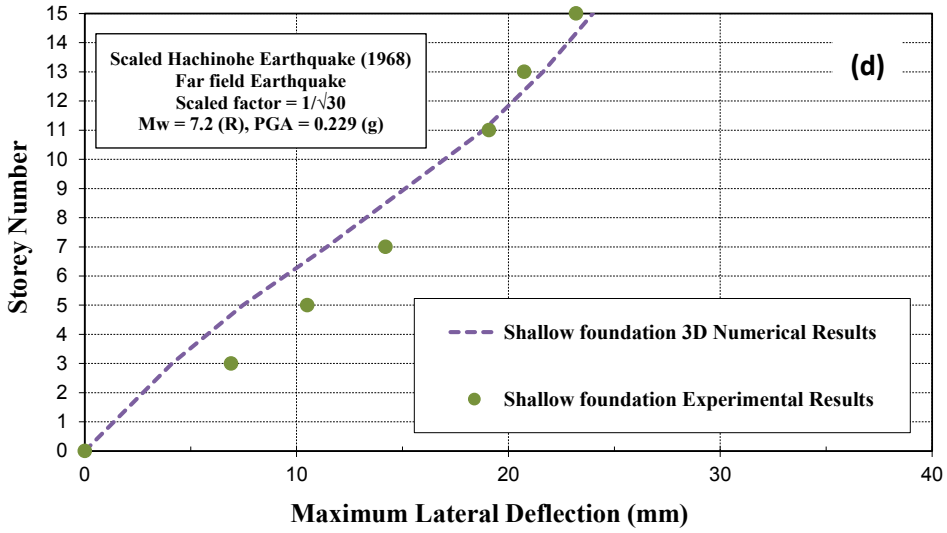


**Figure 5.5** 3D numerical predictions versus experimental measurements of the maximum lateral deformation of the fifteen storey model structure supported by shallow foundation under the influence of: (a) 1994 Northridge earthquake; (b) 1995 Kobe earthquake; (c) 1940 El Centro earthquake; (d) 1968 Hachinohe earthquake

In the 3D numerical simulation of the model structure supported by pile foundations, both floating (Figure 5.6a) and end-bearing piles (5.6b) have the same mesh generation and size as the shallow foundation case, in order to make the results comparable without being affecting by meshing variables. Moreover, similar boundary conditions and soil properties are adopted. In Figure 5.6 just half of the model is shown for more clarification. For the end-bearing pile foundation model, as an example, the generated mesh comprised 10,868 zones and 16,356 grid points. Fast computation facilities at University of Technology Sydney were employed to conduct the time-history analysis, and the computation took approximately 20 hours for a single analysis.

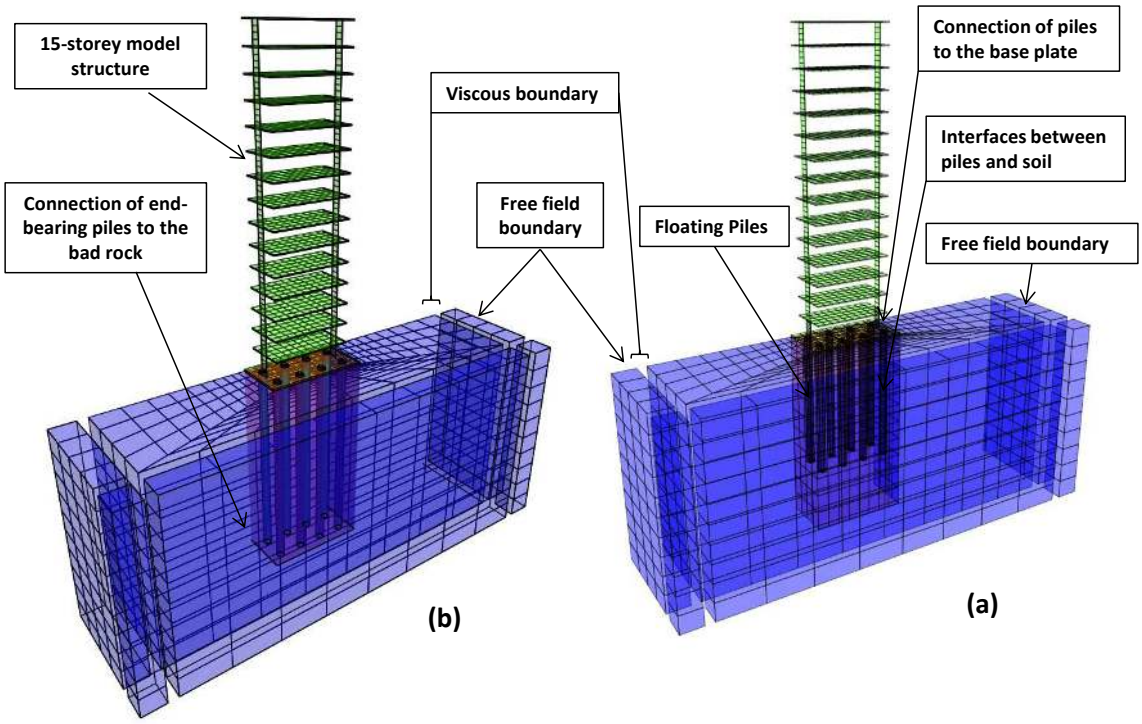


**Figure 5.6** Numerical grid and model components in FLAC3D for: (a) structure supported by floating (frictional) pile foundation; (b) structure supported by end-bearing pile foundation

Pile elements are modelled based on the method explained in Section 3.4. Accordingly, a group of 4×4 model piles with the diameter of 40 mm and the centre to centre spacing of 120 mm (3D) are adopted. The lengths of the end-bearing and floating piles are 1000mm and 660mm, giving the slenderness ratio L/d of 16.6 and 25, respectively. The pile elements, have rigid connection with the pile cap, while appropriate interface elements (see Section 3.6), capable of accounting for possible gap and slide generation in pile elements are defined to connect the pile grid points and the surrounding soil. Moreover, the end-bearing pile are connected to the bedrock with a fixed-base connection in order to avoid any possible sliding between the piles and bedrock during the shaking excitations, simulating typical end-bearing pile foundations. It should be noted that in the pile foundation cases there is no interface or attachment between the foundation and the surface soil as some gap in the shaking table tests is considered to avoid any pile-raft behaviour. Therefore, there is no direct stress transfer between the foundation slab and the subsoil in the pile foundation case. Table 5.4 summarises the mechanical characteristics of the model piles adopted in the 3D numerical simulation in terms of mass density ($\rho$), Shear modulus ($G$), Poisson's ratio ($\upsilon$), and yield stress of pile elements ($F'_y$). It should be noted that the equivalent

mechanical characteristics of the experimental model piles are adopted in the 3D numerical simulation.

**Table 5.4** Mechanical characteristics of the model piles adopted in the 3D numerical simulation

| Model Pile Properties | Value |
|---|---|
| Mass density of pile elements, $\rho$ *(kg/m$^3$)* | 440 |
| Shear modulus of pile elements, G (*kPa*) | 2.73E5 |
| Poisson's ratio of pile elements, υ | 0.4 |
| Yield stress of pile elements, $F'_y$ *(MPa)* | 32 |

After conducting fully nonlinear time-history analyses on the fifteen storey model structure supported by pile foundations, results in terms of the maximum lateral deflections are presented and compared with the experimental measurements in Figure 5.7 and Figure 5.8, for the case of floating piles and end-bearing piles, respectively.

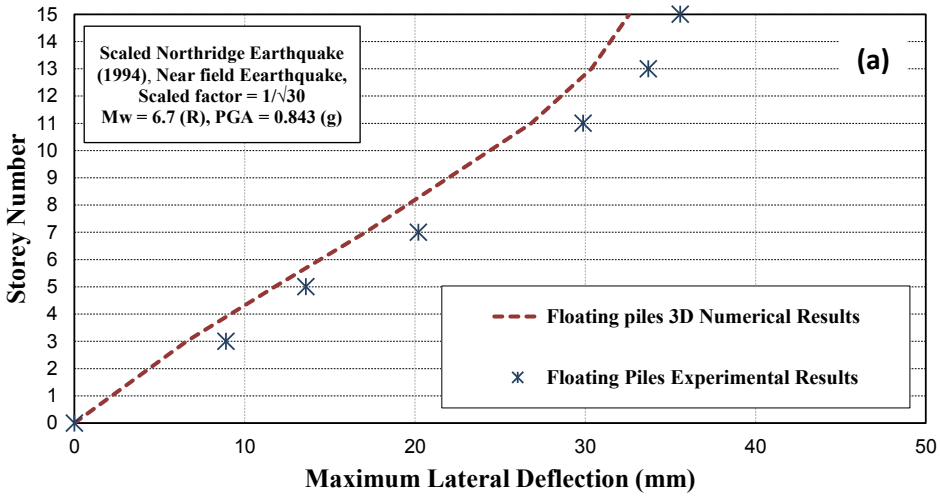

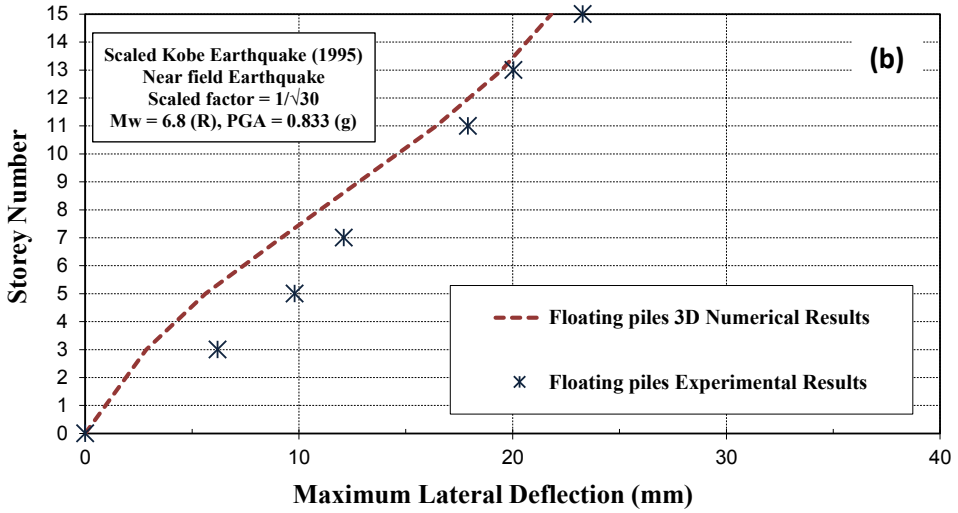


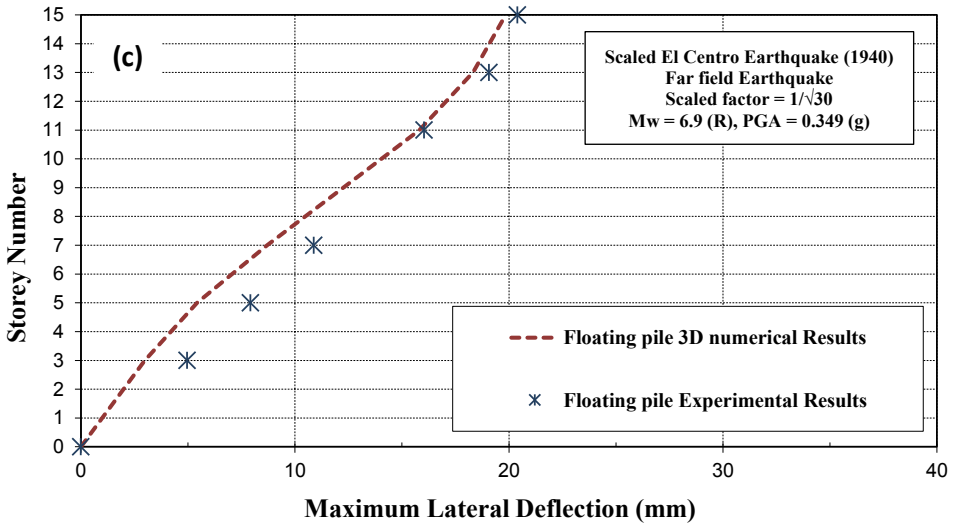


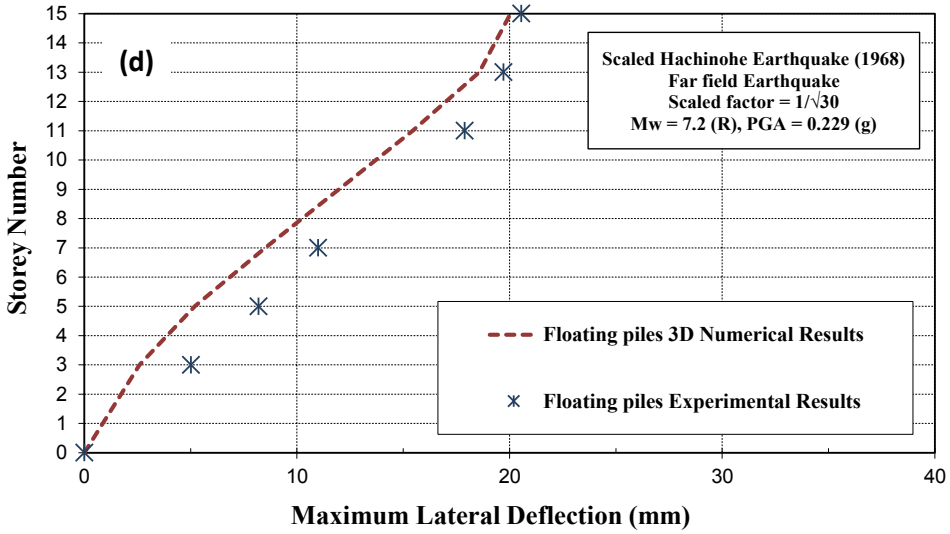


**Figure 5.7** 3D numerical predictions versus experimental measurements of the maximum lateral deformation of the fifteen storey model structure supported by floating pile foundation under the influence of: (a) 1994 Northridge earthquake; (b) 1995 Kobe earthquake; (c) 1940 El Centro earthquake; (d) 1968 Hachinohe earthquake

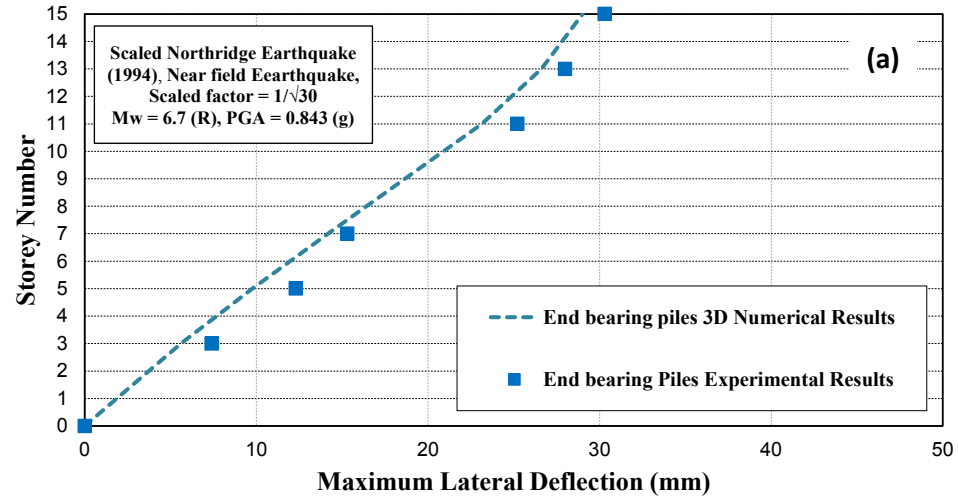
Scaled Northridge Earthquake (1994), Near field Eearthquake, Scaled factor = 1/√30 Mw = 6.7 (R), PGA = 0.843 (g)
(a)
End bearing piles 3D Numerical Results
End bearing Piles Experimental Results
Storey Number
Maximum Lateral Deflection (mm)

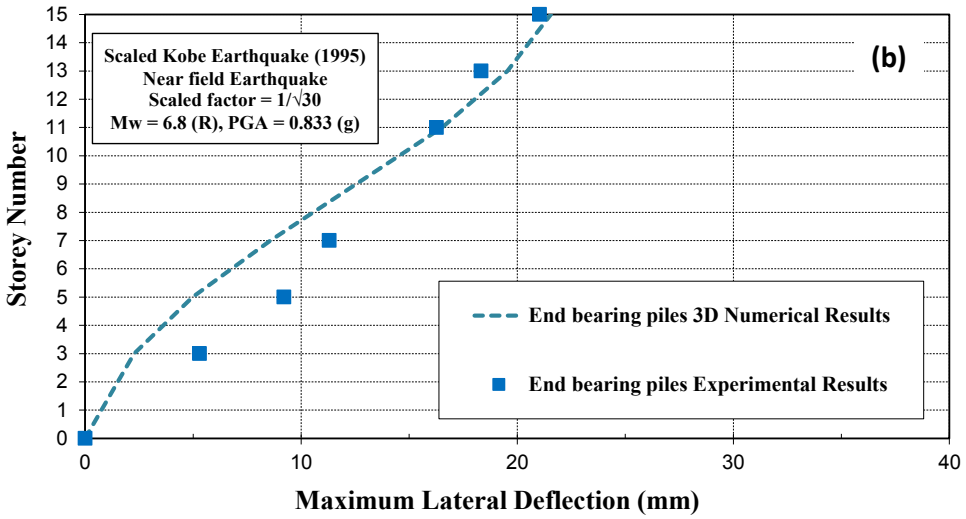
Scaled Kobe Earthquake (1995) Near field Earthquake Scaled factor = 1/√30 Mw = 6.8 (R), PGA = 0.833 (g)
(b)
End bearing piles 3D Numerical Results
End bearing piles Experimental Results
Storey Number
Maximum Lateral Deflection (mm)

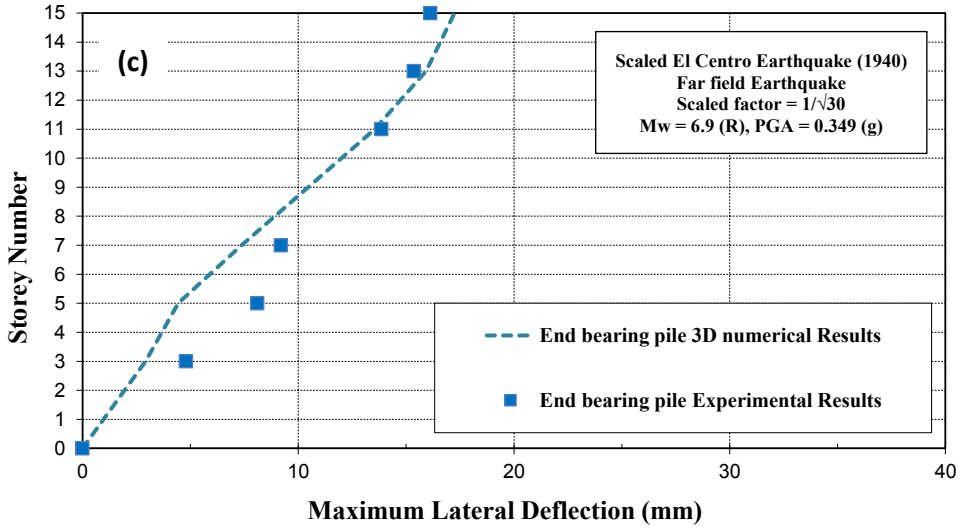
(c)
Scaled El Centro Earthquake (1940) Far field Earthquake Scaled factor = 1/√30 Mw = 6.9 (R), PGA = 0.349 (g)
End bearing pile 3D numerical Results
End bearing pile Experimental Results
Storey Number
Maximum Lateral Deflection (mm)

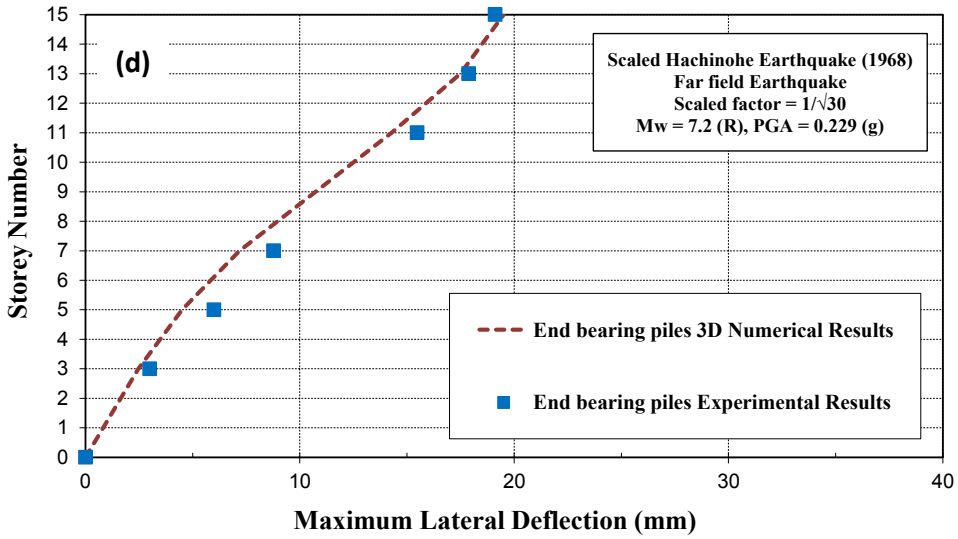


**Figure 5.8** 3D numerical predictions versus experimental measurements of the maximum lateral deformation of the fifteen storey model structure supported by end-bearing pile foundation under the influence of: (a) 1994 Northridge earthquake; (b) 1995 Kobe earthquake; (c) 1940 El Centro earthquake; (d) 1968 Hachinohe earthquake

## 5.3 Results and Discussion

Comparing the results of the conducted shaking table tests and the 3D numerical predictions for the maximum lateral displacements of the fixed-base (Figure 5.2), shallow foundations (Figure 5.5), floating pile foundations (Figure 5.7), and end-bearing pile foundation (Figure 5.8), it is observed that the trend and the values of the 3D numerical predictions are in a good agreement and consistent with the experimental shaking table test results. Therefore, the developed 3D numerical model can replicate the behaviour of the soil-pile-structure system with acceptable accuracy and is a rational and appropriate tool for further studies of the soil-pile-structure interaction effects. The observed disparities between FLAC3D predictions and experimental measurements in the lower levels of the shallow foundation and pile foundation cases can be due to the nature of the numerical method, adopting nonlinear elastic-perfectly plastic Mohr-coulomb model for the soil, assuming ideal rigid connection between the foundation and the pile caps, and unavoidable experimental uncertainties.

In addition, as an example, Figure 5.9 presents the time-history acceleration records at the top of the 15-storey model structure for the fixed-base, shallow foundations, floating pile foundations, and end-bearing pile foundation under the influence of 1940 El Centro earthquake. Comparison of the measurements and the

predictions indicates that the horizontal acceleration - time curves obtained from the 3D numerical analysis and the laboratory experiments are in a reasonable compliance.

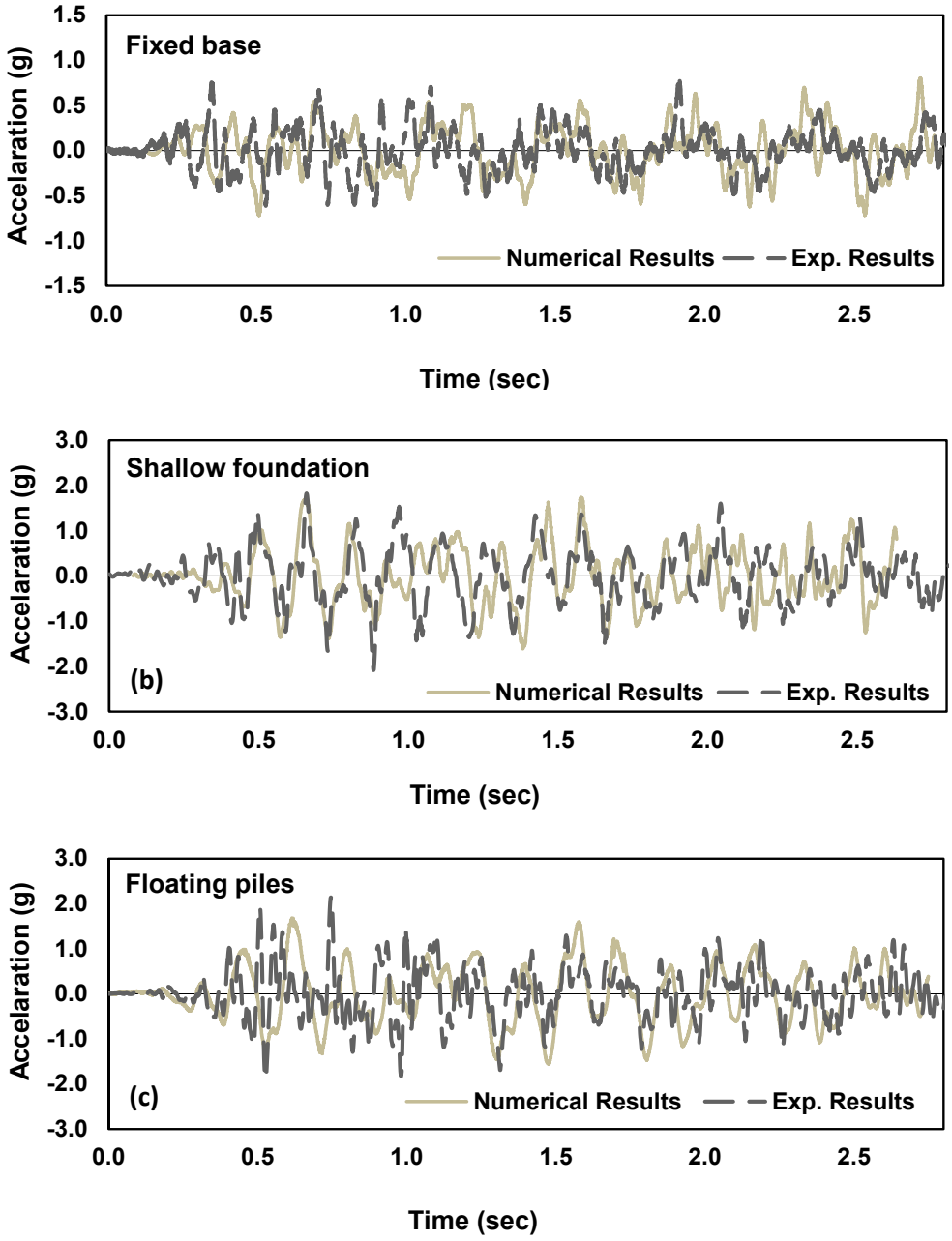

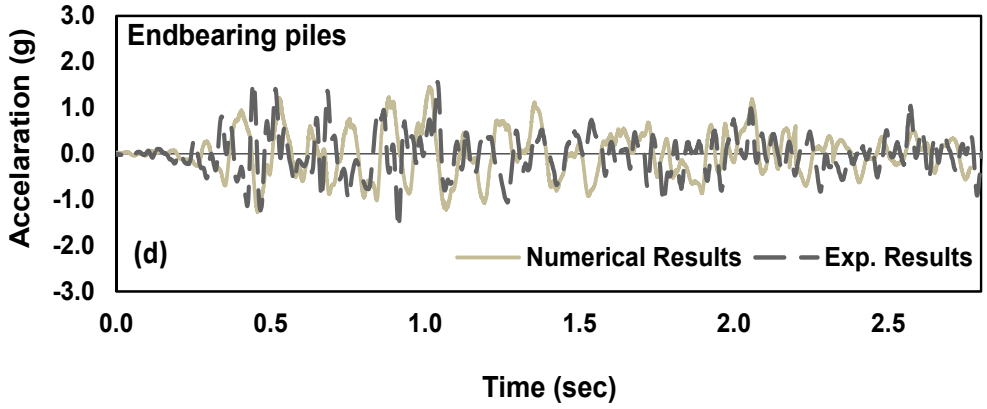


**Figure 5.9** history acceleration records at top of the 15-storey model structure under the influence of 1940 El Centro earthquake for: (a) fixed-base structure; (b) structure supported by shallow foundation; (c) structure supported by floating (frictional) pile foundation; (d) structure supported by end-bearing pile foundation

Rocking of the superstructure during the earthquake, according to Section 2.3, generates an extra degree of freedom which mostly results in excess lateral deformation of the structural and non-structural elements. To observe and measure this phenomenon, a vertical displacement transducer was located at the baseplate level during the shaking table tests (Figure 4.22), and measurements are tabulated in Sections 4.7- 4.9. Based on the developed numerical simulation and conducting nonlinear time-history analysis, the maximum vertical displacement and the rocking angles of the foundation in the instant of the maximum deformation at the top of the structure are predicted as summarised in Tables 5.3 and 5.4, respectively.

In comparison, the numerical predictions of the experienced vertical displacements and rocking angles (Tables 5.5 and 5.6) are in a close adaptation with the experimental measurements for the shallow foundation, floating pile foundation, and end-bearing pile foundation cases, confirming the accuracy of the developed numerical simulation. Referring to Tables 5.5 and 5.6, the fifteen storey model structure supported by shallow foundation experiences the excessive rocking in commission with the fixed-base assumption and pile foundation cases. End-bearing pile foundation provides stiffer support for the superstructure resulting in less rocking in comparison with the floating pile and the shallow foundation. The area replacement ratio of the pile group is 8% in this study and as a result piles attract significant axial forces. It should be noted that, in the floating pile foundation cases, rocking occurs due to the axial deformation of the pile elements together with the deformation of the surrounding and beneath soil

elements, while for the end-bearing pile just the axial deformation of the pile elements governs the maximum rocking experienced by the superstructure.

**Table 5.5** Maximum vertical displacement of the base plate obtained from 3D Numerical model

| **Scaled Earthquake Acceleration Record** | **Maximum Vertical Displacement** | | | |
|---|---|---|---|---|
| | Fixed-base | Shallow foundation | Floating Pile Foundation | End-bearing Pile Foundation |
| 1994 Northridge | 0 | 2.68 mm | 1.98 mm | 0.94 mm |
| 1995 Kobe | 0 | 1.45 mm | 0.52 mm | 0.32 mm |
| 1940 El Centro | 0 | 2.06 mm | 1.34 mm | 0.57 mm |
| 1968 Hachinohe | 0 | 1.58 mm | 1.02 mm | 0.83 mm |

**Table 5.6** Maximum rocking angle of the base plate obtained from 3D Numerical model

| **Scaled Earthquake Acceleration Record** | **Rocking Angle of the Foundation** | | | |
|---|---|---|---|---|
| | Fixed-base | Shallow foundation | Floating Pile Foundation | End-bearing Pile Foundation |
| 1994 Northridge | 0 | 0.61° | 0.45° | 0.21 |
| 1995 Kobe | 0 | 0.33° | 0.12° | 0.07 |
| 1940 El Centro | 0 | 0.47° | 0.31° | 0.13 |
| 1968 Hachinohe | 0 | 0.36° | 0.23° | 0.19 |

Figure 5.10 compares the 3D numerical predictions of the structural demand in terms of the maximum base shear for the fixed-base structure and the structure supported by three types of foundations, including shallow foundations, floating pile foundations, and end-bearing pile foundation. In general, the ratio of the maximum base shear for cases including the soil-structure interaction to those of the fixed-base is less than one, demonstrating the effect of the soil-structure interaction in reducing the maximum base shear of the structure. The maximum base shear of the structure supported by the end-bearing pile foundation, floating pile foundation, and shallow foundation is on average 89%, 78%, and 70% of the fixed-base structure excluding the soil-structure interaction, respectively. Therefore, presence of the pile foundations increases the maximum base shear and in turns the demand of the superstructure, in comparison with the case supported by the shallow foundation. Moreover, the structure

supported by end-bearing pile foundation experiences more base shear in comparison with the structure sitting on the floating pile foundation.

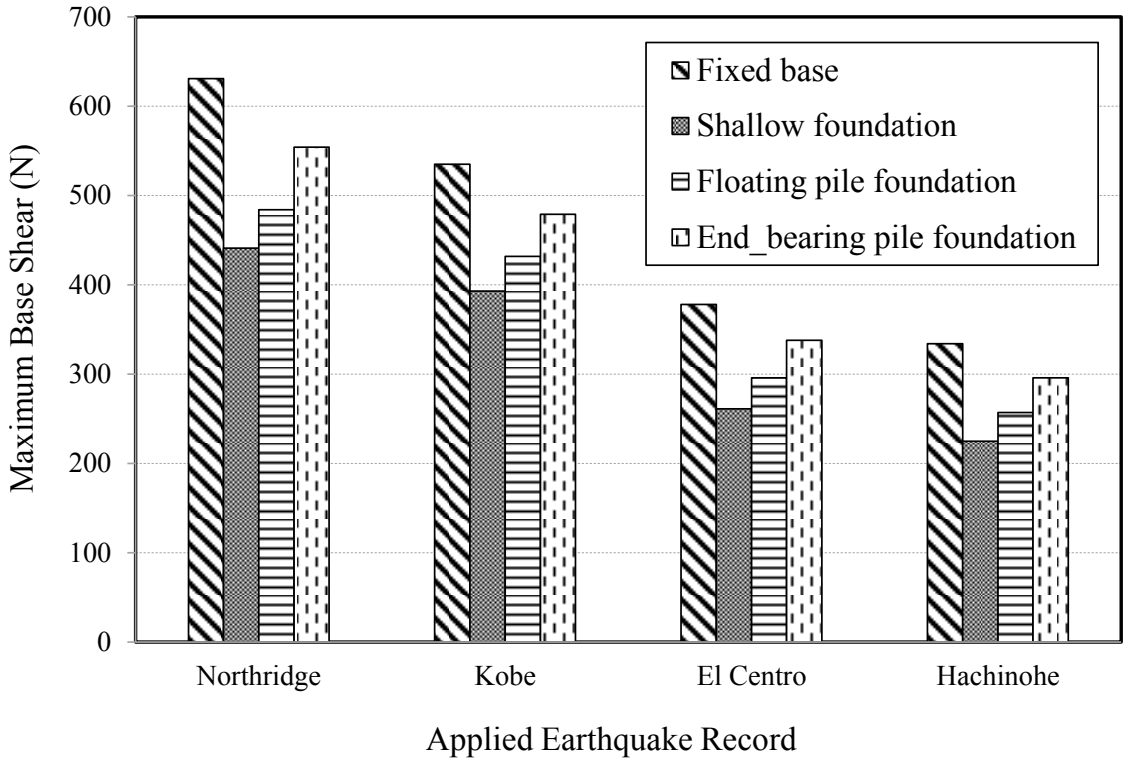


**Figure 5.10** Maximum base shear of the model structure obtained from 3D numerical analysis for: fixed-base structure; structure supported by shallow foundation; and structure supported by floating (frictional) pile foundation

In order to draw a general conclusion to be used by practicing engineers, the average values of the 3D numerical predictions of deformations for each case were determined and compared in Figure 5.11. In comparison to the fixed-base structure, the maximum lateral deflection of the structure supported by the end-bearing and the floating pile foundations increase by 19%, and 27% based on the 3D numerical predictions, respectively. Moreover, the maximum lateral deflection of the structure supported by the shallow foundation is increased by 59% based on the 3D numerical predictions in comparison to the results obtained from the fixed-base structure. The recorded natural frequencies from the 3D numerical predictions (2.11 Hz for the fixed-base condition, 1.93 Hz for the end-bearing pile foundation, 1.88 Hz for the floating pile foundation, and 1.64 Hz for the shallow foundation case) show reduction in the natural frequency of the system due to the soil-structure interaction. Presence of stiff pile elements in the soft soil increases the equivalent stiffness of the ground and influences

the dynamic properties of the whole system such as the natural frequency and the damping.

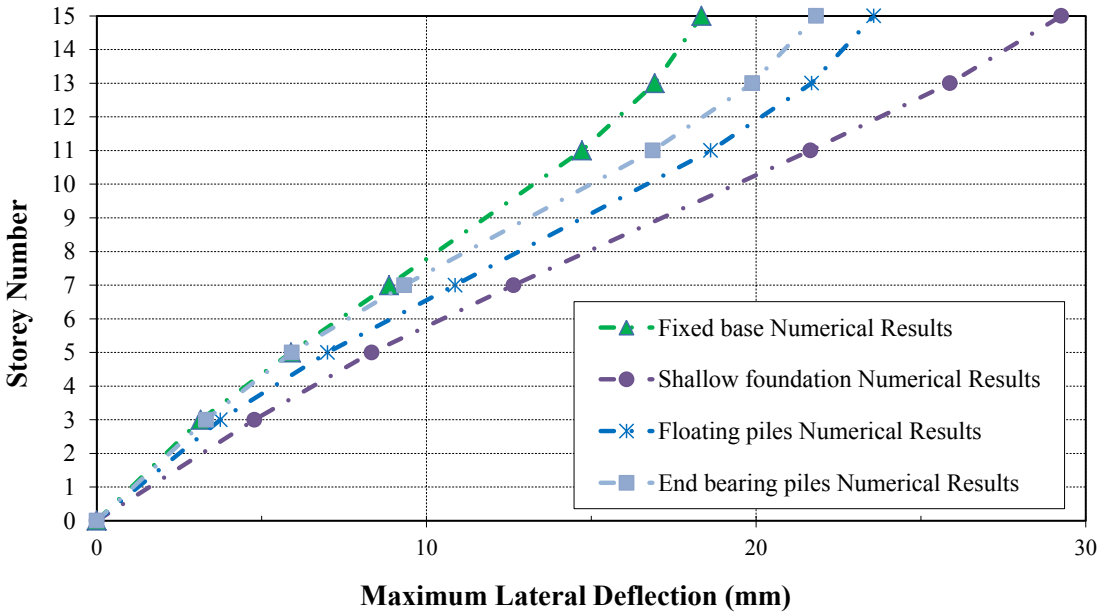


**Figure 5.11** Average 3D numerical values of maximum lateral displacements for: (a) fixed-base structure; (b) structure supported by shallow foundation; (c) structure supported by floating pile foundation; (d) structure supported by end-bearing pile foundation

Since the adopted model is a Multi Degree of Freedom (MDOF) structure, inter-storey drifts can be estimated and employed to investigate the performance levels of the building structures under the influence of dynamic soil-structure interaction. The corresponding inter-storey drifts of the average values of 3D numerical model (Figure 5.12) were calculated using Equating (4.4) based on the Australian standard (AS1170.4, 2007). It should be noted that considering the agreement between the experimental measurements and the numerical predictions in terms of the maximum lateral deformations (Figures 5.7 and 5.8), reasonable agreement between the values of the maximum inter-storey drifts experienced by the superstructure during shaking excitations are observed.

Referring to Figure 5.12, the inter-storey drifts of the structure supported by the pile foundation cases are more than the fixed-base conditions, excluding the soil-structure interaction. However, the structure supported by pile foundations experience less inter-storey drifts in comparison to the structure supported by the shallow foundation. For example, the maximum recorded inter-storey drift of the fixed-base

structure is measured to be 1.48%, while the corresponding value for the end-bearing and floating pile foundation case are 1.7% and 1.83%, respectively. Same value for the shallow foundation case is 2.25%. In other words, effects of the soil-pile-structure interaction (pile foundation) and the soil-structure interaction (shallow foundation) induces up to 23% and 52% increase in the recorded inter-storey drifts, respectively. As a result, considering the influence of the soil-structure interaction with different types of foundations may affect the performance level of the structure and shift the performance level of the structure from life safe zone to near collapse or even collapse levels.

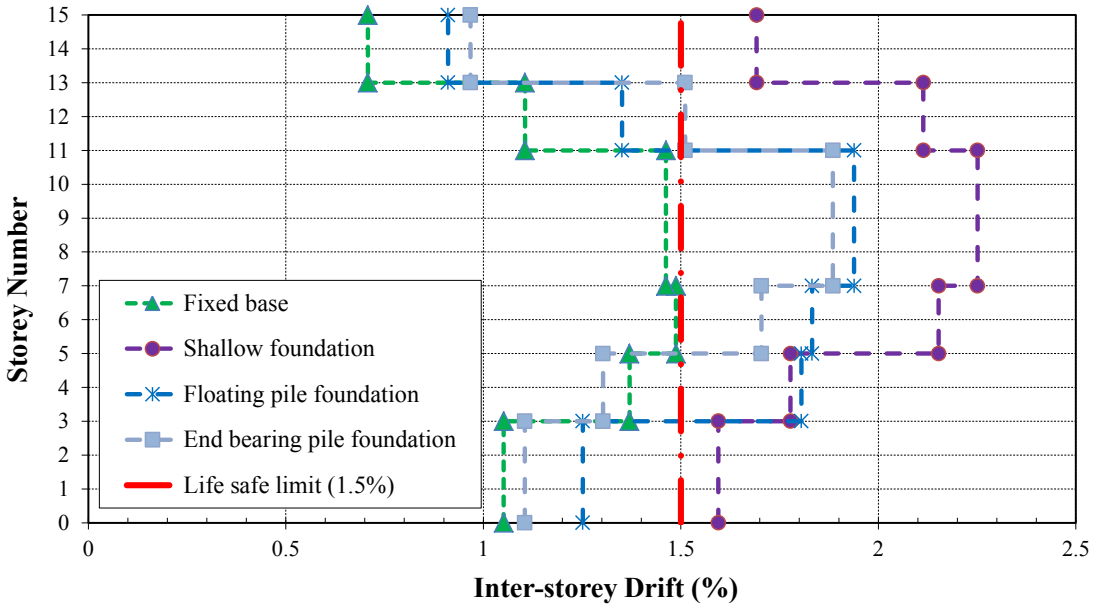


**Figure 5.12** Average 3D numerical inter-storey drifts for: (a) fixed-base structure; (b) Structure supported by shallow foundation; (c) structure supported by floating pile foundation; (d) structure supported by end-bearing pile foundation

The seismic response of the structure built on rock (fixed-base assumption) is different from the same structure supported by shallow or pile foundations in the soft soil. For the fixed-base structure, the shaking events can be applied directly to the base of the structure. Therefore, the acceleration caused by the inertial load over the structure is equal to the acceleration of the bed rock. Although, overturning moment and transverse shear generate at the base of the structure, there is no deformation and rocking motion at the base due to the high stiffness of the bed rock, directly beneath the structure. As a result, response of the fixed-base structure depends mainly on the dynamic characteristics of the superstructure. However, for the structures sitting on the

soft soils, the motion of the foundation is different from the control motion. Presence of the stiff foundation elements like piles alters the motion of the ground. Moreover, the deformation of the foundation may result in the amplification of the lateral deformations of the soil-foundation-structure system.

The soil nonlinearity during the earthquake plays an important role on the dynamic response of soil-structure systems. The amplification ratio in the soil medium and its natural frequency change during the shaking excitations in accordance with the developed shear strain level in the soil elements. The generated shear strain at a particular point in the soil medium changes during the excitation. For instance, the developed shear stresses and shear strains for the case of the end-bearing pile foundation, recorded at the soil surface bellow the foundation, under the influence of El Centro earthquake are presented in Figure 5.13. In order to obtain two- and three-dimensional strain paths in FLAC3D, the shear strain is decomposed into components in strain space, and strain reversals are detected by changes in signs of the dot product of the current increment and the previous mean path (Itasca, 2009).

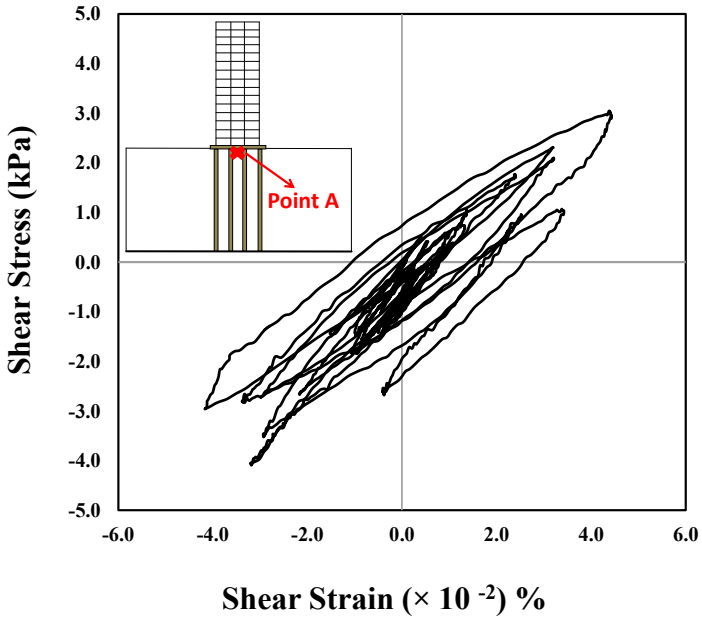


**Figure 5.13** Developed shear stress versus shear strain in the soil medium at Point A for the case of end-bearing pile foundation record at the soil surface bellow the foundation under the influence of El Centro earthquake

In the above mentioned case, point A experiences the shear strain level of up to 4 $\times 10^{-2}$ percent during the excitation. Comparing Figures 5.4 and 5.13, it is evident that the actual secant modulus ratio ($G/G_{max}$) varies from 1 to 0.7, and the damping ratio varies from 0% to 5% during the applied earthquake in this particular point. Soil elements in different locations experience different shear strains during the earthquake. This highlights the advantage of fully nonlinear models over the equivalent linear methods in capturing the cyclic nonlinear behaviour of the soil more accurately, while in the equivalent linear methods, the strain-dependent modulus and damping functions are only taken into account in an average sense, in order to approximate some effects of the soil nonlinearity (e.g. Fatahi and Tabatabaiefar, 2013; Kramer, 1996).

## 5.4 Summary

In this chapter, the developed numerical model is verified against the previously conducted shaking table experimental tests. Employing FLAC3D and following the modelling techniques explained in Chapter 3, a fully nonlinear three-dimensional numerical model was adopted to perform time-history analyses implementing hysteretic damping of the soil to represent the variation of the shear modulus and damping ratio of the soil with the cyclic shear strain. Free field boundary conditions were assigned to the numerical model, and appropriate interface elements, capable of modelling sliding and separation between the pile and the soil elements, were considered.

Comparing the results of the numerical model and the experimental measurements, it can be concluded that the employed numerical model is appropriate for the simulation of the soil-pile-structure interaction under strong ground motions. Consequently, the proposed SSPSI numerical model is a valid and qualified method of simulation with sufficient accuracy which can be employed for further numerical dynamic soil-structure interaction investigations. Practicing engineers can adopt this verified numerical modelling procedure in the design considering the effect of SSPSI with respect to the interface elements, boundary conditions, and hysteretic damping of the soil representing the variations of the shear modulus and the damping ratio of the soil with the cyclic shear strain. Another advantage of the current numerical modelling technique is performing the SSPSI analysis in a fully coupled manner in which main components of the interaction including subsoil, pile foundation, and superstructure are

modelled simultaneously without resorting to independent calculations of site or superstructure response, or application of the pile group interaction factors.

Based on the 3D numerical simulation, although SSPSI reduces the base shear of the structure leading to the reduction in the structural distortion in comparison with the fixed-base structure, considering the effect of SSPSI increases the overall lateral deformation and consequently inter-storey drifts of the structure mainly due to the rocking component. Accordingly, the seismic soil-pile-structure interaction affects the performance level of structures sitting on the soft soil by increasing the inter-storey drifts, which may shift the performance level of the structure from life safe to near collapse or even collapse levels. Moreover, in the seismic response of pile groups, rocking and translation components are coupled and the response of the underneath soils to strong seismic shaking is strongly nonlinear.

# Chapter 6- INFLUENCE OF FOUNDATION TYPE ON SEISMIC PERFORMANCE OF STRUCTURES

## 6.1 General

In the selection of the foundation type for the mid-rise buildings in high risk seismic zones, several options such as shallow foundation, pile foundation, or pile-raft foundation, might be considered by design engineers to carry both static and dynamic loads. However, different types of foundations behave differently during the earthquake considering the soil-structure interaction (SSI), where the properties of the in situ soil and the foundation type change the dynamic characteristics (natural frequency and damping) of the soil-foundation-structure system.

During the strong earthquake excitations, rocking occurs due to the generated inertial forces in the superstructure, causing compression in one side and tension on the other side of the foundation, which in turn results in settlement in one side and possible uplift on the other side of the foundation, respectively. Different types of foundations supporting a superstructure experience different amounts of rocking under a particular earthquake excitation. The rocking component amplifies the lateral displacement of the superstructure and may influence the total stability of the superstructure. However, significant amount of earthquake energy dissipates due to the rocking-dissipation which results in directing less shear forces to the superstructure. Comparing the behaviour of different types of foundations during the earthquake with respect to the soil-structure interaction can help the practicing engineers in selecting the proper foundation type for the structures.

In this chapter, in order to investigate the different characteristics of SSI and its influence on the seismic response of superstructures, parametric studies with respect to different types of foundations have been conducted. For this purpose, the previously verified three-dimensional numerical modelling procedure (see Chapter 5) has been

adopted. A fifteen storey full scale (prototype) structure with four different types of foundations, namely, (i) fixed-base structure representing the situation excluding the soil-structure interaction, (ii) structure supported by a shallow foundation, (iii) structure supported by a pile-raft foundation in soft soil, and (iv) structure supported by a floating (frictional) pile foundation in soft soil, are simulated. Finite difference analyses are performed using real earthquake records taking into account both material (soil and superstructure) and geometric (uplifting, gapping, and P- $\Delta$ effects) nonlinearities. Results are presented and compared in terms of the settlement of the superstructure under the gravity loads, the site effect and soil amplification, the shear force distribution in the superstructure, the rocking of the superstructure, and the lateral deformations and drifts of the fifteen storey superstructure.

## 6.2 Characteristics of Adopted Soil-Foundation-Structure Systems

### 6.2.1 Characteristics of Adopted Superstructure

The adopted prototype structure in this study is a fifteen storey concrete moment resisting building frame with the total height of 45 m and width of 12 m consisting of three spans in each direction, representing the conventional types of mid-rise moment resisting buildings. The structural sections are specified after conducting the routine design procedure as regulated in the relevant building codes (AS3600, 2009; AS1170.4, 2007). For this purpose, SAP2000 (CSI, 2010) software is employed, where the following general steps are required to analyse and design a structure:

- Create or modify a model that numerically defines the geometry, material properties, and loading,
- Analyse the numerical model,
- Review the results of the analysis, and
- Check and optimise the designed structural sections.

This is usually an iterative process that may involve several cycles of the above sequence of steps. For the structural concrete utilised in this analysis and design, specified compressive strength ($f'_c$) and mass density ($\rho$) are assumed to be $32MPa$ and

2400 $kg/m^3$, respectively. The modulus of elasticity of concrete ($E$) was calculated according to clause 3.1.2.a of Australian Standard for Concrete Structures (AS3600, 2009) as follows:

$$E = (\rho)^{1.5} \times (0.043\sqrt{f_c'}) \quad (6.1)$$

where, unit of $E$ is in $MPa$, unit of $\rho$ is in $kg/m^3$, and unit of $f'_c$ is in $MPa$.

The gravity loads imposed to the prototype structure are considered in accordance with AS1170.4 (2007) (Permanent, imposed and other actions). The values of permanent action (dead load) and imposed action (2kPa in this study) are determined as uniformly distributed loads over the floors according to AS1170.4 (2007). Furthermore, the earthquake loads are considered employing nonlinear time-history dynamic analyses under the influence of four earthquake ground motions including 1994 Northridge, 1995 Kobe, 1940 El Centro, and 1968 Hachinohe earthquakes, as characterised in Table 4.6. In the dynamic analyses, geometric nonlinearity and P-Delta effects are considered according to AS3600 (2009). It should be noted that cracked sections for the reinforced concrete sections are taken into account by multiplying moment of inertial of the uncracked sections ($I_g$) by cracked section coefficients ($0.35I_g$ for beams, $0.70I_g$ for columns and piles, and $0.25I_g$ for slabs) according to ACI318-08 (2008).

After finalising the dynamic analyses, concrete sections of the fifteen storey building were designed according to AS3600 (2009) (Australian Standard for Concrete Structures). The following design load combinations are considered for concrete design of the structural members subjected to Permanent ($G$), Imposed ($Q$), and Earthquake ($E_u$) actions according to AS/NZS1170.0-2002 (Australian Standard for structural design actions):

- Load Combination number 1= $1.35G$
- Load Combination number 2= $1.2G + 1.5Q$
- Load Combination number 3= $G + 0.4Q \pm E_u$

In order to incorporate the inelastic structural analysis, as broadly discussed in Section 3.5, the plastic moment capacity ($M_p$) of the concrete members were determined using Equation 3.12, and assigned to the sections considering the yield stress of the concrete

material ($\sigma_y$) equal to the compressive strength of concrete ($f'_c$) referring to Shing and Tanabe (2001).

In the concrete design procedure, ratio of the capacity of each structural member to the maximum factored axial force and bending moments obtained from each load combination results in capacity ratio giving an indication of the stress condition of a structural member with respect to the capacity of the member. In this design, capacity ratio of the structural members has been in the range of 0.85 to 0.95 (all less than 1.0). In addition, shear capacity of the designed members are checked according to Section 8.2 of AS3600 (2009) (Australian Standard for Concrete Structures).

Accordingly, after strength design of the structural sections, inter-storey drifts of the model are checked in a way that the performance level of the designed model stays in the life safe region by limiting the maximum inter-storey drift to 1.5%. The inter-storey drifts have been calculated using the following equation based on the Australian Standard (AS1170.4, 2007):

$$Drift = (d_{i+1}-d_i) / h \tag{6.2}$$

where, $d_{i+1}$ is deflection at ($i+1$) level, $d_i$ is deflection at ($i$) level, and $h$ is the storey height. In practical designs, it is often assumed that the storey deflection is equal to the horizontal displacement of the nodes on the level which may be due to translation, rotation, and distortion. Considering 3 metres storey height and 1.5% maximum inter-storey drift, following form of Equation (6.2) is employed as a criterion to keep the performance level of the designed structure model in the life safe region:

$$Drift = (d_{i+1}-d_i) / 3000 \leq 1.5\% \tag{6.3}$$

Eventually, the final structural sections are specified as shown in Figure 6.1. It can be noted that the selected characteristics for the building represent the structural norms and construction practices of the conventional buildings in mega cities, which is adopted to investigate the influence of SSI in this study. The results of the inelastic analysis in FLAC3D and SAP2000 for the fixed base fifteen storey building were in a very good agreement (less than 5%), satisfying the requirement for the life safe performance level for the fixed base structure.

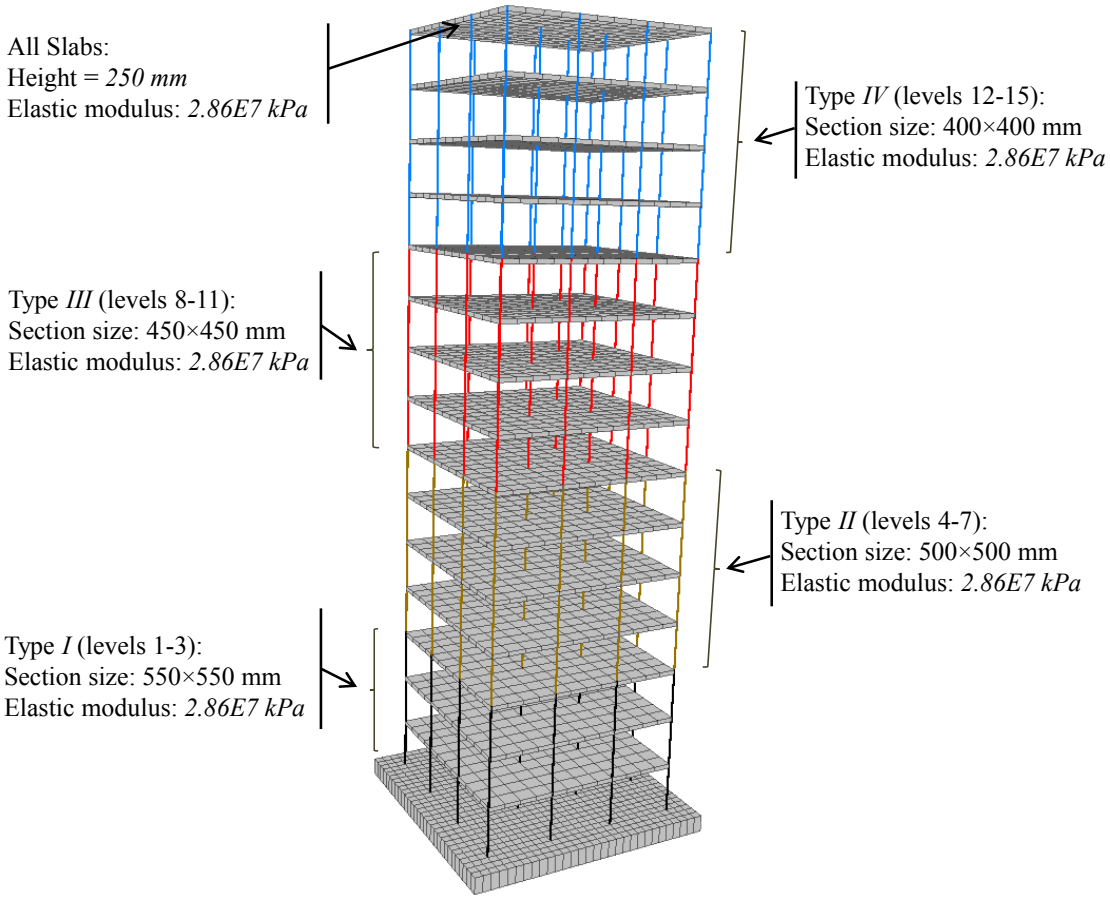


**Figure 6.1** Designed concrete sections for the adopted fifteen storey superstructure

## 6.2.2 Characteristics of Adopted Soil and Foundations

The above designed fifteen storey superstructure is sitting on the soft clayey soil with the shear wave velocity of 150 m/s, density of 1470 kg/m$^3$, and undrained shear strength of 50 kPa. Three different types of foundations are designed to support the superstructure against the static and dynamic loads following the routine engineering procedures (e.g. Bowles, 2001; Poulos and Davis, 1980) and regulated codes and manuals (AS2149, 2009) to satisfy the requirement for the bearing capacity and the maximum settlement, as follows:

- *Shallow square foundation (footing) which is 1 m thick and 15 m wide made of the reinforced concrete*. Both the geotechnical and structural designs of the foundation are conducted referring to Bowles (2001) and Canadian Foundation Engineering Manual (2006), where the ultimate limit state of a shallow

foundation involves the case where the applied loads exceed the resistance of the ground beneath the foundation. The geotechnical resistance at this ultimate limit state is termed the ultimate bearing capacity of the ground that supports the foundation. Moreover, the settlement of a foundation must be within tolerable or acceptable limits to satisfy the specified serviceability limit states criteria for a given project. In this case, the obtained factor of safety for the shallow foundation supporting the fifteen storey superstructure against the gravity loads is equal to 3.2.

- *Pile-raft foundation with the same material and dimensions as the shallow foundation which is connected to a group of 4×4 reinforced concrete piles with diameter and length of 1.2 m and 9 m, respectively, in order to reduce the uplift and rocking behaviour of the structure during the earthquake.* Australian piling standard (AS2149, 2009) and Poulos and Davis (1980) approach are adopted to design the pile-raft foundation. Accordingly, the ultimate geotechnical strength of the pile-raft foundation is calculated as the lesser of (i) the sum of the design ultimate geotechnical strengths of the individual piles in the group, plus the design ultimate geotechnical strengths of the net area of the pile cap (gross area minus the area occupied by the piles); and (ii) the design ultimate geotechnical strength of the block containing the piles and the soil between them, plus the design ultimate geotechnical strength of the area of the cap outside the perimeter of this block. The obtained factor of safety for the pile-raft foundation supporting the fifteen storey superstructure against the gravity loads is equal to 4.5.

- *Floating (frictional) pile foundation in the soft soil, with a 4×4 reinforced concrete pile group with pile diameter and length of 1.2 m and 18 m, respectively*. For this case, unlike the pile-raft foundation, there is no direct stress transfer between the foundation slab and the subsoil, so the foundation gains the required bearing capacity and stiffness from the pile elements only. The design method used for a particular pile foundation will depend on the soil type in which the pile lays, whether the soil is cohesive (clay) or cohesionless (sand), and weather the pile is end-bearing or floating (Canadian Foundation Engineering Manual, 2006). Piles obtain their load-carrying capacity from both toe and shaft resistance, where the relative contribution of each to the total

capacity of the pile depends on the type of the soil and characteristics of the pile elements. Moreover, in the design of pile groups, the group action should be taken in to account. In this case, the obtained factor of safety for the floating pile foundation supporting the fifteen storey superstructure against the gravity loads is equal to 2.9, following the procedure presented in Canadian Foundation Engineering Manual (CGS, 2006).

The centre to centre spacing of piles is 4 m (3.3D), which is in a reasonable agreement with the values used by other researchers (e.g. Small and Zhang, 2002; Shelke and Patra, 2008). Since the superstructure consists of three spans with total width of 12 m, by adopting the mentioned pile setup and allocating one pile under each column, an efficient pile foundation system to carry the applied structural loads has been designed. It should be noted that after designing the above mentioned foundations, the bearing capacity and serviceability (deformations) of the foundations under the applied loads are controlled during the numerical modelling process to satisfy the design requirements for the routine engineering projects.

In summary, from the practicing engineers' point of view, all three mentioned foundation types are acceptable and can be selected to support the superstructure. However, they may behave differently during the earthquake while taking into account SSI. The seismic responses of the above mentioned foundation types are compared and discussed in the following sections employing a 3D numerical simulation.

## 6.3 Utilised Parameters for Soil-Pile-Structure Model in FLAC3D

A numerical modelling procedure in FLAC3D, as broadly explained in Chapter 3, is adopted to conduct a nonlinear time-history analysis on the prototype structure supported by the different types of foundations. For the superstructure, as suggested by other researchers (e.g. Shiming and Gang, 1998b; Lu et al., 2005; Nghiem, 2009), solid elements and beam structural elements (beamSELs) are adopted to simulate the floor slabs and columns, respectively. The adopted parameters for the column sections and slabs in the developed numerical model considering the cracked sections are presented in Table 6.1 and Table 6.2, respectively. Moreover, structural damping ratio ($\xi$) of 5% is

assigned for the reinforced concrete structure referring to the relevant codes (AS1170.4, 2007; ASCE7-10, 2010).

**Table 6.1** Adopted characteristics of column sections for 3D numerical simulation of the prototype soil-foundation-structure system

| Section Type | $I_x$ ($m^4$) | $I_z$ ($m^4$) | $I_{yz}$ ($m^4$) | *Area* ($m^2$) | *E* (*kPa*) |
|---|---|---|---|---|---|
| Type *I* | 5.34E-3 | 5.34E-3 | 10.68E-3 | 0.30 | 2.86E7 |
| Type *II* | 3.65E-3 | 3.65E-3 | 7.3E-3 | 0.25 | 2.86E7 |
| Type *III* | 2.39E-3 | 2.39E-3 | 4.78E-3 | 0.20 | 2.86E7 |
| Type *IV* | 1.49E-3 | 1.49E-3 | 2.98E-3 | 0.16 | 2.86E7 |

Note: cracked sections with 0.7*Ig* have been considered according to ACI318-08 (2008).

**Table 6.2** Adopted characteristics of slabs for 3D numerical simulation of the prototype soil-foundation-structure system

| Slabs Properties | Value |
|---|---|
| Height (*m*) | 0.25 |
| Shear modulus, *G* (*kPa*) | 2.7E6 |
| Poisson's ratio | 0.3 |
| Yield stress, $\sigma_y$ (*kPa*) | 3.2E4 |

Note: cracked sections with 0.25*Ig* have been considered according to ACI318-08 (2008).

In order to simulate the subsoil behaviour during the shaking excitation, the numerical model adopts hysteretic damping algorithm representing the variations of the shear modulus and damping ratio of the soil with the cyclic shear strain capturing the energy absorbing characteristics of the soil. For this purpose, Hardin and Drnevich (1972) built-in tangent-modulus function for clayey soil with the value of $\gamma_{ref} = 0.234$, as explained in Section 3.3, is adopted in the dynamic analysis. As explained earlier, a value of $\gamma_{ref} = 0.234$, giving the coefficient of determination ($R^2$) equal to 0.91, produces the best match to the backbone curves suggested by Sun et al. (1988) for fine grained soils (see Figure 5.4), and thus was adopted in this study. The employed soil parameters in the developed 3D numerical model are summarised in Table 6.3. The adopted soil parameters can be used as a typical values for clayey soils as reported by other

researchers (Tabatabaiefar et al., 2013). The shear wave velocity of soils in the field can be obtained from the downhole test, where soil stiffness properties are determined by analysing direct compressional and shear waves along a borehole down to about 30 m. The downhole test is a low strain in-situ test generating a cyclic shear strain of about$10^{-4}$ percent where the resulting shear modulus is called $G_{max}$.

**Table 6.3** Adopted soil parameters for 3D numerical simulation of the prototype soil-foundation-structure system

| Soil Properties | Value |
|---|---|
| Mass density (kg/m$^3$) | 1470 |
| Maximum shear modulus, $G_{max}$ (kPa) | 33100 |
| Poisson's ratio | 0.4 |
| Shear wave velocity (m/s) | 150 |
| Undrained shear strength, $C_u$ (kPa) | 50 |
| Undrained friction angle, $\varphi_u$ (kPa) | 0 |
| Dilation angle, $\psi$ (degree) | 0 |

Pile elements are modelled with solid elements based on the method explained in Section 3.4. Accordingly, pile elements have rigid connections with the pile cap. The mentioned types of foundations (i.e. shallow, floating pile, and pile-raft) are made of the reinforced concrete adopting the same material properties as the superstructure.

Considering the different mechanical characteristics of the soil and the foundation/piles, and in order to capture the possible uplift (gapping) and sliding of the foundation (piles) during the shaking excitations, three sets of interface elements are modelled in this study as illustrated in Figure 6.2. For the shallow foundation case, the interface elements are placed between the foundation and the soil surface (Figure 6.2a). For the floating pile foundation case, the interface elements are attached to the outer perimeter and bottom of the piles (Figure 6.2b). Finally, for the pile-raft foundation case, interface elements are placed between the foundation and the soil surface as well as to the outer perimeter and bottom of the piles, as shown in Figure 6.2c. Therefore, for the floating pile foundation case, no direct stress transfer between the foundation slab and the subsoil is allowed. However, for the pile-raft foundation case, by placing the

interface elements between the foundation and the soil surface as well as to the outer perimeter and bottom of the piles, the generated stresses in the foundation can be transferred to the subsoil both from the foundation slab and the pile elements. The properties of the adopted interface elements in this study are summarised in Table 6.4, which have been calculated referring to the method explained in Section 3.6.

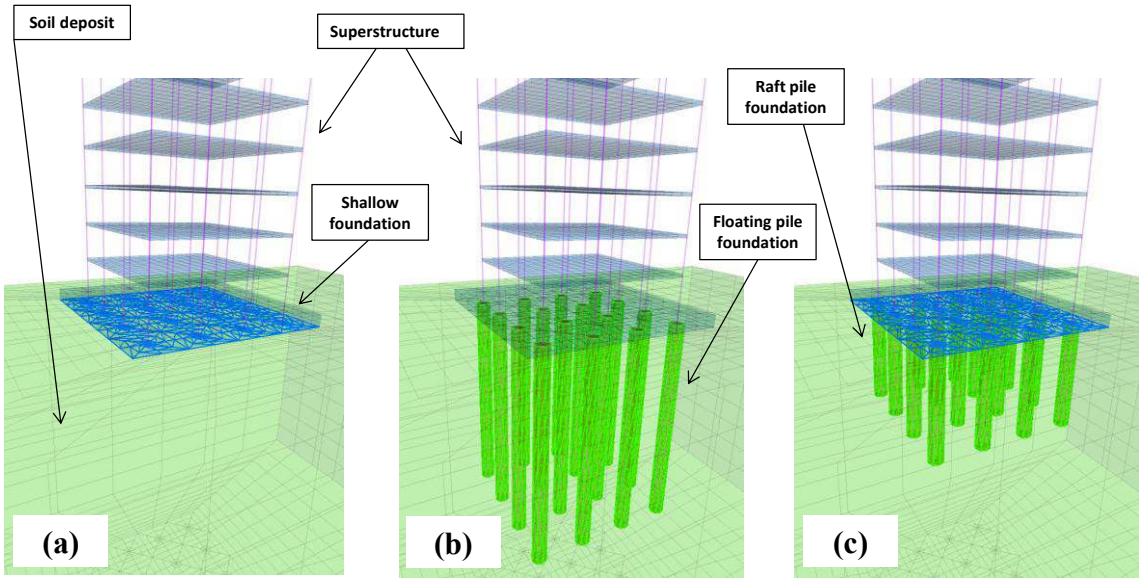


**Figure 6.2** Adopted interface elements in the 3D numerical simulation for: (a) superstructure supported by shallow foundation; (b) superstructure supported by 18m long floating (frictional) pile foundation; (c) superstructure supported by 9m long pile-raft foundation

**Table 6.4** Properties of the adopted interface elements

| Interface Properties | Value |
|---|---|
| Shear stiffness, $K_s$ (kPa/m) | 3E8 |
| Normal stiffness, $K_n$ (kPa/m) | 3E8 |
| Shear strength, $S_s$ (kPa) | 50 |
| Tensile strength, $T_s$ (kPa) | 0 |
| Dilation angle, $\psi$ (degree) | 0 |

The boundary conditions in the numerical models are prescribed at the boundaries of the numerical grids. For the static analysis step, as broadly discussed in Section 3.7, the preliminary boundary conditions are adopted. During the dynamic time-history analysis, free field boundary conditions are assigned to the numerical model at the sides of the main grid by introducing viscous dampers to avoid the reflection of the outward

propagating waves back into the model. Moreover, rigid boundary condition is adopted to simulate the bedrock (bottom of the soil medium grid) in the seismic soil-structure interaction analysis (see Section 3.7.3), and the earthquake input motions are applied at the bedrock horizontally propagating upward through the entire model. Four benchmark earthquake input motions including 1994 Northridge, 1995 Kobe, 1940 El Centro, and 1968 Hachinohe earthquakes, referring to Table 4.6, are imposed to the numerical model while conducting a nonlinear time-history analysis. Figure 6.3 shows the final numerical grid and the model components in FLAC3D for the prototype structure supported by the floating (frictional) pile foundation. It should be noted that, in order to make the results comparable without being affecting by meshing variables, same mesh generation is adopted for all three types of foundations. The generated mesh, as shown in Figure 6.3, comprises 11,352 zones and 16,643 grid points with the dynamic time step of $1.19\times10^{-5}$ second. Fast computation facilities at University of Technology Sydney were employed to conduct the time-history analysis. Results of the 3D numerical simulation are presented and discussed in the following section.

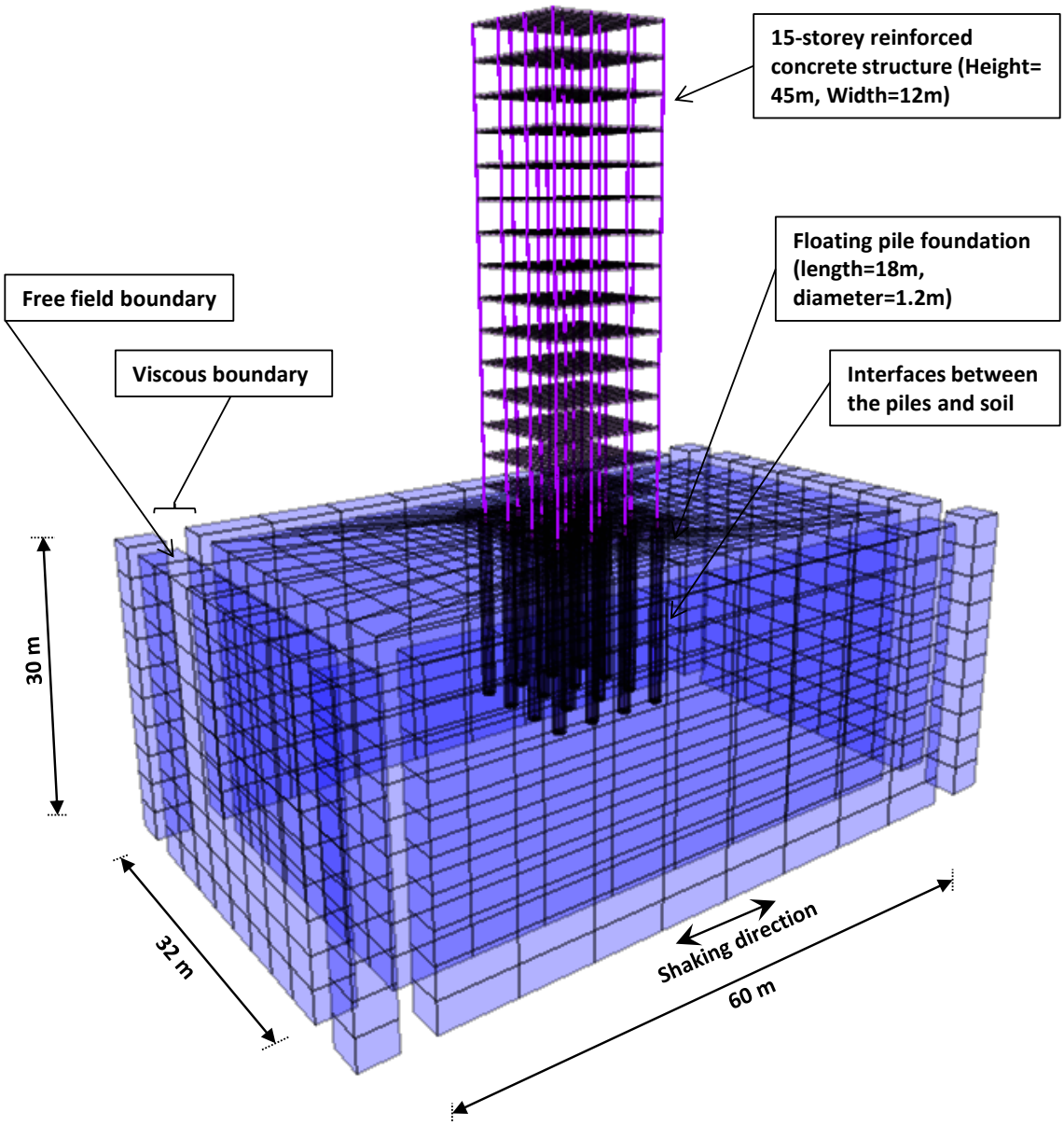


**Figure 6.3** Numerical grid and model components in FLAC3D for prototype structure supported by floating (frictional) pile foundation

## 6.4 Results and Discussion

### 6.4.1 Settlement of Superstructure under Gravity Loads

The numerical analysis of SSI, as discussed in Section 3.7, consists of two main steps: static analysis and dynamic analysis. Each of the two main steps of SSI numerical analysis (i.e. static analysis and dynamic analysis) requires particular types of boundaries. During the static analysis step, the model is subjected to the gravity loads in order to

achieve the static equilibrium. In this stage, preliminary boundary conditions should be adopted at the boundaries of the numerical grids, where as shown in Figure 3.9, soil side boundaries are fixed in the horizontal directions while free movement is allowed in the vertical direction. Lu et al. (2012) emphasised on the influence of the gravity load on contact state of the soil–structure interface mentioning that significant error in the analysis may occur if gravity is not taken into account in the dynamic analysis.

The final vertical settlements of the fifteen storey structure under the gravity loads supported by different types of foundations are shown in Figure 6.4. Accordingly, the structure supported by the 18m floating pile foundation experienced the minimum settlement (15.7mm), while the structure supported by the 15m width shallow foundation had the largest deformation (39.4mm). The settlement of the structure supported by the 9m pile-raft foundation was 38.4mm. It should be noted that all the recorded settlements satisfy the typical requirements for the ordinary residential building frames (AS2149, 2009).

Comparing the static settlements of the superstructure supported by different types of foundations delivers some indication on the provided equivalent static stiffness by each of the mentioned foundation types under the applied static loads. Accordingly, the designed floating pile foundation provides a stiffer foundation in comparison with the pile-raft and shallow foundations under gravity loads.

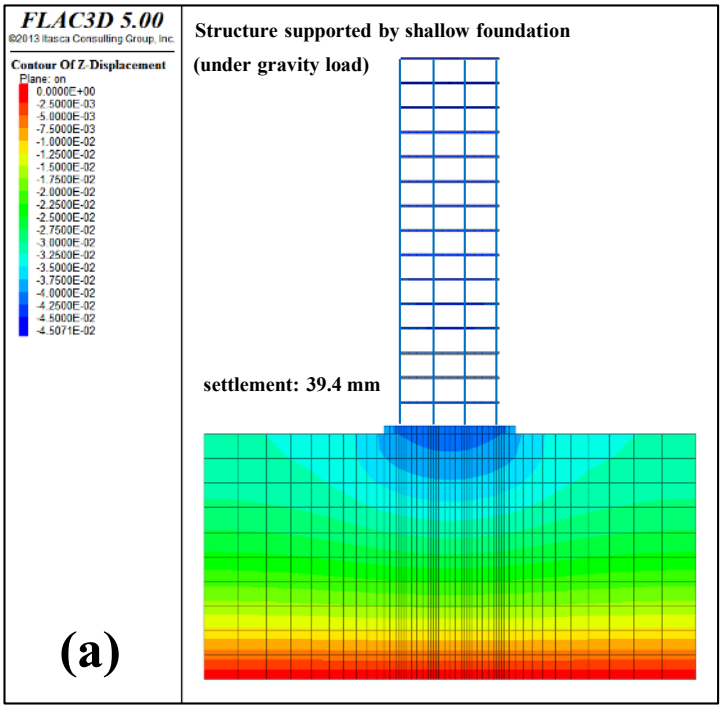

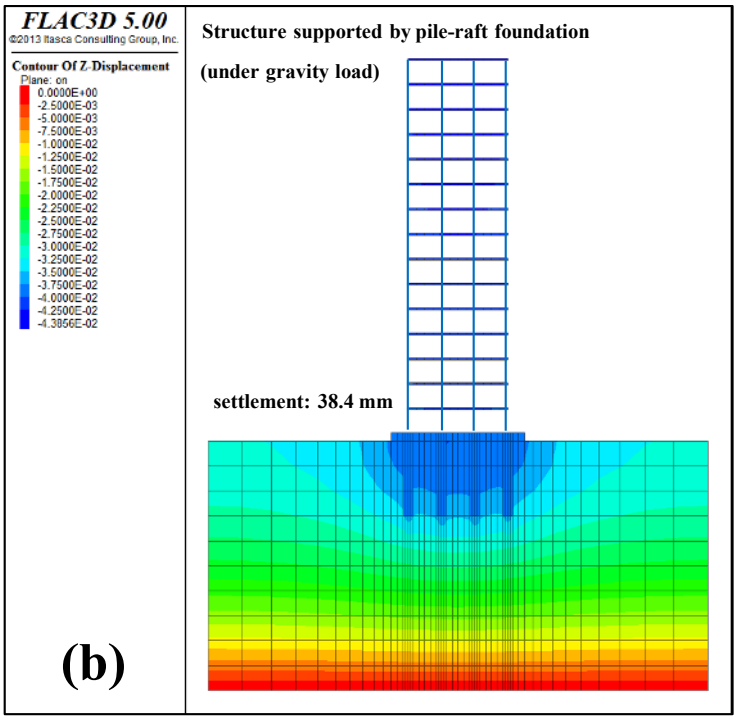


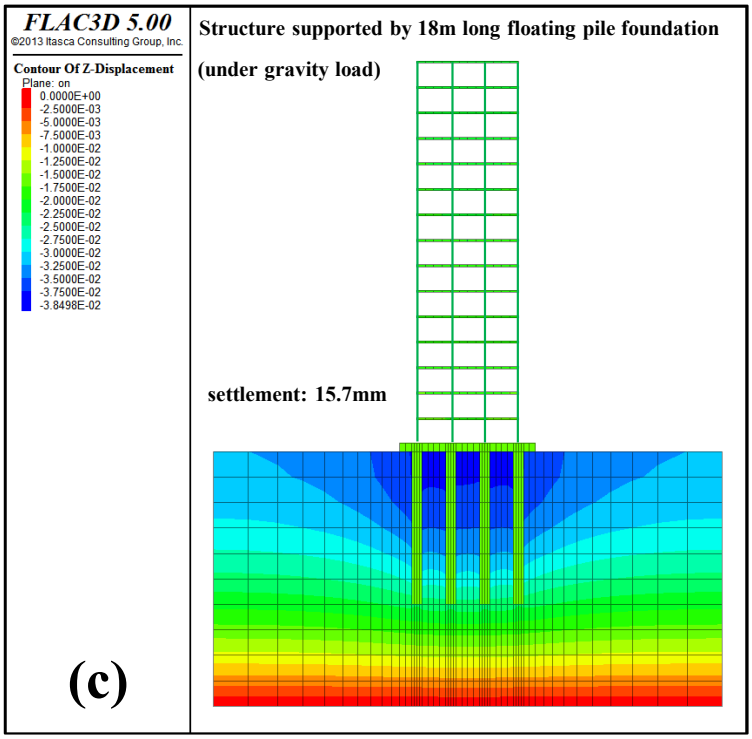


**Figure 6.4** Settlements of the fifteen storey structure supported by: (a) shallow foundation; (b) pile-raft foundation; (c) floating pile foundation under the gravity loads

### 6.4.2 Site Effect and Soil Amplification

Properties of the underlying soil deposit influence the earthquake motions experienced at the base of the superstructure considerably. As discussed in Section 2.2, local site effects can significantly alter the seismic characteristics of the ground motion such as the amplitude and the frequency content. Figures 6.5-6.8 present the time-history acceleration records and the corresponding response spectrum at the bed rock and free field soil surface under the influence of 1940 El Centro, 1995 Kobe, 1940 El-Centro, and 1968 Hachinohe earthquakes, respectively, based on the developed 3D numerical model.

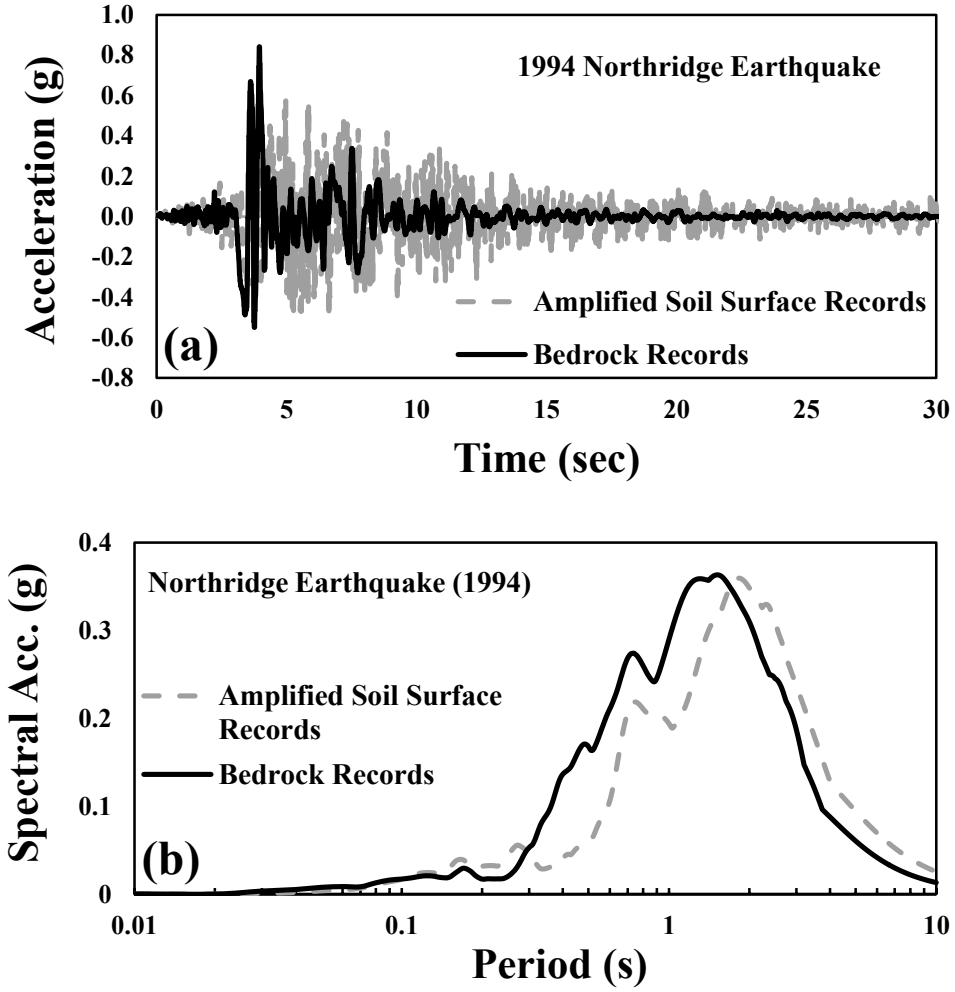


**Figure 6.5** (a) Bedrock record and the amplified free field soil surface record under the influence of 1994 Northridge earthquake; (b) acceleration response spectrum with 5% damping ratio for the structure

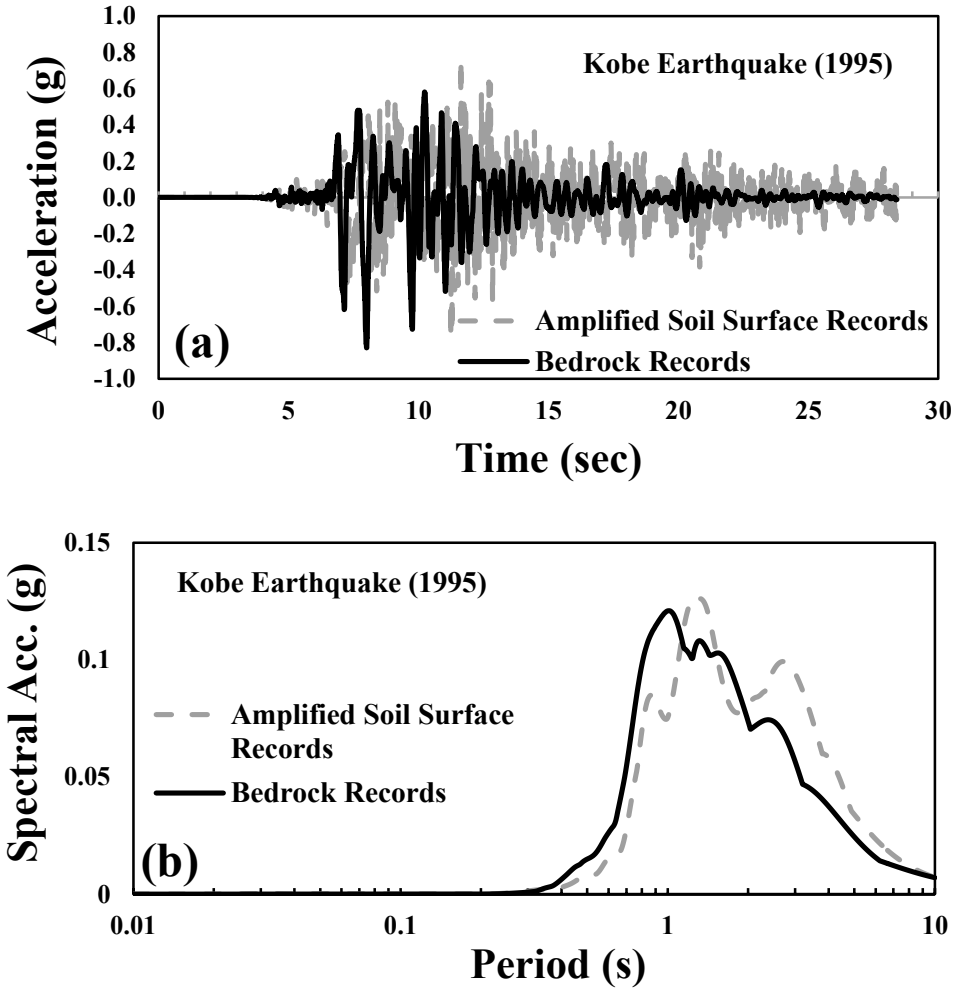


**Figure 6.6** (a) Bedrock record and the amplified free field soil surface record under the influence of 1995 Kobe earthquake; (b) acceleration response spectrum with 5% damping ratio for the structure

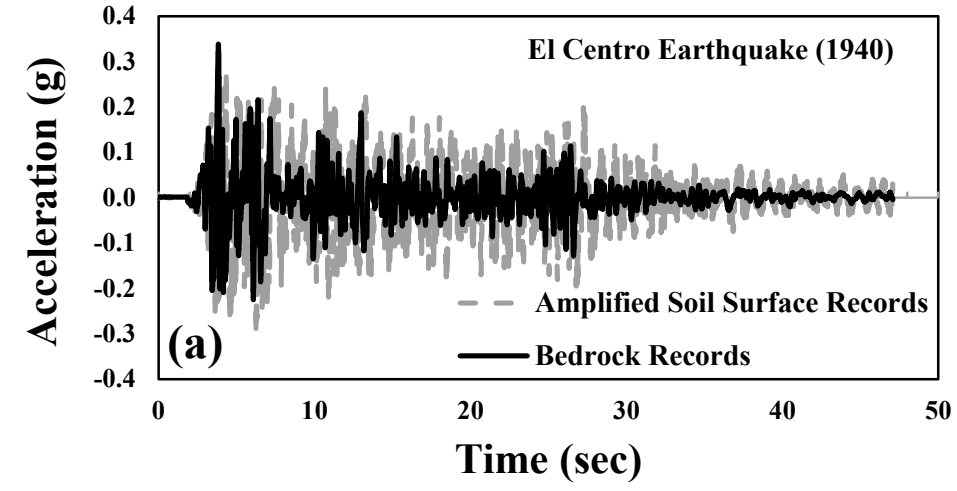

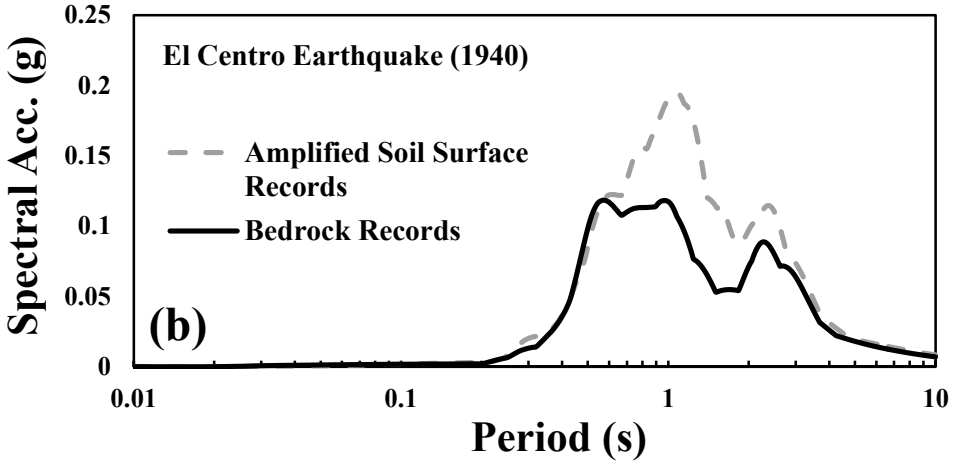


**Figure 6.7** (a) Bedrock record and the amplified free field soil surface record under the influence of 1940 El Centro earthquake; (b) acceleration response spectrum with 5% damping ratio for the structure

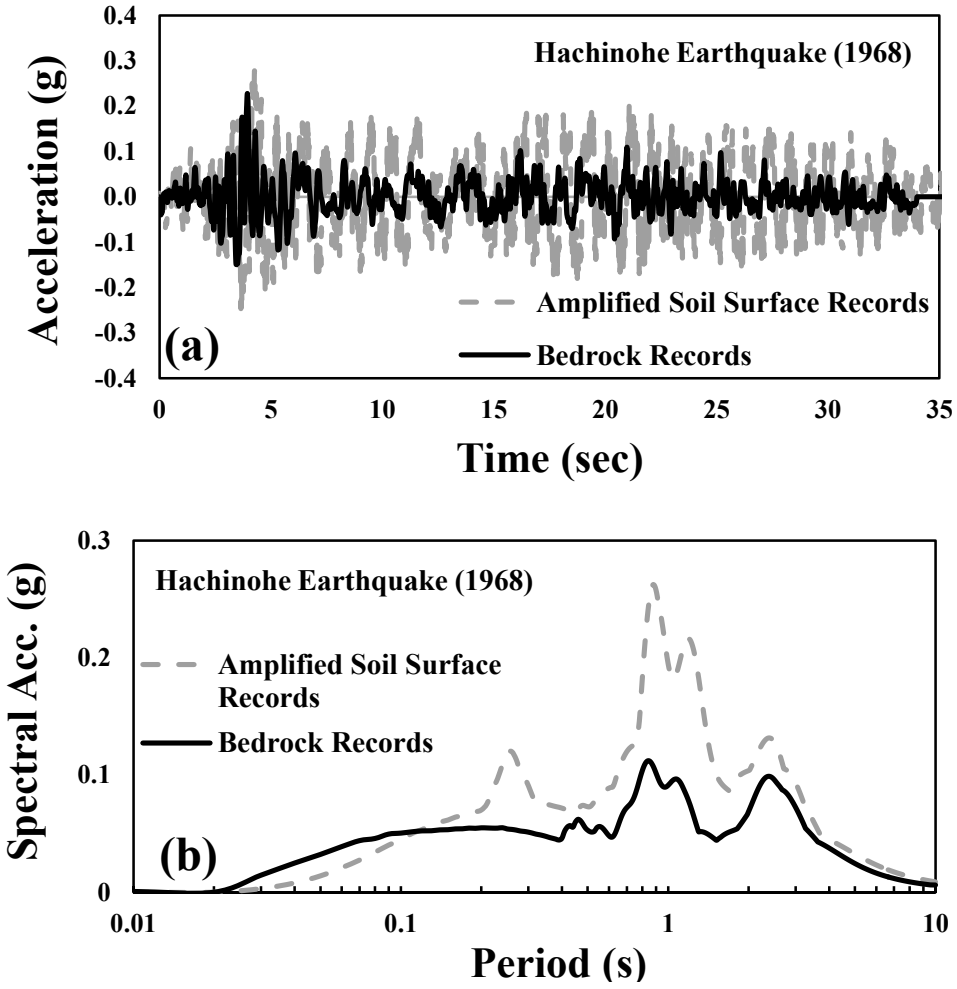


**Figure 6.8** (a) Bedrock record and the amplified free field soil surface record under the influence of 1968 Hachinohe earthquake; (b) acceleration response spectrum with 5% damping ratio for the structure

According to Figures 6.5a-6.8a, the peak accelerations at the soft soil surface are greater than that of on the bedrock for low to moderate acceleration levels. However, at higher acceleration levels, low stiffness and nonlinearity of the soft soil prevent the development of peak accelerations as large as those recorded at the bedrock. For instance, the soil surface acceleration records under 1994 Northridge earthquake (Figure 6.5a) were amplified for the acceleration levels lower than approximately 0.4g. In the meantime, the peak acceleration at the bedrock, which is equal to 0.84g, reduces while passing through the soft soil deposit, giving the peak acceleration of 0.57g at the soil surface. Similar observations were reported by other researchers (e.g. Idriss, 1990; Meymand, 1998; Kramer and Stewart, 2004).

The frequency content of the free field ground motion is also influenced by the local site conditions. Referring to Figures 6.5b-6.8b, the soil surface records consist of greater proportions of long-period (low frequency) motions in comparison with the bedrock records. For instance, the dominant period of 1940 El Centro earthquake at the soil surface is 1.07 second, while the dominant period of the motion at the bedrock is 0.57 second. Findings by other researchers (e.g. Kramer, 1996; Carbonari et al., 2011) confirm this behaviour. This phenomenon is extremely important influencing the seismic response of the superstructure particularly where the modified earthquake motion hits the superstructure close to its natural frequency.

It should be noted that the developed 3D numerical model accounts for the fully nonlinear behaviour of the soil deposit as discussed in Section 3.3. Kim and Roesset (2004) mentioned that by assuming linear elastic soil behaviour the motion at bedrock is greatly amplified over the complete range of periods by the soil deposit. However, referring to the provided results, as the soil softens and behaves nonlinearly, its natural period elongates, shifting the peaks in the amplification curve to the right (longer periods), and the damping increases due to the internal soil damping of a hysteretic nature, reducing the amplitudes of these peaks.

The presence of the superstructure and the foundation type may influence the characteristics of the earthquake motion at the base of the structure. In fact, the reaction of the superstructure to the seismic motion results in the generation of inertial forces in the structural mass. These inertial forces cause further motion at the base of the structure in comparison with the free field motion (kinematic interaction). On the other

hand, as discussed by Kramer (1996), the inability of the foundation to match the free field deformation (kinematic interaction) contributes to the variation of the base motion from the free field motion. Kinematic interaction effects reduce the foundation motion relative to the free field motion due to the difference between the stiffness of the foundation and the surrounding soil, as concluded by Veletsos and Prasad (1989). Therefore, the motion experienced at the base of the foundation can be greater or weaker than that of the free field due to SSI (Rayhani, 2007).

Figure 6.9 illustrates the ground motion at the base of the superstructure for the different types of foundations under the influence of 1940 El Centro earthquake (near-field earthquake) and 1995 Kobe earthquake (far-field earthquake). According to Figure 6.9, although the variation of the base response spectrums is not significant (or it is close to free field motion) for the most of the cases investigated in this study, the influence of SSI on the base motion can be notable in some cases. For instance, the base response spectrum of the pile-raft foundation case under the influence of 1995 Kobe earthquake is considerably different from the free field ground motion, particularly in the higher periods. Therefore, although the adopted simplified methods in the building codes (see Section 2.2) , in which the free field ground motion is taken as base excitation, can provide sufficient accuracy in many cases, considering the influence of SSI with respect to the different types of foundations is required to predict the base motion of the structures with a great rigor.

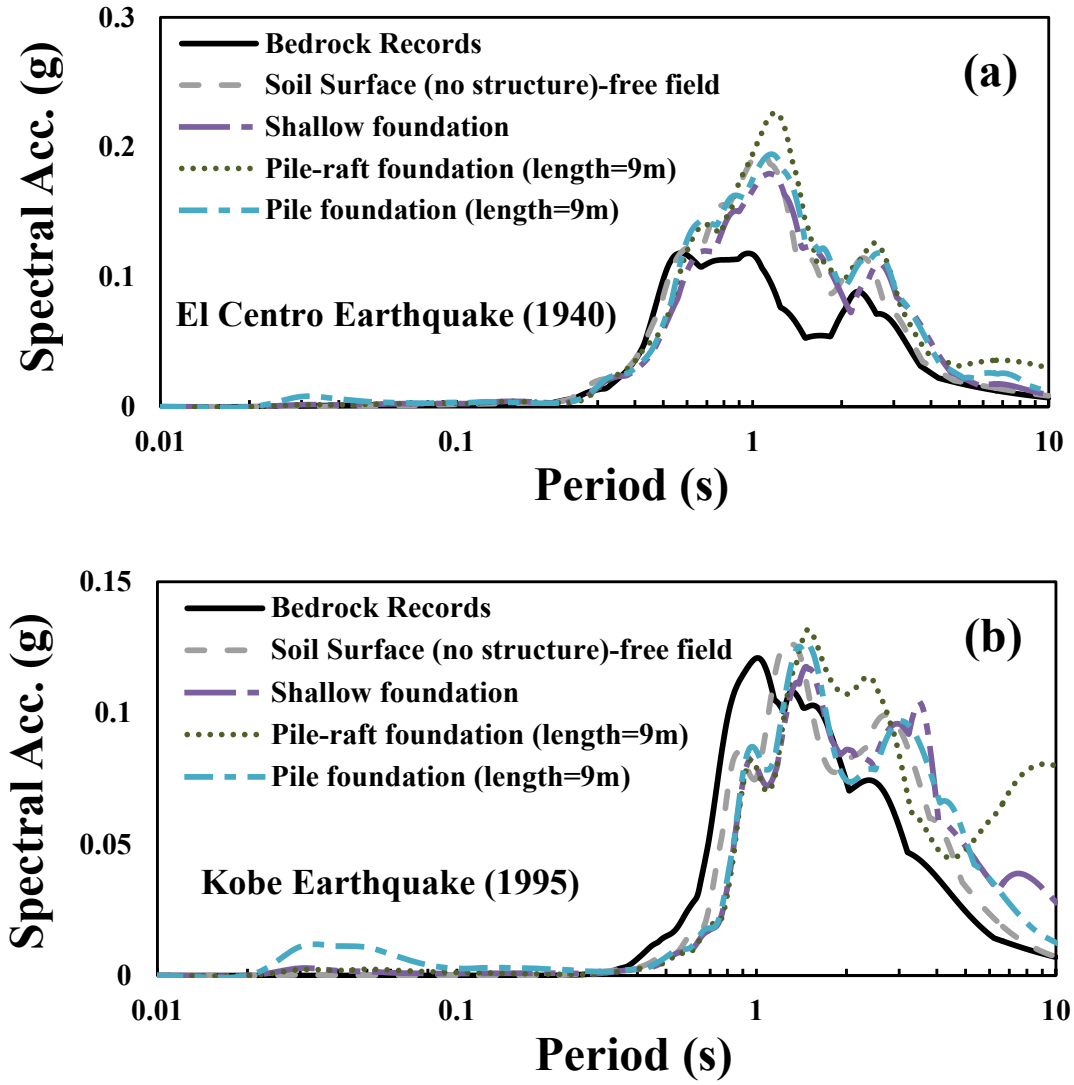


**Figure 6.9** Acceleration response spectrum with 5% damping ratio for the structure with different foundation types under the influence of: (a) 1940 El Centro earthquake; (b) 1995 Kobe earthquake

### 6.4.3 Influence of SSI on Generated Shear Forces in Superstructure

In order to investigate the influence of the soil-structure interaction on the structural demand of the superstructure, the 3D numerical predictions of the shear force distribution in the fixed based structure are compared with the shear force distribution in the structures supported by different types of foundations as shown in Figure 6.10. As mentioned earlier, the adopted 3D numerical model accounts for the inelastic behaviours for both soil and structure. It should be noted that the structural elements experience different shear forces during the shaking excitations. For instance, samples

of time-history shear force records at a corner column on levels 1, 7, and 15 for the fixed base structure under the influence of 1940 El Centro earthquake are shown in Figure 6.11. To determine the maximum shear force in each level, the generated shear forces in all of the columns of that level are summed up in every time increment during the time-history analysis, and the absolute maximum experienced shear force in that level during the earthquake is reported as presented in Figure 6.10. Moreover, the maximum developed base shears (shear force at the first level) of the superstructure under the four mentioned earthquake excitations are compared in Figure 6.12.

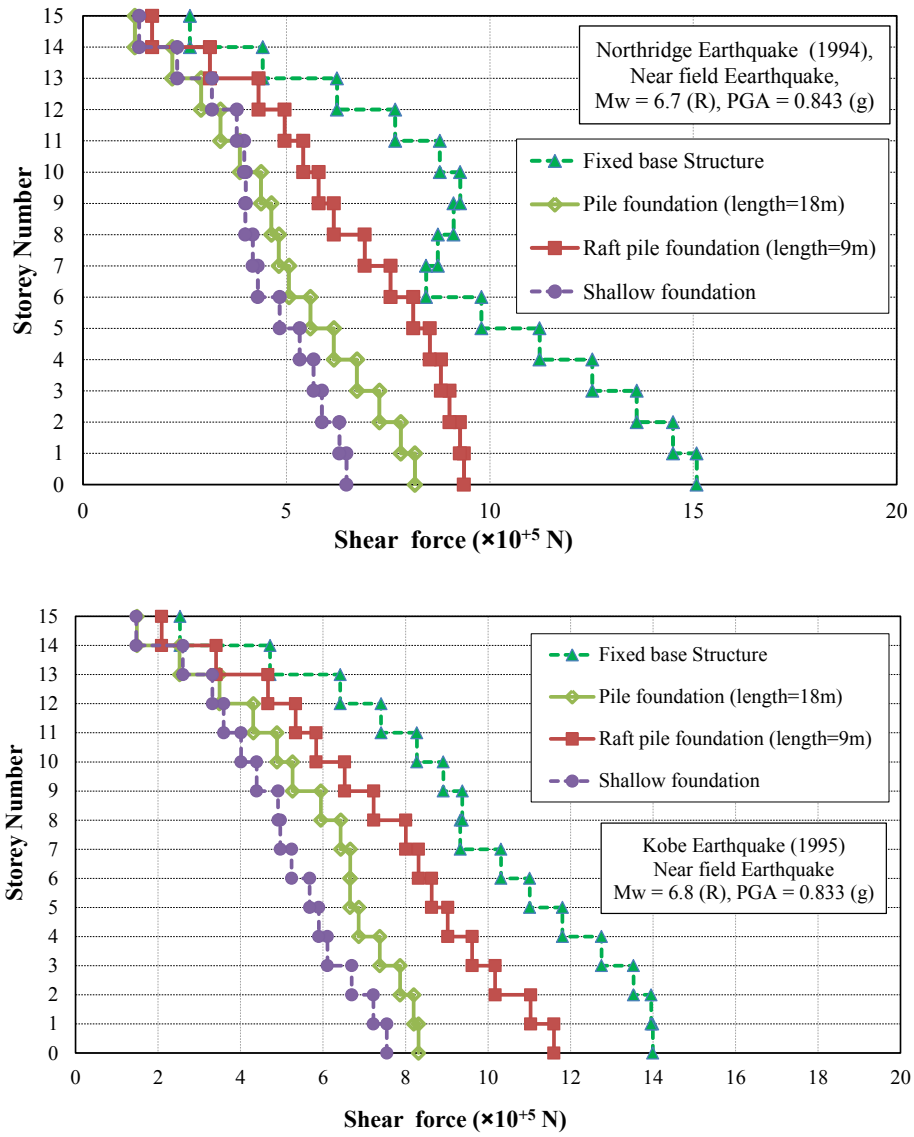

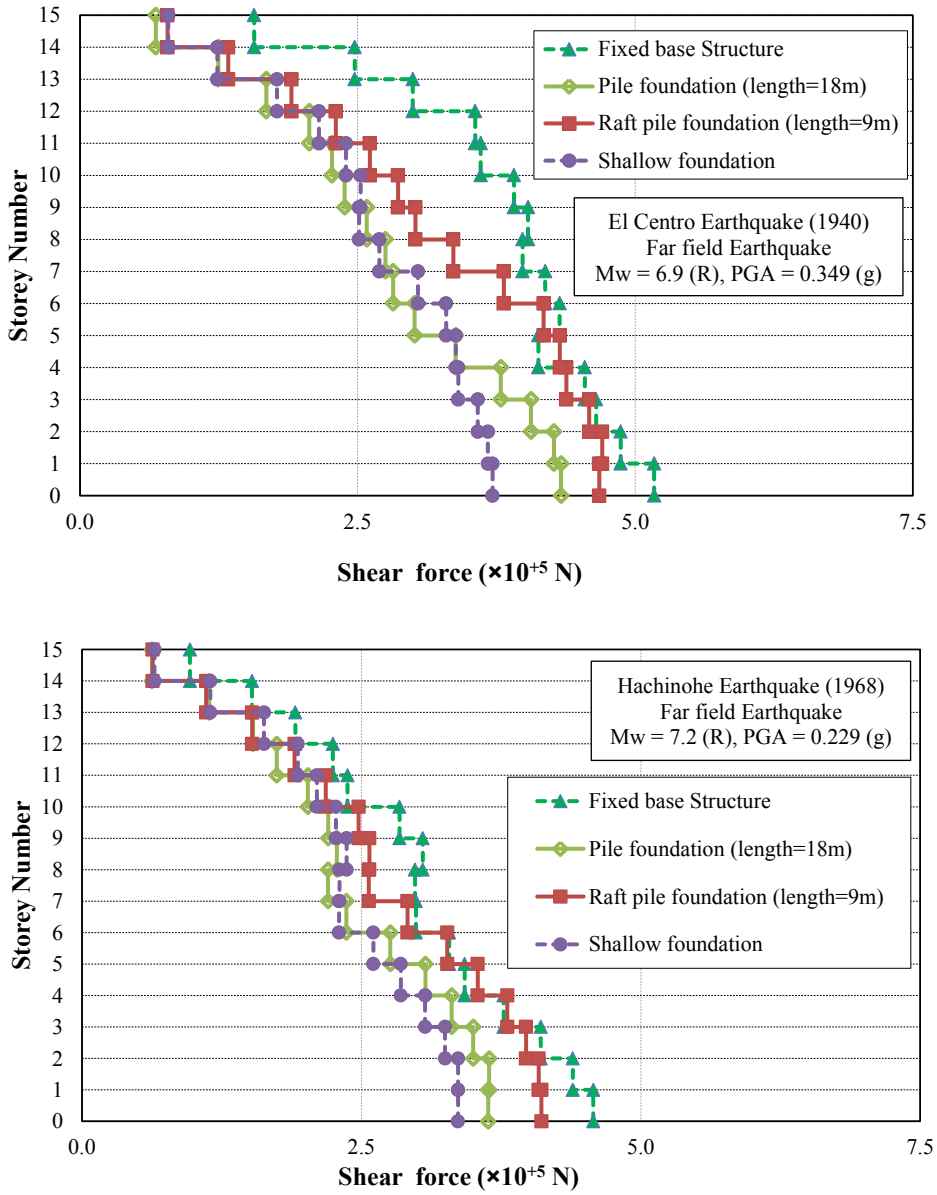


**Figure 6.10** Maximum shear force distribution for the fixed base, shallow foundation, floating pile foundation, and pile-raft cases under the influence of: (a) 1994 Northridge earthquake; (b) 1995 Kobe earthquake; (c) 1940 El Centro earthquake; (d) 1968 Hachinohe earthquake

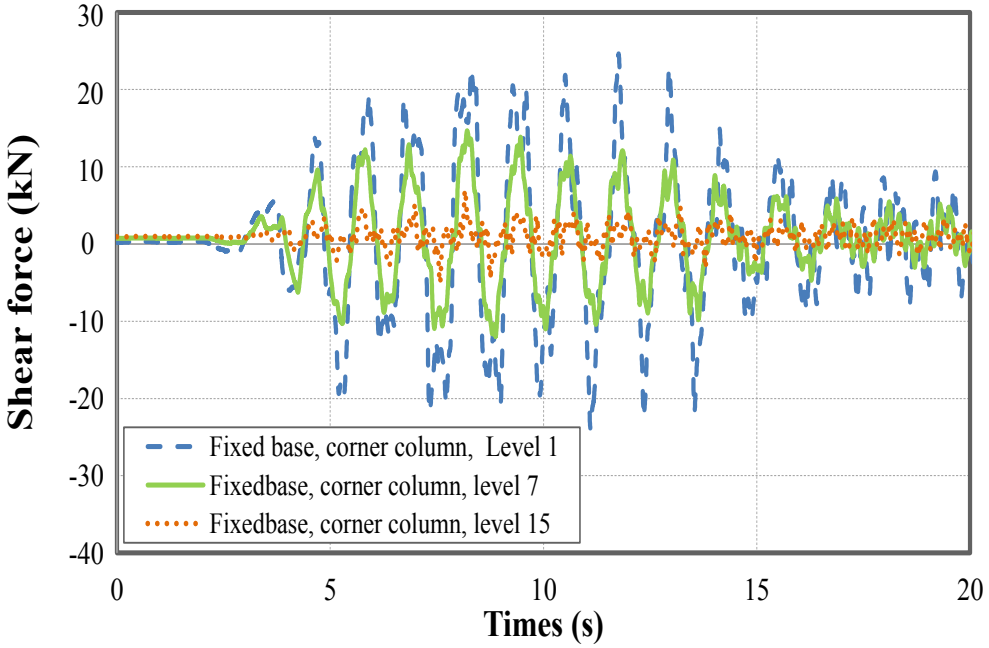


**Figure 6.11** Sample of numerical prediction of time-history shear force generation in corner columns for the fixed base model under the influence of 1940 El Centro earthquake on levels 1, 7, and 15.

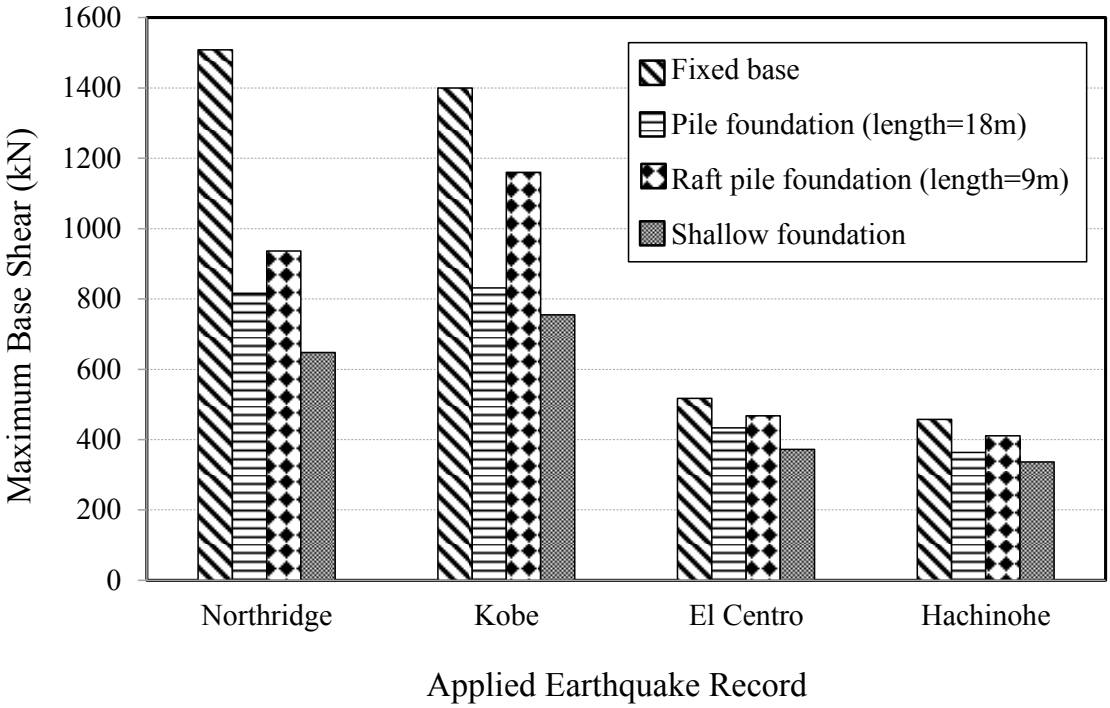


**Figure 6.12** Maximum base shear of the structure for the fixed base, shallow foundation, floating pile foundation, and pile-raft foundation cases under the influence of: (a) 1994 Northridge earthquake; (b) 1995 Kobe earthquake; (c) 1940 El Centro earthquake; (d) 1968 Hachinohe earthquake

In general, the ratio of the base shear for cases including the soil-structure interaction to that of the fixed-base is less than one (see Figure 6.12) demonstrating the effect of the soil-structure interaction in reducing the base shear of the structure. The maximum base shear forces of the structure supported by the floating pile foundation, pile-raft foundation, and shallow foundation are on average 37%, 23%, and 46% less than the maximum base shear force for the fixed base structure excluding the soil-structure interaction. Therefore, the structure supported by the pile-raft foundation experiences greater base shear in comparison to the structure supported by the floating pile and shallow foundations.

Referring to Figure 6.10, SSI influences the shear force distribution along the superstructure significantly. Although the SSI reduces the developed shear forces, the amount and trend of this reduction is not the same for different levels. For instance, the maximum shear force experienced in the first level of the fifteen storey superstructure supported by the pile-raft foundation reduces by 38% in comparison with the fixed base structure under the influence of 1994 Northridge earthquake. However, the seventh level barely experiences any reduction in the generated shear force (less than 10%) during the 1994 Northridge earthquake. In fact, the soil-structure interaction changes the dynamic characteristics (natural frequency and damping) of the system depending on the foundation type. As a result, the input excitation attracts different portions of the structure's higher mode responses contributing to the fluctuations of the shear force distribution along the superstructure. Consequently, the practicing engineers need to be aware that the amount of reduction in the maximum base shear due to SSI (Figure 6.10) cannot be generalised to all levels of the superstructure, otherwise this may result in an unsafe design.

### 6.4.4 Rocking of the Fifteen Storey Superstructure

Rocking occurs when the generated inertial forces in the superstructure cause compression in one side and tension on the other side of the foundation, which in turn results in the settlement in one side and a possible uplift on the other side of the foundation, respectively. For instance, Figure 6.13 shows a sample of 3D numerical prediction of the rocking components for different types of foundations under the influence of 1940 El Centro earthquake. Figure 6.14 compares the maximum experienced vertical

displacements for different types of foundations subjected to the four mentioned earthquake records, and the relevant rocking angles are summarised in Table 6.5. The rocking of the fixed base structure is assumed to be zero.

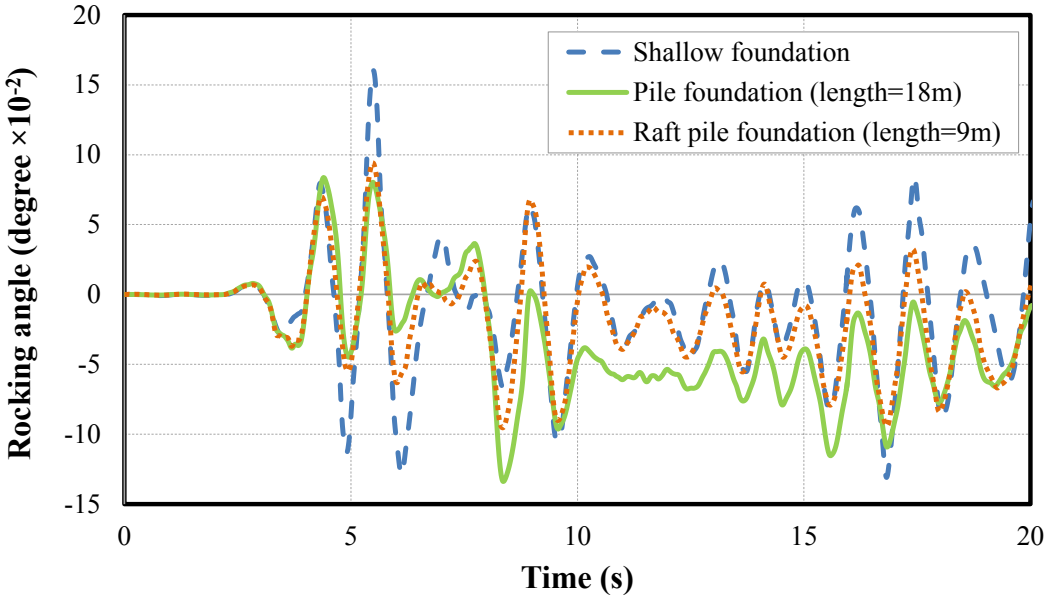


**Figure 6.13** Sample of numerical prediction of rocking component (rocking angle) for shallow foundation, pile foundation, and pile-raft foundation cases under the influence of 1940 El Centro earthquake

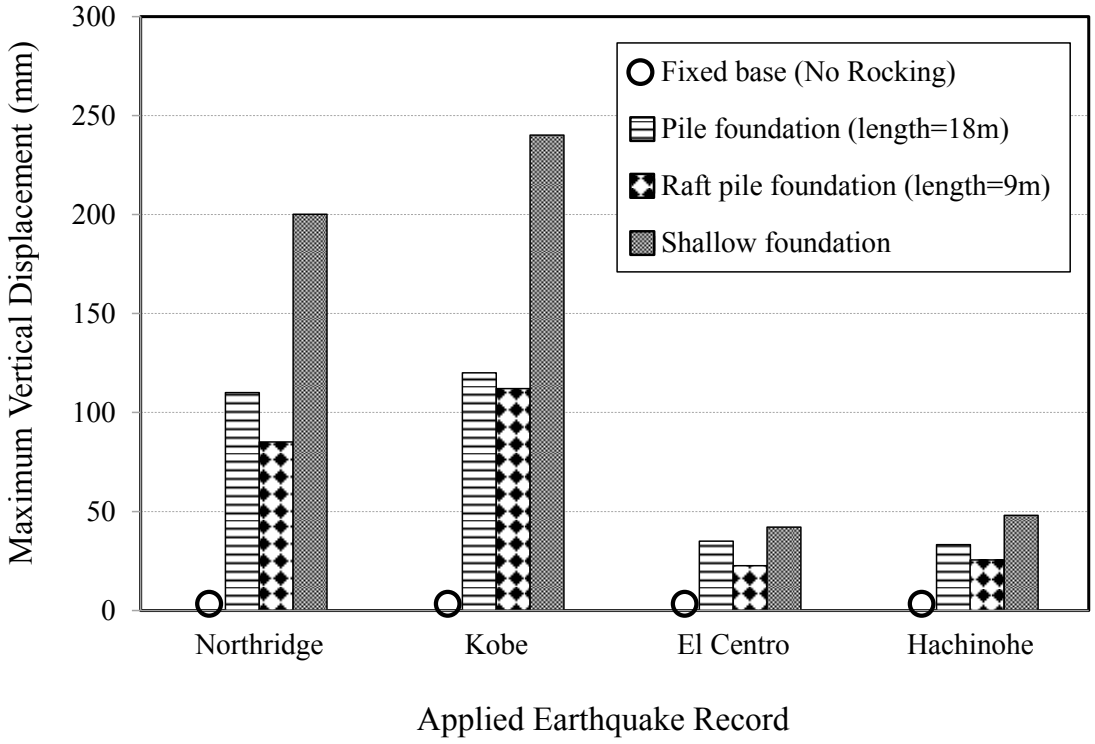


**Figure 6.14** Maximum Rocking of the structure for the fixed base, shallow foundation, floating pile foundation, and pile raft foundation cases under the influence of: (a) 1994 Northridge earthquake; (b) 1995 Kobe earthquake; (c) 1940 El Centro earthquake; (d) 1968 Hachinohe earthquake

**Table 6.5** Maximum rocking angle of foundations obtained from 3D numerical simulation

| Applied Earthquake Record | Rocking Angle of Foundation (degree) | | | |
|---|---|---|---|---|
| | Fixed base | Shallow Foundation | Floating Pile Foundation | Pile-raft Foundation |
| 1994 Northridge | 0 | 0.76° | 0.42° | 0.32° |
| 1995 Kobe | 0 | 0.92° | 0.46° | 0.43° |
| 1940 El Centro | 0 | 0.16° | 0.13° | 0.09° |
| 1968 Hachinohe | 0 | 0.18° | 0.13° | 0.10° |

As expected, earthquakes with higher intensities (near-field) such as 1994 Northridge and 1995 Kobe earthquakes cause more rocking in the building response in comparison with the low intensity (far-field) earthquakes such as 1940 El Centro and 1968 Hachinohe earthquakes due to the generation of higher amount of inertial energy in the structure. For instance, the fifteen storey superstructure supported by the shallow foundation experienced up to 240 mm (0.92°) of rocking under the influence of 1995

Kobe earthquake, while the maximum rocking under the 1940 El Centro Earthquake was less than 50 mm (0.16°).

Comparing different types of foundations, the structure supported by the shallow foundation experienced the most severe rocking as shown in Figure 6.14. However, the presence of pile elements in both floating pile and pile-raft foundations results in considerable reduction in the maximum uplift experienced by the structure which in turn reduces the maximum rocking of the structure. Accordingly, the maximum rocking angle of the floating pile foundation and pile-raft foundation cases are on average 44% and 54% less than the rocking angle of the shallow foundation cases. Moreover, the structure supported by the pile-raft foundation experienced on average 20% less rocking in comparison to the structure supported by the floating pile foundation. This is due to the fact that in the floating pile foundation case, due to the generation of compressive stresses in one side of the foundation, pile elements experience more settlement in comparison to the pile-raft foundation case, where the generated compressive stresses distribute over a larger area resulting in the reduced settlement. It should be noted that the area replacement ratio of the pile group is 8% in this study, and as a result, piles attract significant axial forces. Area replacement ratio is defined as the cross-sectional area of the pile divided by the tributary area for each pile. The same ratio can also be calculated using the cross-sectional area of all piles divided by the area beneath the pile cap.

Consequently, when the key concern of the design engineer is to improve the total stability of the structure by reducing the rocking component, employing the pile-raft foundation might be a good option considering the cases investigated in this study.

### 6.4.5 Lateral Deflection and Inter-storey Drifts of Superstructure

The results of the 3D numerical predictions for the maximum lateral deflections of the fifteen storey structure supported by the fixed-base, the shallow foundation, the floating pile foundation and the pile-raft foundation are summarised and compared in Figure 6.15. As mentioned earlier, the adopted 3D numerical model accounts for the inelastic behaviours for both the soil and the structure. To determine the lateral deflections, the movement of the foundation has been subtracted from the storey

movements. Therefore, all the records are relative to the foundation movements on the soil surface level. It should be noted that the presented data are based on the lateral deformation of each storey when the maximum deflection at the top level occurs. As mentioned earlier, this approach gives a more reasonable pattern of the structural deformation in comparison with the approach that maximum absolute storey deformations irrespective of occurrence time are recorded (Hokmabadi et al., 2012). Figure 6.16 illustrates a sample of time-history deformation records used to obtain the lateral deformations reported in Figure 6.15.

Accordingly to Figure 6.15 and as expected, the near-field earthquakes (i.e. 1994 Northridge and 1995 Kobe earthquakes) cause more lateral deflections in the structure in comparison with the low intensity far-field earthquakes (i.e. 1940 El Centro and 1968 Hachinohe) due to the higher inertial forces generated. For example, the maximum lateral deflection of the fixed base structure under the influence of 1994 Northridge earthquake is 470 mm, while the corresponding value under the 1968 Hachinohe earthquake is 145 mm.

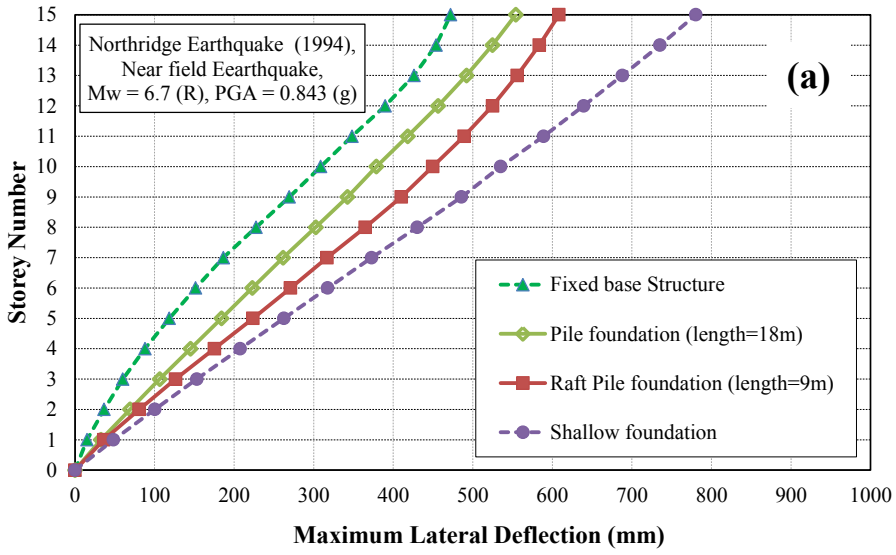

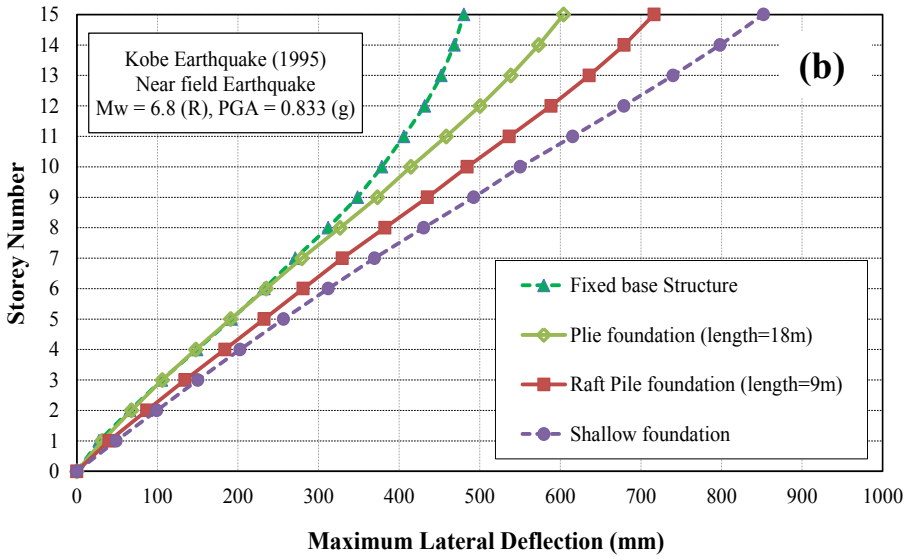
Kobe Earthquake (1995)
Near field Earthquake
Mw = 6.8 (R), PGA = 0.833 (g)
(b)
Fixed base Structure
Plie foundation (length=18m)
Raft Pile foundation (length=9m)
Shallow foundation
Storey Number
Maximum Lateral Deflection (mm)

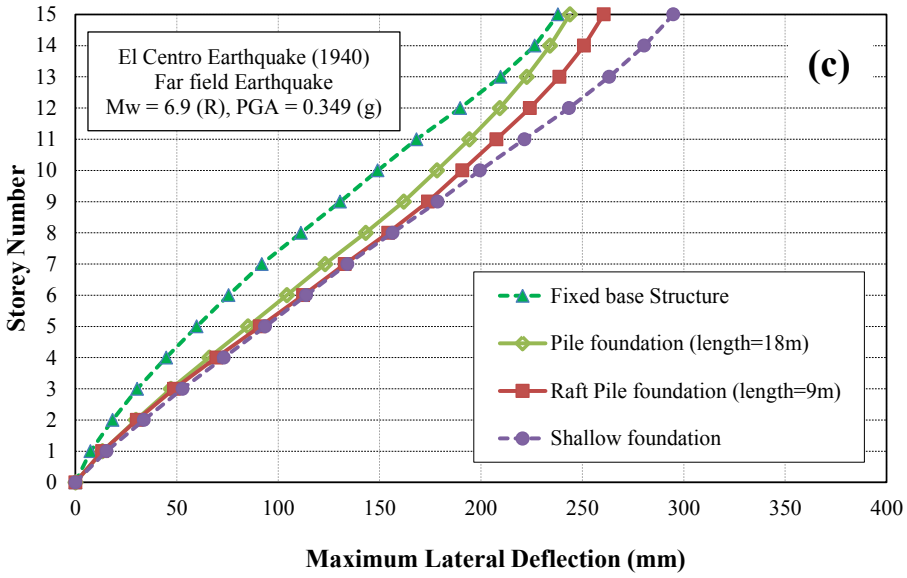
El Centro Earthquake (1940)
Far field Earthquake
Mw = 6.9 (R), PGA = 0.349 (g)
(c)
Fixed base Structure
Pile foundation (length=18m)
Raft Pile foundation (length=9m)
Shallow foundation
Storey Number
Maximum Lateral Deflection (mm)

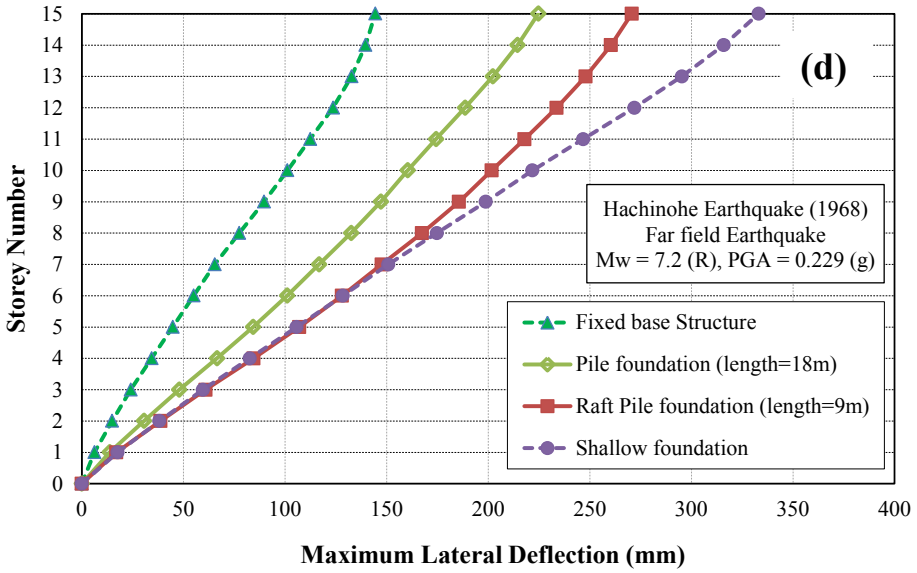


**Figure 6.15** Maximum lateral deflection of the structure for the fixed base, shallow foundation, floating pile foundation, and pile-raft cases under the influence of: (a) 1994 Northridge earthquake; (b) 1995 Kobe earthquake; (c) 1940 El Centro earthquake; (d) 1968 Hachinohe earthquake

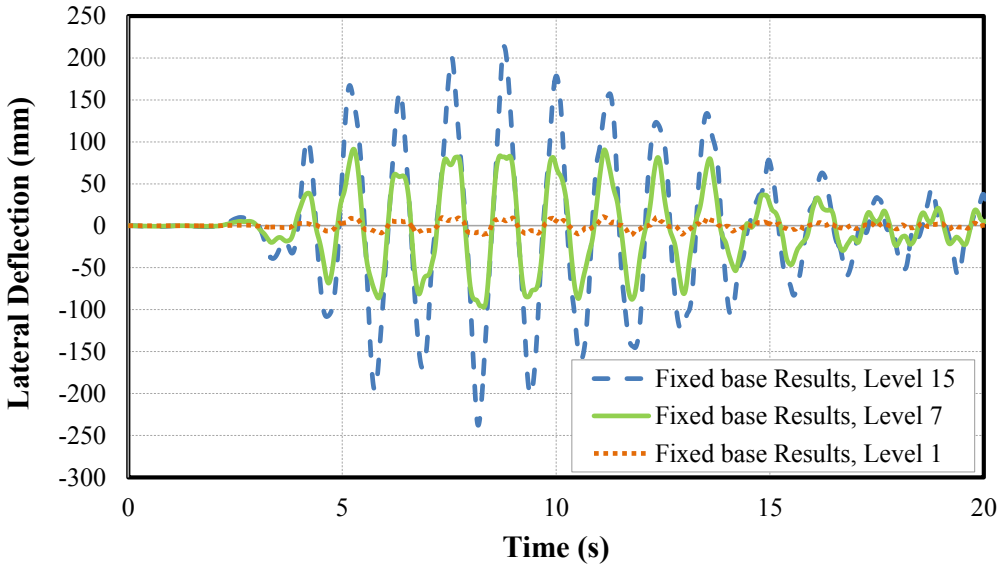


**Figure 6.16** Sample of numerical prediction of time-history deflection for the fixed base model under the influence of 1940 El Centro earthquake in levels 1,7, and 15.

In general, the soil-structure interaction tends to amplify the lateral deflection of the superstructure. Referring to Figure 6.15, the maximum lateral deflection of the structure supported by the floating pile and the pile-raft foundations increase on average by 22%, and 38%, respectively, in comparison to the fixed base structure. Moreover, the maximum lateral deflection of the structure supported by the shallow foundation in soft

soil is increased on average by 69% in comparison to the results obtained from the fixed base structure. Therefore, the amplification factor varies with the foundation type, where the presence of pile elements in the floating pile and pile-raft foundation cases reduces the amplification in the lateral deflections of the structure in comparison with the shallow foundation case.

As discussed earlier, the lateral deflections of the structure are composed of two components, namely structural distortion and rocking. Structural distortion component is directly related to the generated shear forces in the structure. According to Section 6.4.3, SSI reduces the base shear and in turn the structural distortion component. However, according to Section 6.4.4, SSI amplifies the rocking component resulting in the increase in the deflection of the superstructure. The ratio that these two components contribute in the maximum deflection experienced by the structure is a function of the foundation type. Considering the cases investigated in this study, for the shallow foundation case approximately 70% of the maximum lateral deflections were due to the rocking component, while 30% took place due to the structural distortion. These values for the floating pile foundation case are 55% and 45%, respectively, and for the pile-raft foundation cases are 39%, 61% respectively. Therefore, the presence of pile elements in the floating pile foundation and pile-raft foundation cases increases the base shear of the structure (Section 6.4.3) in comparison with the shallow foundation case. In contrast, the presence of pile elements in the floating pile foundation and pile-raft foundation cases reduces the maximum lateral deflections experienced by the structure in comparison with the shallow foundation case, due to the reduced rocking experienced by the structure (see Section 6.4.4).

Figure 6.17 presents the corresponding maximum inter-storey drifts of the superstructure for different types of foundations, calculated using Equation (6.2). As discussed earlier, in the performance-based design which is a modern approach for the earthquake-resistant design, the seismic performance (performance level) is described by considering the maximum allowable damage state (damage performance) for an identified seismic hazard (hazard level). Inter-storey drifts are the most commonly used damage parameters, and based on FEMA (BSSC, 1997), the maximum inter-storey drift of 1.5% is defined as the border between life safe and near collapse levels.

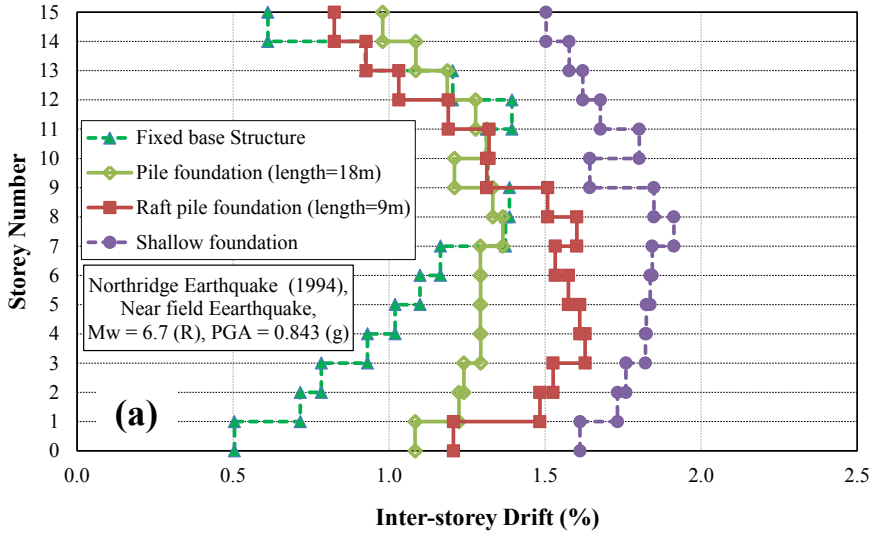
Storey Number
Inter-storey Drift (%)
Fixed base Structure
Pile foundation (length=18m)
Raft pile foundation (length=9m)
Shallow foundation
Northridge Earthquake (1994),
Near field Eearthquake,
Mw = 6.7 (R), PGA = 0.843 (g)
(a)

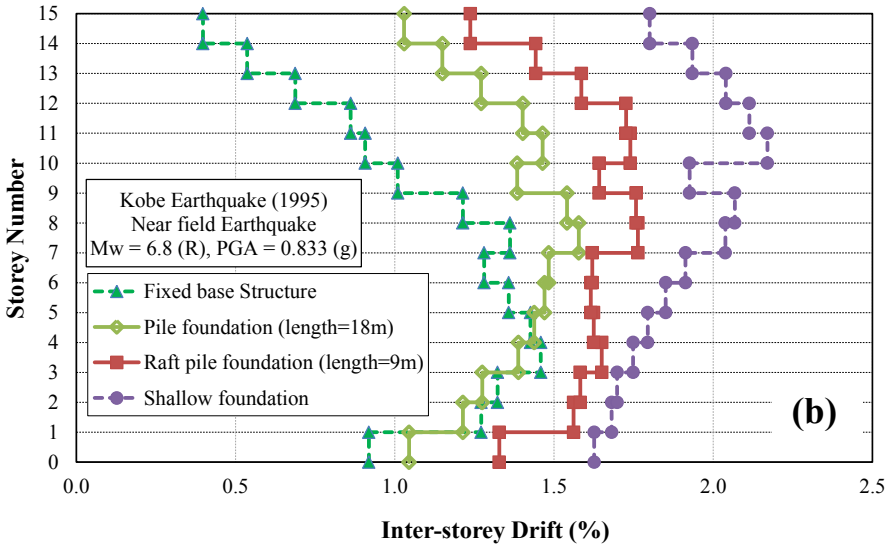
Storey Number
Inter-storey Drift (%)
Kobe Earthquake (1995)
Near field Earthquake
Mw = 6.8 (R), PGA = 0.833 (g)
Fixed base Structure
Pile foundation (length=18m)
Raft pile foundation (length=9m)
Shallow foundation
(b)

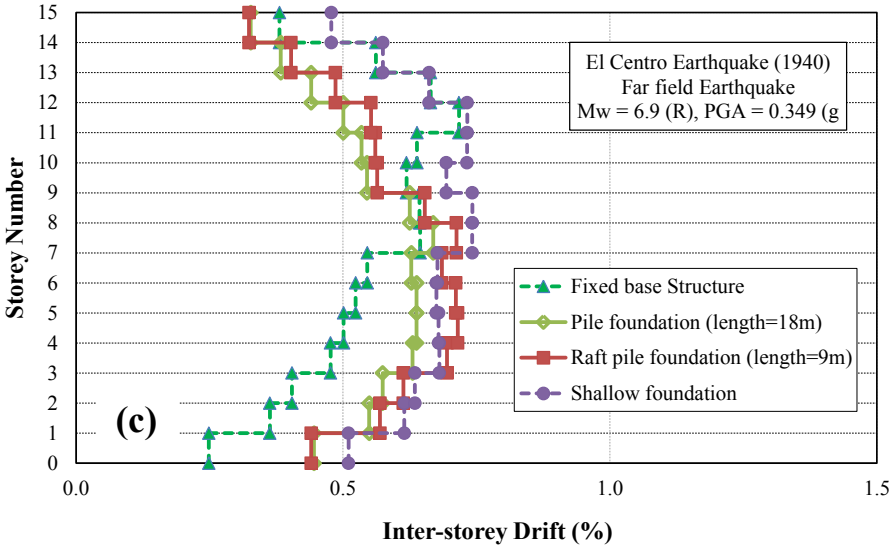
Storey Number
Inter-storey Drift (%)
El Centro Earthquake (1940)
Far field Earthquake
Mw = 6.9 (R), PGA = 0.349 (g
Fixed base Structure
Pile foundation (length=18m)
Raft pile foundation (length=9m)
Shallow foundation
(c)

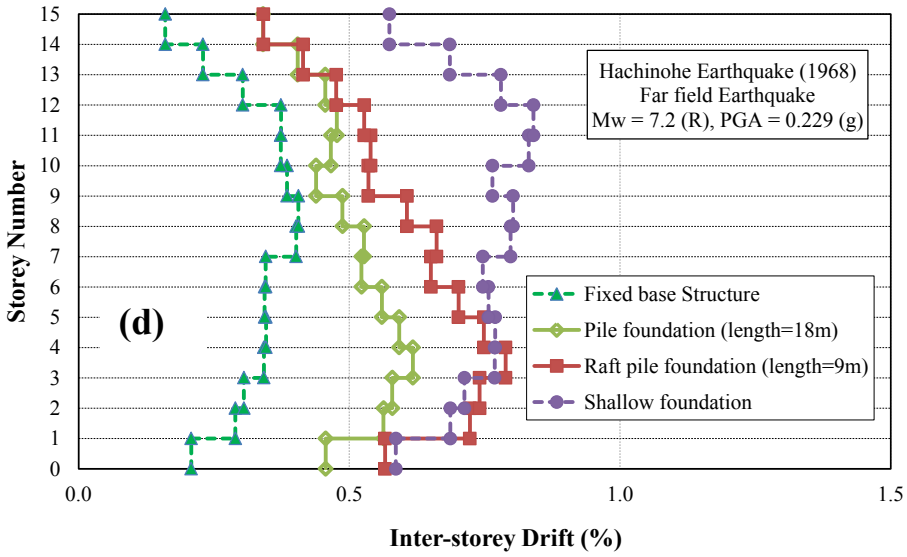


**Figure 6.17** Maximum inter-storey drifts of the structure for the fixed base, shallow foundation, floating pile foundation, and pile-raft cases under the influence of: (a) 1994 Northridge earthquake; (b) 1995 Kobe earthquake; (c) 1940 El Centro earthquake; (d) 1968 Hachinohe earthquake

According to Figure 6.17, SSI tends to increase the inter-storey drifts of the superstructure. In general, the maximum recorde inter-storey drift of the structure supported by the floating pile foundation is more than the corresponding value for the fixed-base condition excluding the soil-structure interaction. However, the structure supported by the floating pile foundation experiences less inter-storey drifts in comparison to the structure supported by the pile-raft and the shallow foundations. For instance, under the influence of 1995 Kobe earthquake, the maximum recorded inter-storey drift of the fixed base structure is measured to be 1.4%, while the corresponding values for the floating pile foundation, the pile-raft foundation, and the shallow foundation cases are 1.57% and 1.76%, and 2.1%, respectively. As a result, the soil-structure interaction may affect the performance level of the structure and shift the performance level of the structure from life safe zone to near collapse or even collapse zones, particular in soft soils.

Moreover, SSI affects the distribution of the inter-storey drifts in the structure. This can be due to the same reasons as discussed in Section 6.4.3, where the soil-structure interaction changes the dynamic characteristics (natural frequency and damping) of the system. As a result, the input excitation attracts different portions of the

structure's higher mode responses depending on the foundation type, contributing to the observed distribution of the inter-storey drifts in the superstructure.

### 6.4.6 Rocking-dissipation due to SSI

In the modern design approaches which are under investigation by a growing number of researchers (e.g. Mergos and Kawashima, 2005; Anastasopoulos et al., 2012b; Deng and Kutter, 2012; Midorikawa et al., 2005) the foundation is allowed to rock in order to reduce the inertial loading that may be transmitted into the superstructure via the foundation. As explained by Anastasopoulos et al. (2014), the basic idea comes from the fact that rocking and settlement do not necessarily imply failure, thanks to the cyclic and kinematic nature of the ground shaking. Therefore, by designing a structure rocking more, further earthquake energy would be spent on rigid body rotation and less energy /force would induce distortion (shear force in the columns), resulting in less detrimental effects.

Based on the results obtained in this study, where the response of the superstructure under seismic loads is compared for different types of foundations, the influence of the rocking-dissipation on the seismic response of the structures can be assessed. Accordingly, if the practicing engineer can satisfy the requirement for the performance level (inter-storey drifts less than 1.5%) and total stability of the structure accounting for SSI, the rocking component can be beneficial for the structure as the rocking can dissipate the energy and reduce the structural demand of the structure as observed in Section 6.4.3. For example, the designed fifteen storey structure supported by a shallow foundation under the influence of 1940 El Centro earthquake stays in the life safe zone even after amplified deflections experienced by the structure due to SSI. Therefore, in this case, the rocking component can be beneficial in the design due to the reduction in the structural demand (base shear) by 28% in comparison with the fixed base structure. Referring to the results presented in Sections 6.4.3 and 6.4.4, this reduction in the structural demand of the superstructure is more considerable for the stronger earthquakes (1994 Northridge and 1995 Kobe earthquakes), where the superstructure is subjected to a higher amount of rocking-dissipation during the shaking excitations.

When earthquakes larger than the design earthquake occur at a particular site, structures with the foundation types experiencing more rocking component would be less damaged structurally, although non-structural members may be destructed more due to the amplified lateral deformations and drifts. However, it should be noted that the reduction in the base shear should be adopted with extreme caution and after assessing the influence of SSI, considering the following points: (1) the reduction factor in the shear forces due to SSI varies for different levels in the structure (see Section 6.4.3); (2) the residual rotation and differential settlements must be critically evaluated; and (3) the total stability of the structure should be checked carefully.

## 6.5 Summary

In this chapter, by employing the verified three-dimensional numerical model, a series of parametric studies on a fifteen storey full scale (prototype) structure with respect to the foundation types, including fixed base, shallow foundation, floating pile foundation, and pile-raft foundation, have been conducted. Material (soil and superstructure) and geometric (uplifting, gapping, and P- $\Delta$ effects) nonlinearities have been considered in the 3D numerical simulation.

Results of the 3D numerical simulation in this study show that the properties of the in situ soil influence the characteristics of the excitation, where the peak accelerations at the soft soil surface are greater than that of on the bedrock for low to moderate acceleration levels. However, at higher acceleration levels, low stiffness and nonlinearity of the soft soil prevent the development of the peak accelerations as large as those recorded at the bedrock. Moreover, earthquake records consist of greater proportions of long-period (low frequency) motion after passing through the soft soil deposit. The nonlinear behaviour of the soft soil deposit influences the dynamic characteristics of the ground motion by shifting the peaks in the amplification curve to the right (longer periods), and reducing the amplitudes of the peak ground accelerations.

In general, the ratio of the structural base shear for cases including the soil-structure interaction to that of fixed-base is less than one demonstrating the effect of the soil-structure interaction in reducing the base shear of the structure. However, the reduction ratio for the base shear is a function of the foundation type. Based on the

results of this study, the structure supported by the pile-raft foundation and the floating pile foundation experience more base shear in comparison to the structure supported by the shallow foundation. Moreover, the amount and trend of this reduction in the the structural shear forces are not the same for different levels in superstructure. Therefore, practicing engineers need to be aware that the reduction factor for the maximum base shear due to SSI cannot be generalised to all levels of the superstructure.

Based on the predicted maximum rocking angles of the superstructure, the structure supported by the shallow foundation experienced the most severe rocking in comparison with the floating pile and pile-raft foundation cases, where the presence of pile elements in both cases results in considerable reduction in the maximum uplift and in turn rocking experienced by the structure. Moreover, the structure supported by the pile-raft foundation experienced on average 20% less rocking in comparison to the structure supported by the floating pile foundation. This is due to the fact that in the floating pile foundation case, due to the generation of compressive stresses in one side of the foundation, pile elements experience more settlement in comparison with the pile-raft foundation case, where the generated compressive stresses distribute over a larger area resulting in a reduced settlement.

The other important influence of the seismic soil-structure is its significant contribution in amplifying the lateral deflections of the structure. The amplification factor varies with the foundation type, where the presence of pile elements in the floating pile and pile-raft foundation cases reduces the amplification of the lateral deflections of the structure in comparison with the shallow foundation case. Accordingly, SSI tends to increase the inter-storey drifts of the superstructure, which may affect the performance level of the structure and shift the performance level of from life safe zone to near collapse or even collapse zones, particularly in soft soil deposits.

Eventually, considering the rocking-dissipation, the results of this study can help the practicing engineers in selecting the proper foundation type for the structures. Accordingly, the foundation types experiencing considerable amount of rocking during an earthquake, dissipate significant amount of earthquake energy in comparison with the other types of foundations, and this rocking-dissipation in turn results in directing less shear forces to the superstructure and reducing the structural demand of the

superstructure. However, accounting for the rocking dissipation should be adopted with extreme caution and after assessing the influence of SSI, considering the following points: (1) the reduction factor in the shear forces due to SSI varies for different levels in the structure; (2) the residual rotation and differential settlements must be critically evaluated; and (3) the total stability of the structure should be checked carefully.

# Chapter 7- CONCLUSIONS AND RECOMMENDATIONS

## 7.1 Conclusions

### 7.1.1 Conclusions based on the Conducted Experimental Shaking Table Tests

In the conducted shaking table tests in this thesis, soil-foundation-structure models were physically simulated with geometric scaling factor of 1:30. Unlike the previous efforts, a multi-storey frame for the superstructure was adopted, representing the dynamic properties of the prototype structure such as natural frequency of the first and higher modes, number of stories, and density. Moreover, an advanced laminar soil container was designed to simulate the free field soil response by minimising the boundary effects. Consequently, in the current shaking table tests, by adopting the same soil properties, same superstructure, same input motions, and same test setup, a clear comparison was provided between the structural responses for different types of foundations (i.e. shallow foundation, floating pile foundation, end-bearing pile foundation). Four sets of shaking events including 1995 Kobe Earthquake, 1994 Northridge Earthquake, 1940 El Centro Earthquake, and 1968 Hachinohe Earthquake were applied. The improved physical modelling techniques in this study such as designing the soil mix and laminar soil container were explained in details which can be used by other researchers to achieve more accurate simulation of the soil-structure interaction in the 1g shaking table test.

According to the shaking table test results, the maximum lateral deflection of the fifteen storey structure supported by end-bearing and floating pile foundations increases on average by 17% and 34% in comparison to the fixed-base structure, respectively. Moreover, the maximum lateral deflection of the structure supported by the shallow

foundation was increased by 55% in comparison to the results obtained from the fixed-base structure. Therefore, comparing different types of foundations, pile foundations increase the lateral displacements of the superstructure in comparison with the fixed-base assumption, and reduce the lateral displacements in comparison to the shallow foundation case due to the rocking components. Consequently, the choice of the foundation type is dominant and should be included in investigating the influence of SSI on the superstructure response during shaking excitations, and conventional design procedures excluding the soil-structure interaction are not adequate to guarantee the structural safety for the moment resisting buildings resting on soft soils.

In addition, further experimental tests were conducted to investigate the influence of SSPSI on the dynamic response of buildings with various heights (i.e. five storey, ten storey, and fifteen storey buildings). By comparing the experimental results obtained from the model structures, it can be concluded that considering the effects of SSPSI can alter the dynamic characteristics of the superstructure. In addition, the lateral deflections of structures siting on end-bearing pile foundations were amplified in comparison to the fixed-base model. Generally, this amplification which is mainly due to the rocking component is more severe for taller buildings considering the range of the buildings investigated in this study. As a particular case, the five storey model structure experienced considerably high amount of amplification under the influence of the 1995 Kobe earthquake, while accounting for SSPSI. This can be due to the nature of the imposed seismic motion and its frequency content which hits the structure (with the modified dynamic properties due to SSPSI) and is close to the natural frequency of the system, resulting in attraction of extra energy by the superstructure and coming close to the resonant conditions.

Consequently, based on the conducted experimental investigations, considering the effects of the soil-pile-structure interaction can alter the dynamic characteristics of the superstructure, and ignoring the real deformability of the soil-pile system may affect the predicted damage level of structural and non-structural elements during earthquake as well as the lateral load carrying mechanism of soil-structure systems.

### 7.1.2 Conclusions based on the 3D Numerical Investigations

In this thesis, a three-dimensional numerical model employing FLAC3D was developed to perform nonlinear time-history analyses on the soil-foundation-structure system. Finite difference analyses were performed using real earthquake records taking into account both material (soil and superstructure) and geometric (uplifting, gapping, and P- $\Delta$ effects) nonlinearities, where hysteretic damping of the soil was implemented to represent the variations of the shear modulus and damping ratio of the soil with the cyclic shear strain capturing the energy absorbing characteristics of the soil. In order to avoid reflection of the outward propagating waves back into the model, quiet (viscous) boundaries comprising independent dashpots in the normal and shear directions were placed at the lateral boundaries of the soil medium. The lateral boundaries of the main grid were coupled to the free-field grids by viscous dashpots of quiet boundaries at the sides of the model to simulate the free-field motion which would exist in the absence of the structure. Moreover, rigid boundary conditions were adopted to simulate the bedrock in the seismic soil-structure interaction analysis, and the earthquake input motions were applied at the bedrock horizontally propagating upward through the entire model.

Comparing the results of the numerical model and the experimental measurements, it can be concluded that the employed numerical model is appropriate for the simulation of the soil-pile-structure interaction under strong ground motions. Consequently, the proposed SSPSI numerical model is a valid and qualified method of simulation with sufficient accuracy which can be employed for further numerical dynamic soil-structure interaction investigations. Practicing engineers can adopt this verified numerical modelling procedure in the design to consider the effect of SSPSI. Another advantage of the current numerical modelling technique is performing the SSPSI analysis in a fully coupled manner in which main components of the interaction including the subsoil, the pile foundation, and the superstructure are modelled simultaneously without resorting to independent calculations of site or superstructure response, or application of the pile group interaction factors.

In this thesis, in order to investigate the different characteristics of SSI and its influence on the seismic response of superstructures, parametric studies with respect to

different types of foundations were conducted. For this purpose, the previously verified three-dimensional numerical modelling procedure was adopted. A fifteen storey full scale (prototype) structure with four different types of foundations, namely, (i) fixed-base structure representing the situation excluding the soil-structure interaction, (ii) structure supported by shallow foundations, (iii) structure supported by pile-raft foundation in soft soil, and (iv) structure supported by floating (frictional) pile foundation in soft soil, were simulated. Results were presented and compared in terms of settlement of the superstructure under gravity loads, site effect and soil amplification, shear force distribution in the superstructure, rocking of the superstructure, and lateral deformations and drifts of the fifteen storey superstructure.

Results of the 3D numerical simulation in this study show that the properties of the in situ soil influence the characteristics of the excitation, where the peak accelerations at the soft soil surface are greater than that of on the bedrock for low to moderate acceleration levels. However, at higher acceleration levels, low stiffness and nonlinearity of the soft soil prevent the development of the peak accelerations as large as those recorded at the bedrock. Moreover, earthquake records consist of greater proportions of the long period (low frequency) motions after passing through the soft soil deposit. The nonlinear behaviour of the soft soil deposit influences the dynamic characteristics of the ground motion by shifting the peaks in the amplification curve to the right (longer periods), and reducing the amplitudes of the peak ground accelerations.

In general, the ratio of the structural base shear for cases including the soil-structure interaction to that of the fixed-base is less than one demonstrating the effect of the soil-structure interaction in reducing the base shear of the structure. However, the amount of this reduction on the base shear is a function of the foundation type. Based on the results of this study, the structure supported by the pile-raft foundation and floating pile foundation experience more base shear in comparison to the structure supported by the shallow foundations. Moreover, the amount and trend of this reduction in the structural shear forces are not the same for different levels in the superstructure. Therefore, practicing engineers need to be aware that the reduction factor for the maximum base shear due to SSI cannot be generalised to all levels of the superstructure.

Based on the results of this study in terms of the maximum rocking of the superstructure, the structure supported by the shallow foundation experienced the most

severe rocking in comparison with the floating pile and pile-raft foundation cases, where the presence of pile elements in both cases results in considerable reduction in the maximum uplift and in turn rocking experienced by the structure. Moreover, the structure supported by the pile-raft foundation experienced on average 20% less rocking in comparison to the structure supported by the floating pile foundation. This is due to the fact that in the floating pile foundation case, due to the generation of compressive stresses in one side of the foundation, pile elements experience more settlement in comparison with the pile-raft foundation case, where the generated compressive stresses distribute over a larger area resulting in a reduced settlement.

The other important influence of the soil-structure interaction on the seismic response of the superstructure is the significant contribution in amplifying the lateral deflections of the structure. The amplification factor varies with respect to the foundation type, where the presence of pile elements in the floating pile and pile-raft foundation cases reduces the amplification of the lateral deflections of the structure in comparison with the shallow foundation case. Accordingly, SSI tends to increase the inter-storey drifts of the superstructure, which may affect the performance level of the structure and shift the performance level of the structure from life safe zone to near collapse or even collapse zones, particularly in soft soil deposits.

Results of this study can help the practicing engineers in selecting the proper foundation type for the structures. Accordingly, the foundation types experiencing considerable amount of rocking during an earthquake, dissipate significant amount of earthquake energy in comparison with the other types of foundations, and this rocking-dissipation in turn results in directing less shear forces to the superstructure and reducing the structural demand of the superstructure. However, accounting for the rocking dissipation should be adopted with extreme caution and after assessing the influence of SSI, considering the following points: (1) the reduction factor in the shear forces due to SSI varies for different levels in the structure; (2) the residual rotation and differential settlements must be critically evaluated; and (3) the total stability of the structure should be checked carefully.

## 7.2 Recommendations for Future Works

Since the purpose of this work was to assess the influence of different types of foundations on the seismic response of regular mid-rise moment resisting building frames, further numerical and experimental studies plus developing new design procedures to consider the effect of the foundation type are recommended. Future research work may be carried out in the following areas:

- Extend the numerical model as well as physical shaking table model to consider the foundations with different characteristics such as foundation size, embedment length, and pile group arrangement. In this case, the results of the current research can be extended to the wider range of common foundation types.
- Conduct the numerical and experimental investigations, adopted in this study, to determine seismic response of regular high-rise moment resisting building frames resting on various soil types under the influence of SSI. Thus, the findings of the current study can be assessed over a wider range of seismic problems in engineering practice.
- Employ rigorous constitutive soil models to simulate nonlinear and strain dependant behaviour of soils with greater accuracy.
- Perform further investigations on the cases where the superstructure is embedded, which are common case in practice, considering the active and passive pressures of the subsoil on the response of the system during the earthquake excitations.
- Adopt the results of this study and similar works to develop a new design procedure and fulfil the current gap in the available design codes. The proposed design procedure should be able to address the influence of foundation type on the seismic response of buildings in a simply but elaborative manner.

# REFERENCES


ACI318-08 2008. Building Code Requirements for Structural Concrete and Commentary. American Concrete Institute.

AKKAR, S. & BOORE, D. M. 2009. On Baseline Corrections and Uncertainty in Response Spectrafor Baseline Variations Commonly Encounteredin Digital Accelerograph Records. *Bulletin of the Seismological Society of America,* 99(3)**,** 1671-1690.

ALLOTEY, N. & EL NAGGAR, M. H. 2008. Generalized dynamic Winkler model for nonlinear soil-structure interaction analysis. *Canadian Geotechnical Journal,* 45(4)**,** 560-573.

AMBROSINI, R. D. 2006. Material damping vs. radiation damping in soil–structure interaction analysis. *Computers and Geotechnics,* 33(2)**,** 86-92.

ANASTASOPOULOS, I., GELAGOTI, F., SPYRIDAKI, A., SIDERI, J. & GAZETAS, G. 2014. Seismic Rocking Isolation of Asymmetric Frame on Spread Footings. *Journal of Geotechnical and Geoenvironmental Engineering,* 140(1)**,** 133-151.

ANASTASOPOULOS, I., KOURKOULIS, R., GELAGOTI, F. & PAPADOPOULOS, E. 2012a. Rocking response of SDOF systems on shallow improved sand: An experimental study. *Soil Dynamics and Earthquake Engineering,* 40(0)**,** 15-33.

ANASTASOPOULOS, I., LOLI, M., GEORGARAKOS, T. & DROSOS, V. 2012b. Shaking Table Testing of Rocking—Isolated Bridge Pier on Sand. *Journal of Earthquake Engineering,* 17(1)**,** 1-32.

AS1170.4 2007. Structural design actions—Earthquake actions in Australia. NSW, Australia: Standards Australia.

AS2149 2009. Pilling-Design and installation. NSW, Australia: Standards Australian.

AS3600 2009. Concrete Structures. NSW, Australia: Standards Australia.

AS5101.4 2008. Methods for preparation and testing of stabilised materials, Method 4: unconfined compressive strength of compacted materials. NSW, Australia: Standards Australian.

AS/NZS3678 2011. Structural steel - Hot-rolled plates, floorplates and slabs. NSW, Australia: Standards Australia.

AS/NZS4130 2009. Polyethylene (PE) pipes for pressure applications. NSW, Australia: Standards Australia.

ASCE7-10 2010. Minimum Design Loads for Buildings and Other Structures American Society of Civil Engineers.

ASHOUR, M., NORRIS, G. & PILLING, P. 1998. Lateral Loading of a Pile in Layered Soil Using the Strain Wedge Model. *Journal of Geotechnical and Geoenvironmental Engineering,* 124(4)**,** 303-315.

ATC-40 1996. Seismic Evaluation and Retrofit of Concrete Buildings. California Department of Transportation.

BAO, Y., YE, G., YE, B. & ZHANG, F. 2012. Seismic evaluation of soil–foundation–superstructure system considering geometry and material nonlinearities of both soils and structures. *Soils and Foundations,* 52(2)**,** 257-278.

BATHURST, R. J., KESHAVARZ, A., ZARNANI, S. & TAKE, W. A. 2007. A simple displacement model for response analysis of EPS geofoam seismic buffers. *Soil Dynamics and Earthquake Engineering,* 27(4)**,** 344-353.

BEATY, M. H. 2001. *A synthesized approach for estimating liquefaction-induced displacements of geotechnical structures.* NQ71436 Ph.D., The University of British Columbia (Canada).

BONELLI, P., RESTREPO, J. I., BOROSCHEK, R. & CARVALLO, J. F. The 2010 Great Chile Earthquake - Changes to Design Codes. International Symposium on Engineering Lessons Learned from the 2011 Great East Japan Earthquake, 2012 Tokyo, Japan.

BOORE, D. M. 2001. Effect of Baseline Corrections on Displacements and Response Spectra for Several Recordings of the 1999 Chi-Chi, Taiwan, Earthquake. *Bulletin of the Seismological Society of America,* 91(5)**,** 1199-1211.

BORJA, R. I., WU, W. H., AMIES, A. P. & SMITH, H. A. 1994. Nonlinear Lateral, Rocking and Torsional Vibration of Rigid Foundations. *Journal of Geotechnical Engineering Structures,* 120(3)**,** 491-513.

BOWLES, J. E. 2001. *Foundation Analysis and Design*, McGraw-Hill International, Editions, 5th edn, Civil Engineering Series.

BREBBIA, C. A., TELLES, J. C. F. & WROBEL, L. C. 1984. *Boundary Element Techniques: theory and applications in engineering*, Springer-Verlag.

BSSC 1997. NEHRP Guidelines for the Seismic Rehabilitation of Buildings, 1997 Edition, Part 1: Provisions and Part 2: Commentary. Federal Emergency Management Agency.

BSSC 2009. NEHRP Recommended Seismic Provisions for New Buildings and Other Structures. Federal Emergency Management Agency.

BYRNE, P. M., NAESGAARD, E. & SEID-KARBASI, M. 2006. Analysis and Design of Earth Structures to Resist Seismic Soil Liquefaction. *59th Canadian Geotechnical Conference & 7th Joint CGS/IAH-CNC Groundwater Specialty Conference.* Vancouver, Canada.

CARBONARI, S., DEZI, F. & LEONI, G. 2011. Linear soil-structure interaction of coupled wall-frame structures on pile foundations. *Soil Dynamics and Earthquake Engineering,* 31(9)**,** 1296-1309.

CARR, A. J. 2008. *Soil-Structure Interaction, Advanced nonlinear seismic structural analysis notes*, Pavia.

CGS 2006. Canadian Foundation Engineering Manual. forth ed. Canada: Canadian Geotechnical Society.

CHAMBON, R., DESRUES, J., HAMMAD, W. & CHARLIER, R. 1994. CLoE, a new rate-type constitutive model for geomaterials theoretical basis and implementation. *International Journal for Numerical and Analytical Methods in Geomechanics,* 18(4)**,** 253-278.

CHAN, S. L. & CHUI, P. T. 2000. *Non-Linear Static and Cyclic Analysis of Steel Frames with Semi-Rigid Connections*, Elsevier.

CHAU, K. T., SHEN, C. Y. & GUO, X. 2009. Nonlinear seismic soil-pile-structure interactions: Shaking table tests and FEM analyses. *Soil Dynamics and Earthquake Engineering,* 29(2)**,** 300-310.

CHEN, J., SHI, X. & LI, J. 2010. Shaking table test of utility tunnel under non-uniform earthquake wave excitation. *Soil Dynamics and Earthquake Engineering,* 30(11)**,** 1400-1416.

CHU, D. 2006. *Three-dimentional nonlinear dynamic analysis of soil-pile-structure interaction.* PhD, Washington University.

CHU, D. & TRUMAN, K. Z. 2004. effects of pile foundation configurations in seismic soil-pile-structure interaction. *13th World Conference on Earthquake Engineering.* Vancouver, B.C., Canada.

COMODROMOS, E. M. & PAPADOPOULOU, M. C. 2012. Response evaluation of horizontally loaded pile groups in clayey soils. *Geotechnique,* 62(4)**,** 329-339.

COMODROMOS, E. M. & PAPADOPOULOU, M. C. 2013. Explicit extension of the p-y method to pile groups in cohesive soils. *Computers and Geotechnics,* 47**,** 28-41.

CRAIG, R. R. J. & KURDILA, A. J. 2006. *Foundamentals of Structural Dynamics,* New Jersey, Joun Wiley & Sons Inc.

CSI 2010. SAP2000 v14 Analysis Reference Manual. California: CSI (Computers and Structures Inc.), Berkley.

CUNDALL, P. A. Explicit Finite Difference Methods in Geomechanics. Proceedings of the EF Conference on Numerical Methods in Geomechanics, 1976 Blacksburg, Virginia. 132-150.

DARVE, F., FLAVIGNY, E. & MEGHACHOU, M. 1995. Constitutive modelling and instabilities of soil behaviour. *Computers and Geotechnics,* 17(2)**,** 203-224.

DAS, B. M. 1983. *Fundamentals of soil dynamics*, Elsevier.

DENG, L. & KUTTER, B. L. 2012. Characterization of rocking shallow foundations using centrifuge model tests. *Earthquake Engineering & Structural Dynamics,* 41(5)**,** 1043-1060.

DESAI, C. S. & ABEL, J. F. 1972. *Introduction to the finite Element Method: A Numerical Method for Engineering Analysis*, Van Nostrand Reinhold Co., New York.

DUTTA, S. C. & ROY, R. 2002. A critical review on idealization and modeling for interaction among soil-foundation-structure system. *Computers & Structures,* 80(20-21)**,** 1579-1594.

ENDO, O. & KOMANOBE, K. Single and Multi Directional Shaking Table Tests on Sand Liquefaction. 1st International Conference on Earthquake Geotechnical Engineering, 1995 IS-Tokyo. 675-680.

FATAHI, B. & TABATABAIEFAR, S. 2013. Fully Nonlinear Versus Equivalent Linear Computation Method for Seismic Analysis of Mid-Rise Buildings on Soft Soils. *International Journal of Geomechanics,* doi:10.1061/(ASCE)GM.1943-5622.0000354.

FEMA 2005. Improvement of nonlinear static seismic analysis procedures. Washington, D.C.

FINN, W. D. 2005. A study of piles during earthquakes: Issues of design and analysis. *Bulletin of Earthquake Engineering, Springer,* 3**,** 141–234.

GAJO, A. & MUIR WOOD, D. 1999. A kinematic hardening constitutive model for sands: the multiaxial formulation. *International Journal for Numerical and Analytical Methods in Geomechanics,* 23(9)**,** 925-965.

GAZETAS, G. 1982. Vibrational characteristics of soil deposits with variable wave velocity. *International Journal for Numerical and Analytical Methods in Geomechanics,* 6(1)**,** 1-20.

GAZETAS, G. 1991. Formulas and Charts for Impedances of Surface and Embedded Foundations. *Journal of Geotechnical Engineering,* 117(9)**,** 1363-1381.

GAZETAS, G. & APOSTOLOU, M. Nonlinear Soil–Structure Interaction: Foundation Uplifting and Soil Yielding. Proceedings Third UJNR Workshop on Soil-Structure Interaction, , March 29-30, 2004 Menlo Park, California, USA.

GAZETAS, G. & MYLONAKIS, G. Seismic Soil-Structure Interaction: New Evidence and Emerging Issues. Proc. 3rd Conf. Geotechnical Earthquake Engineering and Soil Dynamics, 1998 Seattle, USA. ASCE, 1119-1174.

GHEE, E. & GUO, W. 2010. FLAC3D analysis on soil moving through piles. *Frontiers in Offshore Geotechnics II.* CRC Press.

GIBSON, G. 2010. Learning from Earthquakes, Chile, 2010. *Australian Earthquake Engineering Society Conference (AEES 2010).* Perth, Western Australia: Australian Earthquake Engineering Society.

GIRAULT, D. P. Analyses of Foundation Failures. *In:* ASCE, ed. The Mexico Earthquakes—1985: Factors Involved and Lessons Learned, 1986. 178-192.

GOHL, W. B. & FINN, W. D. L. Seismic Response of Single Piles in ShakingTable Studies. Fifith Canadian Conference Earthquake Engineering, 1987 Ottawa. A.A. Balkema, 435-444.

GRATCHEV, I. B., SASSA, K., OSIPOV, V. I. & SOKOLOV, V. N. 2006. The liquefaction of clayey soils under cyclic loading. *Engineering Geology,* 86(1)**,** 70-84.

GUIN, J. & BANERJEE, P. K. 1998. Coupled Soil-Pile-Structure Interaction Analysis under Seismic Excitation. *Journal of Structural Engineering,* 124(4)**,** 434-444.

GUTIERREZ, J. A. & CHOPRA, A. K. 1978. A substructure method for earthquake analysis of structures including structure-soil interaction. *Earthquake Engineering & Structural Dynamics,* 6(1)**,** 51-69.

HA, I.-S., OLSON, S. M., SEO, M.-W. & KIM, M.-M. 2011. Evaluation of reliquefaction resistance using shaking table tests. *Soil Dynamics and Earthquake Engineering,* 31(4)**,** 682-691.

HAN, Y. C. & CATHRO, D. Seismic behaviour of tall building supported on pile foundations. seismic analysis and design for soil-pile-strcutre interaction. Geotechnical Special publications, No. 70, 1997. ASCE, 36-51.

HARDIN, B. O. & DRNEVICH, V. P. 1972. Shear modulus and damping in soils: desing equations and curves. *Journal of the Soil Mechanics and Foundations Division,* 98(7)**,** 667-692.

HAYASHI, Y. & TAKAHASHI, I. Soil-structure interaction effects on building response in recent earthquakes. Third UJNR Workshop on Soil-Structure Interaction, 2004 Vallombrosa Center, Menlo Park, California.

HETENYI, M. 1946. *Beams on Elastic Foundation: Theory with Applications in the Fields of Civil and Mechanical Engineering*, University of Michigan Press, Ann Arbor, Michigan.

HOKMABADI, A. S., FAKHER, A. & FATAHI, B. 2011. Seismic strain wedge model for analysis of single piles under lateral seismic loading. *Australian Geomechanics,* 46(1)**,** 31-41.

HOKMABADI, A. S., FATAHI, B. & SAMALI, B. 2012. Recording inter-storey drifts of structures in time-history approach for seismic design of building frames. *Australian Journal of Structural Engineering,* 13(2)**,** 175-179.

IAI, S. 1989. Similitude for Shaking Table Tests on Soil-Structure-Fluid Model in 1g Gravitational Field. *Soils and Foundations,* 29(1)**,** 105-118.

IBC 2012. International Building Code (IBC). USA: International Code Consortium.

IDRISS, I. M. Response of Soft Soil Sites during Earthquakes. Memorial Symposium to honor Professor Harry Bolton Seed,, 1990 Berkeley, California.

INABA, T., DOHI, H., OKUTA, K., SATO, T. & AKAGI, H. 2000. Nonlinear response of surface soil and NTT building due to soil-structure interaction during the 1995 Hyogo-ken Nanbu (Kobe) earthquake. *Soil Dynamics and Earthquake Engineering,* 20(5-8)**,** 289-300.

ISHIMURA, K., OHTSUKI, A., YOKOYAMA, K. & KOYANAGI, Y. Sway-rocking model for simulating nonlinear response of sandy deposit with structure. Tenth World Conferecne on Earthquake Engineering, 1992. 1897-1903.

ITASCA 2009. FLAC3D version 4.00 Fast Lagrangian Analysis of Continua in three dimentions, User's Manual. Minneapolis, Minnesota, USA: Itasca Consulting Group, Inc.

ITASCA 2010. FLAC Version 6.00, A computer program for seismic response analysis for soil deposits. Minneapolis, Minnesota, USA: Itasca Consulting Group, Inc.

IVŠIĆ, T. 2006. A model for presentation of seismic pore water pressures. *Soil Dynamics and Earthquake Engineering,* 26(2–4)**,** 191-199.

JAFARZADEH, F. & YANAGISAWA, E. Settlement of Sand Models under Unidirectional Shaking. 1st International Conference on Earthquake Geotechnical Engineering, 1995 IS-Tokyo. 693-698.

JAKRAPIYANUN, W. 2002. *Physical modeling of dynamics soil-foundation-structure-interaction using a laminar container.* University of California, San Diego Ph.D.

KANATANI, M., NISHI, K. & TOUMA, J. Large Shake Table Tests on Saturated Sand layer and Numerical Simulation by Nonlinear Analysis Mwethod. First International Conference on Earthquake Geotechnical Engineering, 1995 IS-Tokyo. 705-710.

KARAMODIN, A. K. & KAZEMI, H. H. 2010. Semi-active control of structures using neuro-predictive algorithm for MR dampers. *Structural Control and Health Monitoring,* 17(3)**,** 237-253.

KATSIKADELIS, J. 2002. *Boundary Elements Theory and Applications*, Elsevier, Oxford.

KIM, Y. & ROESSET, J. 2004. Effect of Nonlinear Soil Behavior on Inelastic Seismic Response of a Structure. *International Journal of Geomechanics,* 4(2)**,** 104-114.

KOCAK, S. & MENGI, Y. 2000. A simple soil–structure interaction model. *Applied Mathematical Modelling,* 24(8–9)**,** 607-635.

KRAMER, S. L. 1996. *Geotechnical earthquake engineering*, Prentice Hall.

KRAMER, S. L. & STEWART, J. P. 2004. Geotechnical Aspects of Seismic Hazards. *In:* BOZORGNIA, Y. & BERTERO, V. V. (eds.) *Earthquake Engineering: From Engineering Seismology to Performance-Based Engineering.* LLC: CRC Press.

KUTANIS, M. & ELMAS, M. 2001. Non-Linear Seismic Soil-Structure Interaction Analysis Based on the Substructure Method in the Time Domain. *Turkish Journal of Engineering & Environmental Sciences,* 25(6)**,** 617-626.

LANGHAAR, H. 1951. *Dimensional Analysis and Theory of Models,* New York, John Wiley and Sons.

LEE, C.-J., WEI, Y.-C. & KUO, Y.-C. 2012. Boundary effects of a laminar container in centrifuge shaking table tests. *Soil Dynamics and Earthquake Engineering,* 34(1)**,** 37-51.

LO, R. C. & WANG, Y. 2012. Lessons Learned from Recent Earthquakes – Geoscience and Geotechnical Perspectives. *In:* MOUSTAFA, A. (ed.) *Advances in Geotechnical Earthquake Engineering - Soil Liquefaction and Seismic Safety of Dams and Monuments.* InTech.

LU, J., ELGAMAL, A., YAN, L., LAW, K. & CONTE, J. 2011. Large-Scale Numerical Modeling in Geotechnical Earthquake Engineering. *International Journal of Geomechanics,* 11(6)**,** 490-503.

LU, J., ELGAMAL, A., YAN, L., LAW, K. H. & CONTE, J. P. 2012. Large-scale numerical modeling in geotechnical earthquake engineering. *International Journal of Geomechanics,* 11(6)**,** 490-503.

LU, X., LI, P., CHEN, B. & CHEN, Y. 2005. Computer simulation of the dynamic layered soil-pile-structure interaction system. *Canadian Geotechnical Journal,* 42(3)**,** 742-751.

LU, X., LI, P., CHEN, Y. & CHEN, B. SHAKING TABLE MODEL TESTING ON DYNAMIC SOIL-STRUCTURE INTERACTION SYSTEM. 13th World Conference on Earthquake Engineering, August 1-6, 2004 2004 Vancouver, B.C., Canada.

LYSMER, J. & KUHLEMEYER, R. L. 1969. Finite Dynamic Model for Infinite Media. *Journal of the Engineering Mechanics Division,* 95(6)**,** 859-877.

LYSMER, J. & WAAS, G. 1972. ShearWaves in Plane Infinite Structures. *ASCE J. Eng. Mech.,* 98**,** 85-105.

MAHESHWARI, B. & SARKAR, R. 2011. Seismic Behavior of Soil-Pile-Structure Interaction in Liquefiable Soils: Parametric Study. *International Journal of Geomechanics,* 11(4)**,** 335-347.

MAHESHWARI, B. K. & WATANABE, H. 2006. Nonlinear dynamic behavior of pile foundations: Effects of separation at the soil-pile interface. *Soils and Foundations,* 46(4)**,** 437-448.

MALHOTRA, S. Seismic Soil-Pile-Structure Interaction: Analytical Models. *In:* DANTE, F., ANAND, J. P. & BALASINGAM, M., eds., 2010. ASCE, 310.

MARTI, J. & CUNDALL, P. A. 1982. Mixed Discretization Procedure for Accurate Solution of Plasticity Problems. *Int. J. Num. Methods and Anal. Methods in Geomech.,* 6**,** 129-139.

MASSIMINO, M. R. & MAUGERI, M. 2013. Physical modelling of shaking table tests on dynamic soil–foundation interaction and numerical and analytical simulation. *Soil Dynamics and Earthquake Engineering,* 49(0)**,** 1-18.

MATLOCK, H. & REESE, L. 1960. Generalized Solutions for Laterally Loaded Piles. *Soil Mechanics and Foundation Div.,* 86(5)**,** 63-91.

MAUGERI, M., MUSUMECI, G., NOVITÀ, D. & TAYLOR, C. A. 2000. Shaking table test of failure of a shallow foundation subjected to an eccentric load. *Soil Dynamics and Earthquake Engineering,* 20(5–8)**,** 435-444.

MENDOZA, M. & ROMO, M. Behavior of Building Foundations in Mexico City During the 1985 Earthquake: Second Stage. Lessons Learned from the 1985 Mexico Earthquake, 1989. Earthquake Eng. Research Inst., 66-70.

MERGOS, P. E. & KAWASHIMA, K. 2005. rocking isolation of a typical bridge pier on spread foundation. *Journal of Earthquake Engineering,* 9(sup2)**,** 395-414.

MEYMAND, P. J. 1998. *Shaking table scale model tests of nonlinear soil-pile-superstructure in soft clay.* PhD thesis in Civil Engineering, University of California, Berkley.

MIDORIKAWA, M., AZUHATA, T., ISHIHARA, T. & WADA, A. 2005. seismic response analysis of rocking structural systems with yielding base plate by the finite element method. *Earthquake Resistant Engineering Structures,* 81(1)**,** 333-341.

MINDLIN, R. D. 1936. Force at a Point in the Interior of a Semi-Infinite Solid. *Physics,* 7(5)**,** 195-202.

MIZUNO, H., IIBA, M. & HIRADE, T. Pile Damage During the 1995 Hyogoken-Nanbu Earthquake in Japan. Proc. 11th World Conf. Earthquake Eng., 1996 Acapulco.

MONCARZ, P. & KRAWINKLER, H. 1981. Theory and Application of Experimental Model Analysis in Earthquake Engineering. John Blume Earthquake Engineering Ctr., Stanford Univ.

MOSS, R. E., CROSARIOL, V. & KUO, S. Shake Table Testing to Quantify Seismic Soil Structure Interaction of Underground Structures. International Conference on Recent Advances in Geotechnical Earthquake Engineering and Soil Dynamics, 2010 San Diego.

MOSTAFA, Y. E. & EL NAGGAR, M. H. 2002. Dynamic analysis of laterally loaded pile groups in sand and clay. *Canadian Geotechnical Journal,* 39(6)**,** 1358-1383.

NAGTEGAAL, J. C., D. M. PARKS, D. M. & RICE, J. R. 1974. On Numerically Accurate Finite Element Solutions in the Fully Plastic Range. *Comp. Meth. Appl. Mech. & Eng.,* 4**,** 153-177.

NGHIEM, H. 2009. *Soil-pile-structure interaction effects on high rises under seismic shaking.* PhD Thesis, University of Colorado at Denver.

NZS1170.5 2004. Strcutural Design Actions, part5: earthquake actions-New Zealand Commentary. Standards New Zealand.

PEER 2012. PEER Ground Motion Database. *Pacific Earthquake Engineering Research Centre.* University of California, Berkeley, CA.

PITILAKIS, D., DIETZ, M., WOOD, D. M., CLOUTEAU, D. & MODARESSI, A. 2008. Numerical simulation of dynamic soil-structure interaction in shaking table testing. *Soil Dynamics and Earthquake Engineering,* 28(6)**,** 453-467.

POULOS, H. & DAVIS, E. 1980. *Pile Foundation Analysis and Design*, John Wiley and Sons.

POULOS, H. G. 1971. Behaviour of laterally loaded piles: I-single piles and II- pile groups. *Journal of Soil Mechanics and Foundation Divsion, ASCE,* 97(SM5)**,** 711–731, 733–751.

PRASAD, S., TOWHATA, I., CHANDRADHARA, G. & NANJUNDASWAMY, P. 2004. Shaking table tests in earthquake geotechnical engineering. *Current science,* 87(10)**,** 1398-1404.

RAYHANI, M. 2007. *Centrifuge modeling of seismic site response and soil-structure interaction.* PhD Thesis, The University of Western Ontario.

RAYHANI, M. & EL NAGGAR, M. 2008. Numerical Modeling of Seismic Response of Rigid Foundation on Soft Soil. *International Journal of Geomechanics,* 8(6)**,** 336-346.

RAYHANI, M., EL NAGGAR, M. & TABATABAEI, S. 2008. Nonlinear Analysis of Local Site Effects on Seismic Ground Response in the Bam Earthquake. *Geotechnical and Geological Engineering,* 26(1)**,** 91-100.

RICHARDS, J. R., ELMS, D. G. & BUDHU, M. 1990. Dynamic Fluidization of Soils. *Journal of Geotechnical Engineering,* 116(5)**,** 740-759.

RIEMER, M., GOOKIN, W., BRAY, J. & WARTMAN, J. Using Reflected Waves to Measure Small Strain Dynamic Properties. 5th Caltrans Seismic Research Workshop, 1998 Sacramento. 16-18.

ROESSET, J. M. & ETTOUNEY, M. M. 1977. Transmitting Boundaries: A Comparison. *Int. J. Num. & Analy. Methods Geomech.,* 1**,** 151-176.

ROESSET, J. M., WHITMAN, R. V. & DOBRY, R. 1973. Modal Analysis for Structures with Foundation Interaction. *Journal of the Structural Division,* 99(4)**,** 399-416.

SATO, H., TANAKA, Y., KANATANI, M., TAMARI, Y. & SUGISAWA, M. An Experimental and Numerical Study on the Behaviour of Improved Grounds. 1st International Conference on Earthquake Geotechnical Engineering, 1995 IS-Tokyo. 767-772.

SCHNABEL, P. B., LYSMER, J. & SEED, H. B. 1972. SHAKE: A computer program for earthquake response analysis of horizontally layered sites. Earthquake Engineering Research Centre, University of California, Berkeley, California. .

SEED, H. B. & IDRISS, I. 1969. Influence of Soil Conditions on Ground Motion during Earthquakes. *Journal of Soil Mechanics and Foundations, Division, ASCE,* 95**,** 99-137.

SEED, H. B., MURARKA, R., LYSMER, J. & IDRISS, I. M. 1976. Relationships of maximum acceleration, maximum velocity, distance from source, and local site conditions for moderately strong earthquakes. *Bulletin of the Seismological Society of America,* 66(4)**,** 1323-1342.

SEED, H. B., WONG, R. T., IDRISS, I. M. & TOKIMATSU, K. 1986. *Moduli and Damping Factors for Dynamic Analyses of Cohesionless Soils*, ASCE.

SHELKE, A. & PATRA, N. 2008. Effect of Arching on Uplift Capacity of Pile Groups in Sand. *International Journal of Geomechanics,* 8(6)**,** 347-354.

SHIMING, W. & GANG, G. 1998a. Dynamic soil-structure interaction for high-rise buildings. *In:* ZHANG, C. & JOHN, P. W. (eds.) *Developments in Geotechnical Engineering.* Elsevier.

SHIMING, W. & GANG, G. 1998b. Dynamic soil-structure interaction for high-rise buildings. *In:* ZHANG, C. & JOHN, P. W. (eds.) *Developments in Geotechnical Engineering.* Elsevier.

SHING, B. P. & TANABE, T. 2001. *Modeling of inelastic behavior of RC structures under seismic loads,* Reston, VA, American Society of Civil Engineers (ASCE).

SMALL, J. & ZHANG, H. 2002. Behavior of Piled Raft Foundations Under Lateral and Vertical Loading. *International Journal of Geomechanics,* 2(1)**,** 29-45.

SPYRAKOS, C. C., MANIATAKIS, C. A. & KOUTROMANOS, I. A. 2009. Soil–structure interaction effects on base-isolated buildings founded on soil stratum. *Engineering Structures,* 31(3)**,** 729-737.

STANTON, J. F., BANERJEE, S. & HASAYEN, I. 1998. Shaking table tests on piles. *Final report, Research Project Y-2811, Task 26* Repared for Washington State Trasportation Communication.

STEEDMAN, R. S. & ZENG, X. Physical Modelling of Earthquake Excitation for Geotechnical Engineering. Sixth Canadian Conference Earthquake Engineering, 1991.

STEWART, J., FENVES, G. & SEED, R. 1999a. Seismic soil-structure interaction in buildings. I: Analytical aspects. *J. Geotech. & Geoenv. Engrg.,* 125(1)**,** 26-37.

STEWART, J., FENVES, G. & SEED, R. 1999b. Seismic soil-structure interaction in buildings. II: Empirical findings. *J. Geotech. & Geoenv. Engrg.,* 125(1)**,** 38-48.

STEWART, J. P., SEED, R. B. & FENVES, G. L. 1998. Empirical evaluation of inertial soil-structure interaction effects. Berkeley: Pacific Earthquake Engineering Research Center, University of California.

STEWART, J. P. & STEWART, A. F. 1997. Analysis of Soil-Structure Interaction Effects on Building Response from Earthquake Strong Motion Recordings at 58 Sites. *Rpt. No. UCB/EERC-97/01.* Earthquake Eng. Research Ctr., Univ. of California.

SULAEMAN, A. 2010. *The Use of Lightweight Concrete Piles for Deep Foundation on Soft Soils*. PhD thesis in Civil Engineering, University of Tun Hussein Onn, Malaysia.

SUN, J., GOLESORKHI, R. & SEED, H. B. 1988. Dynamic moduli and damping ratio for cohesive soils. University of California Berkeley-Earthquake Engineering Research Center.

TABATABAIEFAR, H. R., FATAHI, B. & SAMALI, B. 2013. Seismic Behavior of Building Frames Considering Dynamic Soil-Structure Interaction. *International Journal of Geomechanics,* 13(4)**,** 409-420.

TAJIMI, H. Dynamic Analysis of a Structure Embedded in an Elastic Stratum. Proc. 4th World Conf. Earthquake Eng., 1969 Santiago, USA. 53-69.

TANG, L., LING, X., XU, P., GAO, X. & WANG, D. 2009. Shake table test of soil-pile groups-bridge structure interaction in liquefiable ground. *Earthquake Engineering and Engineering Vibration***,** 1-12.

TAO, X., KAGAWA, T., MINOWA, C. & ABE, A. Verification of Dynamic Soil-Pile Interaction. Geotechnical Special Publication No. 75, 1998. ASCE, 1199-1210

TAYLOR, C. A. 1997. Large Scale Shaking Tests of Geotechnical Structures. Earthquake Engineering Research Centre, University of Bristol.

TAYLOR, C. A., DAR, A. R. & CREWE, A. J. Shaking Table modelling of seismic geotechnical problems. 10th European Conference on Earthquake Engineers, 1995 Vienna, Austria. 441-446.

TIMOSHENKO 1940. *Strenght of materials*, D. Van Nostrand company, Lnc.

TOWHATA, I. 2008. *Geotechnical Earthquake Engineering,* Berlin Heidelberg, Springer-Verlag.

TSUKAMOTO, Y., ISHIHARA, K., SAWADA, S. & FUJIWARA, S. 2012. Settlement of Rigid Circular Foundations during Seismic Shaking in Shaking Table Tests. *International Journal of Geomechanics,* 12(4)**,** 462-470.

TURAN, A. 2009. *Physical modeling of seismic soil-structure interaction of embedded structures.* Ph.D. NR50400, The University of Western Ontario (Canada).

TURAN, A., HINCHBERGER, S. & EL NAGGAR, H. 2009. Design and commissioning of a laminar soil container for use on small shaking tables. *Soil Dynamics and Earthquake Engineering,* 29(2)**,** 404-414.

UKAJA, K. 1975. Analysis of soil foundation structure interaction. Stanford University, Department of Civil and Environmental Engineering.

VALSANGKAR, A. J., DAWE, J. L. & MITA, K. A. shake Table Studies of Sesimic Response of Single Partially Suppported Piles. Sixth Canadian Conference Earthquake Engineering, 1991. 327-334.

VELETSOS, A. & PRASAD, A. 1989. Seismic Interaction of Structures and Soils: Stochastic Approach. *Journal of Structural Engineering,* 115(4)**,** 935-956.

VELETSOS, A. S. 1993. *Design concepts for dynamics of soil-structure interaction. Developments in Dynamic Soil-Structure Interaction,* Netherlands, Kluwer Academic Publishers.

VUCETIC, M. & DOBRY, R. 1991. Effect of Soil Plasticity on Cyclic Response. *Journal of Geotechnical Engineering,* 117(1)**,** 89-107.

WARTMAN, J. 1996. *A Laboratory Study of the Effects of Fly Ash on the Geotechnical Properties of Soft Clay.* MEng, University of California, Berkeley.

WOLF, J. 1998. *Soil-Structure Interaction Analysis in Time Domain*, Prentice Hall Co, New Jersey.

WOLF, J. P. 1985. *Dynamic soil-structure interaction*, Prentice-Hall, Englewood Cliffs, New Jersey.

YAN, L. & BYRNE, P. M. 1989. Application of hydraulic gradient similitude method to small-scale footing tests on sand. *Canadian Geotechnical Journal,* 26(2)**,** 246–259.

ZEN, K., YAMAZAKI, H., TORIIHARA, M. & MORI, T. Shaking Table Test on Liquefaction of Artificially Cemented Sands. Tenth World conference on Earthquake Engineering, 1992 Madrid, Spain. 1417-1420.

ZENG, X. & SCHOFIELD, A. N. 1996. Design and performance of an equivalent-shear-beam container for earthquake centrifuge modelling. *Geotechnique,* 46(1)**,** 83-102.

ZHANG, Z., CHO, C., QIANG PAN, Q. & LU, X. 2009. Experimental Investigation on Excess Pore Water Pressure in Soft Soil-Foundations under Minor Shocks. *World Academy of Science, Engineering and Technology,* 3(2)**,** 508-512.

ZIEMIAN, R. 1993. Examples of Frame Studies Used to Verify Advanced Methods of Inelastic Analysis. *Plastic hinge based methods for advanced analysis and design of steel frames: an assessment of the state-of-the-art Workshop.*